Development of a murine model of colorectal cancer; application to the optimisation of irinotecan therapy.

Thesis submitted in accordance with the requirements of the University of Liverpool for the degree of Doctor of Philosophy by Jonathan Evans

September 2017

Contents

Declaration

The work presented in this thesis was carried out in the Institute of Translational Medicine, University of Liverpool and was undertaken while working as a research fellow at the Liverpool Cancer Research (UK) Centre. The material contained within this thesis has not been, nor is currently being presented wholly, or in part, for any other degree or qualification.

I declare that all the work presented in this thesis has been carried out by me except where indicated below:

- Cation exchange prior to iTRAQ analysis was performed by Mrs Jane Hamlett
- iTRAQ mass spectrometry was performed by Dr Roz Jenkins
- Histopathological and immunohistochemical assessment of murine caecal tumours was performed by Dr Lorenzo Ressel

Acknowledgments

Many people have supported and advised me during the time taken to complete this thesis.

Firstly, my wife Jenny who has provided invaluable support, not just in completing this thesis, but for the last 12 years. I am eternally grateful for all you do and consider myself extremely lucky to be married to such an intelligent, insightful and beautiful lady. You have always been there for me throughout the long hours, multiple examinations and trials of pursuing a career in surgery.

I am very grateful for the advice and guidance of my supervisory team; Dr Neil Kitteringham, Professor Dan Palmer, Dr Eithne Costello and Ms Elizabeth Tweedle; as I made the transition from a full-time practicing clinician to laboratory-based scientist. Dr Neil Kitteringham's open door policy and logical approach has been invaluable as I met the challenges and frustrations of laboratory based experimentation.

I am also grateful to all the staff in the Medical Research Council Centre for Drug Safety Science who assisted me in the acquisition of laboratory technique, particularly Dr Boleslaw Winiarski whose meticulous technique and teaching allowed me to relatively rapidly acquire the necessary skills. Working in collaboration on overlapping projects facilitated discussion and the exchange of ideas that would not have been possible working in isolation. Many others have provided advice and a watchful eye as I learnt to perform the varying experimental techniques required for this thesis. Dr Holly Bryan, Dr Laleh Kamalian and Dr James Heslop all guided me through cell culture, transfection and drug-dosing in my early experiments. My office mates, Dr Rowena Sison-Young, Dr Joanne Walsh, Dr Rowena Eakins, Dr Shiva Forootan and Dr Emma Wilkinson, have acted as a sounding board for ideas and more importantly provided cake on a relatively regular basis!

My fellow surgical trainees have also made the research process much easier, and I wish to thank Mr Paul Sutton, Mr Rob Jones, Mr Mohammed Elmasry, Mr Derek McWhirter, Mr David Bowden and Mr Nicholas Bird.

Finally, I wish to thank Cancer Research (UK) who funded me and this work.

Abstract

Introduction

Outcomes in colorectal cancer (CRC) might be improved by identification of novel drug targets. Nrf2 is a transcription factor that regulates cellular stress response and irinotecan-metabolising pathways; it is inhibited by the naturally occurring quassinoid brusatol. This thesis assessed the expression of Nrf2 in CRC and explored the effect of Nrf2 modulation alone and in combination with irinotecan *in vitro* and in an orthotopic syngeneic mouse model, developed as part of this thesis.

Methods

Tissue microarrays (TMA) were constructed from normal colon, primary CRC tumours and liver metastases from the same patient and stained for Nrf2. Cell viability and irinotecan cytotoxicity were assessed in murine (CT26) and human (HCT116) CRC cell lines following siRNA or pharmacological modulation of Nrf2. *In vitro* findings were validated in the murine model, utilising bioluminescent imaging to quantify disease burden following caecal implantation of luminescent CT26 cells. iTRAQ proteomic pathway analysis was subsequently undertaken on liver tissue from mice exposed to brusatol over a two-week period in attempt to determine the specificity of brusatol as an Nrf2 inhibitor and its safety profile.

Results

An orthotopic syngeneic murine model of CRC was developed using the CT26 cell line transfected with the luciferase gene and cloned by serial dilution. This model allowed the monitoring of disease burden in mice through the measurement of luminescent signal longitudinally over the study period. Disease development in mice was a reasonable recapitulation of the disease process in humans; tumours developed in the correct microenvironment in the presence of an intact immune system with up to 20% of mice developing liver metastases.

Nrf2 expression was significantly higher in primary CRC and metastatic tissue than in normal colon ($p<0.01$), with a positive correlation between Nrf2 expression in matched primary and metastatic samples included in the TMA. *In vitro* viability was decreased in human and mouse CRC cell-lines by Nrf2 siRNA, confirming a role for Nrf2 in cell survival. The Nrf2 inhibitor, brusatol, also resulted in a loss of cell viability, in concordance with the effect of Nrf2 siRNA. Furthermore, inhibition of Nrf2 by siRNA or brusatol significantly enhanced the cytotoxicity of irinotecan *in vitro*, with drug synergy noted for combinations of brusatol with irinotecan in both cell lines.

Brusatol effectively abrogated tumour growth in orthotopically-allografted mice, resulting in an average 8-fold reduction in luminescence at the study end-point ($p=0.02$). There was a trend toward enhanced cytotoxicity of irinotecan when combined with brusatol in the mouse model.

Nrf2 inhibition was confirmed in the livers of mice receiving brusatol treatment by western immunoblotting prior to iTRAQ analysis. Many of the pathways significantly altered in the analysis of murine livers following prolonged brusatol therapy could be linked to Nrf2, implying that brusatol may exert much of its effect through Nrf2.

Conclusions

Nrf2 offers a promising drug target in the treatment of CRC. Brusatol provides the potential for translation to clinical trials, although further work is required to determine the mechanism by which brusatol achieves inhibition on Nrf2 and how specific this effect is.

Abbreviations

3D	3-dimensional
5-FU	5-fluorouracil
ABC	Adenosine-triphosphate binding cassette
AFAP	Attenuated familial adenomatous polyposis
AOM	Azoxymethane
APC	Adenomatous Polyposis Coli
APER	Abdomino-perineal excision of the rectum
ARE	Antioxidant response element
ATP	Adenosine-triphosphate
ADP	Adenosine-diphosphate
BaE	Barium enema
BCA	Bicinchoninic acid
BCSP	Bowel cancer screening program
BER	Base excision repair
BLI	Bioluminescence imaging
BMI	Body mass index
CCD	Charge-couple device
CDDO-me	Methyl-2-cyano-3,12-dioxooleano-1,9-dien-28-oate
CES	Carboxylesterases
CESTA	Cellular thermal shift assay
CI	Combination indexes
CIMP	CpG island methylator phenotype
CIN	Chromosomal instability
CMV	Cytomegalovirus
COX	cyclooxygenase
CpG	Cystoceine preceeding guanine
CRC	Colorectal cancer
Cre	Cre-recombinase
CRISPR	Clustered regularly interspaced short palindromic repeats
CRM	Circumferential resection margin
CRUK	Cancer Research United Kingdom
CS	Cowden wyndrome
CT	Computerised tomography
CTC	Computerised tomography colonography
CYP3A	Cytochrome P450 3A
DACH	1,2-diaminocyclohexane
DCC	Deleted in colon cancer
DHFU	Dihydrofluorouracil
DILI	Drug induced liver injury
DLIT	Diffuse light imaging tomography
DMEM	Dulbecco's modified Eagle's medium
DMH	1,2-dimethylhydrazine

DMSO	Dimethyl sulfoxide
DNA	Deoxyribonucleic acid
DPD	Dihydropyrimidine dehydrogenase
DSS	Dextran sodium sulfate
EDTA	Ethylenediaminetetraacetic acid
EGFR	Endothelial growth factor receptor
EMEM	Eagle's minimum essential medium
EMR	Endoscopic mucosal resection
ERK2	Extracellular signal regulated kinase 2
ESD	Endoscopic submucosal dissection
Fabp	Fatty acid-binding protein
FACS	Fluorescence-activated cell sorting
FAP	Familial adenomatous polyposis
FDR	False discovery rate
FdUDP	Fluorodeoxyuridine diphosphate
FdUMP	Fluorodeoxyuridine monophosphate
FdUTP	Fluorodeoxyuridine triphosphate
FFPE	Formalin-fixed and paraffin-embedded
FI	Fluorescence imaging
FIT	Faecal immunochemical test
FOB	Faecal occult blood
FOLFIRI	5-FU, irinotecan and leucovorin
FOLFIRINOX	5-FU, oxaliplatin, irinotecan and leucovorin
FOLFOX	5-FU, oxaliplatin and leucovorin
FS	Flexible sigmoidoscopy
FUDP	Fluorouridine diphosphate
FUDR	Fluorodeoxyuridine
FUMP	Fluorouridine monophosphate
FUR	Fluorouridine
FUTP	Fluorouridine triphohate
FXR	Farnesoid X receptor
g	Gram
GA	General anaesthesia
GEMMS	Genetically engineered mouse models
gFOBT	Guaiac-based FOB Test
GST	Glutathione S-transferase
H&E	Haematoxylin and eosin
HCAs	Heterocyclic amines
HNPCC	Hereditary non-polyposis colorectal cancer
HO-1	Hemeoxygenase-1
HRT	Hormone replacement therapy
IBD	Inflammatory bowel disease
IC50	Half maximal inhibitory concentration

IHC	Immunounhistochemistry
ip	Intra-peritoneal
IPA	Isopropanol
IQ	2-amino-33-methylimidazo[4,5-f]quinoline
iTRAQ	Isobaric tagging for relative and absolute quantification
IV	Intravenous
JPS	Juvenile polyposis syndrome
Keap1	Kelch-like ECH-associated protein 1
LB	Luria Bertani broth
LC-MS	Liquid chromatography–mass spectrometry
LCCRT	Long-course neoadjuvant chemoradiotherapy
LITT	Laser induced thermotherapy
LOH	Loss of Heterozygosity
LS	Lynch Syndrome
M	Molar
MAM	Methylazoxymethanol
MAP	*MUTYH*-associated polyposis
MAPK	Mitogen-activated protein kinase
mCRC	Metastatic colorectal cancer
min	Minutes
MMR	Mis-match repair
MMTS	Methylmethanethiosulfate
MNNG	N-Methyl-N-nitro-N-nitrosoguanidine
MNU	N-methyl-N-nitrosourea
MRI	Magnetic iesonance imaging
mRNA	Messenger RNA
MS	Mass spectrometry
MSI	Microsatellite instability
MSI-H	Microsatellite instability High
MSI-L	Microsatellite instability Low
MSS	Microsatellite stable
MWA	Microwave ablation
NICE	National Institute for Health and Care Excellence
nM	Nanomolar
NQO1	NAD[P]H:quinone oxidoreductase-1
Nrf2	Nuclear factor-erythroid 2-related factor 2
OPRT	Orotate phosphoribosyltransferase
p	Pico
PAT	Photoacoustic tomography
PBS	Phosphate buffered saline
PCR	Polymerase chain reaction
PDX	Patient derived xenograft
PET	Positron emission tomography

PET-CT	Positron emission tomography-CT
PHiP	2-amino-1-methyl-6-phenylimidazo[4,5-b]pyridine
PJS	Peutz–Jeghers syndrome
PRPP	Phosphoribosyl pyrophosphate
qPCR	Quantitative polymerase chain reaction
RFA	Radiofrequency ablation
RLU	Relative luminescent units
ROI	Region of interest
ROS	Reactive oxygen species
rpm	Revolutions per minute
RPMI	Roswell Park Memorial Institute
RR	Relative risk
rr	Ribonucleotide reductase
s	Seconds
sc	Subcutaneous
SCID	Severe combined immune deficiency
SCPRT	Short-course pre-operative radiotherapy
SD	Standard deviation
SDS	sodium dodecyl sulphate
siRNA	Small-interfering RNA
SN-38	7-ethyl-10-hydroxycamptothecin
SPECT	Single photon emission computed tomography
SPS	Serrated (hyperplastic) polyposis syndrome
TAMIS	Transanal minimally invasive surgery
TCEP	Tris (2-carboxyethyl) phosphine hydrochloride
TE	Transanal excision
TEMS	Transanal endoscopic microsurgery
TFA	Trifluoroacetic acid
TK	Thymidine kinase
TLDA	TaqMan low density array cards
TMA	Tissue microarray
TME	Total mesorectal excision
TNM	Tumour, node and metastases
TS	Thymidylate synthase
u	Micro
UGT	UDP-glucuronosyltransferases
UICC/AJCC	Union for International Cancer Control/American Joint Committee for Cancer
UK	United Kingdom
UK	Uridine kinase
UP	Uridine phosphorylase
USA	United States of America
v/v	Volume/volume
VEGF	Vascular endothelial growth factor

List of Tables

	density array card.	
4.2	Microfluidic TaqMan low density array card layout. Eight samples were run on each plate. Each loading well corresponds to two adjacent rows of the plate. The gene names for each gene code are detailed in table 4.1.	210
4.3	The 137 proteins significantly upregulated in the livers of BALB/c mice following chronic dosing with brusatol in comparison to the vehicle treated controls. All values are expressed relative to the common pooled sample included in duplicate on the iTRAQ run. An unpaired t-test was utilised to compare between treatment groups. Proteins are listed according to their expression in brusatol-treated mice relative to control animals in ascending order of the fold-change value. (Acc. = accession, Avg. = average, C = control, Bru = brusatol).	219
4.4	The 125 proteins with significantly lower expression in the livers of BALB/c mice following chronic dosing with brusatol in comparison to the vehicle-treated controls. All values are expressed relative to a common pooled sample included in duplicate on the iTRAQ run. An unpaired t-test was utilised to compare between treatment groups. Proteins are listed according to their expression in brusatol-treated mice relative to control animals in ascending order of the fold-change value. (Acc. = accession, Avg. = average, C = control, Bru = brusatol).	224
4.5	Pathway analysis for proteins both upregulated and downregulated in the in the livers of BALB/c mice following chronic dosing with brusatol. The ratio identifies the number of focus molecules identified (numerator) in the pathway (denominator).	226

List of Figures

2.7	a) Light microscopy images of HCT116 cells in culture at varying magnifications (x100-x200) taken before the application of 1000µg/ml G418 and 2 and 7 days after dosing in treated cells. The increasing confluence of untreated control cells is also displayed for comparison. Despite significant cell death, some viable cells were visible in the treated cells by 7 days, appearing brighter and with a more normal morphology than the surrounding necrotic cells. These data were represented graphically, displayed as mean +/- SD, after a 7-day incubation with G418 using both b) the total viable cell count /ml and c) the percentage of the total cells counted that were viable for each concentration. (N=3 in duplicate)	128
2.8	Cytotoxicity dose-response curves, displayed as mean + SD, after a 7-day incubation with Zeocin were performed in a) CT26 and b) HCT116 cells using the MTS assay. Results are expressed as a percentage of untreated control cells left to proliferate for 7 days. There were no viable cells detectable at 7 days with 400µg/ml of zeocin in both cell lines. (N=3 in triplicate, graphs display mean +/- SD)	129
2.9	a) Transfection in 40µl/ml of Lipofectamine® 2000 resulted in the highest luminescent signal at 48 hours, as measured by the Varioskan™ using the Bright-Glo™ Assay, in CT26 cells when normalised to the protein content of the well. b) The luminescent signal decreased proportionally with the dilution of the 1:1 cell suspension. (RLU = relative luminescent units)	130
2.10	Varioskan™ assessment of luminescence in HCT116 cells 48 hours after transfection with the pSELECT-zeo-LucSh vector. Transfection in 20µl/ml of Lipofectamine® 2000 resulted in the highest luminescent signal with this population of cells continued in culture. Luminescent signal reflected the number of cells plated, with a halving of signal for every 1 in 2 serial dilution. (Performed in triplicate with graph displaying mean +/- SD)	131
2.11	a) IVIS® imaging demonstrated luminescent signal in only one (CT26lucA6) of the 13 clones represented by the image in b) (performed in duplicate). c) This was confirmed using Varioskan™ assessment at two cell concentrations (performed in triplicate). d) Luminescent signal was compared between clones and the CT26luc population transfected with the pGL4.51 vector using the Varioskan™ and VivoGlo™ luciferin. The CT26lucA2 clone (transfected with pSELECT-zeo-LucSh) was 10-fold more luminescent than the CT26lucA6 (performed in triplicate). (Graphs display mean +/- SD, s = seconds)	132
2.12	Varioskan™ assessment with VivoGlo™ luciferin demonstrated luminescence in 15 of the 17 clones, with the HCT116lucB4 clone the most luminescent of these. (Performed in triplicate, graph displays mean + SD).	133
2.13	Kinetic imaging assessment of luminescence in CT26lucA6 cells using IVIS® imaging after the application of in VivoGlo™ firefly Luciferin. This curve was generated to guide the timing of imaging after the application of luciferin in subsequent experiments. (N =3 in triplicate with graph displaying mean +/- SD, min = minutes)	134

2.14	A positive correlation was noted between luminescence and the live cell count / well in a) and b) CT26lucA6 cells (r2 = 0.98, p<0.0001, Pearson R) and c) and d) HCT116lucB4 cells (r2 = 0.99, p<0.0001, Pearson R). (N=3, performed in triplicate, graphs display mean +/- SD)	135
2.15	Graphs display the minimal differences in luminescent signal in the a) CT26lucA6c and b) HCT116lucB4 clonal cell lines at increasing time-points following clonal selection.	136
2.16	Representative kinetic imaging curves from two individual BALB/c mice 14 days after the flank injection of CT26lucA6 cells, displaying total flux from their tumours against time after the injection of luciferin.	137
2.17	a) Representative images of 3 BALB/c immune-competent mice serially imaged in the IVIS® after the sc injection of CT26A6 cells. b) Luminescence signal increased throughout the study period in a relatively exponential manner, as displayed for individual mice in a graph of time versus luminescence. c) When data were combined the standard error in the mean (SEM) was relatively wide, reflecting the variable growth rates and therefore luminescent signal in mice. (N=6, Graph displays mean +/- SEM)	138
2.18	Initial pilot study involving orthotopic implantation of the CT26lucA2 cell line into 4 BALB/c mice. a) Representative images acquired using the IVIS® demonstrate a decrease in luminescent signal from day 13. b) This occurred in all mice with detectable signal at the initial imaging point, as demonstrated graphically by plotting total flux against time for each individual mouse.	140
2.19	Findings were similar in the 2nd group of 9 BALB/c mice following caecal injection of the CT26lucA2 clone, with a fall in luminescent signal, as demonstrated in a) representative images and b) graphically for each individual mouse, noted from day 7 onwards. The inclusion of a flank grafted mouse in this group allowed visual confirmation of tumour regression.	141
2.20	a) Photographic image of a tiny tumour nodule (long arrow) in the caecum of a BALB/c mouse, taken 23 days after the orthotopic injection of the CT26lucA2 cell line. b) Light microscopy (x400) confirmed a poorly differentiated adenocarcinoma but with a c) dense T-cell (solid triangles) infiltrate when stained for the CD3 antigen.	142
2.21	a) Representative IVIS® images from the first attempt at caecal implantation using the CT26lucA6c clone. Imaging was consistent with development of a primary tumour in the left iliac fossa of the mouse, with ectopic signal developing on day 17 in the right upper quadrant, consistent with the development of a liver metasatsis. b) Results were combined as fold change in luminescence for graphical display, confirming an increase in luminescence throughout the study period. (N=5, Graph displays mean +/-SEM)	143
2.22	3D spectral un-mixing imaging can be useful for estimating the depth of luminescent signal within the mouse, suggesting luminescent signal arising from within the liver. Ex-vivo assessment confirmed the presence of a liver metastasis, with signal present in both the caecum and liver on IVIS® imaging.	144

3.14	Assessment of reproductive integrity following exposure to brusatol confirmed inhibition of colony formation, represented graphically by calculation of surviving fractions expressed as a percentage of untreated cells, and as representative images of wells, in a) CT26 and b) HCT116 cells. (N=5 in triplicate, graphs display mean +/-SD, * C= 0.5% DMSO vehicle control)	180
3.15	Graphs display the effect of siRNA modulation of Nrf2 on cell lines dosed with irinotecan as measured by the MTS assay. siRNA inhibition of Nrf2 significantly increased the cytotoxicity of irinotecan in a) CT26 and c) HCT116 cells as reflected by the decreased IC50 values when compared with treatment with irinotecan alone, displayed in tables b) for CT26 cells and d) for HCT116 cells (extra sum-of-squares F test). The cytoprotective effect of overexpression of Nrf2 by Keap1 inhibition was non-significant in the CT26 but reached significance in the HCT116 cell line. (IR = irinotecan, siRNA cont = siRNA control, N=3 in triplicate, graphs display mean +/-SD, NS = non-significant, NA = not applicable)	181
3.16	Graphs display the effect of pharmacological modulation of Nrf2 with brusatol and CDDO-me in combination with irinotecan dosing of cell lines using the MTS assay. The same trends were noted as observed with siRNA in both the a) CT26 and b) HCT116 cell lines. Tables c) and d) demonstrate the change in the irinotecan IC50 values with the pharmacological modulation of Nrf2 in the CT26 and HCT116 cell lines respectively (extra sum-of-squares F test). (IR = irinotecan, N=3 in triplicate, graphs display mean +/-SD, NS = non-significant, NA = not applicable)	182
3.17	Heat map tables displaying calculated combination indexes for treatment with varying concentrations of irinotecan and brusatol. These confirm drug synergy in a) CT26 and b) HCT116 cells across a range of concentrations. Red, yellow and orange signify decreasing degrees of synergy, with cells highlighted in green demonstrating an antagonistic effect. (Synergy assumed at CI<1)	183
3.18	Graphs display the effect of siRNA modulation of Nrf2 on cell lines dosed with 5-FU as measured by the MTS assay. siRNA inhibition of Nrf2 significantly increased the cytotoxicity of 5-FU in a) CT26 and c) HCT116 cells, as reflected by the decrease IC50 values, when compared with treatment with 5-FU alone as displayed in tables b) for CT26 cells and d) for HCT116 cells (extra sum-of-squares F test). The cytoprotective effect of overexpression of Nrf2 by Keap1 inhibition meant IC50 values could not be calculated. (siRNA cont = siRNA control, N=3 in triplicate, graphs display mean +/-SD)	184
3.19	Graphs display the effect of pharmacological modulation of Nrf2 with brusatol and CDDO-me in combination with 5-FU dosing of cell lines using the MTS assay. The same trends were noted as observed with irinotecan in both the a) CT26 and b) HCT116 cell lines, although to a lesser extent. Tables c) and d) demonstrate the change in the 5-FU IC50 values with the pharmacological modulation of Nrf2 in the CT26 and HCT116 cell lines respectively (extra sum-of-squares F test). (N=3 in triplicate, graphs display mean +/-SD, NS = non-significant, NA = not applicable)	185

Chapter 1 - General Introduction and literature review

1.1 Epidemiology of Colorectal Cancer

According to the 2011 data set published by Cancer Research United Kingdom (UK), colorectal cancer (CRC) is the fourth most common carcinoma and the second leading cause of cancer related death in the UK. CRC makes up 12.4% of the total cancer burden in the UK and the incidence continues to increase, rising by 6% over the last ten years. There were approximately 41 600 new cases of CRC diagnosed in the UK in 2011 with a slight preponderance for the disease in men. The lifetime risk of CRC is 5% in the general population and increases with age; 95% of cases occur in those over the age of 50. (http://www.cancerresearchuk.org/cancer-info/cancerstats/types/bowel/)

Duke's Stage	TNM Stage	Frequency	5-year survival
A	T1-2, N0,M0	8.70%	80-95%
B	T3, N0, M0	24.20%	72-75%
	T4, N0, M0		65-66%
C1	T1-2, N1, M0	23.60%	55-60%
	T3-4, N1, M0		35-42%
C2	Any T, N2, M0		25-27%
D	M1	9.20%	0-7%
Unknown		34.30%	35.40%

Table 1.1 - Percentage of cases and 5 year survival by Dukes' and TMN (Tumour, Node and Metastases) stage at diagnosis for colorectal cancer patients [1, 2].

The best predictor of prognosis remains radiological and histopathological staging (Table 1.1), and whilst survival across all stages of CRC continues to improve, with 57% of patients alive at five years, outcomes for those presenting with metastatic disease remain poor (7% five-year survival). Metastatic disease may be confined to the lymphatic nodal tissue which follows the arterial blood supply of the tumour or to the liver through haematological spread via the portal venous system. Approximately 25% of CRC patients present with metastases while an additional 25–35% will develop them during the course of their disease. Metastatic disease is confined to the liver alone in 20-30% of patients at presentation and 50% of recurrent disease following resection occurs in the liver [3]. Spread may also be transcoelomic to the omentum or peritoneal cavity and metastatic to the lungs.

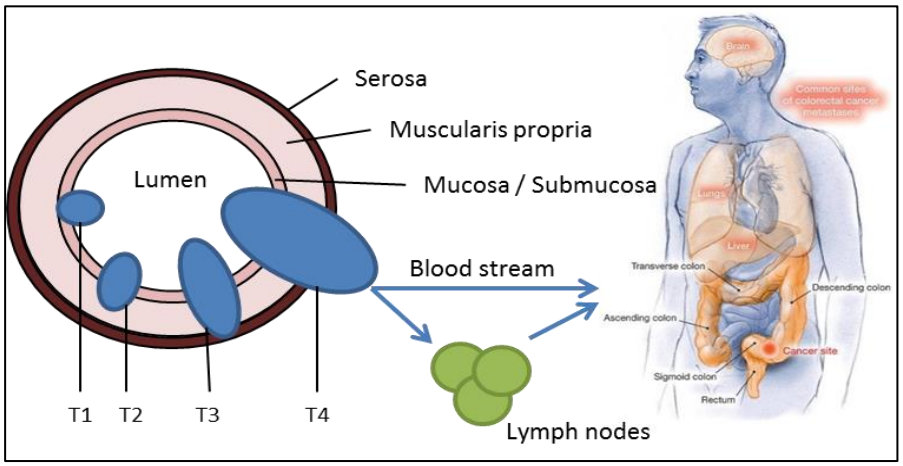

Figure 1.1 – Local staging of colorectal cancer by T (local tumour stage) stage with common sites of metastases

Surgical resection remains the cornerstone of curative treatment but is not always possible or advantageous in those with advanced disease, whose only therapeutic options are chemo- or radiotherapy. Others will benefit from adjuvant or neoadjuvant chemo- or radiotherapy in conjunction with oncological resection. Advances in chemotherapy have increased survival, reduced recurrence rates and prolonged life in advanced disease but more can be accomplished through the utilisation of improved or novel therapies. Achieving this will require a greater understanding of the pathogenesis of CRC and the pharmacology of chemotherapeutic and biological treatment agents on an individual patient basis. The ultimate aim is the personalisation of treatment for all CRC patients based on the genetic and biological characteristics of their tumour, and the enhancement of chemotherapy through the manipulation of novel targets to improve tumour response, whilst minimising side effect profiles.

1.2 Aetiology of Colorectal Cancer

The aetiological factors and patho-genetic mechanisms underlying CRC development are complex and heterogeneous. Contributory agents and mechanisms in CRC include lifestyle factors in addition to inherited and genetic mutations. Many factors have been examined for their influence on the development of sporadic CRC and, although knowledge of molecular genetics has increased in recent years, the stimuli that lead to malignant change remain obscure.

1.2.1 Diet

Numerous dietary factors have been linked with the development of or protection against CRC. There is good evidence that eating red and processed meat increases CRC risk as assessed in four separate meta-analyses. These reported a 17-30% increase in the risk of CRC with ingestion 100-120g of red meat per day and a 9-50% increase on consuming 25-50g of processed meat per day [4-7]. High quality level 4 evidence suggests that a diet high in fibre reduces the risk of developing CRC. Meta-analysis of 25 prospective studies involving over 2 million participants revealed that CRC risk was reduced by 10% for every 10g of total dietary fibre ingested per day [8]. Evidence consistently reports that garlic and milk have a protective effect against CRC, while limited inconsistent evidence suggests vegetable and fruit consumption may offer some risk reduction, although this may be due to the fibre content [9-11]. It is possible that eating cheese [10] and sugary foods [12, 13] may increase risk, but evidence is inconsistent and no definite conclusions can be drawn. Other possible dietary influences on CRC pathogenesis include calcium, vitamin D [14, 15], folate [16-19], vitamin B6 [20] and vitamin B12 [21, 22] but published data reveal conflicting outcomes between studies.

1.3.2 Alcohol

Evidence consistently demonstrates that alcohol intake increases CRC risk, even at relatively moderate levels of consumption. In 2011 a systematic review reported relative risks (RR) were 1.21 for moderate (2-3 drinks/day) and 1.52 for heavy (≥4 drinks/day) alcohol drinkers when compared with light drinkers (≤1 drink/day). Dose-response analysis revealed a 7% increase in risk for every 10g per day of alcohol consumed [23]. The association between an increased risk of CRC and alcohol have been confirmed by two other meta-analyses conducted in 2007 [24] and 2011 [25].

1.3.3 Smoking

Three meta-analyses explored the effect of having been a smoker on bowel cancer risk, finding smokers were significantly more likely to develop CRC than those who have never smoked [26-28]. Laing *et al.* included 36 studies, involving over 3 million participants, in their 2009 review. Separate analyses were performed for smoking status, daily cigarette consumption, duration, pack-years and age of initiation. Compared with those who had never smoked, current smokers had a 17% higher chance of developing CRC while in former smokers the RR for CRC incidence was 1.25 [26].

1.3.4 Obesity

Studies consistently report an association between CRC risk and increasing Body Mass Index (BMI). Meta-analysis of 56 case-control and cohort studies involving 93 812 individuals with CRC examined this relationship. Compared with those whose BMI was less than 23.0 kg/m^2, the increased risk of colorectal cancer was 14% for individuals with a BMI of 23.0 to 24.9 kg/m^2, 19% for a BMI of 25.0 to 27.4 kg/m^2, 24% for a BMI of 27.5 to 29.9 kg/m^2 and 41% for a BMI of 30.0 kg/m^2 or more. The association was stronger for men than women and for the colon than the rectum [29]. In a separate meta-analysis of prospective studies colon cancer risk increased by 33% and 16% for men and women respectively per 10-cm increment in waist circumference [30].

1.3.5 Physical activity

Three meta-analyses report that physically active individuals have a lower risk of colon cancer. The association between physical activity levels and rectal cancer risk is less well defined with one of these studies reporting a non-significant 6% reduction in risk [31], the second no reduction in risk [32] and the third only focusing on colon cancer [33]. These studies report that the most active men and women can reduce their risk of colon cancer by up to 28% and 32% respectively in comparison to the least active. These analyses suffer from a lack of consistency in defining activity levels in individuals between studies. Examined outcomes varied significantly with some studies focusing on the duration of activity with no assessment of intensity.

1.3.6 Medication

Aspirin taken for several years at doses of at least 75 mg daily reduced long-term incidence and mortality due to colorectal cancer in a review of four randomised control trials. These trials were conducted to assess the benefit of aspirin in reducing thromboembolic events but it was noted that allocation to daily aspirin reduced the 20-year risk of colon cancer significantly (incidence hazard ratio 0·76, p=0.02). This effect was more pronounced for proximal than distal tumours and there was no significant reduction in the risk of rectal cancer. There was no increase in benefit as the dose of aspirin was increased from 75 mg daily [34]. Aspirin may be considered in patients deemed to be a high risk of colon cancer based on family history or previous polyp disease.

Preclinical studies have suggested that statins may protect against CRC by inducing apoptosis, an upregulation of pro-apoptotic proteins and inhibiting tumour angiogenesis. No definitive conclusions can be drawn from meta-analysis of clinical data. These report a modest trend towards reduced CRC risk (RR 0.94, p=0.23) with statin therapy [35]. Current evidence is too inconsistent to recommend the routine use of statins in preventing CRC.

Two meta-analyses from the late 1990s reported a reduction in the incidence of CRC in women who had or were taking hormone replacement therapy (HRT). The more recent of these examined 18 epidemiologic studies of postmenopausal hormone therapy and colorectal cancer. They found a 20% reduction (RR = 0.80) in colon cancer risk and a 19% decrease (RR = 0.81) in the risk of rectal cancer for postmenopausal women who had ever taken hormone therapy [36]. More recent studies report mixed findings. Oestrogen-only HRT was found to have no effect on bowel cancer risk in a randomised trial [37], but a significant risk-reducing effect in a large nested case-control study [38]. Combined HRT did not affect CRC risk in the two large cohort studies [39, 40] and did not reduce colon cancer risk significantly in a randomised trial of women with pre-existing cardiovascular disease [41]. This contrasts findings from a randomised control trial demonstrating a significant 44% decrease in the risk of CRC with hormonal therapy versus placebo [42]. The evidence is not consistently in favour of supplementation with HRT to reduce CRC risk, especially given the well-publicised side-effects associated with hormonal therapy.

1.3.7 Inflammatory bowel disease

Inflammatory bowel disease (IBD) is associated with an increased risk of developing CRC. A 2001 meta-analysis reported cumulative probabilities of 2% by 10 years, 8% by 20 years, and 18% by 30 years in patients with ulcerative colitis [43]. More recent data publish a cumulative risk of CRC in patients with ulcerative or Crohn's colitis of 1%, 2%, and 5% after 10, 20, and >20 years of disease duration, respectively [44]. This decreased risk may reflect improving treatments of IBD reducing the incidence of CRC, in combination with improved surveillance identifying those at high risk of malignancy due to polyps or dysplasia and selection to resection.

The sheer number of causative factors associated with CRC is indicative of the complex genetic alterations associated with its development. Knowledge of these continues to improve through gene sequencing and bioinformatics, leading to a better understanding of potential therapeutic targets.

1.3 Genetics of Colorectal Cancer

The development of a colorectal malignancy was believed to follow a series of genetic mutations in oncogenes and tumour suppressor genes from benign polyp to invasive cancer (figure 1.2) [45]. The genes responsible for the various stages were identified as Adenomatous Polyposis Coli (*APC*), *KRAS* and *TP53* and the process labelled the adenoma-carcinoma sequence. Since this model was proposed, understanding of the molecular pathogenesis of CRC has advanced considerably. Sequencing of CRC genomes has revealed numerous mutations in the average colon cancer, determining which of these mutations have a pathogenic role is challenging. Analysis of approximately 13,000 genes revealed mutations in the coding sequences of approximately 67 of these [46], while recent genome sequencing highlighted twenty-four genes that were commonly mutated in CRC. As expected, mutations commonly occurred in *APC, TP53, SMAD4, PIK3CA* and *KRAS* but there were also frequent mutations in *ARID1A, SOX9* and *FAM123B* [47].

It is now appreciated that there are multiple molecular pathways associated with the development of CRC and it is possible separate CRC into three phenotypical groups based on their genetic profile; tumours with microsatellite instability (MSI), those that are microsatellite stable but have chromosomal instability (CIN) and those with CpG island methylator phenotype (CIMP).

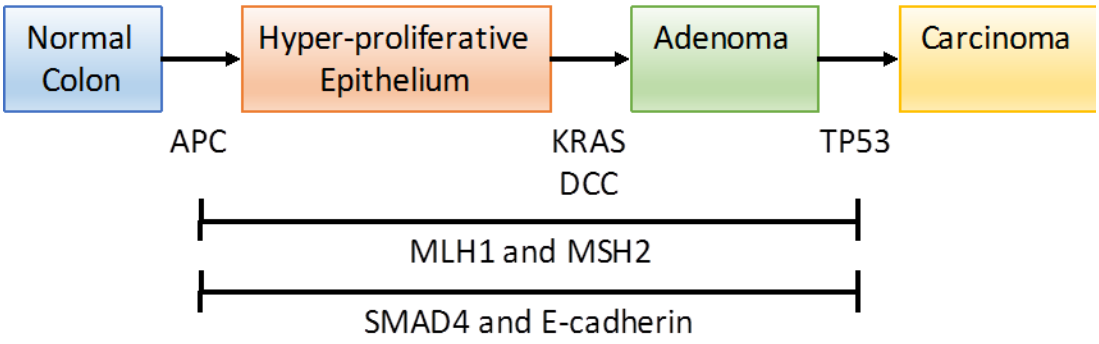

Figure 1.2 – The adenoma-carcinoma sequence; from normal colonic epithelium through adenoma to carcinoma. The increasing loss of cellular differentiation and capacity to metastasise correspond to the accumulation of genetic mutations as originally described by Vogelstein.

1.3.1 Microsatellite instability

MSI is identified by the presence of frequent insertion and deletion mutations in short tandem repeats of nucleotide sequences that are 1-6 base pairs long and known as microsatellites. These make up 3% of Deoxyribonucleic acid (DNA) and are found throughout the genome. Microsatellites are prone to errors in replication that, if missed by DNA polymerase, are corrected by the mismatch repair (MMR) system in normal cellular function. As microsatellite sequences are present in the coding regions of genes that regulate cell growth and apoptosis, defective MMR can result in frameshift mutations that create an environment promoting cell survival and carcinogenesis. Inactivation of the MMR system may be due to epigenetic mechanisms or mutations that alter the function of the MMR genes, for example *MLH1, MSH2, MSH6* and *PMS2* [48].

In 1998 the National Cancer Institute recommended the testing of five microsatellite biomarkers by polymerase chain reaction (PCR) and immunohistochemistry (IHC) for determination of MSI status; these markers include BAT-25, BAT-26, D2S123, D5S346 and D17S250 [49]. Two or more positive markers demonstrate instability and define the tumour as microsatellite high (MSI-H). Although this is often adequate for determining MSI-H tumours it may not select between microsatellite low (MSI-L) and microsatellite stable (MSS) tumours. A large number of markers may be required to make this distinction with MSI-H tumours defined as having instability in ≥30% of the markers tested; MSI-L defined as the presences of instability in 10%–29% of markers, and MSS defined as no unstable markers [48].

MSI tumours account for approximately 15%−20% of sporadic CRCs and have specific clinical and histopathological features [50, 51]. These tumours tend to be proximal to the splenic flexure, have a high histological grade, a mucinous histology with prominent numbers of tumour-infiltrating lymphocytes and display a Crohn's like inflammatory response. They are associated with an improved prognosis despite studies suggesting a lack of efficacy with 5-fluorouracil (5-FU) based chemotherapy [52].

1.3.2 Chromosomal instability

CIN refers to accelerated rates of gain or loss of whole or large portions of chromosomes and fits more with the traditional view of the adenoma-carcinoma sequence [45]. The genomic changes associated with the CIN pathway include activation of *KRAS*, inactivation

of *APC*, loss of *TP53* and loss of heterozygosity at chromosome 18q, which contains the tumour suppressor genes *SMAD2*, *SMAD4* and deleted in colon cancer (*DCC*). These mutations were believed to occur in a stepwise fashion as the tumour progressed from adenoma to carcinoma. This model continues to be refined as evidence emerges on the complexity and number of mutations associated with the development of CRC. However, it did establish the key principle that multiple genetic hits were required for the progression to CRC. Genome-wide sequencing has demonstrated up to 80 mutated genes per CRC but a smaller group of mutations (less than 15) were considered to be drivers of tumourigenesis [53]. The consequence of CIN is aneuploidy, genomic amplifications and loss of heterozygosity leading to the activation of pathways initiating the development and progression of CRC. (Table 1.2)

CIN is observed in 65%–70% of sporadic colorectal cancers with tumours occurring predominantly in the descending colon and rectum. It is accepted that most MSS tumours follow the CIN mechanism of tumourigenesis, but the MSI and CIN phenotypes are not mutually exclusive with up to 25% of MSI colorectal cancers exhibiting chromosomal abnormalities [54]. Data indicate that the CIN phenotype is associated with less favourable outcomes in patients in comparison to those with tumours that exhibit MSI [53, 55].

Gene	Chromosomal location	Prevalence of mutations	Function of gene product
Oncogenes			
KRAS	12p12	~ 30–50%	Cell proliferation, survival, and transformation
CTNNB1	3p22	~ 4–15% (~ 50%*)	Regulation of Wnt pathway target genes that promote tumour growth and invasion
PIK3CA	3q26	~20%	Cell proliferation and survival
Tumour suppressor genes			
APC	5q21	~ 30–70%	Inhibition of Wingless/Wnt signalling; cytoskeletal regulation
TP53	17p13	~ 40–50%	Cell cycle arrest, apoptosis induction
SMAD4, SMAD2	18q21	~ 10–20%	Intracellular mediators of the TGF-β pathway
DCC	18q21	~ 6%	Cell surface receptor for netrin-1

Table 1.2 - Overall Prevalence of common genetic mutations in CIN-positive CRCs as adapted from Pino and Chung, 2014 [53]. *Identified in 50% of tumours without APC mutations.

1.3.3 CpG island methylator phenotype

CIMP is a subset of CRCs that occur through an epigenetic instability pathway characterised by hypermethylation of promoter CpG island sites [56]. Methylation refers to the enzymatic addition of a methyl group to cytosine by DNA methyltransferases. CpG (cytosine preceding guanine) islands are regions within the genome where the percentage of the CpG dinucleotides is higher than expected. CpG islands overlap the promoter region of 60–70% of genes and tend to be protected from methylation. However, they can become abnormally methylated in cancer resulting in epigenetic silencing of several tumour suppressor genes. The mechanisms involved in aberrant methylation are unclear but could include overexpression, hyper-activation or misdirection of enzymes, such as DNMT1, DNTM3a, and DNMT3b, that mediate DNA methylation or impairment of the control elements that normally prevent DNA methylation [56]. Hundreds to thousands of genes can be aberrantly methylated in the average CRC and only subsets of these are likely to be important in its pathogenesis. (Table 1.3)

Meta-analysis of 19 studies suggested CIMP tumours to be independently associated with a worse overall survival but highlighted the inconsistent definitions of CIMP positivity employed. However, unlike the MSI phenotype tumours, CIMP tumours do not seem to be associated with a poor response to 5-FU based adjuvant therapy [57, 58].

Gene	Protein	Effect of loss of function
APC	Adenomatous polyposis coli	Increased Wnt/β-catenin signalling
MLH1	MutL homolog 1	Microsatellite instability
MGMT	O-6-methylguanine-DNA methyltransferase	Increased G>A mutation frequency
RASSF1A	Ras association domain family 1 (isoform A)	Increased RAS/RAF/MAP kinase signalling, death-receptor-dependent
SLC5A8	Sodium solute symporter family 5 member 8	Not known
RUNX3	Runt-related transcription factor 3	Decreased TGF-β/BMP signalling
MINT1*	Methylated in tumour locus 1	Not applicable
MINT31*	Methylated in tumour locus 31	Not applicable
SFRP1	Secreted frizzled-related protein 1	Increased Wnt/β-catenin signalling
SFRP2	Secreted frizzled-related protein 2	Increased Wnt/β-catenin signalling
CDH1	E-cadherin	Loss of cell adhesion, possible increased Wnt/β-catenin signalling
CDH13	Cadherin 13	Increased PI3K/Akt/mTOR signalling, MAPK signalling
CRABP1	Retinol-binding protein 1	Not known
CDKN2A/p16	Cyclin-dependent kinase inhibitor 2A	Increased cell proliferation
HLTF	Helicase-like transcription factor	Impaired DNA repair
CDKN2A (P14,ARF)	p14(ARF)	Decreased p53 stabilization and activation
ESR1	Oestrogen receptor 1	Loss of oestrogen receptor signalling
TIMP3	Tissue inhibitor of metalloproteinase 3	Increased EGFR signalling, TNF signalling
CXCL12	Chemokine (CXC motif) ligand 12	Increased tumour cell metastases
ID4	Inhibitor of DNA binding 4	Not known
IRF8	Interferon regulatory factor 8	Interferon signalling
THBS1/TSP1	Thrombospondin 1	Decreased TGF-β1 signalling
DAPK	Death associated protein kinase	Interferon gamma signalling, TNF alpha signalling, Fas/APO1 signalling
VIM	Vimentin	No known biological effect
SEPTIN 9	Septin 9	Impaired cytokinesis and loss of cell cycle control

Table 1.3 – Genes commonly hypermethylated and silenced in CRC as adapted from Lal and Grady, 2011 [56]. * MINTs are 'methylated in tumour' loci and not specific genes.

1.3.4 Adenomatous polyposis coli (APC)

Many of the gene mutations now known to be associated with the development of CRC were originally identified and described in the adenoma-carcinoma sequence as described by Volgestein [45]. The *APC* tumour suppressor gene encodes for a protein known to regulate cell-adhesion, migration, apoptosis and proliferation; halting the progression from G1 to S phase of the cell cycle. The defect is present in 30-70% of CRCs and is widely believed to be an early step in sporadic carcinogenesis due to its reported presence across the adenoma-carcinoma sequence [59]. The majority (95%) of *APC* mutations are either frameshift or nonsense leading to the synthesis of a truncated protein [60]. The downstream effect of *APC* mutations is disruption of the WNT pathway. APC targets β-catenin for proteasomal degradation and therefore mutation results in the nuclear accumulation of β-catenin, increased WNT activity and cellular proliferation. The end product of this over-proliferation is the overgrowth of colonic epithelial cells, resulting in the formation of polyps. Malignant transformation of a polyp may then occur as further genetic mutations accumulate [61].

1.3.5 KRAS/BRAF

The RAS family (KRAS, HRAS and NRAS) are membrane bound guanine nucleotide binding proteins that predominantly act as molecular switches. *KRAS* is a proto-oncogene which, after activation by the endothelial growth factor (EGFR) receptor, triggers downstream signalling through the PI3K/AKT/MTOR and RAF/MEK/ERK pathways resulting in cellular proliferation and growth factor induced differentiation [62, 63]. *KRAS* is mutated in 30%-50% of CRCs with single nucleotide point mutations occurring in codons 12 and 13 of exon 2 and to a lesser extent in codon 61 of exon 3. These lock KRAS in the guanine-triphosphate bound activated form, leading to constitutive activation of RAS downstream signalling [53].

The RAF family (ARAF, BRAF and RAF1) were the first downstream effectors of RAS to be identified. BRAF exhibits a high propensity to MEK/ERK activation, explaining why only *BRAF* mutations have been associated with malignancy and not *ARAF* or *RAF1*. *BRAF* mutations have been reported in 10% of CRCs and are associated with a significantly higher proportion of MSI tumours [64, 65].

1.3.6 TP53 (p53)

TP53 is a tumour suppressor gene located on the short arm of chromosome 17. It induces arrest of the cell-cycle in the G1 phase and facilitates DNA repair prior to a cell committing to DNA replication; if DNA repair is unsuccessful p53 induces apoptosis [66]. Referred to as the 'guardian of the genome' p53 is implicated in a number of malignancies. *TP53* mutations occur as a late event in the transition from adenoma to carcinoma in CRC; they are present in 4% to 26% of adenomas and in 50 to 75% of CRCs [67, 68]. Most of *TP53* mutations are missense mutations occurring most frequently in codons 175, 248 and 273, leading to the synthesis of an inactive protein [69].

1.3.7 18Q loss of heterozygosity

Loss of heterozygosity (LOH) is defined as loss of one of the two alleles or copies of a gene and is frequently noted in chromosome 18Q in advanced CRC. The *DCC* gene is located on the long arm of chromosome 18 and was initially proposed to be a colorectal cancer tumour suppressor gene. This was debated when its product was found to be a cell surface receptor for the neuronal protein netrin-1, involved in axon guidance in the developing nervous system [70]. However, DCC also has a role in intracellular signalling, blocking cell growth in the absence of netrin-1 and mutations may promote cell survival and tumour development [71]. In normal conditions netrin-1 is produced deep in the crypts of the colorectal mucosa and as epithelial cells differentiate and migrate to the surface netrin-1 concentrations fall. This results in reduced activation of the DCC surface receptor and reduced cell survival and growth. However, mutation of the *DCC* gene results in failure of netrin-1 to bind to the transmembrane protein, causing abnormal cell survival [48]. Approximately 70 % of CRC show allelic losses in *DCC* with studies suggesting that loss of DCC expression occurs more frequently in the later clinical stages and higher pathological grades of CRC [72, 73].

The tumour suppressor gene SMAD4 is also located on chromosome 18Q and is an intracellular mediator of the transforming growth factor pathway; involved in the regulation of cell growth, differentiation and apoptosis. SMAD4 mutations have been found in 10% of CRCs with the frequency of mutation increasing with stage [74].

1.4 Familial Colorectal Cancer Syndromes

Although the majority of CRC are believed to be sporadic, estimates indicate that familial CRC, defined by the presence of two or more first-degree relatives affected with CRC, may account for 20% of cases [75]. CRC can be directly attributed to one of the well-characterised familial syndromes in 5-10% of cases, these include: Lynch syndrome (LS), familial adenomatous polyposis (FAP), attenuated familial adenomatous polyposis (AFAP), *MUTYH*-associated polyposis (MAP), Peutz–Jeghers syndrome (PJS), juvenile polyposis syndrome (JPS), Cowden syndrome (CS) and serrated (hyperplastic) polyposis syndrome (SPS) [76]. Each syndrome is associated with a specific phenotype that often include extra-colonic manifestations [77]. (Table 1.4)

1.4.1 Lynch Syndrome (LS)

LS is the most common of the inherited CRC syndromes, accounting for up to 3% of all colorectal cancers [78]. It is an autosomal-dominant condition defined by the presence of a germline mutations in MMR genes resulting in MSI-high tumours that tend to occur in the right side of the colon with the histological findings matching those discussed in section 1.3.1. Patients with LS typically develop colorectal and endometrial cancers in their 40s and are also at increased risk of developing adenocarcinomas of the stomach, small intestine, upper urinary tract, ovary, pancreatobiliary tract, brain and skin. Tumours are often synchronous or metachronous and 70% of patients with LS will develop CRC by the age of 70 [79].

The revised Bethesda guidance are helpful in determining when a patient is at increased risk of LS and state patients should have their tumour assessed for MSI if they fulfil any of the following conditions:

1. diagnosed with CRC under 50 years of age
2. present with synchronous or metachronous CRC or other LS-related tumours, regardless of age
3. diagnosed with a MSI-high CRC under 60 years of age
4. have one or more first-degree relatives with an LS-related cancer, with one of the cancers being diagnosed under 50 years of age
5. have two or more first- or second-degree relatives with LS-related cancer, regardless of age [76]

In 2015 the American College of Gastroenterology released comprehensive guidance stating that individuals at risk for or affected with LS should be screened for CRC by colonoscopy at least every two years, beginning between the ages of 20 and 25. These also state that colectomy with ileo-rectal anastomosis is the preferred treatment for LS patients diagnosed with a colon cancer or colonic neoplasia not controllable by endoscopy. Segmental colectomy is an option in patients unsuitable for total colectomy if regular postoperative surveillance is conducted [76].

1.4.2 Familial Adenomatous Polyposis (FAP)

FAP was the first hereditary CRC syndrome to be fully characterised. FAP is due to a germline mutation in the *APC* gene located on the long arm of chromosome 5 (5q21-22) and is inherited in an autosomal dominant fashion with a high penetrance. FAP is the defined by the presence of ≥100 synchronous colorectal adenomas. It carries a 100% lifetime risk of CRC, with most malignancies occurring before the age of 40 [80]. However, some germline mutations, particularly those at either the 5' or 3' ends of the gene, lead to a milder phenotype known as AFAP, defined by the presence of 10-100 adenomas that tend to be confined to the right-colon [77].

Individuals who have a personal history of more than 10 colorectal adenomas, a family history of one of the adenomatous polyposis syndromes or a history of adenomas and FAP-type extra-colonic manifestations (duodenal or ampullary adenomas, desmoid tumors, papillary thyroid cancer, congenital hypertrophy of the retinal pigment epithelium, epidermal cysts and osteomas) should undergo assessment for the adenomatous polyposis syndromes. Those found to be at risk for or affected should be screened annually for CRC by colonoscopy, beginning at puberty. The absolute indications for immediate colorectal surgery in FAP and AFAP include the presence of malignancy or significant symptoms. Relative indications for surgery include the presence of multiple adenomas greater than 6mm in size, a significant increase in adenoma number, the presence of an adenoma with high-grade dysplasia and/or inability to adequately survey the colon because of multiple polyps.

Pan-proctocolectomy with ileo-anal pouch formation or an end-ileostomy is often preferred for patients with FAP. Subtotal colectomy may be more appropriate in AFAP as polyp numbers are fewer and have a predilection to the right-colon. Postsurgical

surveillance should include yearly endoscopy of rectum or ileal pouch and examination of an ileostomy every two years [76].

1.4.3 MUTYH-associated polyposis (MAP)

First described in 2002, MAP is a recessively inherited syndrome due to bi-allelic *MUTYH* mutations. *MUTYH* is a base excision repair gene involved in DNA oxidative damage. Failure of base excision repair results in CG–AT transversions in multiple genes, including APC and KRAS [81]. Although MAP was believed to mimic AFAP, it is now known that MAP patients frequently develop serrated type polyps (hyperplastic polyps and sessile serrated lesions) in addition to classical adenomas [77]. MAP is most commonly found in patients presenting with 20 to 99 adenomas but patients may present with over a 1000 colonic polyps. Guidelines recommend the same screening, management and surveillance regimens as FAP or AFAP. Colectomy and ileo-rectal anastomosis is possible in those with relative rectal sparing [76].

1.4.4 Peutz–Jeghers syndrome (PJS)

PJS is an autosomal-dominantly inherited syndrome that includes histologically distinctive hamartomatous polyps of the gastrointestinal tract and characteristic mucocutaneous pigmentation. Most (94%) cases are associated with a germline mutation in the serine/threonine kinase 11 (*STK11*) gene on chromosome 19p [82]. Affected individuals have an increased risk of the colorectal, pancreatic, gastric, small intestine, oesophageal, breast, ovarian, endometrial and lung carcinomas [77].

The lifetime risk for CRC in PJS is estimated at 39% and any individual with perioral or buccal pigmentation and/or two or more histologically characteristic gastrointestinal hamartomatous polyps or a family history of PJS should be tested for *STK11* mutations. In affected individuals colonoscopic surveillance should begin at eight years old and, if polyps are present, repeated every three years. If no polyps are found, colonoscopy should be repeated at 18 years of age and then every three years or earlier if symptoms occur. Treatment involves endoscopic excision of polyps with colectomy sometimes necessary to control colonic especially if neoplastic change is identified [76].

1.4.5 Juvenile Polyposis Syndrome (JPS)

JPS occurs as a result of mutations of the *SMAD4* or *BMPR1A* genes and is inherited in an autosomal dominant fashion, although 25% of newly diagnosed cases represent a new mutation without a family history [76]. JPS is a pure intestinal polyposis syndrome without the extra-intestinal manifestations seen in many of the others. Patients develop characteristic polyps throughout the gastrointestinal (GI) tract, typically by the age of 20 years, with a reported cumulative lifetime risk for developing colorectal adenocarcinoma of 40–70%. The World Health Organization stated an individual with any of the following should be tested for JPS:

1. more than five juvenile polyps in the colon or rectum
2. juvenile polyps throughout the gastrointestinal tract
3. any number of juvenile polyps in a person with a family history of juvenile polyposis

Screening with colonoscopy should begin at 12 years old and continual annually if polyps are found and every three years in the absence of polyps. Indications for surgery are the same as the other polyposis syndromes [83].

1.4.6 Cowden's syndrome (CS)

CS is the most common variant of the PTEN-hamartoma tumour syndromes which are caused by germline mutations in the tumour suppressor phosphatase and tensin (*PTEN*) homologue, situated on chromosome 10q23. CS is inherited in an autosomal dominant fashion, although up to 30% of patients may have *de-novo* mutations [84]. Patients can develop hamartomas in multiple organ systems, with an increased risk of malignancy of the breast, thyroid, endometrium and kidney. Nearly 95% of patients develop a polyposis, which can include hyperplastic-, adenomatous-, hamartomatous-, ganglioneuromatous- and inflammatory-type polyps. Colonic involvement is typical resulting in an increased risk of CRC with prevalence of approximately 14% and a mean age of 47 at diagnosis [77].

Individuals with multiple gastrointestinal hamartomas or ganglioneuromas should be evaluated for CS by testing for mutations in *PTEN*. Screening with colonoscopy should continue annually from diagnosis [76].

1.4.7 Serrated (hyperplastic) Polyposis Syndrome (SPS)

The exact mode of inheritance of SPS remains unclear but 40 to 60% of affected individuals report a family history of CRC in first or second-degree relatives. Individuals develop serrated polyps which can include a mixture of hyperplastic polyps, sessile serrated lesions and traditional serrated adenomas [77]. The lifetime risk of colorectal in SPS has been estimated to be greater than 50% [85]. Diagnosis is made clinically and is based on the World Health Organization diagnostic criteria which includes any one of the following:

1. at least five serrated polyps proximal to the sigmoid colon with two or more of them >10 mm in diameter
2. any number of serrated polyps proximal to the sigmoid colon in an individual who has a first-degree relative with SPS
3. >20 serrated polyps of any size, but distributed throughout the colon

It is recommended that patients with SPS should undergo colonoscopies every one to three years with attempted removal of all polyps >5 mm diameter. Surgery is indicated when the growth of polyps cannot be controlled by colonoscopy or malignant change is identified [76].

Syndrome	Gene(s) involved	Inheritance	Mean age CRC	Polyp type(s)	Polyp number	Extra-intestinal features
FAP	APC 5q21	Autosomal dominant	39 years	Conventional adenomas	>100–1000s	CHRPEs Fundic gland polyps Desmoids Thyroid carcinoma Hepatoblastoma Osteomas, cysts and fibromas
Attenuated FAP	APC 5q21	Autosomal dominant	55 years	Conventional adenomas	<100	(as FAP)
Lynch syndrome	MLH1 3p21.3 PMS2 7p22.1 MSH2 2p21 MSH6 2p16.3	Autosomal dominant	45 years	Conventional adenomas	0–10	Endometrial adenocarcinoma TCC of upper urogenital tract Ovarian carcinoma Pancreatobiliary carcinoma Brain tumours Skin tumours
MYH-associated polyposis	MUTYH 1p34.3	Autosomal recessive	48 years	Conventional adenomas. Serrated polyps	Typically, <100 (may be 1000s)	Some FAP-type extra-intestinal features but at low incidence
Peutz-Jegher's syndrome	STK11 19p13.3	Autosomal dominant	46 years	Hamartomas (PJ polyps)	1–10s	Carcinomas in multiple organs
Juvenile polyposis	SMAD4 18q21.1 BMPR1A 10q23	Autosomal dominant	34 years	Hamartomas (juvenile polyps)	5–200	No
Cowden Syndrome	PTEN 10q23	Autosomal dominant	47 years	Conventional adenomas Hyperplastic polyps Hamartomas Ganglioneuromas Inflammatory polyps	0–50	Breast carcinoma
Serrated polyposis	Unknown	Unknown	Uncertain	Serrated polyps (Conventional adenomas)	2–200	No

1. CHRPE: Congenital hypertrophy of the retinal pigment epithelium 2. TCC: transitional cell carcinoma

Table 1.4 – Summary of the familial CRC syndromes with their associated extra-colonic manifestations. Adapted from Novelli, 2015 [77].

1.5 Clinical Presentation, Diagnosis and Staging of Colorectal Cancer

CRC is a potentially preventable disease with tumours often arising from malignant change in an adenomatous polyp [86]. It is hoped that CRC screening programs, with endoscopic control of polyp disease, will reduce the incidence of CRC in the future [87]. However, the majority of patients still present with symptoms which may include a change in bowel habit, iron deficiency anaemia, weight loss, abdominal pain, rectal bleeding, tenesmus or the presence of an abdominal or rectal mass. Patients may also present acutely with bowel obstruction, perforation or haemorrhage, requiring emergency management. Staging is an assessment of local and metastatic CRC burden completed by endoscopic and radiological investigation and used to guide evidence based treatment. A number of systems have been used for staging of disease in CRC and will be discussed below. Most utilise a description of tumour invasion (T stage), lymph node positivity (N stage) and the presence of metastatic disease (M stage) to guide treatment and estimate prognosis.

1.5.1 Screening

Population based screening for CRC, labelled the Bowel Cancer Screening Program (BCSP), commenced in the UK in June 2006. This involves all individuals between 60 and 74 years old being offered testing for Faecal Occult Blood (FOB) every two years. Those with a positive test are then considered for colonoscopy. Meta-analyses of published randomised control trial data demonstrates that FOB testing strategies appear to be effective in reducing the CRC mortality but not in reducing CRC incidence [88, 89]. Two forms of the FOB test are available for use in clinical practice, the guaiac-based FOB test (gFOBT) and Faecal Immunochemical Test (FIT). Evidence from randomised trials suggest that FIT has a significantly higher sensitivity but non-significantly lower specificity for CRC that gFOBT and therefore may be considered a superior method [87].

From 2013 to 2014 trials of an alternate screening protocol were conducted at six centres in the UK. This utilised visualisation of the left colon with a one off flexible-sigmoidoscopy (FS) at the age of 55 years old; preliminary published data report uptake rates of only 43% [90]. Results from a meta-analysis of five randomised control trials demonstrate that an FS-based strategy is effective in reducing the CRC mortality (by 28%) and incidence (by 18%) in a population with an average risk of CRC [91].

1.5.2 Clinical Assessment

Clinical assessment of patients with a suspected CRC should include a history and examination focusing on disease specific symptoms (described in 1.5), the coexisting comorbidity and the signs of malignant disease such as a palpable mass on abdominal or *per rectal* examination. Subsequent investigations or treatment should take into account the nature of the disease itself, such as the presence of metastatic disease, in addition to the general comorbidities of the patient.

1.5.3 Endoscopic Assessment

Flexible-sigmoidoscopy refers to endoscopic assessment of the colon from the rectum to the splenic flexure. Colonoscopy involves examination of the entire colon up to and sometimes including the terminal ileum. Colonoscopy is the recognised gold standard investigation for the identification of colonic polyps or malignancies. It allows direct visualisation of the entire colon colonic mucosa, biopsy of suspected malignant lesions for histological diagnosis and the removal of polyps for the prevention of progression to invasive tumours. The marking of colonic tumours with tattoo ink at colonoscopy has become invaluable in the modern era of laparoscopic surgery where tumour localisation can be challenging. Examination of the entire colon is especially important given the relatively high incidence of synchronous CRC (5%) or colonic polyps (28%) which may alter management decisions [92]. Complications from colonoscopy are rare and were reported at 0.5% in the Nottingham FOB test trial, including post-polypectomy bleeding, perforation and snare entrapment [93]. Missed lesions are reported in the literature with a recent review of tandem colonoscopy reporting a miss rate of 2.1% for adenomas larger then 1cm. However, the miss rate for a small polyp of less than 5mm was very high at 26% [94].

1.5.4 Radiological Assessment

Radiological staging in CRC is essential prior to selection to treatment in the non-emergency setting; allowing assessment of the feasibility of surgical resection and guiding patient selection to specific neoadjuvant therapies, for example long course chemo-radiotherapy in rectal cancer. Radiological imaging in the form of Computerised Tomography Colonography (CTC) or, less frequently, Barium Enema (BaE) may also be used for diagnostic purposes in patients in which complete colonoscopy is not possible due to comorbidity, colonic anatomy or the presence of an impassable stenosing tumour.

Computerised Tomography (CT) scanning is the most widely utilised imaging modality for the local staging of CRC and the detection of distant metastases. It accurately distinguishes between tumours confined to the bowel wall and those invading beyond it. Nodal staging of CRC by CT is unreliable as it relies on lymph node size as a criterion for positivity [95, 96]. The sensitivity (74%-78%) and specificity (93-97%) of CT for the detection of liver metastases is good [97]. CTC allows the use of CT scanning as a diagnostic tool in CRC. Gas insufflation of the colon provides contrast between the colonic mucosa and lumen which, in combination with CT imaging, allows detection of even small colonic polyps. This can be used for diagnostic purposes with meta-analyses reporting a sensitivity of 100% for the detection of CRC and 87.9% for adenomas less than 10mm [98].

Positron Emission Topography (PET) can be combined with CT (PET-CT) and uses the increased glucose metabolism in tumour cells to uptake 18-fluorodeoxyglucose and aid the detection of small malignant deposits. A meta-analysis reported that PET had a slightly lower sensitivity than CT on patient based assessment (93 % and 98 % respectively) and lesion based assessment (66 % and 79 % respectively) but appeared to be more specific than CT (86 % and 67 % respectively). PET findings were shown to alter the management in 24 % of patients [99].

Magnetic Resonance Imaging (MRI) supplements CT staging in two specific situations. Firstly, in the local staging rectal cancer high resolution MRI can provide information previously only available on histological assessment of the resection specimen. Details on local tumour stage, lymph node status and extramural vascular invasion can all be observed with varying degrees of accuracy on T2-weighted images [100]. The MERCURY study group reported that tumour visualised within 1mm of the mesorectal fascia on MRI to be a sensitive predictor of circumferential resection margin (CRM) positivity at surgery [101]. Pre-operative knowledge of these details can allow the selection of patients to neoadjuvant chemoradiotherapy, potentially preventing positive resection margins and reducing recurrence. Secondly, MRI with gadolinium contrast can be employed for the characterisation of indeterminate liver lesions found on CT with improved sensitivity and specificity [102].

1.5.5 Histopathological Assessment

As endoscopic examination of the colon allows the acquisition of tissue from the primary tumour, histopathological assessment is possible prior to surgical resection. Tissue for analysis is formalin-fixed, paraffin-embedded (FFPE), sliced for examination and stained with haematoxylin and eosin (H&E). The histological diagnosis of colorectal cancer is based on invasion through the muscularis mucosae into the submucosa. Further classification into a number of histopathological subtypes is also possible and include; adenocarcinoma, mucinous adenocarcinoma, signet-ring cell carcinoma and medullary carcinoma. Pre-operative histopathological examination of metastatic disease, particularly of the liver, remains a controversial issue due to the risks of tumour seeding and the poor outcomes reported in the literature following biopsy and should be avoided [103]. (Table 1.5)

Grading of tumour tissue allows an interpretation of the degree of de-differentation from the morphology of the original tissue assigned on a scale of G1-G3. Assignment of tumour grade considers nuclear features such as pleomorphism, cellular architecture and mitotic count. G1-2 tumours and G3 tumours are often grouped together for simplicity as low and high grade respectively. Grading of a colorectal cancer may offer some prognostic information to guide management, although this has not been formally incorporated into specific grading systems [104].

Histopathological assessment of the post-resection specimen provides further information on the morphology of primary tumour and on the presence of lymph node disease; allowing staging of disease burden and allocation to treatment as discussed below.

Authors	Year	Design	Number of Patients	Findings
Al-Leswas *et al.*	2008	Case report	2	2 cases of implantation
Jones *et al.*	2005	Retrospective review	17	19% seeding rate; poorer long term survival after biopsy
Rodgers *et al.*	2003	Retrospective review	7	16% risk of seeding irrespective of route of biopsy
Metcalfe *et al.*	2004	Case report	1	Biopsy added nothing to diagnostic pathway
Ohlsson *et al.*	2002	Case series	5	10% seeding rate
Scheele & Altendorf-Hofmann	1990	Case report	2	Seeding following biopsy of resectable lesion
Ferrucci *et al.*	1979	Case report	1	First documented case of tract seeding

Table 1.5 - Summary of the evidence highlighting the complications of percutaneous needle biopsy of colorectal liver metastases. Adapted from Cresswell, Welsh and Rees, 2009 [103].

1.5.6 Staging Systems

The first staging system for CRC was described by Dr Cuthbert Dukes and initially only applied to rectal cancers. Tumours were classified from Dukes' stage A to C with stage A cancers confined to the bowel wall, stage B through the bowel wall and stage C used to describe lymph node involvement [105]. This was system was later correlated with prognosis and stage C subdivided into stages C1 and C2 (apical node involvement) [106]. In 1967 stage D was added, representing the presence of metastatic disease [107]. (Table 1.1)

As a result of the increasing understanding of cancer biology and the advances in radiological techniques, allowing more accurate pre-operative characterisation of CRC, updated staging systems have been developed. The Union for International Cancer Control/American Joint Committee for Cancer (UICC/AJCC) TNM classification is now regarded as the standard of care [108]. Three variables are used to describe cancer stage, including: the degree of invasion of the primary tumour as described by a T stage; the presence and extent of local lymph node invasion referred to as N stage; and M stage describing the presence or absence of metastatic disease. (Table 1.6)

Tumour (T) Stage		Nodal (N) Stage		Metastatic (M) Stage	
TX	Primary tumour cannot be assessed	NX	Regional lymph nodes cannot be assessed	M0	No distant metastasis
T0	No evidence of primary tumour	N0	No regional lymph node metastasis	M1	Distant metastasis
Tis	Carcinoma in situ: intraepithelial or invasion of lamina propria	N1	Metastasis in 1-3 regional lymph nodes	M1a	Metastasis confined to one organ or site
T1	Tumour invades submucosa	N1a	Metastasis in 1 regional lymph node	M1b	Metastases in more than one organ/site or the peritoneum
T2	Tumour invades muscularis propria	N1b	Metastasis in 2-3 regional lymph nodes		
T3a	Tumour extends <1 mm beyond muscularis propria	N1c	Tumour deposit(s) in the subserosa, mesentery, or non-peritonealised pericolic or perirectal tissues without regional nodal metastasis		
T3b	Tumour extends 1-5 mm beyond muscularis propria	N2	Metastasis in 4 or more regional lymph nodes		
T3c	Tumour extends 5-15 mm beyond muscularis propria	N2a	Metastasis in 4-6 regional lymph nodes		
T3d	Tumour extends 15 mm beyond muscularis propria	N2b	Metastasis in 7 or more regional lymph nodes		
T4a	Tumour penetrates to the surface of the visceral peritoneum				
T4b	Tumour directly invades or is adherent to other organs or structures				

Table 1.6 - UICC/AJCC TNM staging of colorectal cancer; 7th edition (2010). Adapted from https://cancerstaging.org/references-tools/quickreferences/Pages/default.aspx

The UICC/AJCC staging system was simplified by grouping into disease stages to allow easier selection to treatment. This divides the CRC staging into four major groups (I to IV) with further subdivision to A or B, including:

- Stage 0: Tis, N0, M0
- Stage I: T1, N0, M0; T2, N0, M0
- Stage IIA: T3, N0, M0
- Stage IIB: T4a, N0, M0
- Stage IIC: T4b, N0, M0
- Stage IIIA: T1-T2, N1/N1c, M0; T1, N2a, M0
- Stage IIIB: T3-T4a, N1/N1c, M0; T2-T3, N2a, M0; T1-T2, N2b, M0
- Stage IIIC: T4a, N2a, M0; T3-T4a, N2b, M0; T4b, N1-N2, M0
- Stage IVA: Any T, any N, M1a
- Stage IVB: Any T, any N, M1b.

Due to the unreliability of radiological assessment for predicting nodal disease in the resection specimen accurate TNM staging is often only available on post-operative histopathological inspection. For this reason, a number of prefixes to the TNM system have been created to describe the origin of the information used for staging. These include:

- c - for clinical classification
- p - for histopathological staging of a surgical specimen
- y - indicating the stage is assessed after chemotherapy and/or radiotherapy
- r - for recurrent tumours after a substantial disease-free period
- A - determined at post mortem

Histopathological assessment of the post-resection specimen can provide further prognostic information beyond nodal staging, which may be beneficial in predicting outcome. The presence of tumour budding and poorly differentiated clusters of cancer cells or invasion into lymphatic vessels, blood vessels and perineural tissue has been shown to influence prognosis. However, these variables have not been incorporated in to a formal staging system, perhaps due to the significant observer error reported in the literature [109]. The Jass classification is currently the best utilised staging system that takes into

account some of the genetic abnormalities discussed previously, in addition to the macro- and microscopic characteristics of the tumour. It is used for the molecular classification of CRC [110].

Accurate staging of patients is essential as it allows prognostication and allocation to treatment. Currently patients with nodal disease are recommended to receive adjuvant chemotherapy. Further studies are needed to clarify whether a select group of node negative patients would benefit from adjuvant therapy based on histopathological assessment of the primary tumour.

Feature	Group 1	Group 2	Group 3	Group 4	Group 5
MSI status	H	S/L	S/L	S	H
Methylation	+++	+++	++	+/–	+/–
Ploidy	Dip > An	Dip > An	An > Dip	An > Dip	Dip > An
APC	+/–	+/–	+	+++	++
KRAS	–	+	+++	++	++
BRAF	+++	++	–	–	–
TP53	–	+	++	+++	+
Location	R > L	R > L	L > R	L > R	R > L
Gender	F > M	F > M	M > F	M > F	M > F
Precursor	SP	SP	SP/AD	AD	AD
Serration	+++	+++	+	+/–	+/–
Mucinous	+++	+++	+	+	++
Dirty necrosis	+	+	?	+++	+
Poor differentiation	+++	+++	+	+	++
Circumscribed	+++	+	?	++	++
Tumour budding	+/–	+	?	+++	+
Lymphocytes	+++	+	?	+	+++

MSI, microsatellite instability; H, high; S, stable; L, low; Dip, diploid; An, aneuploid; Serration, serrated morphology; SP, serrated polyp; AD, adenoma; Circumscribed, circumscribed invasive margin.

Table 1.7 – Jass classification system for CRC as adapted from Jass, 2007 [110].

1.6 Surgical management of colorectal cancer

The surgical resection of the primary tumour, with the draining lymph nodes or metastatic disease where possible, remains the mainstay of treatment in CRC. The exact oncosurgical strategy employed can vary considerably with local T stage, the location of the primary tumour or the presence and location metastases, as can the timing of resection in relation to other treatment modalities.

1.6.1. Local resection of the primary tumour

Local excision is possible for adenomas or early CRC, such as those confined to the submucosa. This can be undertaken at colonoscopy for colonic tumours or using a variety of transanal techniques for rectal lesions. Endoscopic Mucosal Resection (EMR) and Endoscopic Submucosal Dissection (ESD) have allowed the local resection of larger colonic polyps, with ESD resulting in a deeper margin of resection into the layers of the colonic wall and excision of larger lesions. Local recurrence rates for EMR and ESR are 13% and 1% respectively, with no statistical differences in complication rates reported on meta-analysis. However, ESD is a more difficult technique and procedures take longer to complete [111]. Transanal excision (TE), Transanal Endoscopic Microsurgery (TEMS) and Transanal Minimally Invasive Surgery (TAMIS) are all utilised for the local excision of larger rectal lesions specifically. TEMS has been compared with radical resection for T1 and T2 rectal tumours, with an increased risk of local recurrence reported with TEMS (11% versus 3%); distant recurrence rates were equivocal [112]. However, local resection is associated with fewer postoperative complications and lower mortality in T1 lesions specifically [113]. TAMIS is a relatively recent development with published data consisting mostly of small case-series [114].

A concern with local resection of colorectal cancer is incomplete histopathological staging. Excision and examination of the draining lymph nodes is not undertaken and nodal staging is reliant on radiology. This may result in under-treatment, as lymph node positive patients may be incorrectly excluded from the benefit of adjuvant chemotherapy. Local excision for CRC is therefore only advisable in early low-risk tumours or in patients unfit for formal resection. Identifying those patients considered to have low risk lesions is challenging with positive nodes reported in at least 6% of T1 tumours [115, 116].

1.6.2 Radical resection of the primary tumour

Radical resection of CRC refers to the removal of the section of bowel containing the primary tumour with its draining lymph nodes, which follow the vascular supply to that segment. The arterial supply is divided at the highest point possible, while preserving the bloody supply to non-resected segments. For tumours in the right colon a right hemi-colectomy is performed with division of the ileo-colic artery close to its origin from the superior mesenteric artery, which supplies much of the small bowel. For tumours in the left colon and rectum the inferior mesenteric artery is ligated as it branches from the abdominal aorta. If the patient is deemed to be at a lower risk for a leak, then an anastomosis is created to restore intestinal continuity and avoid the formation of a stoma. The anastomotic leak rate was 8.7% in patients undergoing colonic resection for malignant disease in a large multicentre prospective study. An increased risk of leak was noted with obesity, male sex, poor nutrition, anticoagulation treatment, emergency surgery and intraoperative complications [117].

The proximal division of vessels maximises the mesenteric resection and therefore lymph node yield, allowing more accurate histopathological staging and prognostication. The National Cancer Institute and the National Quality Forum recommend that at least 12 lymph nodes are examined for adequate staging [118].

Anterior resection with total mesorectal excision (TME) has become the standard surgical technique for the radical resection of rectal cancers in which clear distal margins can be achieved. First described in 1988, TME involves removal of the rectum with its supporting mesentery from the pelvis, allowing wider resection margins. The anal canal is not removed and intestinal continuity can be restored with the option to perform a de-functioning loop-ileostomy. TME dissection reduced local recurrence rates from 30% to 3-6% [119, 120]. Involvement of the circumferential resection margin is now believed to be a predictor of local recurrence, distant metastasis and survival [121].

The widespread adoption of this technique has reduced the number of abdomino-perineal excisions of the rectum (APER) performed. This entails removal of the rectum and anal canal in its entirety with formation of a permanent colostomy. Combinations of neoadjuvant chemoradiation, total mesorectal excision, intersphincteric proctectomy and colonic-J pouch to anal anastomosis means that sphincter preservation can be achieved in most patients, reducing the rate of APER [122].

Resections for CRC may be performed using an open, laparoscopic or robotic approach. International multi-centre studies have attempted to confirm the oncological equivalence of laparoscopic colorectal cancer surgery to open. Early results from the Colon Cancer Laparoscopic or Open Resection (CoLOR) trial reported equivalent short-term outcomes, including complication rate, mortality, positive resection margins and blood loss during surgery between groups [123]. While the Conventional versus Laparoscopic-Assisted Surgery in Colorectal Cancer (CLASSIC) trial concluded that, for colonic resections, laparoscopic techniques are oncologically equivalent but reported a non-significant increased rate of circumferential margin positivity for laparoscopic anterior resections. This could translate to a higher rate of local recurrence in the longer-term, despite a higher rate of TME in the laparoscopic-assisted group [124]. Longer-term analysis of data from the CoLOR trial found no difference in overall and disease free survival, but could not rule out a difference in disease-free survival at three years in favour of open colectomy. However, this difference was felt to be small enough to justify the use of laparoscopic surgery in daily practice [125]. Studies agree that laparoscopic surgery reduces wound infection rates, allows earlier recovery of bowel function, reduces narcotic use, decreases overall morbidity and results in a shorter hospital stay, at the cost of modest increase in operative times.

Robotic surgery for rectal cancer remains in its relative infancy. Published data consists of short-term outcome reporting of small single centre experience. Meta-analysis of four randomised control trials comparing robotic to laparoscopic resection for rectal cancer reported no differences in complication rates, length of hospital stay, proximal margin, distal margin or harvested lymph node yield between techniques [126], but a lower conversion rate to open surgery has been reported for robotic rectal resection [127]. Results of an international, multicentre, prospective, randomised, controlled, unblinded, parallel-group trial of robotic-assisted versus standard laparoscopic surgery for the curative treatment of rectal cancer (ROLARR) are awaited [128].

1.6.3 Resection of metastatic disease

Increasing numbers of patients are now offered potentially curative surgery for CRC metastases, particularly those confined to the liver. A more aggressive approach to neoadjuvant chemotherapy, combined with improved surgical techniques, brings more patients to resection. Variable survival rates are reported in those patients who undergo resection of liver metastases, ranging from 16% to 74% at five years [129].

Traditionally there was a conservative approach to the management of metastatic disease in the liver. Patients with 1-3 unilobar metastases which were resectable with a generous margin were considered for surgical management. Presenting with stage IV disease, a rectal primary, multiple diffuse metastases, metastases larger than 5cm, a disease free interval of less than one year from the diagnosis of the primary and high serum carcinoembryonic antigen (CEA) were considered relative contraindications to curative surgical resection due to a poor prognosis [130].

The approach to the surgical resection of liver metastases is now more a consideration of both technical and oncological feasibility. Resection is considered when it is possible to remove all macroscopic disease with negative margins (refered to as an R0 resection), preserve blood supply and leave sufficient future remnant liver to ensure adequate hepatic function. The volume of liver remnant required to ensure adequate hepatic function depends on the quality of the remaining liver parenchyma; those with cirrhosis, steatosis or drug induced liver injury (DILI) require a larger liver remnant to maintain function [131]. National Institute for Health and Care Excellence (NICE) guidance (CG131) now recommends that surgery for metastatic disease in the liver be considered in those patients fit enough and in whom complete resection can be obtained leaving adequate a hepatic remnant.

Radiofrequency ablation, microwave ablation and laser induced thermotherapy, performed at open surgery or percutaneously, offer less invasive alternatives to the surgical resection of liver metastases. Given the varying local progression rates reported with these techniques their role in the curative management of patients is unclear [132]. They are often reserved for unfit patients with low volume disease, as an adjunct to formal resection or in the non-curative setting.

Guidance on the surgical management of extra-hepatic metastases from CRC is less clear. Pulmonary metastasectomy in a select group of patients with lung limited metastases resulted in five year survival rates greater than 50% [133]. Results of the Pulmonary Metastasectomy in Colorectal Cancer (PulMICC) trial, a feasibility study randomising to surgical resection or active monitoring, will hopefully add clarity to the role of surgery for metastatic colorectal cancer in the thorax when results are published [134].

The best surgical approach for patients presenting with a resectable primary tumour and synchronous metastatic disease requires clarification due to a lack of high-level prospective data. Options include a classical approach (primary first and then liver), reverse approach (liver first and then primary) or to synchronously (simultaneously) resect disease at both sites within a single procedure. All of these approaches would need to be integrated with neoadjuvant or adjuvant chemotherapy and possibly radiotherapy in some cases of rectal cancer specifically. A systematic review of the surgical management of synchronous metastatic disease identified 18 papers in which 21 comparisons had been performed between two or more of these strategies; concluding that no strategy is inferior to the others [135]. A more recent review noted no difference in survival between the three surgical approaches [136]. Based on the evidence to date, patients with synchronous metastatic disease should be managed on an individual basis by a specialist multidisciplinary team.

1.7 Radiotherapy in the treatment of rectal cancer

Radiotherapy is a recognised treatment utilised in the management of patients with rectal cancer to shrink locally advanced tumours and facilitate complete surgical resection, or to reduce the risk of local recurrence. The potential complications of radiotherapy, such as increased bowel frequency, incontinence and delayed wound healing, should always be balanced against the potential benefits.

1.7.1 Effect of radiation

Radiotherapy works through the direct and indirect ionisation of atoms. Direct effects occur when radiation causes ionisation of atoms in DNA, resulting in double strand breaks or adducts, essential to the survival and reproduction of the cell. The indirect action is the result of the ionisation of water leading to the formation of free radicals. Oxygen is required for free radical formation and therefore radiotherapy is less effective in relatively

hypoxic cells, such as those found in central areas of large solid tumours [137]. The effect of radiotherapy is more marked in malignant cells due to their rapid replication rate, with progeny requiring the correct DNA to survive or replicate. The relative mobility of the colon and small bowel within the abdomen, combined with the risk of radiation enteritis due to the rapidly dividing small bowel epithelial cells, limits the use of radiotherapy to the treatment of rectal cancer. The fixed position of the rectum in the pelvis allows more accurate tumour targeting and reduces the risk of small bowel irradiation.

1.7.2 Resistance to radiotherapy

The ability of cancer cells to repair DNA damage is at least partially responsible for the variation in response seen in tumours. Base excision repair (BER) mechanisms remove damaged bases that could otherwise cause mutations by mispairing or lead to breaks in DNA during replication. AP endonuclease 1, DNA polymerase β and DNA ligase III with its cofactor XRCC1 are all believed to be key proteins involved in BER and have been investigated as both biomarkers and therapeutic targets for radiotherapy treatment [138].

The tumour microenvironment may also influence radiotherapy response. Vascular, stromal and immunological changes following radiotherapy treatment may all alter tumour regression. There are numerous potential targets within the tumour microenvironment which could be manipulated for radio-sensitisation. These are categorised as hypoxia, fibrosis, cancer-associated fibroblast and immune related, dependent on their area of action [139]. (Table 1.8)

All these factors mean a number of patients treated with radiotherapy will receive little or no benefit but are still exposed to the potential risks and complications. Up to 40% of patients have been shown to experience no tumour regression following radiotherapy [140]. Predicting and modifying this response is essential to improving outcomes and reducing overtreatment.

Resistance mechanism	Drugs	Targets	Mode of action
Immune response	Ipilimumab	CTLA4	T cell activation
	Nivolumab and pembrolizumab	PD1	T cell exhaustion
	Imiquimod	TLR7	DC activation
	Oncolytic viruses	Tumour cells	Activate immune response
	Future inhibitors	IL-6 and IL-10	T cell activation
		PDL1, TIM3 and LAG3	Prevent T cell exhaustion
	Future agonists	GM-CSF, CXCL16, OX40, CD40L, CD80 and CD137	T cell recruitment and activation
		CCL3, CCL5, IL-2, IL-4, IL-12 and IRX-2	Activate immune response
Hypoxia	Nitroimidazole derivatives (that is, nimorazole)	Hypoxic cells	Reduce tumour hypoxia
	Bioreactive albumin–MnO2 nanoparticles	Hypoxic cells	Reduce tumour hypoxia
	Acriflavine and YC-1	HIF1α	Reduce hypoxia response pathway activity
	Aflibercept	All VEGF molecules and PlGF	Vessel normalization
	AMG386	ANG1 and ANG2	Inhibit pBMDC recruitment
	Endostar	VEGF, TGFβ, HIF1α and bFGF	Inhibit angiogenesis
	AMD3100	CXCL12 and CXCR4	Inhibit BMDC recruitment and vasculogenesis
	Integrin inhibitors (cilengitide, vitaxin and volociximab)	Integrins αvβ3, αvβ5 and α5β1	Inhibit angiogenesis
	Future inhibitors	Integrins α6β1 and α6β4	Reduce endothelial cell survival and inhibit angiogenesis
		PlGF and ANG2	Vessel normalization and overcome resistance to anti-VEGF therapies
Fibrotic processes	BIBF1000 and BIBF1120	PDGF, VEGF and bFGF receptors	Reduce GF signalling and TME remodelling; fibrosis
	Imatinib, nilotinib and dasatinib	TGFβ and PDGF	GF signalling; collagen synthesis
	Vismodegib, saridegib and sonidegib	SMO	Reduce HH signalling; fibrosis
	Suramin	PDGF, EGF, TGFβ, FGF2 and IGF receptors and heparanase enzymes	Reduce GF signalling and TME remodelling; fibrosis
	ST0001, PG545 and M402	Heparanase	Inhibit TME remodelling
	SD-208	TGFβR1	Inhibit TGFβ signalling
	Simtuzumab	LOXL2	Reduce TME remodelling; liver fibrosis
	81C6 and F16SIP	TNC	Reduce CAF-mediated TME remodelling
	Future inhibitors	HGF, CTGF, MMP2, MMP3, and integrins α11β1, αvβ6 and α3β1	TME activation and remodelling; radiation-mediated fibrosis

ANG, angiopoetin; bFGF, basic fibroblast growth factor; BMDC, bone marrow-derived cell; CAF, cancer-associated fibroblast; CTGF, connective tissue growth factor; CTLA4, cytotoxic T lymphocyte antigen 4; CXCL, chemokine (C-X-C motif) ligand; CXCR4, C-X-C chemokine receptor 4; DC, dendritic cell; EGF, epidermal growth factor; FGF2, fibroblast growth factor 2; GF, growth factor; GM-CSF, granulocyte–macrophage colony-stimulating factor; HGF, hepatocyte growth factor; HH, Hedgehog; HIF1α, hypoxia-inducible factor 1α; IGF, insulin-like growth factor; IL, interleukin; IRX2, iroquois homeobox 2; LAG3, lymphocyte activation gene 3; LOXL2, lysyl oxidase-like 2; MMP, matrix metalloproteinase; pBMDC, perivascular bone marrow-derived cell; PD1, programmed cell death protein 1; PDL1, programmed cell death protein ligand 1; PDGF, platelet-derived growth factor; PlGF, placental growth factor; SMO, Smoothened; TGFβ, transforming growth factor-β; TGFβR1, transforming growth factor-β receptor 1; TIM3, T cell immunoglobulin mucin 3; TLR7, Toll-like receptor 7; TME, tumour microenvironment; TNC, tenascin C; VEGF, vascular endothelial growth factor.

Table 1.8 - Tumour microenvironment therapeutic biomarkers for radio-sensitisation. Adapted from Barker, 2015 [139].

1.7.3 Short-course pre-operative radiotherapy (SCPRT)

Short-course pre-operative radiotherapy (SCPRT) is given to patients to reduce the risk of post-surgical local recurrence. SCPRT is an irradiation regimen designed to not delay definitive surgical treatment; a typical regimen is 25Gy in five equal fractions delivered over five days. This approach was supported by a number of randomised trials, the most significant of which was the Swedish Rectal Cancer Trial which demonstrated improved survival and reduced local recurrence rates with compared with surgery alone, with median follow up of 13 years in the more recently published data [141, 142]. Some caution should be exercised in interpreting these data, with many of the patients operated on before the widespread introduction of TME.

More recent trials do confirm similar benefits. The Dutch Colorectal Cancer Study Group trial compared SCPRT and TME surgery with TME surgery alone. Overall survival at two years was comparable between groups but the rate of local recurrence was 2.4% in those receiving SCPRT-TME and 8.2% in the group receiving TME alone [143]. Similarly the Medical Research Council CR07 trial compared SCPRT with selective post-operative chemoradiotherapy for patients with CRM involvement. Eighty centres randomised 1350 patients to treatments with a 61% reduction in local recurrence and 6% increase in disease free survival at three years in those patients undergoing SCPRT [144].

1.7.4 Long-course neoadjuvant chemoradiotherapy (LCCRT)

Long-course radiotherapy involves the delivery of 45-50Gy over 5-6 weeks at 1.8 or 2.0Gy per fraction, generally followed by surgery 4-8 weeks later. As with SCPRT, there is good evidence for improved local control but no evidence of an increase in survival benefit. Controversy exists as to whether there is any additional benefit to LCCRT when compared with SCPRT; the Trans-Tasman Radiation Oncology Group trial 01.04 concluded there were no statistically significantly differences between the two treatments in 326 randomised patients with T3 lesions [145]. Long-term results of the Stockholm III Trial of radiotherapy regimens for rectal cancer are awaited. This three-armed trial randomises patients with primary operable rectal cancers to either SCPRT with immediate surgery, SCPRT with surgery delayed 4-8 weeks or long-course RT with surgery delayed 4-8 weeks. Interim results have only compared SCPRT to SCPRT with delayed surgery, suggesting an improved tumour regression in delayed surgery [146].

A potential benefit of LCCRT is the ability to combine it with neoadjuvant chemotherapy. Trials (FFCD 9203 and EORTC Radiotherapy Group 22921) compared preoperative chemoradiotherapy to radiotherapy alone for the management of T3-T4 rectal cancer concluding that, despite a moderate increase in acute toxicity and no impact on overall survival, the addition of chemotherapy significantly improves local control [147, 148]. Only one trial has compared SCPRT and LCCRT in patients with operative disease; longer courses of radiotherapy were associated with greater tumour down-staging and CRM-negative resections but resulted in higher rates of radiation toxicity and no improvement in local recurrence or survival [149]. More recently the German CAO/ARO/AIO-04 study concluded that the addition of oxaliplatin to fluorouracil-based neoadjuvant chemoradiotherapy alone significantly improved the disease-free, but not overall, survival of patients with clinically staged T3-4 or N1-2 rectal cancer [150]. The potential benefits of LCCRT to local disease control must always be balanced with the risk of side effects.

The timing of LCCRT relative to surgical excision has been subject to debate. However, the recent CAO/ARO/AI0 94 trial, comparing pre-and post-operative chemoradiotherapy in the context of standardised TME surgery and adjuvant chemotherapy, reported lower recurrence rates when the radiotherapy is delivered pre-operatively (7.1% vs. 10% at 10 year follow up) [151].

1.7.5 Selection of patients to radiotherapy

With the universal acceptance of TME surgery for rectal cancer the routine use of radiotherapy has become more controversial. However, for patients with a threatened CRM or at high risk of local recurrence, radiotherapy may be indicated.

More accurate prediction of CRM involvement, defined as a tumour encroaching upon the mesorectal fascia and therefore likely to result in a positive CRM given a satisfactorily performed TME resection, has become possible with the routine use of MRI staging in rectal cancer. The MERCURY study group reported the best cut-off distance for predicting CRM involvement post-resection using pre-operative MRI was 1mm; five year follow-up highlighted a fall in disease free and overall survival in patients whose tumour was closer than this to the CRM on MRI [152]. It has also been suggested that MRI prognostication can be used to define tumours likely to have a poor prognosis which should receive radiotherapy prior to resection, despite a low risk of CRM involvement [153]; poor prognosis tumours were defined by the criteria displayed in table 1.9.

MRI feature	Good Prognosis	Poor Prognosis
CRM	>1mm clear	<1mm involved
Low rectal <5cm	Intersphincteric plane clear	Intersphincteric plane involved
T stage	T1, T2 or T3a-b	T3c-d or T4
Extra-mural venous invasion	Absent	Present
N stage	Any	Any

Table 1.9 - Good and poor prognosis rectal cancers as defined by MRI pre-operative local staging. Adapted from Taylor, 2011 [153].

Attempts to select between SCPRT or LCCRT in patients with rectal cancer lead to the publication of NICE guidance in 2011 (CG131). These divide rectal cancers into low, moderate or high risk groups; low risk tumours proceed straight to surgery, moderate risk tumours with no CRM involvement receive SCPRT and high risk tumours are treated with LCCRT. Criteria for defining risk groups are displayed in table 1.10.

Risk of local recurrence	Characteristics of rectal tumours predicted by MRI
High	A threatened (<1 mm) or breached resection margin or
	Low tumours encroaching onto the intersphincteric plane or with levator involvement
Moderate	Any cT3b or greater, in which the potential surgical margin is not threatened or
	Any suspicious lymph node not threatening the surgical resection margin or
	The presence of extramural vascular invasion
Low	cT1 or cT2 or cT3a and
	No lymph node involvement

Table 1.10 - Risk of local recurrence for rectal tumours as predicted by MRI according to NICE guidance CG131. Low risk tumours are recommended to proceed straight to surgery, moderate to SCPRT if no CRM involvement and high risk to LCCRT. Adapted from NICE guidance CG131.

1.7.6 Other uses for radiotherapy in rectal cancer

Discussion so far has focused on the use of radiotherapy to reduce the risk of local recurrence in rectal cancer in combination with surgical resection but it may have a role in other scenarios.

The Papillon system has been used for the delivery of direct contact local radiotherapy to rectal cancer, often in patients not suitable for TME resection or in conjunction with a local resection technique such as TEMS. A case series of 220 patients with T1-T3 tumours less than 3cm in diameter was reported from the Clatterbridge Centre of Oncology. A local control rate of 93% was reported, with no significant morbidity, accepting that their population was highly selective and that close follow-up and plans for salvage surgery are advised [154].

Radiotherapy may also help to alleviate symptoms, such as pain or bleeding, in the palliative setting when disease is unresectable or has reoccurred post-resection. A total radiotherapy dose of 20-60Gy was shown to relieve pain and bleeding in 75% of patients for a median duration of 6-9 months [155].

1.8 Chemotherapeutics used in colorectal cancer

The use of chemotherapy for advanced and metastatic CRC (mCRC) began in the late 1950s with the development of 5-FU. The use of alternative agents has dramatically altered the approach to the management of these patients. Combination regimens have become standard practice since their introduction in the early 2000's and include; 5-FU, oxaliplatin and leucovorin (FOLFOX); 5-FU, irinotecan and leucovorin (FOLFIRI); and 5-FU, oxaliplatin, irinotecan and leucovorin (FOLFIRINOX) [156]. The increasing understanding of tumour biology had led to the development of additional biological agents, such as cetuximab, panitumumab and bevacizumab, which can be combined with the standard chemotherapy regimens.

1.8.1 5-Fluorouracil (5-FU)

The fluotopyrimidine anti-metabolite 5-FU remains the primary chemotherapeutic agent used in the treatment of CRC. Analogous to uracil, it substitutes hydrogen with a fluorine atom at the C5 position and acts as a specific uracil antagonist. Misincorporation of 5-FU into RNA and DNA arrests RNA synthesis and inhibition of the nucleotide synthetic enzyme thymidylate synthase (TS) results in the arrest of cell division and tumour growth.

After entering the cell via a facilitated transport mechanism, 5-FU is converted to three main active metabolites: fluorodeoxyuridine monophosphate (FdUMP), fluorodeoxyuridine triphosphate (FdUTP) and fluorouridine triphoshate (FUTP). The predominant mechanism of 5-FU activation is conversion to fluorouridine monophosphate (FUMP) by orotate phosphoribosyltransferase (OPRT), with phosphoribosyl pyrophosphate (PRPP) as the cofactor, or via fluorouridine (FUR) through the sequential action of uridine phosphorylase (UP) and uridine kinase (UK). FUMP is subsequently phosphorylated to fluorouridine diphosphate (FUDP) which can then be further phosphorylated to FUTP, or further converted to fluorodeoxyuridine diphosphate (FdUDP) by ribonucleotide reductase (rr). FdUDP is then phosphorylated or dephosphorylated to FdUTP and FdUMP respectively. Alternatively, 5-FU can undergo thymidine phosphorylase catalysed conversion to fluorodeoxyuridine (FUDR) which is phosphorylated by thymidine kinase (TK) to FdUMP. The rate-limiting step in 5-FU catabolism is the enzyme dihydropyrimidine dehydrogenase (DPD) that converts 5-FU to dihydrofluorouracil (DHFU); it is believed that up to 80% of administered 5-FU is broken down by DPD in the liver (figure 1.3) [157].

Frequently occurring side effects of 5-FU therapy include nausea, vomiting, diarrhoea, mucositis, headache, myelosuppression and alopecia.

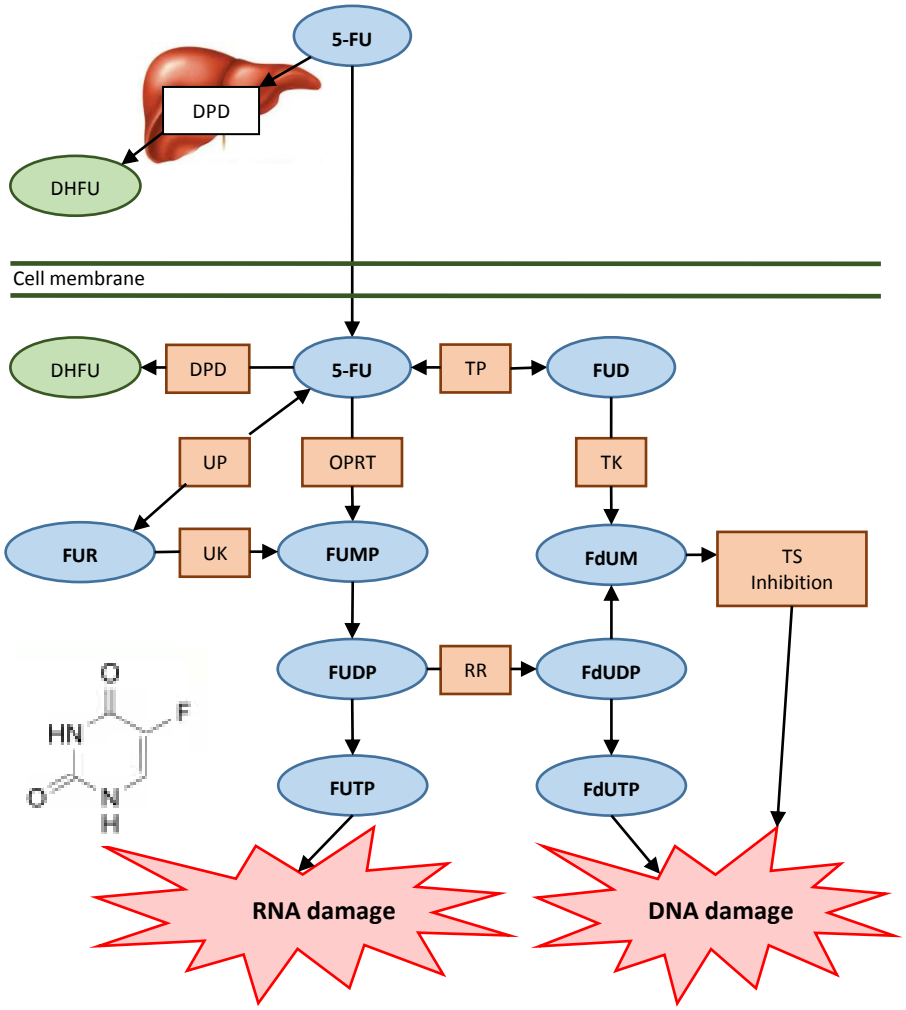

Figure 1.3 – The activation and metabolism of 5-FU. Adapted from Longley, 2003 [157].

1.8.2 Leucovorin

High intracellular levels of the reduced folate CH2 THF are necessary for optimal binding of FdUMP to TS. As a result, 5-FU is given in combination with leucovorin (LV, 5'-formyltetrahydrofolate) to expand the intracellular concentration of CH2 THF and potentiate the effects of 5-FU. Leucovorin is transported into cells via the reduced folate transporter, anabolised and polyglutamated. This not only increases intra-cellular retention but further help stabilise the complex formed with FdUMP and TS [158].

1.8.3 Oxaliplatin

Oxaliplatin is a third-generation platinum compound with a 1,2-diaminocyclohexane (DACH) ring. It undergoes intra-cellular transformation into a number of active metabolites all of which contain the DACH ring. The primary target of all platinum complexes is DNA, particularly guanine, resulting in DNA inter- and intra-stand cross link adducts which prevent replication and transcription [159]. The main side effect of oxaliplatin is polyneuropathy, but patients may also experience nausea, vomiting, diarrhoea, mucositis, headache and myelosuppression [160]. Hepatic sinusoidal obstruction syndrome has also been reported following the administration of oxaliplatin based regimens. Evidence of this process was reported in the livers of 51% patients receiving oxaliplatin on histological assessment [161].

1.8.4 Irinotecan

Irinotecan (7-ethyl-10[4-(1-piperidino)-1-] carbonyloxycamptothecin (CPT-11, Camptostar) is a camptothecin analogue derived from *Camptotheca acuminate* [162]. It is a pro-drug metabolically activated to 7-ethyl-10-hydroxycamptothecin (SN-38) by cleavage of a dipiperidino side chain [163]. Although more cytotoxic than irinotecan (100-1000-fold), SN-38 is poorly soluble and highly cytotoxic, meaning it cannot be administered systemically [164]. The primary therapeutic target of SN-38 is Topoisomerase 1 (Topo1), which is responsible for the relaxation of supercoiled DNA by the cutting of one DNA strand. It then allows the intact strand to pass through the DNA-Topoisomerase cleavage complex and re-joins the cleaved DNA strand without damage [165]. The persistence of single-stranded DNA breaks can lead to double-stranded breaks due to the interaction at advancing replication forks and cell division subsequently stalls in S phase [166]. If these DNA breaks remain unrepaired then apoptotic cell death results [167].

Irinotecan administration can result in severe neutropenia and diarrhoea. The incidence of early-stage diarrhoea is as high at 80% and is dose dependent. Late-stage diarrhoea, occurring over 24 hours after administration, occurs in 60–87% of patients [168]. Although early-stage diarrhoea is often treatable with atropine, late-stage diarrhoea is more difficult to manage and can result in severe colitis. Hepato-toxicity is also reported, with 12-15% developing steatohepatitis [169].

A number of intracellular proteins play a role in the activation, transport, metabolism and excretion of irinotecan including the carboxylesterases (CES), CYP3A, UDP-glucuronosyltransferases (UGT), adenosine-triphosphate binding cassette (ABC) transporters and β-glucuronidase. Variations in these proteins are thought to contribute to inter-patient differences in the side effects, pharmacokinetic profile and response rates seen with irinotecan therapy; there is a growing interest in using these as potential predictors of response and toxicity (figure 1.4).

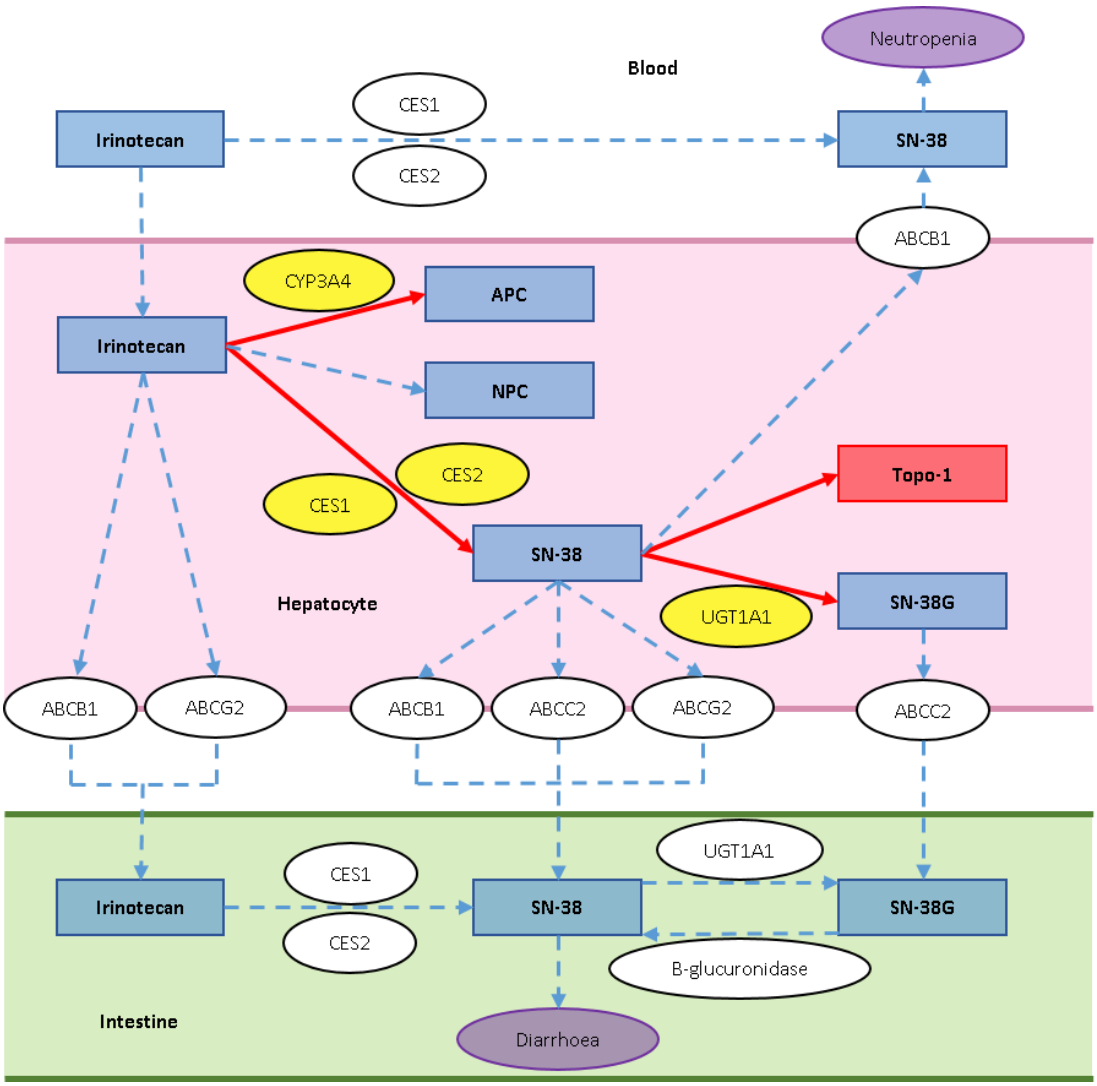

Figure 1.4 – Diagram displaying the metabolism of irinotecan. The key pathways and enzymes are highlighted (key pathway = red arrow and key enzyme = yellow bubble).

1.8.4.1 Carboxylesterase mediated hydrolysis

The CES are phase 1 drug metabolism enzymes located in the endoplasmic reticulum and responsible for the hydrolysis of irinotecan to the active metabolite SN-38. The most abundant and well-studied human enzymes are CES1 and CES2. CES2 has been demonstrated to be a better converter of irinotecan to SN-38 with a 64-fold higher catalytic efficiency [170]. Relative CES expression across tissue types has also been explored in an attempt to establish the primary site of irinotecan activation. CES2 expression was found to be greater than CES1 in normal colon and in CRC, while in normal liver CES1 was six times more abundant than CES2. Despite the lower expression of CES2 than CES1 in hepatic parenchyma, CES2 is still two to three times more abundant than in CRC tissue and, as a result, the liver may be responsible for up to 50% of the conversion of irinotecan to SN-38 [171, 172]. The anti-tumourigenic effects of irinotecan are most likely to be the result of both local production of SN-38 in tumour tissue and SN-38 produced in the liver and transported to the tumour site either through the bloodstream or directly after excretion in bile.

In primary and metastatic tumour tissue there was a good correlation between CES2 expression and irinotecan activity; large variations in CES expression were noted between patient samples [168]. A study investigating the hepatic metabolism of irinotecan as a potential predictor of tumour response to irinotecan-eluting beads found response to treatment positively correlated with CES2 expression in human liver tissue [173]. Additionally, CES2 mRNA expression in peripheral blood mononuclear cells was demonstrated to predict irinotecan to SN38 activation [174]. These findings suggest that induction of CES expression could improve the conversion of irinotecan to SN-38 and therefore the efficacy of therapy. This theory was been explored in CRC cell lines and xenograft studies, demonstrating improved sensitivity to irinotecan with overexpression of CES2 using a recombinant adenoviral vector [175].

1.8.4.2 Cytochrome P450 3A (CYP3A) metabolism

Irinotecan can also be metabolised directly to the pharmacologically inactive compounds APC and NPC by the Cytochrome P450 3A subfamily members CYP3A4 and CYP3A5 [176]. APC is the more abundant of these metabolites and is formed by oxidation of the terminal piperidine ring, while NPC results from cleavage of the distal piperidine ring [177, 178]. CYP3A expression is highest in human hepatic parenchyma, but with a 30-fold difference in protein and mRNA expression reported between individuals, suggesting most direct inactivation of irinotecan occurs in the liver [179]. CYP3A4 expression, which is believed to produce the majority of the inactive metabolites, is lower in colorectal tumour tissue than in normal colon, perhaps implying that reduced direct deactivation of irinotecan may make CRC tissue more chemo-susceptible [180]. Within the setting of a randomised control trial, modifying the dose of irinotecan based on CYP3A function; calculated by an algorithm based on the patient's midazolam clearance, gamma-glutamyl-transferase level and height; resulted in an improved predictability of the pharmacokinetic and toxicity profile of the drug, lowering the incidence of severe neutropenia [181].

1.8.4.3 UDP-glucuronosyltransferase

UDP-glucuronosyltransferase (UGTs) are a group of enzymes, bound to the endoplasmic reticulum, involved in the phase II metabolism of irinotecan. UGTs are responsible for the glucuronidation of SN-38 to the inactive metabolite SN-38G, allowing its conjugation and excretion. The liver is the predominant site of glucuronidation, but considerable variation exists (52-fold) in the conversion of SN-38 to SN-38G by microsomes isolated from human liver homogenate [177, 182].

Several studies have investigated the effects of polymorphisms in UGT's on SN-38 glucuronidation, the most extensively investigated of which are the isoforms of UGT1A1. UGT1A1 is involved in the conjugation of bilirubin and therefore plays a key role in drug excretion; mutations in UGT1A1 are implicated in Gilbert's syndrome, characterised by an inability to conjugate bile and intermittent hyperbilirubinaemia. The UGT1A1*28 polymorphism results in reduced enzyme production and therefore SN-38 glucuronidation due mutations in the promoter region [183]. The effect of the UGT1A1*28 polymorphism on irinotecan toxicity in CRC has been the subject of a number of studies (Table 1.11), the results of which have been assessed by meta-analysis. This study concluded that homozygosity (Odds ratio = 4.79, $p<0.00001$) and heterozygosity (Odds ratio = 1.68,

p<0.0001) of UGT1A1*28 was associated with an increased risk of neutropenia, regardless of the dose of irinotecan. The incidence of severe diarrhoea was only significantly higher in the homozygote group (Odds ratio = 1.78, p = 0.009) at medium and higher doses of irinotecan [184]. As a result of these data UGT1A1*28 genotyping should be considered prior to commencing irinotecan based therapies to allow dose modification. It could be hypothesised that impaired glucuronidation of SN-38 could lead to accumulation of the active metabolite and increased irinotecan efficacy, but this theory was not supported in the conclusions of a high quality meta-analysis [185].

Study	Country, race	Phase of clinical trial	No. of patients (male%)	Age (a)	Population source	Mutation detection methods	Regimen	IRI dose (mg m^{-2})/schedule	Grade criteria	Neutropenia grade 3–4 (%)	Diarrhoea grade 3–4 (%)	Study design
Lamas *et al.*	Spain, U	U	100 (63.4)	67	U	SPR	FOLFIRI	180/biweekly	N3	18 (18.0)	12 (12.0)	R
Shulman *et al.*	Israel, C	I	214 (46.3)	63	M	SPR	TEGAFIRI, XELIRI, FOLFIRI, IFL	U	U	48 (22.4)	19 (8.9)	R
Martinez *et al.*	Spain, C	III	149 (U)	U	M	Sequencing	FOLFIRI, FUIRI	80/weekly or 180/biweekly	U	31 (20.8)	45 (30.2)	R
McLeod *et al.*	USA/UK/Canada, mainly C	III	212 (U)	61	M	PYRS	IFL, IROX	100–125/weekly or 200/every 3 weeks	N2	Only grade 4: 28 (13.2)	60 (28.3)	P
Glimelius *et al.*	Sweden/UK/Norway, mainly C	III	136 (U)	62	M	SPR	FLIRI, Lv5FU-IRI	180/biweekly	N2	18 (13.2)	10 (7.4)	R
Braun *et al.*	UK, U	III	326 (U)	64	M	SPR	IrFu, IRI	300–350/every 3 weeks, 180/biweekly	C2	35 (10.7)	18 (5.5)	P
Parodi *et al.*	USA, U	III	110 (52.2)	60	M	SPR	FOLFIRI, mIFL, CapeIRI	125 or 180/ biweekly, 250/every 3 weeks	U	42 (38.2)	/	P
Ferraldeschi *et al.*	UK, mainly C	U	92 (69.0)	63	S	SPR	FOLFIRI/ IRI—VEGF inhibitor, CapeIRI, UFT-Lv- IRI- OX	180/biweekly	N2	16 (17.4)	6 (6.5)	P
Toffoli *et al.*	Italy, C	I	250 (64.8)	61	M	PYRS	FOLFIRI, mFOLFIRI	180/biweekly	N2	35 (14.0)	21 (8.4)	P
Kweekel *et al.*	Netherlands, C	III	218 (62.8)	61	M	PYRS	CapeIRI, IRI	250 or 350/every 3 weeks	N2	/	48 (22.0)	R
Ruzzo *et al.*	Italy, C	U	146 (55.6)	61	M	SPR	FOLFIRI	180/biweekly	N2	34 (23.0)	/	P
Côté *et al.*	France, C	III	89 (U)	U	M	SPR	FOLFIRI	180/biweekly	N2	19 (21.3)	/	P
Massacesi *et al.*	Italy, C	II	56 (52.7)	64	M	Sequencing	IRI- raltitrexed	80/weekly	N2	4 (7.1)	10 (17.9)	P
Carlini *et al.*	USA, mainly C	II	62 (55.0)	61	M	SPR	CapeIRI	100 or 125/weekly	N2	2 (3.3)	20 (32.3)	P
Rouits *et al.*	France, C	U	73 (61.1)	62	S	PYRS	FOLFIRI, mFOLFIRI	85/weekly or 180/biweekly	N2	22 (30.1)	13 (17.8)	R
Marcuello *et al.*	Spain, C	U	95 (63.3)	68	U	SPR	IRI-Tomudex, IRI-5FU-LV, IRI-5FU, IRI	80/weekly or 180/biweekly or 350/every 3 weeks	C2	/	29 (30.5)	P

Abbreviations: C, Caucasian; CAPe, capecitabine; C2/3, CTCAEv2/3, Common Terminology Criteria for Adverse Events version 2/3; IRI, irinotecan; LV, leucovorin; M, multicentre; N2/3, NCI-CTC v2/3, National Cancer Institute-Common Cytotoxicity Criteria version 2/3; OX(A), oxaliplatin; P, analysis was planned prospectively; PYRS, pyrosequencing; R, analysis was planned retrospectively; S, single centre; SPR, sizing of PCR products; Sequencing, other DNA sequencing methods; TEGAF, UFT/LV; U, unknown; 5FU, 5-fluorouracil; UFT, uracil/tegafur; VEGF, vascular endothelial growth factor; XEL, xeloda. a = median or mean age.

Table 1.11 - Studies assessing the effect of UGT1A1*28 polymorphism on irinotecan toxicity. Adapted from Liu, 2014 [184].

1.8.4.3 Adenosine-triphosphate binding cassette (ABC) transporters

ABC transporters are adenosine-triphosphate (ATP) dependent transmembrane proteins responsible for the movement of a number of molecules across cell membranes. Irinotecan, SN-38, and their metabolites are all excreted by ABC transporters via a hepatobiliary pathway into the faeces and urine [186]. ABC transporters are classified into 7 groups (ABCA to ABCG) based on the topology of their transmembrane domains [187]. ABCB1 (P-glycoprotein), ABCC2 (canalicular multi-specific organic anion transporter), and ABCG2 (breast cancer resistance protein) are the most studied of these and believed to be the most influential in the excretion of irinotecan and its metabolites [164, 188].

Published data suggest a role for the ABC transporters in predicting irinotecan toxicity. In a study of 167 patients with metastatic CRC ABCC5 and ABCG1 polymorphisms were a predictor of severe diarrhoea following irinotecan therapy. ABCC1, ABCC2, ABCC5, and ABCG2 were shown to predict neutropenia in the same study [189]. There are conflicting data on the effect variations in these proteins have on the efficacy of irinotecan. Two variants of the *ABCG2* gene were found to predict response to FOLFIRI treatment in 71 patients with metastatic CRC [190].

However, tissue microarray assessment of ABCB1 and ABCG2 protein expression in the primary tumours of 566 patients with metastatic CRC, recruited in the CAIRO study, found no correlation between expression and irinotecan response [191].

1.8.4.4 β-glucoronidase

β-glucoronidase allows the reactivation of SN-38G by cleavage of the glucuronide group and, although also present at the colonic epithelium due to its release from bacteria, it accumulates in the tumour microenvironment due to lysosomal excretion from inflammatory cells and necrotic tumour tissue [192]. Plasmid transduction of CRC cells resulting in membrane tethering and overexpression of β-glucoronidase was found to increase cytotoxicity to SN-38G by up to 80-fold. These finding were confirmed *in vivo* where an enhanced response to irinotecan was confirmed in mice flank grafted with β-glucoronidase overexpressing CRC cell lines [193].

1.8.4.5 Enterohepatic reactivation

Faecal excretion accounts for 64% of the elimination of irinotecan and its metabolites. Most of this is this result of biliary excretion into the lumen of the gastrointestinal tract [186]. Due to the conversion of SN-38G to SN-38 by β-glucoronidase produced by bacteria present in the bowel lumen; including Escherichia coli, Bacteroides species, and Clostridium perfringens; the amount of SN-38 in faeces is higher than seen in bile [194]. Although SN-38 and SN-38G may be reabsorbed to some extent by the intestinal epithelium and re-enter the portal circulation, the accumulation of active SN-38 in the intestinal lumen is believed to contribute to irinotecan induced diarrhoea through direct mucosal damage and the resulting inflammation [195, 196].

1.8.5 Biological agents

Biological small molecule inhibitors are increasingly incorporated in treatment regimens used in the treatment of CRC. They can be categorised by their target protein and currently include: extracellular EGFR receptor inhibitors (e.g. cetuximab and panitumumab); tyrosine kinase inhibitors (e.g. gefitinib, elotinib and lapatanib); and vascular endothelial growth factor (VEGF) inhibitors (e.g. bevacizumab, ramucirumab, regorafenib and aflibercept).

Cetuximab is a chimeric mouse/human monoclonal antibody and panitumumab a human monoclonal antibody. Both target the extracellular side of the membrane bound EGFR receptor directly by preventing the binding of epidermal growth factor and transforming growth factor α to the receptor. This inhibits activation of the PI3K/AKT/MTOR and RAS/RAF/MEK/ERK pathways (see section 1.3.5) and subsequently a number of cell-cell adhesion, DNA synthesis and cellular proliferation pathways associated with carcinogenesis [197]. In an example of individualised treatment, their use is restricted to tumours expressing EGFR that are *KRAS* wildtype. A mutated *KRAS* will continue to trigger downstream signalling even after EGFR inhibition rendering these drugs ineffective in this scenario [198].

Gefitinib and elotinib act of the cytoplasmic side of the receptor by reducing tyrosine kinase activity. This prevents the autophosphorylation and activation of the EGFR receptor required for downstream signalling and pathway activation. None of the drugs in this category are used routinely in the current treatment of CRC [199, 200].

Over-activation of VEGF is a feature of a number of malignancies. VEGF activation promotes angiogenesis, essential to the survival of cancer cells requiring the delivery of oxygen and glucose to meet their high metabolic demand [201]. Bevacizumab is a human monoclonal antibody which inhibits angiogenesis by binding directly to VEGF, forming a complex which is unable to bind to any other receptors. It is the only anti-angiogenic drug approved for first line use in metastatic CRC.

Other small molecule inhibitors are under investigation, with a number now undergoing testing in clinical trials.

1.9 The treatment of colorectal cancer with chemotherapy

The use of chemotherapy regimens based around 5-FU in combination with other chemotherapeutics is now routinely employed in the treatment of qualifying patients with CRC. In the adjuvant setting chemotherapy significantly improves absolute survival compared with surgery alone (hazard ratio 0.62 versus 0.76) [202]. As a result of the clear benefits to overall survival, NICE guidance (CG131) recommends the use of chemotherapeutics in all high-risk Stage II and all Stage III tumours following resection. The use of chemotherapy in Stage IV disease is less well defined but the combination of hepatic resection with chemotherapy was shown to improve outcomes in a retrospective review of 2470 patients [203].

1.9.1 Chemotherapy in advanced colorectal cancer

Advanced disease in this setting refers to patients with high-risk Stage II or Stage III disease who are currently recommended to receive chemotherapy following surgical resection of the primary tumour. A number of trials have sort to clarify the most effective regimen, with FOLFOX favoured as the first line therapy in the UK and FOLFIRI in the United States of America (USA).

The first trial to combine 5-FU with leucovorin, the NSABP (National Surgical Adjuvant Breast and Bowel Project) C-03 study, reported a significant 11% increase in disease free survival compared with treatment with 5-FU combined with the alkylating nitrosourea lomustine and the alkaloid vincristine [204]. Following this IMPACT (International Multicenter Pooled Analysis of Colorectal Cancer Trials) pooled data from 3 randomised trials investigating high-dose 5-FU/leucovorin compared with no adjuvant therapy.

Adjuvant therapy significantly increased three-year disease free and overall survival by 9% and 5% respectively [205]. The intergroup-0089 study then evaluated four of the mostly commonly used combination regimens, including; the Mayo Clinic regimen (20 mg/m2 intravenous (IV) bolus of leucovorin and 425 mg/m2 IV bolus of 5-FU daily for 5 consecutive days repeated every 4 to 5 weeks), and the Roswell Park regimen (500 mg/m2 IV bolus of leucovorin and 500 mg/m2 IV bolus of 5-FU weekly for 6 weeks). This study reported no difference in overall or disease free survival between treatment arms [206]. Finally the GERCOR C96.1 study compared the Mayo regimen with the de Gramont regimen (twice-monthly IV 5-FU/leucovorin) with no statistically significant differences in disease free or overall survival observed between arms. However, the de Gramont regimen was associated with significantly fewer side effects than the Mayo regimen [207].

More recently a number of trials have combined 5-FU with other chemotherapy agents. The MOSAIC trial of 2246 patients compared 5-FU/ leucovorin with 5-FU/ leucovorin Acid/Oxaliplatin, reporting an increase in 3-year disease free survival of 5%. A subgroup analysis within this study also reported an improvement (5%) in overall survival for stage III but not stage II patients [208]. The NSABP C-07 trial similarly reported an increase in 3-year disease free survival rates of 5% with the addition of oxalipatin [209]. Both trials noted significant neurosensory toxicity associated with the use of oxaliplatin but despite this the FOLFOX regimen was widely adopted across Europe. Three major trials have also examined the benefit of combining irinotecan with 5-FU (FOLFIRI). PETACC (Pan-European Trial in Adjuvant Colorectal Cancer) compared FOLFIRI to 5-FU/leucovorin with no significant improvement in disease free survival reported with the addition of irinotecan [210]. These findings were reproduced in the CALGB (Cancer and Leukemia Group B) 89803 and ACCORD (Action Clinique Coordonnées en Cancérologie Digestive) 02 trials [211, 212]. Interestingly, in the USA a large trial performed by the Irinotecan Study Group randomised patients with palliative disease to 5-FU/leucovorin, irinotecan or FOLFIRI. The used of FOLFIRI resulted in a significant increase progression free and overall survival. Tumour response rates were also increased and on this basis FOLFIRI is considered first line therapy in the USA [213].

Neoadjuvant chemotherapy in the context of non-metastatic disease, except for the radio-sensitisation of rectal cancer, is currently not common in clinical practice. The feasibility study has been completed for the FOXTROT trial which randomises patients with T3/4 colonic tumours to preoperative 5-FU, oxaliplatin, leucovorin and panitumumab followed

by surgery and adjuvant chemotherapy, or surgery and adjuvant chemotherapy combined with panitumumab [214]. The trial is currently recruiting in multiple centres across the UK.

1.9.2 Adjuvant chemotherapy for metastatic disease in the liver

The purpose of chemotherapy following the resection of colorectal liver metastases (stage IV disease) is to increase survival by treating occult residual disease. The evidence for adjuvant chemotherapy in this setting is unclear. The FFCD (Fédération Francophone de Cancérologie Digestive) AURC 9002 trial randomised 173 patients to liver resection alone or resection followed by 5-FU/leucovorin but failed to reach significance on its primary endpoint of 5-year overall survival despite a 6% increase in the adjuvant therapy group [215]. The EORTC (European Organisation for Research and Treatment of Cancer) 0923 trial, which randomised to the same treatment arms, again failed to demonstrate any significant changes in overall survival. Both studies were underpowered, but a pooled multivariate analysis did report marginal but significant improvements in both disease free and overall survival [216].

The benefit of adjuvant combination regimens for stage IV liver disease is also unclear. Trials have compared the use of different combination regimens but are missing the important control arm of surgery alone. In one such study 306 patients were randomised to either FOLFIRI or 5-FU/leucovorin. Although median disease free survival was higher in the FOLFIRI group, this difference was not statistically significant (24.7 versus 21.6 months, $p = 0.44$) [217]. Despite the lack of evidence in the literature most clinicians still choose to manage this patient group with adjuvant combination chemotherapy.

1.9.3 Neoadjuvant chemotherapy for metastatic disease in the liver

Neoadjuvant chemotherapy can be utilised to reduce disease volume, allowing the preservation of liver parenchyma and therefore function following resection, and treat micro-metastases not detectable on cross-sectional imaging.

Attempts were made in early phase 2 studies to address the initial safety concerns of treating patients with cytotoxic agents prior to major surgery. Nearly 100% compliance was achieved in patients receiving preoperative chemotherapy, suggesting they are well tolerated. The perioperative morbidity was high, with complications reported in 21-50% of patients, but no perioperative deaths were recorded [218, 219].

Studies have also attempted to define the benefit of neoadjuvant chemotherapy in patients with liver-limited metastatic disease. A retrospective study of 1474 patients presenting with a solitary, metachronoues liver metastases treated by surgery alone (n=169) or surgery with perioperative chemotherapy (n=1302) found an increased rate of complications in those receiving preoperative chemotherapy (37.2% versus 24%, p=0.006) with no improvement in overall survival. In contrast, postoperative chemotherapy was associated with better overall five-year survivals (65% versus 55%, p<0.01) [220].

The international multicentre randomised EORTC Intergroup 40983 trial randomised 364 patients with up to four resectable colorectal liver metastases to 12 cycles of perioperative FOLFOX or surgery alone. Powered for three-year progression free survival, with primary analysis performed on an intention to treat basis, it reported an improvement of 7% (p=0.04) in progression free survival in the chemotherapy group. However, reversible postoperative complications did occur more frequently in patients who received chemotherapy [221]. A more recent update of this trial confirmed the benefit to progression free survival with perioperative chemotherapy but found no difference in overall survival. Despite this, it did recommend that perioperative FOLFOX remain the reference treatment for this group of patients [222].

1.9.4 Chemotherapy for unresectable disease

Chemotherapy may be given to patients with initially unresectable disease, with the aim of bringing them to resection through a reduction in disease volume, or as a palliative treatment to prolong survival and control symptoms. An unresectable primary tumour is unlikely to change significantly with systemic treatment, but a proportion of patients with colorectal liver metastases will have such a significant treatment effect that their disease may become technically resectable.

Conversion to resection is estimated to be possible in 6-60% of patients, with the large variation reflecting many factors, including the local unit approach to chemotherapy and surgical resection, in addition to patient and disease factors [130]. The evidence for this management option is promising; five-year survivals for patients converted to resection are 35-50%, similar to those who underwent resection at presentation [223]. This was confirmed in a more recent randomised trial, patients were allocated to FOLFIRI/cetuximab or FOLFOX/cetuximab with two monthly imaging to reassess resectability as part of the CELIM study. Patients converted to resection showed favourable outcomes with a 46% five-

year overall survival rate [224]. Disease recurrence in this population is high (94%) but repeat resection is often feasible and can have a significant impact on survival [225].

NICE currently recommends the use of FOLFOX (with cetuximab if appropriate) as first line treatment for all patients with unresectable liver-limited metastatic colorectal cancer; FOLFIRI is reserved for second line treatment. The efficacy of the two regimens is believed to be equivocal in patients with initially unresectable liver disease, a survival difference of approximately 1 month (21.5 versus 20.6 months) was reported in a two arm randomised cross-over study of FOLFIRI then FOLFOX versus FOLFOX then FOLFIRI respectively. However, FOLFIRI has been associated with increased toxicities, attributed to irinotecan, including diarrhoea and neutropenia [226].

1.9.5 Biological therapy in metastatic colorectal cancer

A number of trials have now investigated the use of monoclonal antibodies to EGFR and VEGF in the treatment of CRC.

1.9.5.1 Cetuximab

Cetuximab targets the EGFR receptor and has been the subject of a number of phase III clinical trials in combination with standard chemotherapy regimens. The large EPIC trial aimed to determine whether adding cetuximab to irinotecan prolonged survival in 1298 patients with metastatic colorectal cancer who had failed therapy with 5-FU and oxaliplatin. Cetuximab added to irinotecan significantly improved progression free survival (Hazard ratio 0.7; P<0.0001) and recurrence rate (16.4% v 4.2%; P < .0001) compared with irinotecan alone. Despite this, there was no difference to overall survival between groups [227].

The randomized phase II OPUS (Oxaliplatin and Cetuximab in First-Line Treatment of Metastatic Colorectal Cancer) study demonstrated that the addition of cetuximab to FOLFOX significantly improved response rate (odds ratio 2.6, p=0.003) and progression free survival (hazard ratio 0.6, p=0.006) time in 309 patients with KRAS exon 2 wild-type tumours [228].

In the same setting, the phase III CRYSTAL (Cetuximab Combined with Irinotecan in First-Line Therapy for Metastatic Colorectal Cancer) trial randomised 1198 patients with EGFR receptor positive unresectable metastatic colorectal cancer to FOLFIRI with or without cetuximab as a first line treatment [229]. No difference was seen in overall survival between groups but a significant increase was seen in tumour response rate in those receiving cetuximab (47% versus 39%, p=0.005) [229]. A retrospective assessment of KRAS status was performed in 1063 patients and confirmed no benefit to cetuximab in the KRAS mutant group, in contrast to the wild type group (response rate 57% versus 39%) [230].

The publication of pooled data from the OPUS and CRYSTAL trials adds power to the findings of each study in KRAS wild type patients, providing some of the most compelling evidence to date. The addition of extended survival data for 845 patients with KRAS wild-type tumours demonstrated that the use of cetuximab with standard chemotherapy led to a significant improvement in overall survival (hazard ratio 0.8, p=0.0062), progression free survival (hazard ratio 0.7, p<0.001) and recurrence rate (odds ratio 2.2, p<0.0001) [231].

1.9.5.2 Bevacizumab

Large observational studies have highlighted the benefit of bevacizumab in the treatment of CRC. One such example is the BRiTE (Bevacizumab Regimens: Investigation of Treatment Effects and Safety) study. This large prospective observational study of 1445 previously untreated patients with metastatic colorectal cancer from the USA classified patients who experienced disease progression into; no treatment post disease progression (n=253), treatment without bevacizumab (n=531), and treatment with bevacizumab (n=642) with reported overall survival rates of 12.6, 19.9 and 31.8 months respectively. Multivariate analyses associated the use of bevacizumab with improved survival (hazard ratio 0.5, p<0.01) [232].

A number of clinical trials have also investigated the benefit of bevacizumab in combination with standard chemotherapy regimens. One of the largest of these compared FOLFIRI alone to FOLFIRI plus bevacizumab in a phase III randomised trial. The addition of bevacizumab significantly increased overall survival by five months (hazard ration for death 0.7, p<0.001), progression free survival by four months (hazard ratio for progression 0.5, p<0.001) and the response rate increased from 35% to 45% in this study of 823 patients [233]. Similar outcomes were illustrated in the Tree-1 and Tree-2 studies which compared various 5-FU/oxaliplatin based regimens with or without the addition of bevacizumab. The

addition of bevacezimab to fluoropyrimidine based chemotherapy increased survival by approximately six months. These studies highlight the benefit of bevacizumab as a first line therapy in the treatment of metastatic colorectal cancer.

Comparisons have also been made between the efficacy of cetuximab and bevacizumab as a first line therapy in patient with metastatic CRC. FIRE-3 compared cetuximab or bevacizumab in combination with FOLFIRI in this setting. They concluded that the proportion of patients who achieved an objective response did not differ significantly between groups. However, FOLFIRI plus cetuximab resulted in significantly longer overall survival (29 versus 25 months, p=0.02) and could be the preferred first-line regimen for patients with KRAS exon 2 wild-type metastatic colorectal cancer [234].

The safety of bevacizumab has also been explored with a meta-analysis of randomised trials highlighting a statistically significant higher risk for eight of the 15 evaluated secondary endpoints including: a four-fold higher risk for hypertension, epistaxis, and gastrointestinal haemorrhage/perforation; a three-fold higher risk for any bleeding events; and an elevated risk for proteinuria, leukopenia, diarrhoea, and asthenia [235]. The use of bevacizumab must therefore be considered on an individual patient basis taking into account their personal risk.

1.9.6 Predicting and modifying response to chemotherapy

There is an extremely variable response to chemotherapeutics, irrespective of the setting in which the treatment is delivered. Variation in the pattern of disease and tumour biology, coupled with the mode of presentation, rapidity of diagnosis and treatment strategy employed may explain some of the differences in response.

The ability to accurately predict the response, or the likelihood of acute toxicity, to chemotherapy would be extremely beneficial, allowing the avoidance of unnecessary over-treatment and the associated side effects and toxicities. If response to a particular drug or combination of treatments could be predicted, then the regimen could be tailored to that individual. The value of KRAS testing in predicting the response to EGFR inhibitors has already been discussed in section 1.8.5, however a number of studies have sort to identify other potential predictive molecular biomarkers of response. These biomarkers are potentially identifiable through the analysis of mRNA, DNA or protein expression in the tumour itself or from the patient's blood, stool, urine or any other accessible material.

The MRC FOCUS (Medical Research Council Fluorouracil, Oxaliplatin and Irinotecan: Use and Sequencing trial) demonstrated that expression of topoisomerase I, as established by IHC, could predict the response to irinotecan containing regimens, with higher expression associated with a more favourable response [236]. The value of assessing UGT1A1 polymorphisms in predicting irinotecan toxicity has already been discussed section 1.8.4, as have the other pathways associated with irinotecan metabolism. Other studies have sort to identify subsets of patients who are more or less likely to respond to specific regimens. For example, it was demonstrated that MSI-H tumours are less likely to respond to 5-FU based regimens [237].

The other approach to improving the efficacy of chemotherapeutics involves modulation of pathways in the tumour associated with either resistance to therapy or the metabolism of chemotherapeutics, allowing a modification of response. Successful adoption of this approach requires, not only the identification of potential candidate targets, but the development of target modulators that can be safely translated to the treatment of patients. Drug resistance to anti-cancer agents is complex and involves several biological processes including: drug uptake, efflux and metabolism; detoxifying and intra-cellular translocation systems; drug target modification; DNA repair processes; and cell cycle control. This variety of possible resistance mechanisms mean it is difficult to translate this approach to clinical practice, as highlighted by the dearth of phase II trials in CRC, despite a number pre-clinical and phase I studies [238]. Indeed, the combination of leucovorin with 5-FU, as discussed in section 1.8.2, is one of the only examples of an enhancer of chemotherapy response that has been incorporated into the routine management of CRC to date.

1.10 Nuclear factor-erythroid 2-related factor 2

Reactive oxygen species (ROS) are the by-products of different human physiological functions and have important functions in essential intracellular signalling pathways. The imbalance or overproduction of ROS produces oxidative stress. To counteract the oxidative or electrophilic stress in cells, human bodies organise an antioxidant response through signalling mechanisms, such as the Kelch-like ECH-associated protein 1 (Keap1)–nuclear factor-E2-related factor 2 (Nrf2)–antioxidant response element (ARE) pathway.

The transcription factor Nrf2 is a member of the CNC-bZIP family. Often referred to as the master regulator of cytoprotection, Nrf2 is at least partially responsible for the regulation of an array of genes associated with intracellular redox balance, phase II detoxifying genes and drug transportation. These defensive mechanisms increase the chance of a cell surviving chemical or oxidative stress and allow the detoxification of potentially harmful drug metabolites [239]. Nrf2 has also been associated with the regulation of energy metabolism, inflammation and cellular proliferation [240].

1.10.1 Regulation of the Nrf2 pathway

Under basal conditions Nrf2 expression is controlled at the post-transcriptional level by its interaction with Keap1, which sequesters Nrf2, targeting it for ubiquitination and rapid proteasomal degradation. As a result of this mechanism, Nrf2 is a high turnover protein with a half-life of less than 20 minutes, making detection difficult under basal conditions. Studies have established that Nrf2 binds to the dimeric Keap1 via two motifs, the 'DLG' and 'ETGE' motifs, which have a low and high binding affinity respectively [241]. This two-site binding positions the lysine residues in the α-helix between the 'DLG' and 'ETGE' motifs in the correct orientation for ubiquitination by the Cullin-3–ring-box protein 1 E3 ubiquitin ligase. Consequently, ubiquitinated Nrf2 is released from Keap1 and degraded by the proteasome and free Keap1 is regenerated, maintaining Nrf2 homeostasis in the basal state [242].

Under conditions of stress the interaction of Keap1 with Nrf2 is disrupted and the transcription factor rapidly accumulates in the cell, translocates to the nucleus and enables the transcription of downstream genes. Keap1 is a cysteine-rich molecule well adapted to act as a sensor for cellular stress; oxidative and electrophilic species can modify the sulfhydryl groups of Keap1, altering its confirmation. This conformational change results in

detachment of the 'DLG' site and a subsequent alteration in the orientation of Nrf2, preventing its targeting for ubiquitination [243]. Keap1 molecules rapidly become saturated with Nrf2 and newly synthesised Nrf2 is free to translate to the nucleus.

Once in the nucleus Nrf2 induces a number of cytoprotective genes containing a common ARE sequence in their promoter regions, including hemeoxygenase-1 (HO-1) and NAD[P]H:quinone oxidoreductase-1 (NQO1) [244, 245]. In order to bind to the ARE, Nrf2 must form a heterodimer with other bZIP factors, including the Maf proteins. This results in the recruitment of coactivator proteins and transcription of ARE genes [239].

A number of other signalling pathways have been implicated in the regulation of Nrf2, most involve protein kinases and phosphorylation of Nrf2. For example, activation of the PI3 kinase pathway is believed to induce Nrf2 expression at the genetic and protein level [246-248]. Mutation of the proto-oncogene KRAS, resulting in its constitutive activation, has also been demonstrated to increase Nrf2 expression [249-251]. Many of these pathways are believed to be independent of Keap1, but their effects on Nrf2 signalling are relatively modest compared with Keap1 mediated regulation.

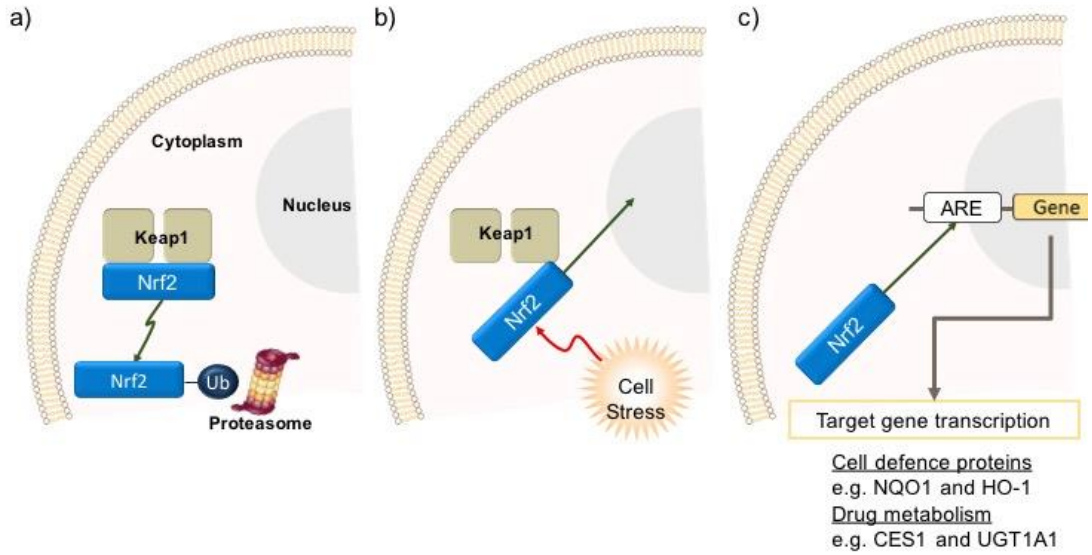

Figure 1.5 – The Nrf2 pathway. (a) Under basal conditions, Nrf2 is bound to Keap1, which targets Nrf2 for ubiquitination and subsequent proteosomal degradation. (b) Under conditions of oxidative stress, the interaction between Nrf2 and Keap1 is disrupted and Nrf2 is no longer targeted for degradation and is free to translocate to the nucleus. (c) In the nucleus Nrf2 dimerises with partners including small Maf proteins and binds to the ARE, mediating the transcription of cytoprotective genes. (Ub = ubiquitin)

1.10.2 The protective role of Nrf2

Activation of Nrf2 can offer protection against the effects of a number of diseases, including cancer. Induction of Nrf2 has been studied in neurodegenerative conditions such as Parkinson's disease and Huntington's disease, multiple sclerosis, diabetes, heart disease, kidney diseases, lung disorders and liver diseases [252]. In a phase II, double-blind, randomised, placebo-controlled trial of 227 adults with diabetes and chronic kidney disease pharmacological Nrf2 induction improved glomerular filtration rates [253]. However, a higher rate of cardiovascular events in the treatment group prompted early termination of the phase III trial [254]. Given its role in drug metabolism, detoxification and excretion it is unsurprising that induction of Nrf2 has also been demonstrated to protect against drug induced liver injury [255]. This could be particularly relevant to the study of chemotherapeutics, many of which cause significant hepatotoxicity.

Multiple studies comparing Nrf2 knockout to wild-type mice describe the benefits of Nrf2 signalling in chemoprevention. A 2-fold increase in the incidence of gastric cancer was

noted in Nrf2 knockout mice after the administration of the carcinogen benzo[a]pyrene [256]. These findings have been replicated in similar studies focusing on bladder cancer caused by N-nitrosobutyl(4-hydroxybutyl)amine [257] and skin cancer induced by 7,12-dimethylbenz[a]anthracene/TPA [258]. In CRC, Nrf2 knockout mice were found to be more susceptible to colitis induced by dextran sulfate sodium (DSS), a risk factor for CRC [259, 260]. This was explored further by co-dosing mice with DSS and the carcinogen azoxymethane, confirming that Nrf2 knockout mice had an increased incidence, multiplicity and size of all colorectal tumours in comparison to wild-type mice. The proportion of these tumours found to be adenocarcinomas was significantly higher in knockout (80%) than wild-type (29%) mice [261].

The cancer-preventative role of Nrf2 is attributed to its ability to induce, not only phase I and phase II drug-metabolising enzymes, but also antioxidant systems to optimise the capacity of the host to detoxify carcinogens, limit the formation of ROS and prevent DNA damage by the secondary metabolites formed by ROS.

1.10.3 The exploitation of Nrf2 by malignant tumours

In contrast to the acute physiological upregulation of Nrf2 in response to cellular stress, in neoplasia there is evidence for increased basal activation of Nrf2. Increased Nrf2 expression has been noted in tumour tissue taken from patients with head and neck cancer [262], lung cancer [263], gall bladder cancer [264], ovarian cancer [265], osteosarcoma [266], breast cancer [267], bladder cancer [268], gastric cancer [269], pancreatic cancer [270] and colorectal cancer [271]. Many of these studies demonstrate poor outcomes and resistance to chemotherapy with increased Nrf2 expression. *In vitro* and *in vivo* data reflect the findings of these observational patient based studies. In CRC specifically, small-interfering RNA (siRNA) or short-hairpin RNA knockdown of Nrf2 reduced cancer cell viability and tumour growth and increased sensitivity to 5-FU *in vitro* and *in vivo* respectively [272, 273].

A number of mechanisms could account for the increased expression of Nrf2 observed in malignant tissue. Loss of function somatic mutations in Keap1 were found to be relatively common in solid malignant tumours. An analysis of 499 cancer tissues from lung, breast, colon, stomach, liver, larynx and prostate by single-strand conformation polymorphism analysis detected somatic mutations of Keap1 in gastric (11.1%), hepatocellular (8.9%), colorectal (7.8%), lung (4.6%), breast (2.0%) and prostate (1.3%) carcinomas. Allelic losses

of the Keap1 locus were identified in 42.9% of cancers with Keap1 mutations, but no NRF2 mutations were detected in these cancers indicating that Keap1 and Nrf2 mutations are mutually exclusive. Detected mutations tended to cluster in areas coding for Nrf2 binding sites and are therefore likely to result in increased Nrf2 expression [274]. Mutations of Nrf2 itself have also been reported in lung (8%), head and neck (13%), oesophageal (11%) and skin (6%) cancer. In a study of 1145 cancer tissues nearly all of these mutations were found within or near the ETGE and DLG motifs, again preventing the binding of Nrf2 to Keap1 [275]. Epigenetic modifications of Keap1 have also been demonstrated to decrease its expression. A gene sequencing study of ten CRC cell lines and 40 patient samples confirmed aberrant promoter methylation of Keap1 in 80% of the cell lines and 53% of tumour samples, resulting in decreased expression of Keap1 and a subsequent increase in the expression of Nrf2 [276].

Nrf2 serves a major function in oxidative stress-related disease and has thus been considered a therapeutic target. By contrast, persistent activation of Nrf2 has been shown to increase proliferation, reduce apoptosis and protect against chemotherapeutics in different types of cancer cells. This dual function of Nrf2 raises the question of whether induction or inhibition of Nrf2 is required in cancer therapy.

1.10.4 The role of Nrf2 in irinotecan metabolism

In addition to its effect on cell survival, proliferation and protection against chemotherapy cytotoxicity in cancer, Nrf2 is believed to induce expression of a number of the genes and proteins involved in the metabolism of irinotecan.

Activation of Nrf2 increased mRNA expression of CES1A1 in three cell lines from different primary tumours (HepG2, Caco-2 and HeLa), this induction was lost when Nrf2 was inhibited using siRNA [277]. Similar findings have been reported i*n vivo* with pharmacological induction of Nrf2 significantly increasing the expression of CES1G mRNA in murine liver tissue excised 24 hours after dosing [278]. In addition to exerting control on the inducible expression of the CES, Nrf2 may also influence the basal expression. CES1 expression was 50% lower in liver tissue from Nrf2 knockout mice in comparison to their wild type counterparts on proteomic assessment using mass spectrometry [279]. Given that Nrf2 can alter the expression of CES, required for hydrolysis of irinotecan to SN-38, it is reasonable to hypothesize that induction of Nrf2 could increase the response to irinotecan through increased conversion to the active metabolite.

Balanced against this is the effect of Nrf2 on the expression of CYP3A, UGT1A1 and the ABC transporters, all of which can theoretically reduce the beneficial effects of irinotecan through conversion to inactive metabolites or increased excretion of SN-38. Members of the CYP3A family were found to be basally regulated by Nrf2 *in vivo*, as evidence by the significant reduction (50%) seen in the proteomic assessment of liver tissue from Nrf2 knockout mice compared with wild-types [278]. UGT1A1 was induced in HepG2 cells following pharmacological activation of the Nrf2 pathway, with this effect blocked when Keap1 was overexpressed or Nrf2 inhibited by siRNA [280]. In the CRC cell line Caco-2 induction of UGT1A1 was at least in part attributable to activation of the Nrf2 pathway [281]. *In vivo* data confirm these findings, demonstrating that UGT1A1 mRNA expression was increased in the hepatic parenchyma and small intestine of mice dosed with activators of the Nrf2 pathway. It was noted that UGT1A1 was inducible by four other transcription factors, implying the control of UGT1A1 to involve multiple pathways [282]. Finally, quantitative investigation of the induction of human ABC transporters mRNA by a redox-active compound tert-butylhydroquinone (tBHQ) in HepG2 cells revealed increased mRNA expression with Nrf2 induction. Following siRNA inhibition of Nrf2 tBHQ-induced mRNA levels of ABCC2 and ABCG2 were significantly suppressed, suggesting this is a Nrf2 dependent induction [283].

Given its multiple roles in cytoprotection and drug metabolism, particularly in the context of the pro-drug irinotecan, the effect of Nrf2 modulation on irinotecan efficacy in the management of CRC is unpredictable. Especially considering the relationship between host and tumour, where hepatic activation of irinotecan may play a significant role and Nrf2 induction may protect against the complications and side effects of therapy, including hepatotoxicity and chemotherapy induced colitis.

1.10.5 Pharmacological induction of Nrf2

The activation of Nrf2 by dietary compounds has been traditionally considered to prevent cancer development. Natural phytochemicals; including sulforaphane (found in broccoli), curcumin, resveratrol, lycopene, and carnosol; have been reported to induce Nrf2 and act as chemoprevention agents in different human and animal models [284, 285]. Ten of 14 dietary compounds were reported to induce Nrf2 in HepG2 cells with a combination extract made of coffee, thyme, broccoli, rosemary, turmeric and red onion fed orally to mice inducing Nrf2 activity in lung and adipose tissue [284].

As a result of this protective effect of Nrf2 activation in cancer prevention and chronic illness a number of synthetic Nrf2 inducers have been described. The synthetic triterpenoid methyl-2-cyano-3,12-dioxooleano-1,9-dien-28-oate (CDDO-me) is the most potent of these, inducing Nrf2 at nanomolar (nM) concentrations. CDDO-me is an analogue of oleanolic acid, believed to induce Nrf2 through competitive binding to Keap1 [286]. Naturally occurring triterpenoids like oleanolic acid are weak Nrf2 inducers and CDDO-me was one of a number novel derivatives synthesised to increase this effect [287]. Multiple studies have confirmed the effectiveness of CDDO-me as a potent and relatively specific inducer of Nrf2 at nM concentrations *in vivo* [278, 288], resulting in its administration to patients with diabetes and chronic kidney disease in the context of a phase III trial. Unfortunately the trial had to be abandoned die to cardiac complication in high-risk patients, but it did confirm significant improvements in glomerular filtration rates in patients receiving CDDO-me [254].

At higher concentrations CDDO-me has been reported to lose its specificity to Nrf2 and can target other proteins and pathways, including Actin-related protein 3 and other components of the cytoskeleton, and inhibit cell proliferation. Micromolar (uM) concentrations of CDDO-Me can even selectively induce apoptosis in cancer cells by targeting a number of key regulatory proteins and pathways that are frequently constitutively activated or overexpressed in cancer cells [289]. A phase I clinical trial administered CDDO-me to patients with a variety of solid malignancies and lymphomas, finding it was well tolerated to doses of 900mg/ml and anecdotally noting complete response in one patient with lymphoma and partial response in a patient with an anaplastic thyroid cancer [290].

1.10.6 Pharmacological inhibition of Nrf2

As initial studies suggested a beneficial effect in Nrf2 induction there are less data focusing on the therapeutic benefit of Nrf2 inhibition. A few compounds are reported to be Nrf2 inhibitors in the literature. Chrysin (5,7-dihydroxyflavone) is a natural flavonoid that is found in many plant extracts. In doxorubicin resistant hepatocellular carcinoma cell line (BEL-7402/ADM), it significantly reduced Nrf2 expression by downregulating the PI3K-Akt and ERK pathways. Chemosensitivity was also improved through downregulation of Nrf2-downstream genes including HO-1 [291]. Luteolin (3',4',5,7-tetrahydroxyflavone) is a polyphenolic flavonoid found in high concentrations in celery, green pepper, and parsley. In a study using a cell-based ARE-reporter assay, luteolin was found to be a potent Nrf2 inhibitor and significantly sensitized A549 lung cancer cells oxaliplatin, bleomycin, and doxorubicin [292].

Perhaps one of the most widely studied Nrf2 inhibitors, brusatol is a quassinoid extracted from the aerial parts of the *Brucea javanica* plant. Fruit and seed oil from *Brucea javanica* was originally used in Chinese medicine for the treatment of various ailments, including a number of malignancies, before brusatol was isolated from the aerial parts of the plant [293]. Studies suggest brusatol is a potent inhibitor of Nrf2, selectively reducing Nrf2 at the protein level through enhanced ubiquitination and degradation of Nrf2 at nM concentrations. This resulted in an enhanced response to cisplatin treatment in A549 cells flank grafted into nude mice, with this effect lost in a variant of the same cell line following chronic ectopic overexpression of Keap1, suggesting the enhanced cisplatin response was mediated by Nrf2 [294]. These data were replicated in a mouse model of mutant KrasG12D-induced lung cancer; suppression of the Nrf2 pathway with the chemical inhibitor brusatol again enhanced the antitumor efficacy of cisplatin [249]. The cytotoxic effect of seven quassinoids was also investigated in pancreatic cancer cell lines (PANC-1 and SW1990), with brusatol displaying the lowest half maximal inhibitory concentration (IC50) value [295]. There are currently no published data investigating the effects of brusatol in CRC.

1.11 Murine models of colorectal cancer

Only 5 % of anticancer candidate therapies that enter clinical testing are approved by the Food and Drug Administration for clinical practice, suggesting that current murine models do not faithfully reflect the human disease [296, 297]. Maximising the conversion of potential therapeutic strategies from bench to bedside in the treatment of CRC, by selection and optimisation of the most appropriate murine model, requires an understanding of the options available, including: carcinogen-induced, genetically engineered and tumour implantation murine models.

1.11.1 Spontaneous and chemically induced CRC in rodents

The incidence of spontaneous CRC in rodents is less than 1% [298]. Higher incidences (30-40%) have been reported in in-bred WF-Osaka rats, but none of these developed metastases and many of the tumours showed signs of spontaneous regression [299, 300]. Although these rats may develop carcinoma at an early age, the unpredictability of this model makes it inadequate for routine experimental use. This has resulted in the use of CRC-inducing carcinogens in rodents, the effectiveness of which varies between species and dose used as well as the duration of exposure.

1.11.1.1 Dimethylhydrazine and azoxymethane

1,2-dimethylhydrazine (DMH) and the metabolite azoxymethane (AOM) are methylazoxymethanol (MAM) precursors and the two most commonly used CRC inducing carcinogens. MAM, the carcinogen in cycad flour, yields a methyl diazonium ion that can alkylate macromolecules such as guanine in the liver and colon leading to tumour development [301, 302]. The majority of these tumours contain mutations in the β-catenin gene (*Ctnnb1*) which stabilise β-catenin and increases WNT signalling, driving tumourigenesis [303]. AOM is used more frequently due to increased potency and greater stability, inducing colonic malignancy in rodents when administered repeatedly over 6-8 weeks via subcutaneous (*sc*) or intra-peritoneal (*ip*) injection; assessment of disease burden is undertaken from approximately 30 weeks [304].

AOM administered with DSS can provide a useful model of colitis induced CRC; 100% of Crj:CD-1 mice given a single *ip* injection of AOM followed by a week of oral DSS developed CRC within 20 weeks [305]. This AOM combined with DSS model has proved useful in

studying dietary chemoprevention of CRC by targeting factors that drive inflammation [306].

1.11.1.2 Heterocyclic amines

The heterocyclic amines (HCAs) 2-amino-1-methyl-6-phenylimidazo[4,5-b]pyridine (PhIP) and 2-amino-33-methylimidazo[4,5-f]quinoline (IQ) are genotoxic compounds in cooked meat and fish. HCAs are activated by cytochrome P450s in the liver with conversion of an amino group to a hydroxyamino group. These are further activated by forming esters which induce carcinogenic DNA adducts [307, 308]. PhIP is the most abundant HCA in cooked meat and although it only induces aberrant crypt foci in mice it can cause colonic carcinomas in rats with prolonged administration; 50% of F344 rats fed continuously with high doses of PhIP for 52 weeks developed CRC [309]. In a recent study only 35% of the same animals developed carcinomas after 20 weeks of PhIP ingestion [310].

Interestingly many of the genetic mutations associated with colon cancer in humans are not noted in PhiP induced tumours, notably K-Ras and P53, an important consideration when undertaking studies on gene targeting therapies or interactions [311].

1.11.1.3 N-Methyl-N-nitro-N-nitrosoguanidine and N-methyl-N-nitrosourea

N-Methyl-N-nitro-N-nitrosoguanidine (MNNG) and N-methyl-N-nitrosourea (MNU) are DNA alkylating agents that can induce malignancy in any organ through direct action. By transferring a methyl group to nucleobases these direct carcinogens lead to the accumulation of genetic mutations that can result in the development of carcinomas. Originally reported to cause gastric carcinoma following oral administration [312] it was later found that intra-rectal instillation caused carcinoma in the distal colon and rectum of rodents [313, 314] with 43% of F344 rats developing rectal cancers after 20 weeks of weekly administration [313]. Increasing the dosing frequency to three time a week in the same rat strain increased tumour incidence to 78% [315].

1.11.1.4 Advantages, Limitations and Applications

Many of the cellular and biochemical defects found in human carcinomas are present in chemically induced rodent models making them advantageous in the study of gene–environment interactions and chemoprevention [316]. For example, the administration of the cyclooxygenase (COX)-2 inhibitor NS-398 to AOM-treated rats significantly reduced the

formation of preneoplastic lesions [317]. More recently diet induced obesity was found to promote CRC development in an AOM induced murine model [318].

The use of chemically induced CRC for therapeutic testing is limited. Assessment of disease burden is often only possible at necropsy with advanced imaging techniques required for longitudinal disease monitoring. Long latency periods of up to 52 weeks mean prolonged follow up periods are required and the formation of metastases is rare making this model unsuitable for studies on advanced disease [319, 320]. Significant variation in tumour development has been noted between murine strains and standardised dosing regimens are required to allow comparisons between studies [305, 321]. Despite their limitations, these models remain useful in improving our understanding of the molecular events underlying colorectal carcinogenesis and in the testing of chemo-preventative agents. (Table 1.12)

Carcinogen	Example dosing regimens	Common Applications	Advantages	Limitations	Examples in literature
AOM and DMH	10mg/kg AOM injected weekly for 6 weeks	Chemoprevention Assessing the influence of carcinogens Dietary influence on tumour development	Inexpensive Heterogeneous tumours Similar mutations to those seen in human CRC (e.g. APC, β-catenin and K-Ras) Can combine with genetically predisposed animals to reduce lead time	Long lead times (e.g. 30 weeks) Rarely metastatic Limited options for non-invasive imaging (CT / MRI) Large variations in tumour development between mouse strains	Chemoprevention with COX2 inhibition Effect of obesity on CRC incidence
AOM + oral DSS	Single dose AOM then 5 ml 2.5% (wt/vol) DSS solution orally per day for a week	Studies of colitis induced CRC	Low mortality Reliable (high tumour incidence) Shortened lead time (e.g. 20 weeks)		Dietary chemoprevention with cinnamon
PhIP	Commonly Fischer 344/NHsd rats fed 0.2 g/kg daily for 20-52 weeks	Chemoprevention of HCA induced tumours	Inexpensive Heterogeneous tumours	Lack many of the mutations found in human CRC (e.g. K-Ras) Unreliable / low incidence Very long lead times (52 weeks)	Dietary chemoprevention with tomato and broccoli
MNNG and MNU	MNU 0.5ml of 0.4% rectal instillation 3 x per week	Chemoprevention Dietary influence on tumour development	Inexpensive Heterogeneous tumours	Direct action; needs rectal instillation Variable incidence (only 43% F344 rats dosed weekly for 20 weeks)	Chemopreventive effect of benzoic Acid

Table 1.12 - Summary of carcinogen induced murine models of colorectal cancer. Adapted from Evans, 2016 [322].

1.11.2 Genetically Engineered Mouse Models (GEMMs)

The mutations that mediate colonic carcinogenesis were discovered through studies on the hereditary CRC syndromes FAP and HNPCC. Mice with mutations in these genes have revealed phenotypes that are similar to human colon cancer and polyposis.

1.11.2.1 Adenomatosis Polyposis Coli mouse (models of FAP)

As discussed in section 1.4.2, the APC gene was identified on chromosome 5q as one of the genes commonly deleted in FAP [323]. It is associated with activation of the Wnt pathway, one of the key events in polyp initiation [324]. The first report of a mutation of *Apc* located on chromosome 18, the mouse homologue of human APC, occurred randomly in C57BL/6 mice treated with ethylnitrosourea. Multiple intestinal neoplasia (Apc^{Min}) mice carry a truncation mutation at codon 850 of the *Apc* gene. They develop tumours throughout their gastrointestinal tract, more frequently in the small intestine. Invasive cancers are reported in older mice but without metastases [325]. Most *Apc* mutant mice die young (4–5 months) as a result of anaemia and cachexia, often before developing invasive cancers.

Several *Apc* mutations have been constructed using gene knockout technology in embryonic stem cells, allowing investigation of the complex genetics associated with the development of CRC. Both $Apc^{\Delta 716}$ and Apc^{1638N} mice have a truncation mutation of *Apc* and develop histologically identical polyps. However, $Apc^{\Delta 716}$ knockouts typically develop approximately 300 polyps in comparison to 3 in Apc^{1638N} mice [326, 327]. Both predominantly develop small bowel polyps but the addition of a heterozygous knock down of *Cdx2* in the $Apc^{\Delta 716}$ mouse results in numerous polyps in the distal colon [328].

The malignant potential of *Apc* mutant mice can be modified through the introduction of further genetic mutations. Inactivation of Smad4 through loss of heterozygosity in $Apc^{\Delta 716}$ (*cis-Apc/Smad4*) mice results in the development of locally invasive carcinomas [329]. While an increase in the number and invasive potential of colonic polyps is also noted with a deficiency in the Wnt-target genes EphB receptor family [330, 331]. In contrast, transgenic loss of *Prox1* in the intestinal epithelial cells of Apc^{Min} mice reduces the progression of colonic adenomas to adenocarcinomas-in-situ [332].

1.11.2.2 Mouse Models for Lynch Syndrome

As discussed in section 1.4.1, LS is characterised by mutations in MMR genes; commonly the MutL or MutS homologs MLH1, MSH2 and MSH6. MMR mutant mice are useful in determining how the loss of MMR function results in tumourigenesis. Despite the genetic abnormalities in MMR knockout mice correlating with those in humans there are significant differences in phenotype. Unlike humans with mutations in MLH1, MSH2 and MSH6, heterozygous mice carrying the corresponding mutations do not develop early-onset tumours. However, homozygous *Mlh1, Msh2* and *Msh6* knockout mice are prone to forming malignant tumours, including CRC, but die prematurely due to aggressive lymphomas [333-335]. Mice have been generated with disruptions in all known mammalian MutS and MutL homologues. Combining homozygous mutations for the MMR genes with various *Apc* mutations has allowed the development of mice with multiple early-onset colonic tumours [336].

1.11.2.3 Conditional genetic models of colorectal cancer

Cre-Lox recombination has allowed the conditional inactivation of genes associated with the development of CRC in transgenic mice by flanking the gene with 'Lox-P' binding sites. Cre-recombinase (Cre) recombines these two Lox-P sites, causing the gene to be skipped and preventing its transcription. Conditional inactivation can be used to reduce embryonic lethality or extra-intestinal features which often result in the premature death of the animal.

The first conditional knockout mice were generated by flanking exon 14 of the *Apc* gene. Rectal instillation of recombinant adenovirus expressing Cre resulted in inactivation of both *Apc* alleles in the distal colon. Mice developed an average of 7 adenomas at this site, with 50% developing invasive adenocarcinoma within a year [337]. Cre-Lox technology has subsequently been used to conditionally inactivate a number of the genes associated with the development of CRC.

Combining Cre with specific promoters has allowed its expression to be targeted to the organ of interest. The fatty acid-binding protein (*Fabp*) promoter has been used to target Cre expression in murine colonic and small bowel epithelium with temporal control provided through the administration of doxycycline (*Fapb-Cre mice*) [338]. When *Fabp-cre* mice are crossed with *Apc* conditional knockout mice they develop colonic adenomas, with

half developing adenocarcinomas [339]. More recently the combination of Villin, an actin binding protein expressed mainly in the brush border of epithelia, with Cre has been used to target the expression of many CRC oncogenes or tumour suppressor gene in the murine intestine [340-344].

1.11.2.4 Advantages, Limitations and Applications

GEMMs are most useful in studies of chemoprevention, for example exploring the links between diet and CRC [345]. Such studies are likely to be translational to the clinical setting as they represent the natural history of tumour development in the correct microenvironment. The role of GEMMs in translational research was proven when it was found COX-1 and 2 inhibition significantly reduced polyp burden in Apc^{Min} mice, providing the rationale for treating FAP patients with COX inhibitors [346-348].

The use of GEMMs in pre-clinical drug discovery is more limited due to the following: necropsy is required to assess disease burden unless advanced imaging techniques are employed; the incidence of invasive cancers is unpredictable; they are expensive and time consuming to develop and the development of small bowel tumours and other extra-colonic manifestations limits their life span. Although the formation of spontaneous tumours in immune-competent mice more closely mimics the heterogeneity of CRC in humans, this can be disadvantageous in therapeutic studies as increased variance within groups necessitates large sample sizes to confidently detect significant effects. Additionally, the low metastatic rate means they are not a good mimic of advanced CRC. Conditional gene models have made it possible to generate tumours in a narrow time window and with greater confidence and consequently their use in chemotherapeutic studies may well increase. (Table 1.13)

GEMM model	Examples of variations and modifiers	Common applications	Advantages	Limitations
All		Studying the role of genes involved in carcinogenesis Studies of chemoprevention Assessing the influence of carcinogens Lifestyle / Dietary influence on tumour formation		Limited options for non-invasive imaging (would need CT / MRI capability) Expensive and time consuming to develop Rarely metastases
Apc^{Min} Mice / models of FAP	*Apc*^{1638N} and *Apc*$^{\Delta 716}$ *Apc*$^{\Delta 716}$/Cdx2 *Apc/Smad4* *Apc/Prox1* *Apc/*EphB2-B3		Multiple adenomas, useful for studies of the early events in CRC tumourogenesis Reduced polyp numbers in Apc$^{\Delta 716}$ than seen with Apc^{1638N} Increases polyp number in distal colon in comparison to small bowel Develop locally invasive cancers Develop adenocarcinomas Develop invasive intestinal adenomas	Most tumours located in small bowel Die early of anaemia / cachexia Rarely invasive cancers Develop ampulla of Vater adenocarcinomas Carcinoma-in-situ only
HNPCC mice	**MutS homologues:** *MSH2*$^{-/-}$ *MSH6*$^{-/}$ **MutL homologue:** *MLH1*$^{-/-}$		High tumour incidence High tumour incidence Live longer than *MSH2*$^{-/-}$ (up to 18 months) High MSI	Develop life-limiting aggressive lymphomas Develop endometrial carcinoma Less MSI than *MSH2*$^{-/-}$ Develop life-limiting aggressive lymphomas and skin tumours
Combination	*Mlh1/Apc1638N* mice		Early-onset of intestinal tumours No increase in incidence of lymphomas	
Conditional GEMMs	*APC*$^{flox/flox}$ Targeted promoters (e.g. Villin-Cre and Fapb-Cre)		Allow studies of mutations that would otherwise result in embryonic lethality Reduce premature deaths associated with extra-intestinal manifestations Temporal control possible by drug administration (e.g. tamoxifen, doxycycline) Use tissue specific promoters in intestinal mucosa to target gene knockout Some invasive adenocarcinomas seen Can be used to target specific tumour suppressor or oncogenes (e.g. *k-Ras, APC, MSH2)*	Requires rectal instillation of recombinant adenovirus expressing Cre

Table 1.13 - Summary of genetically engineered mouse models of colorectal cancer. Adapted from Evans, 2016 [322].

1.11.3 Tumour Implantation Models

CRC cells have been implanted in mice since the 1960s; the simplicity and relatively low cost of this model make it popular in the testing of novel therapeutics. Immortalised human CRC cell lines are commercially available for orthotopic, intra-portal, intra-splenic or intra-hepatic implantation into nude or severe combined immune deficiency (SCID) mice. As a result of prolonged *in vitro* propagation, cell lines may not recapitulate the inherent heterogeneity of spontaneous CRC and patient derived xenografts (PDX) have been used to overcome this problem. Establishment rates of 67%-77% are reported for subcutaneous grafting using this method and the resulting tumours in nude mice have been found to maintain the genetic and molecular profile of the patient tumours they were derived from [349, 350]. This approach is labour intensive and requires access to human CRC tissue.

The development of immortalised murine CRC cell lines, usually through chemical induction, has allowed the utilisation of syngeneic models in preclinical research. This involves the implantation of cell lines originally derived from a particular strain of rodent back into an immune-competent rodent of the same strain, allowing testing of immune-therapies. Common examples include Ct26 cells in BALB/c mice [351-356], MCA38 cells in C57BL/6J mice [357, 358], CC531 cells in Wag/Rij rats [359] or DHD/K12-TRb cells in BDIX rats [360]. The rodent species used in these studies are usually cheaper and more robust than their immune-deficient counter-parts, reducing costs.

1.11.3.1 Subcutaneous grafts

The most commonly utilised model involves the subcutaneous inoculation of a suspension of CRC cells into the flank of a mouse. The main advantage of this model is its simplicity, allowing screening of candidate therapies in large numbers with longitudinal measurement of tumour growth possible via caliper measurements. The major disadvantage is the micro-environment in which the tumour develops, which is markedly different from that of the colon. As interactions between the host environment and the tumour graft can determine tumour cell expression profiles, growth rates, tumour angiogenesis and metastatic behaviour the true translational benefit of this model may be limited. Metastatic liver disease has not been reported in subcutaneously grafted rodents [361-364] limiting their use in studies of advanced CRC treatment or cell migration and invasion. Lung metastases have been reported from subcutaneously implanted primary cells derived from advanced

human CRC tissue and from cell lines established through serial propagation of tumours arising in GEMMs [365, 366].

1.11.3.2 Orthotopic implantation

Orthotopic implantation refers to the grafting of tissue or cells to their natural position, for a murine model of CRC this would involve either the injection of a suspension of tumour cells or implantation of a fragment of tumour into the colon or rectum. This can overcome the problems associated with tumour development in an artificial micro-environment and allows replication of tumour invasion, vascular spread and metastasis to distal organs. It is therefore one of the truest mimics of the progression to advanced CRC in humans. For caecal implantation a midline laparotomy is performed aseptically under general anaesthesia, the caecum is exteriorised and a suspension of tumour cells injected into the bowel wall or a small fragment of tumour grown in another animal sutured onto it after lifting or damaging the serosa [367, 368]. Transanal injection of tumour cells has also been utilised as a model of rectal cancer, avoiding the need for laparotomy. This method again requires general anaesthesia, followed by anal dilatation with blunt forceps and the injection of a suspension of cells into the rectal mucosa [369, 370].

Metastatic rates vary depending on the cell line, site of implantation and murine strain. One of the first studies utilising this method reported the development of metastasis in 65-75% of C57BL/6J mice 8 weeks after the intra-mural caecal injection of MCA38 cells [371]. A more recent study of immune-deficient mice orthotopically grafted with tissue fragments grown subcutaneously from 12 different human CRC cell lines found primary tumour uptake rates and metastatic potential varied significantly between cell lines. Six cell lines (KM20L2, HCT116, HCT15, SW480, SW620 and Colo320DM) had a 100% uptake rate, whereas intermediate uptake rates were observed for Co115 (90%), HCC2998 (88%) and HT29 (69%) and only 40% of mice implanted with CaCo2, WiDr and Co205 developed tumours. Liver metastases were only seen in 20% of mice grafted with SW620 tumours but nodal disease was common across all but two of the cell lines (SW480 and Colo320DM) [372]. Similar uptake rates were seen with HCT116 cells injected into the caecal submucosa using a specially designed micro-pipette technique with 75% developing a colonic primary; of these 100% had nodal disease, 67% hepatic metastases and 50% lung metastases [373]. Primary tumour uptake rates of 65% have also been reported using rectal injection, however only 3.3% developed metastases [374]. An orthotopic model was recently used to

investigate the effect of Weichang'an (a Chinese traditional medicine) and 5-fluorouracil on CRC development, highlighting the role of this model in the validation of candidate therapies prior to considering clinical trials [375].

PDX have also been utilised in a caecal injection model; cell suspensions isolated from five different patients resulted in primary tumours in 92% of NOD-SCID mice. Metastatic rates were not high (27% developed liver metastases and 23% lung metastases) but are similar to those observed in patients. It is noted that the highest tumour establishment rates were seen with tumours derived from patients with node positive disease and poor differentiation. Importantly the generated tumour xenografts maintain the same mutational status as the original patients' carcinoma [376].

Isolation, culture and re-implantation of cells from liver metastases or from primary tumours with the highest metastatic potential improved metastatic rates to 90% in a syngeneic model [377]. This process is time consuming and labour intensive and should be reserved for studies where metastatic disease in essential.

1.11.3.3 Ectopic implantation to sites of metastasis

Approximately 50% of patients with CRC develop liver metastases over the duration of their disease, with poor overall survivals seen in this group [378]. Lung metastases are less common, developing in 5 to 15 % of CRC patients [379]. Increased understanding of the metastatic process and the testing of novel therapies requires models that develop metastases more reliably than seen with orthotopic implantation. Inoculation of tumour cells to the spleen, portal vein or liver parenchyma of rodents can be used to mimic liver metastases, whilst tail vein injection can model lung metastases [380]. Although these models do require a degree of technical skill, high rates of metastatic disease can be achieved with a degree of certainty.

Early attempts at intra-splenic injection of CRC cells generated through primary cell culture of primary or metastatic tumour from eight patients produced varying rates of liver metastases in nude mice sacrificed at 90 days. The rate of liver metastases varied considerably from 16% with one of the cell lines generated from liver metastases to 100% in a number of the other cells developed from rectal primary tumours or liver metastases [362]. Established cell lines give similar metastatic rates with 78% of mice inoculated with HT-29 cells developing macroscopic liver metastases within 6 weeks [381]. Similar success

has been reported with the use of syngeneic cell lines with 100% of C57Bl/6 mice injected with MCA38 cells developing hepatic metastases [382]. Uptake rates can be further improved by injection of cells isolated from liver metastases grown *in vivo* [383]. Splenectomy is often required following this technique to reduce haemorrhage and prevent formation of splenic metastases. A syngeneic model was recently used to assess the combined therapeutic efficacy of ^{188}Re-liposomes and sorafenib on liver metastases, highlighting the role of this model in drug development [384].

Intra-portal injection is technically more challenging but is a good mimic of the venous migration of CRC to the liver. It may be more reliable than intra-splenic injection with metastases reported in 100% of animals [385, 386]. However, a more recent publication highlighted the variability between cell lines with HCT116 cells exhibiting the highest rate of hepatic metastases (90% of animals within 30 days) [387]. A recent study utilising this model demonstrated a reduction in hepatic metastases formation following administration of pyrvinium pamoate [388].

Direct injection of CRC cells or implantation of tumour tissue into the liver parenchyma can reliably produce metastases in both immune-deficient and syngeneic models. This technique is particularly advantageous when a single metastasis or tumour confined to a single lobe is required and was recently utilised to study the effect of FOLFOX on the murine liver in the presence of colorectal metastases [358].

1.11.3.4 Advantages, Limitations and Applications

CRC implantation models offer a reproducible means of screening potential therapies in statistically significant numbers of animals. Before utilising such a model, it is important to consider a number of factors including: the site of implantation, bearing in mind the impact of tumour development outside its natural environment and the importance of metastatic disease; the importance of the immune system to treatment success; the resources and time available for development of the model; and whether the treatment may be dependent on human specific factors, as is generally the case with antibody-based therapies.

Immune-deficient implantation models allow relatively rapid testing of candidate therapeutics on malignancies developed from human cell lines and therefore with human specific genes and proteins. The major disadvantage is the lack of host immunity which

rules out the testing of immune-therapies or the study of immuno-tumoural interactions. Immune-deficient rodents are less robust and more expensive than their immune-competent counterparts. Syngeneic tumour models offer several advantages; they are relatively low cost, more robust and are generally non-immunogenic. However, the tumours express the rodent homologues of human tumour genes and this may limit-testing of targeted therapies. PDX may offer a solution to the lack of heterogeneity seen in established cell lines. Capturing the genetic profile of a patient's tumour in a mouse model will allow validation of potential biomarkers *in vivo* but may also permit assessment of the metastatic potential and drug-response of an individual tumour, allowing therapy to be tailored to that specific case [389].

Subcutaneous implantation allows rapid screening in relatively large numbers with minimal technical expertise. Validation of these results should subsequently be considered in the presence of more advanced or orthotopically implanted disease. Although orthotopic implantation offers the most realistic replication model of the development of CRC it is unreliable with respect to metastases formation. If metastases are essential to the study then intra-splenic, intra-portal or liver parenchymal injection of tumour cells should be considered. (Table 1.14)

Implantation site	Common Applications	Advantages	Limitations	Examples in literature
All	Screening of candidate therapies and chemotherapeutics	Options for longitudinal disease follow up	Reliant on cell lines which may not be as heterogeneous as spontaneous tumours	
Subcutaneous	Screening cytotoxic agents in large numbers of animals	Relatively inexpensive Minimal technical skill required Reproducible / good tumour uptake rates	Tumour develops in an artificial micro-environment, may not translate well Non-metastatic	The anti-tumour effect of simultaneously targeting VEGF and PROK1
Orthotopic	Analysing the pathogenesis of metastases Assessing the effect of therapies on metastases Evaluating drugs that influence the tumour microenvironment Evaluation of tumour stroma Confirmation of the results of subcutaneous grafting	Mimics colon tumour invasion, vascular spread, and metastasis Technically challenging	Metastasis rates depend on cell lines and rodent strains and can be unreliable	Combination of Weichang'an and 5-fluorouracil therapy on tumour growth and metastases
Intrasplenic inoculation	Investigation of therapies for suppression of metastatic disease Assessing the effect of therapies on liver metastases Drug safety (e.g. hepatoxicity in the presence of liver metastases)	Reproducible Mimics vascular spread of colorectal cancer Technically less challenging	Metastasis rates depend on cell lines and rodent strains No primary tumour	Therapeutic efficacy of ^{188}Re-liposomes and sorafenib
Intraportal inoculation	Investigation of therapies for suppression of metastatic disease Assessing the effect of therapies on liver metastases Drug safety	Mimics vascular spread of colorectal cancer metastasis Technically challenging	No primary tumour	Impact of pyrvinium pamoate on colon cancer cell viability
Intrahepatic inoculation	Investigation of therapies for suppression of metastatic disease Assessing the effect of therapies on liver metastases Drug safety	Reproducible Can limit disease to a single lobe / segment if required Technically less challenging	Does not mimic the generally accepted hypothesis of hematogenous spread No primary tumour	FOLFOX induced sinusoidal obstruction syndrome in the presence of metastases
Tail vein injection	Assessing the effect of therapies on lung metastases Studying the pathophysiology of lung metastasis	Reproducible Technically less challenging	No primary tumour	Mechanism of tumour vascularization in lung metastases

Table 1.14 - Summary of tumour implantation models of colorectal cancer. Adapted from Evans, 2016 [322].

1.11.4 In vivo imaging techniques

Although simple caliper measurements are adequate for subcutaneous tumours, advanced imaging techniques are required for assessment of disease burden in other models without necropsy. Imaging live animals reduces the number of animals required for an experiment and provides increased statistical power with each animal functioning as its own control. MRI, CT, PET, single photon emission computed tomography (SPECT), fluorescence imaging (FI), bioluminescence imaging (BLI) and photoacoustic tomography (PAT) have all been used for *in vivo* imaging with each technique suited to a specific application [390]. Direct visualisation of the colonic mucosa via endoscopy has also been utilised for the monitoring of tumour development and growth. Endoscopy may be most beneficial in carcinogen induced models that previously required necropsy for the evaluation of tumour growth [391-393]. CT and MRI are best applied to the detailed anatomical reconstruction of tissues while nuclear imaging techniques (PET and SPECT) allow imaging of radiotracer molecules providing quantitative, longitudinal and functional images of tumour biology [394]. BLI and FI are ideal for the longitudinal assessment of disease burden but lack anatomical details with signals superimposed on a photo of the animal. PAT uses nonionizing laser illumination to generate an internal temperature rise which is converted to pressure waves via thermoelastic expansion. These waves are detected via an ultrasonic transducer and reconstructed to form an image [395]. Anatomical, functional and molecular assessment is possible by combining endogenous and exogenous contrasts. For example, haemoglobin can provide both anatomical and functional assessment such as the speed of blood flow based on endogenous contrast [396]. Exogenous contrast agents such as labelling dyes, nanoparticles and fluorescent proteins have enabled molecular imaging including assessment of tumour growth [397-399].

MRI, CT, PET SPECT and endoscopy do not require implantation of genetically modified cells but they are expensive and user dependent; considerable skill is required for accurate interpretation of results and quantification of tumour growth can be challenging. Additionally, if the study requires frequent imaging then techniques reliant on radiation, such as CT, should be avoided [400]. The time for image acquisition with MRI particularly can also be a problem, with animals requiring prolonged general anaesthesia. Endoscopy is also time consuming (approximately one hour per animal) and carries a risk of bowel perforation. In contrast, FI and BLI offer rapid image acquisition with easy longitudinal disease monitoring but require stable gene transfections of cell lines prior to implantation

with either one of the luciferase family of photo-proteins for BLI or a fluorescent probe for FI. A number of plasmids are now commercially available for this, utilising antibiotic selection to maintain gene expression through co-transfection [401, 402]. A very sensitive charge-coupled device (CCD) detector, super-cooled to -90°C, is then used for detection after visible light is used to excite the subject for FI or after the administration of the substrate luciferin to the subject for BLI. This allows quantification of light emission and therefore disease burden without the need for sacrifice. BLI is limited by loss of signal as light passes through the animal, this can be as much as 10-fold for every centimetre of tissue, while background auto-fluorescence can limit assessment in FI [403]. PAT can offer a solution to this problem by providing higher penetration depths of 5-6cm with various photosensitizers available including fluorescent probes [404].

Multimodal imaging allows images of disease burden acquired by BLI and FI to be superimposed over the anatomical details provided by CT or MRI. However, the limited resources available in most centres mean selection of the most relevant imaging technique remains essential.

1.11.5 Selecting the most appropriate murine model

Selection of the most appropriate murine model is essential in the study of CRC. Understanding the ideal application of each increases the chance of acquiring relevant and translational results. The carcinogen induced murine models and GEMMs are most useful in studies of CRC development and chemoprevention whilst tumour implantation models are preferred for screening candidate therapeutics, with subcutaneous implantation allowing high throughput assessment of drugs for subsequent verification in orthotopic models. If the proposed intervention is designed solely for the treatment of metastatic disease then ectopic implantation to the liver or lungs offers the most reproducible assessment tool. The key is selecting the most appropriate model for each experimental application in order to achieve results translational to CRC and its treatment in humans.

1.13 Summary

CRC is the fourth most common carcinoma and the second leading cause of cancer related death in the UK. Survival is worst for those patients presenting with advanced or metastatic disease. A number of dietary and lifestyle factors have been linked to the development of colorectal cancer including diets rich in unsaturated fats, red meat, excess alcohol, smoking and a sedentary lifestyle. Inflammatory bowel disease also increases the risk of developing CRC.

The understanding of the genetics of colorectal carcinogenesis has improved significantly. The vast majority of colorectal tumours reflect a series of hereditary and somatic mutations in key genes (APC, KRAS, BRAF, DCC and p53). These mutations are most frequently associated with a CIN phenotype and are often acquired in a different order. A subset of tumours are initiated through inactivation of MMR function, which may be through inherited or somatic mutation, or alternatively epigenetic inactivation through hypermethylation (CIMP) leading to MSI-H.

Patients presenting with CRC are assessed and staged through clinical, endoscopic and radiological investigation. Radiological assessment normally consists of CT, PET and, for rectal tumours or further evaluation of liver metastases, MRI. Commonly used staging systems include the Dukes', UICC/AJCC TNM and Jass classifications, with complete pathological staging only possible post-resection. Surgery remains the mainstay of curative treatments but patients may be recommended to neoadjuvant or adjuvant chemo- or radiotherapy based on their disease stage, those with advanced or metastatic disease are normally offered chemotherapy.

Irinotecan is a chemotherapy agent used in the combination treatment of CRC (FOLFIRI), it is often used as a second line therapy in the UK after failure of FOLFOX therapy. It is a prodrug converted to the active metabolite SN-38. A number of proteins including the CES, CYP3A, UGT1A1, ABC transporters and β-glucuronidase are involved in the metabolism and excretion of irinotecan.

The tumour response to chemotherapy can vary significantly between patients and predicting or modifying this response could avoid unnecessary treatment and reduce the side effects or complications of treatment. This may be possible through the identification

and modulation of proteins associated with chemo-protection and drug metabolism. This is particularly relevant to irinotecan where inter-patient variations in any of the proteins associated with its metabolism can have an effect on chemo-response.

Nrf2 is a transcription factor, controlled by the regulatory protein Keap1 in the quiescent state, that can induce expression of many of the proteins associated with irinotecan metabolism. It also activates the ARE genes, associated with cell survival and protection against cellular stress, in addition to having a role in cellular proliferation. Nrf2 is overexpressed in a number of malignancies, allowing them additional protection against cellular stress and perhaps playing a role in chemoresistance. It is feasible that induction of Nrf2 is useful in the protection of non-malignant tissue, reducing the damage done by cellular stress and protecting against DNA damage which can lead to mutations and malignant change. However, in cancer tissue Nrf2 inhibition may reduce cellular survival, proliferation and chemoresistance. The effects of modulation of Nrf2 on cancer cell survival and chemotoxicity are unpredictable, particularly in relation to irinotecan therapy where it could potentially alter metabolism and excretion of the drug.

In order to investigate the translational benefit of potential therapies in the management of CRC and increase the conversion to clinical practice, robust and reproducible *in vivo* models are required. Tumour implantation models are most appropriate for the high through-put investigation of chemotherapeutics and chemo-sensitizers. Orthotopic implantation allows a tumour to be grown in the correct tumour environment with the potential to metastasise to the liver, while bioluminescent imaging provides an option for the longitudinal assessment of disease burden, with each animal acting as its own control.

1.14 Hypothesis and study plan

From review of the literature it is clear that new treatments and modifiers of the response to chemotherapy are required to improve outcomes in advanced CRC, and that modulation of Nrf2 may offer a potential strategy, particularly in the context of irinotecan based therapy. The effects of Nrf2 modulation in this setting are unpredictable and robust *in vivo* modelling is required to increase the chance of translating the findings to clinical practice. In order to attempt to investigate the potential benefits of Nrf2 modulation in the treatment of CRC a number of questions need to be addressed:

1. Is Nrf2 a relevant target for therapy in CRC?
2. Is it possible to modulate Nrf2 expression in CRC cell lines either genetically (using siRNA) or pharmacologically (using CDDO-me and brusatol)?
3. Does genetic or pharmacological modulation of Nrf2 in CRC cell lines effect cell viability and proliferation?
4. Does modulation of Nrf2 in CRC cell lines alter their response to irinotecan based therapy?
5. Can *in vitro* findings be replicated in a murine model of CRC that more accurately represents the development of the disease in humans?
6. Can pharmacological modulation be achieved *in vivo?*
7. Is Nrf2 modulation safe *in vivo?*

In order to attempt to answer these questions the study plan will involve:

1. Development and cloning of stably luminescent CRC cell lines to allow serial *in vivo* imaging and assessment of disease burden.
2. Development of a murine model of CRC that allows longitudinal imaging and quantification of disease.
3. Relative quantification of Nrf2 in matched CRC and normal colonic specimens from patients with stage IV disease.
4. Assessment of Nrf2 expression in CRC cell lines and modulation of its expression by siRNA inhibition of Nrf2 or Keap1 or by the pharmacological inhibitor brusatol and inducer CDDO-me.
5. Investigation of the effect of Nrf2 modulation on CRC cell viability and proliferation *in vitro.*
6. Assessment of the effect of Nrf2 modulation on irinotecan CRC cell line cytotoxicity *in vitro*.
7. Translation of *in vitro* findings into the murine model.
8. Investigation of the effect of brusatol treatment on the proteome *in vivo.*

Chapter 2 – The development of a murine model of colorectal cancer

2.1 Introduction

The ideal murine model would provide an exact recapitulation of human CRC. It should develop spontaneously throughout the colon and rectum, have a high incidence in the animals with a short latency period, follow the same metastatic pattern, occur in immune-competent animals, allow non-invasive monitoring of disease progression and have the same molecular characteristics as the human disease. Perhaps not surprisingly, current animal models fail to fulfil all these criteria, but with advanced imaging modalities, numerous cell lines and improved transgenic modelling methods available there is a growing choice. Selection of the correct model for the individual research question is essential to ensure the timely acquisition of data that answers the study hypothesis.

Specifically for the pre-clinical study of potential novel therapies in the treatment of CRC, a murine model is required that reliably and rapidly develops disease, allows serial longitudinal investigation of malignant burden in a single animal and mimics the disease pattern in humans as closely as possible. This requires a tumour that grows in the correct microenvironment with the potential to metastasise, particularly to the liver. Imaging assessment of disease burden should allow data acquisition from several animals in a short time frame and at a relatively low cost.

Developments in bioluminescent imaging have allowed the detection of a relatively small numbers of cells in rodents and facilitated the assessment of disease burden without necropsy, resulting in a reduction in the number of mice required in experimental studies. Bioluminescence imaging (BLI) is considered superior to fluorescence imaging (FI) in animal studies as the background signal in FI can limit the detection of low cell numbers [403]. BLI also allows detection of signal in a number of animals simultaneously, decreasing the cost and time required for data acquisition considerably when compared with CT or MRI assessment. The main limitation of BLI is light quenching and scattering, significant light absorption can occur as a result of the melanin found in the skin of pigmented mice. Animal fur can also scatter light and attenuate signal and therefore shaving is required in furred animals [405].

BLI relies on the induced expression of the foreign protein luciferase, which is not normally expressed in the cell or organism of interest. Upon exposure to the luciferase enzyme the substrate luciferin is oxidised to the excited-state molecule that emits light. This reaction

requires oxygen and adenosine triphosphate (ATP) and therefore is only possible in viable cells, making luminescence a good marker of the number of live cells [406]. The light emitted from the reaction can be detected using a luminometer, usually utilised in the assessment of cells in culture, or a cooled charge-couple device (CCD) camera for animal studies. Luciferase expression, under promotor control, is frequently introduced into the cell of interest by plasmid transfection, with stability of luciferase expression achieved by antibiotic selection and clonal expansion (figure 2.1).

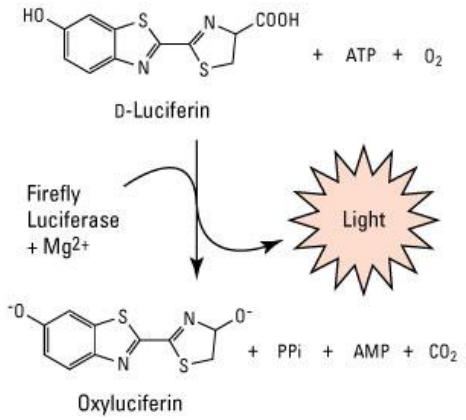

Figure 2.1 – The ATP dependent conversion of D-luciferin to oxyluciferin, catalysed by luciferase, and resulting in the emission of light. (AMP = adenosine monophosphate and PPi = pyrophosphoric acid)

The work in this chapter describes the development of a murine model of CRC through the caecal implantation of luminescent CRC cell lines, allowing the longitudinal assessment of disease burden and the detection of metastatic disease through serial BLI. This model was selected to allow the high-throughput investigation of novel therapies and the optimisation of irinotecan chemotherapy in a murine model that more accurately reflects the pattern of disease in humans, with a primary tumour growing in the correct microenvironment and with the potential to metastasise. A human and murine cell line were both used in model development, with the aim of developing both a nude and immune-competent syngeneic model.

2.2 Materials and methods

2.2.1 Luminescent vectors

Two vectors were utilised in the creation of luminescent CRC cell lines, pGL4.51[luc2/CMV/Neo] (Promega, Southampton, UK) and pSELECT-zeo-LucSh (Invivogen, Toulouse, France). The pGL4.51 vector encodes the luciferase reporter gene *luc2* (Photinus pyralis), which has been codon optimised for mammalian expression. Luciferase expression is under control of the cytomegalovirus (CMV) promotor with a SV40 late poly(A) signal sequence downstream to ensure termination of transcription. The synthetic Neomycin resistance gene (G418) allows selection of successfully transfected cells and the Ampicillin resistance gene is included for bacterial amplification of the vector (figure 2.2).

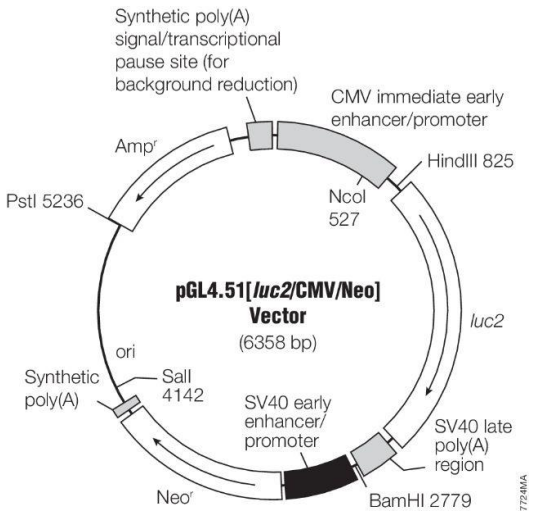

Figure 2.2 – The pGL4.51[luc2/CMV/Neo] vector

The pSELECT-zeo-LucSh vector contains two expression cassettes. The first cassette relies on the hEF1-HTLV promotor to drive expression of luciferase (LucSh) with the SV40 promotor again terminating transcription. The second cassette contains a CMV promotor to drive expression of the Zeocin resistance gene with the bacterial promotor EM7 allowing selection in both mammalian cells and E. coli, while the BGlo pAn sequence arrests transgene transcription (figure 2.3).

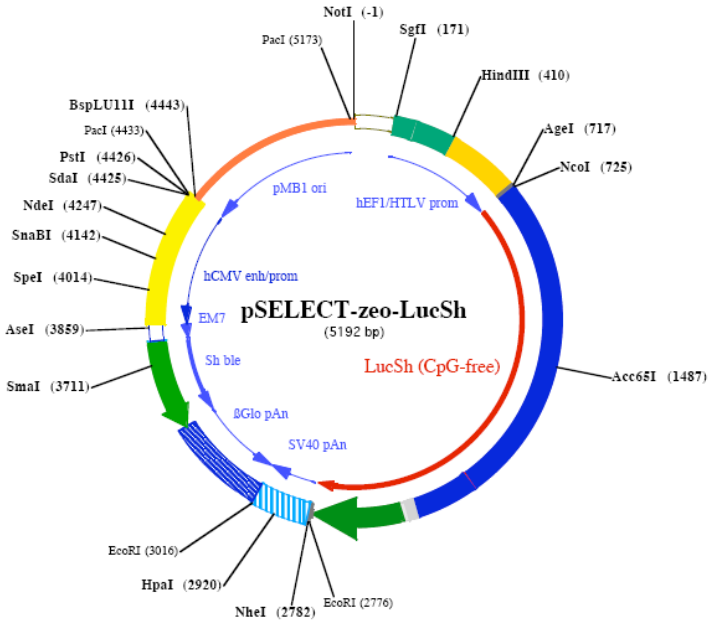

Figure 2.3 – The pSELECT-zeo-LucSh vector

2.2.2 Transformation and amplification of vector

In order to increase the quantity of the vectors available for subsequent experiments plasmids were transformed and amplified in E.coli bacteria. Four vials (50µl per vial) of One Shot® TOP10 Chemically Competent E. coli bacteria (ThermoFisher Scientific, Paisley, UK) were thawed on ice. Under aseptic conditions, 1µl of vector DNA was added to each vial, including the positive control DNA for transformation pUC19 (ThermoFisher Scientific, Paisley, UK, 10 pg/ul), which provides ampicillin resistance to transformed cells. Distilled water was added to the final vial as a negative control.

Following the addition of DNA or water, vials were incubated on ice for 30 minutes prior to heating to 42°C for 30 seconds. After a further 3 minutes on ice, 900µl of pre-warmed SOC medium (ThermoFisher Scientific, Paisley, UK) was added to each vial. The contents of each vial were subsequently moved to separate 15ml Falcon tubes (Fisher scientific, Loughborough, UK) and gently shaken in a rocking-incubator at 250 revolutions per minute (rpm) and 37°C for one hour.

Luria Bertani Broth (LB)-Agar-ampicillin coated 100mm petri dishes (Greiner Bio-One, Stonehouse, UK) were made by combining 20g LB powder (Sigma-Aldrich, Dorset, UK) with 15g agar granules (Melford Laboratories Ltd., Ipswich, UK) in 1L of sterile distilled water and adding ampicillin (Sigma-Aldrich, Dorset, UK) to a final concentration of 100µg/ml, with this mixture poured into the petri dishes and left to solidify. To ensure the development of individual well-spaced colonies, four different volumes of the contents from each falcon tube were spread over individual coated petri dishes and incubated at 37°C overnight, after which a 10µl filter tip was used to pick colonies. The 10µl tip was placed directly into a LB broth-ampicillin mixture in a 15ml Falcon tube and incubated overnight at 37°C. Once cloudy, the mixture was added to 1L of LB broth (20g LB powder in 1L water) and incubated at 37°C for 24 hours prior to the extraction of plasmid DNA.

2.2.3 DNA / plasmid extraction from bacteria

Plasmid DNA was extracted and purified using the QIAGEN-tip 500 Plasmid Midi Kit (QIAGEN, Manchester, UK) as per the manufacturer's instruction. In brief, the bacteria were harvested from the culture / LB broth mixture by centrifugation at 6000g for 15 minutes at 4°C. The bacterial pellet was resuspended in the buffers provided by the manufacturer and the plasmid DNA released into suspension by lysis of the bacterial pellet. The suspension was passed though the filters in the QIAGEN-tip before the DNA was eluted into a fresh 15ml falcon tube. DNA was precipitated by the addition of isopropanol (IPA), separated by centrifugation at 15 000g for 10 minutes and resuspended in 2ml TE buffer [10mM Tris base, 1nM Ethylenediaminetetraacetic acid (EDTA), pH 7.5] for storage.

The concentration and purity of the plasmid DNA was determined by reference to the 260:280nm ratio by placing 1µl of the buffered DNA on the Nanodrop™ ND-1000 UV spectrophotometer (Labtech International, East Sussex, UK) a per the manufacturer's instructions. Only samples with a ratio ≥ 1.8 were used in subsequent experiments.

2.2.4 Cell culture

Human (HCT116) cells and murine (CT26) CRC cell lines were purchased from the European Collection of Cell Cultures (ECACC) and American Type Culture Collection (ATCC) respectively. The CT26 cell line was developed from a colonic carcinoma induced by the administration of the carcinogen N-nitroso-N-methylurethane to BALB/c mice [407]. HCT116 and CT26 cells were cultured in Dulbecco's modified Eagle's medium (DMEM) and Roswell Park Memorial Institute (RPMI) 1640 medium (both Sigma-Aldrich, Dorset, UK) respectively at 37°C in a humidified incubator containing 5% CO2. Media were supplemented with 10% heat inactivated fetal bovine serum, 584mg/L L-glutamine, 100 units/ml penicillin G and 100 µg/ml streptomycin (all Sigma-Aldrich, Dorset, UK). The transfected luminescent cell lines were co-cultured with the selection antibiotics G-418 (Promega, Southampton, UK) or Zeocin (Invivogen, Toulouse, France) at a pre-determined cytotoxic concentration.

Cells were routinely cultured in 75cm^2 Nunclon cell culture flasks (Nalge-Nuc international, C/O VWR International, Lutterworth, UK) and passaged under aseptic conditions in a class-2 cell-culture hood when approximately 80% confluent. For passage, or when required for experiments, cells were washed with 5ml of unsupplemented medium prior to the addition of 5ml 0.25% trypsin-EDTA (Sigma-Aldrich, Dorset, UK). Flasks were returned to the incubator for up to 5 minutes to allow detachment of cells. The contents of the flask were transferred to a 15ml Falcon tube and a further 5ml of medium added before centrifugation at 2000 rpm for 3 minutes. The cell pellet was resuspended in 5ml of supplemented medium and dissociated with a 21-gauge needle and 5ml syringe. A 1:10 split of the cell suspension was routinely used for continuity of the cell line in culture.

For experiments where a specific number of cells were required, cells were counted using 0.4% Trypan Blue solution and the Countess™ automated cell counter (both Invitrogen, Paisley, UK). After trypsinisation and suspension in media, an equal volume of trypan blue and the cell suspension were mixed by pipetting and 10µl injected into the chamber of the Countess™ automated cell counter slide (Invitrogen, Paisley, UK). The slide was inserted into the cell counter and the image focused prior to the determination of the concentration of viable cells (those that did not take up trypan blue). The volume required for the specific cell count could consequently be calculated and diluted in medium for seeding.

2.2.5 Determining lethal concentrations of selection antibiotics in cells

To allow antibiotic selection of transfected cells the concentration required to kill all cells within a week was determined. To establish the lethal concentrations of G418 and zeocin, allowing selection following transfection with either vector in both cell lines, cells were plated out at $1x10^5$ cells/well in 500µl of medium on a 24-well culture plate (Nalge-Nuc international, C/O VWR International, Lutterworth, UK) for assessment of cell viability using trypan blue and the Countess™ automated cell counter, or at 5000 cells/well in 100µl of medium on a 96-well culture plate (Nalge-Nuc international, C/O VWR International, Lutterworth, UK) for assessment by the MTS cell viability assay, and left to adhere overnight.

For dosing with G418 a stock solution was made by dissolving the antibiotic to 1mg/ml in the appropriate growth media. Cells were dosed across a range of 12 concentrations from 0 to 1000µg/ml in triplicate by dissolving the stock solution in the appropriate volume of growth medium and applying this to the cells in culture. For zeocin dosing the master stock solution (100mg/ml) was diluted in medium to 500µg/ml and then further diluted in appropriate volumes of medium for application to cells in triplicate across a range of eight concentrations from 0 to 500µg/ml.

Media, containing the selection antibiotics, were changed every two to three days before the assessment of cell viability after 7 days using trypan blue and the Countess™ automated cell counter, as described in 2.2.4, or the MTS assay as described in 2.2.6. The concentration of antibiotic that caused complete cell death was subsequently used for the selection of transfected cells.

2.2.6 MTS cell viability assay

An MTS [3-(4,5-dimethylthiazol-2-yl)-5-(3-carboxymethoxyphenyl)-2-(4-sulfophenyl)-2H-tetrazolium, inner salt] colorimetric assay was used to assess cell viability. The assay utilises MTS tetrazolium, which is reduced to a soluble formazan-coloured product by NAD(P)H-dependent oxidoreductase enzymes in viable cells. This rapid colour change causes a detectable alteration in the absorbance of light [408]. 20µL of MTS reagent (CellTiter 96® AQueous One Solution Cell Proliferation Assay, Promega, Southampton, UK) was introduced to all wells and the plates incubated for 2 hours at 37°C. Light absorbance, at a wavelength of 490nm, was assessed using the Varioskan™ Flash Multimode Reader (ThermoFisher Scientific, Paisley, UK) and cell viability expressed as a percentage of control cells.

2.2.7 Transfection of cells with luminescent vectors

For the stable incorporation of luciferase expression into cell lines a liposomal transfection was carried out using Lipofectamine® 2000 (Invitrogen, Paisley, UK) as per the manufacturer's instructions with both vectors. Cells were plated out at $1x10^5$ cells/well in 500µl of complete medium on a 24-well plate and left overnight to adhere. Lipofectamine® 2000 was subsequently diluted in Opti-MEM Reduced Serum Media (Invitrogen, Paisley, UK) in sterile Eppendorf's (Eppendorf UK Limited, Stevenage, UK) with varying volume/volume (v/v) ratios; Lipofectamine® 2000: Opti-MEM = 2µl : 50µl, 3µl : 50µl, 4µl : 50µl and 5µl : 50µl. 5µg of plasmid DNA was also diluted in 250µl of Opti-mem before 50µl of the diluted DNA was mixed with 50µl of the four diluted Lipofectamine® 2000 mixtures. Following a 15-minute incubation at room temperature, the resulting four DNA-lipid complexes were added in duplicate to the medium on the cultured cells in a drop-wise fashion. This resulted in a final quantity of DNA of 500ng per well. As a Lipofectamine® 2000 only control 5µl of the transfection reagent was added to 100µl of Opti-MEM and 50µl added to duplicate wells of the 24-well plate. Cells were incubated at 37°C for 48 hours before the assessment of luminescence as described below. The most luminescent population of cells were kept in culture and serially passaged in the appropriate selection antibiotic, at the pre-determined cytotoxic concentration.

2.2.8 Assessment of luminescence by the Bright-Glo™ Assay

The Bright-Glo™ Luciferase Assay System (Promega, Southampton, UK) allows quantitation of firefly luciferase expression in mammalian cells and was one of the methods used to assess luminescence in cell lines. To assess the optimum transfection conditions, cells from one well of each pair of duplicates were lysed by aspirating the medium and adding 200µl of the supplied lysis buffer as per the manufacturer's instructions. Following this the plate was rocked at 70rpm for 5 minutes. The lysis buffer was aspirated from each well and two serial 1:2 dilutions of the buffer performed before 80µl of each dilution was added to a separate well of a 96-well white-backed plate (Greiner Bio-One, Stonehouse, UK). 20µl of the Bright-Glo™ reagent was added to each well, the plate spun at 700rpm for 15 seconds and luminescence assessed on the Varioskan™ Flash Multimode Reader with an open filter. Luminescence was normalised to the protein content in each well in duplicate to prevent bias due to unequal loading. The bicinchoninic acid (BCA) assay [409], utilising the Pierce™ BCA Protein Assay Kit (ThermoFisher Scientific, Paisley, UK), was used for protein quantification. Samples were compared with a standard curve created by a serial 1:2 dilution of bovine serum albumin with absorbance at 570nm read on the Varioskan™ Flash Multimode Reader.

2.2.9 Assessment of luminescence with in vivo grade luciferin

For the assessment of luminescence *in vitro*, without the need for cell lysis, *in vivo* grade luciferin can be applied to cells in culture. Cells were seeded on 96-well plates at the required cell count and left to adhere. A stock solution of VivoGlo™ firefly Luciferin (Promega, Southampton, UK) was created by diluting the powder to 15mg/ml in 1x phosphate buffered saline (PBS) (Invitrogen, Paisley, UK). This stock solution was further diluted 100-fold to 150µg/ml in growth medium and 100µl added to cells in culture on a 96-well white backed plate for assessment in the Varioskan™ Flash Multimode Reader or on a clear plastic plate for the IVIS® Spectrum *in vivo* imaging system (Perkin-Elmer, Massachusetts, USA). For plate imaging in the IVIS® the stage was set to position C with the default settings of auto-exposure and medium binning used for image acquisition with an open filter.

To establish the optimum imaging time after the application of luciferin to cells, plates were imaged every 5 minutes until peak signal was obtained and subsequent imaging performed at this time-point.

2.2.10 Clonal selection and expansion of cell lines

Once a sufficient population of luminescent cells were available, through serial culture in increasing volumes to a 75cm^2 Nunclon cell culture flask, clonal selection and expansion was performed. By selecting a single luminescent clone for subsequent experiments luminescent signal can be increased, the chances of achieving stable luminescence is improved and the heterogeneity associated with a mixed population of transfected cells is removed. This was achieved through serial dilution in 96-well culture plates to a single cell per well. A cell suspension of 2x10^4 cell/ml was created from the luminescent population and 200µl of this added to the first well (A1) of a 96-well plate. 100µl of culture medium was added to every other well on the plate before a 1:2 first dilution series was completed down the first column. An additional 100µl of medium was added to each well in column one to give wells in this column a total volume of 200µl. A second 1:2 serial dilution series was subsequently performed, moving 100µl from the first column to second, and this process repeated across the plate, with 100µl discarded from the final column. This was performed across 3 culture plates to increase the number of wells diluted to a single cell (figure 2.4).

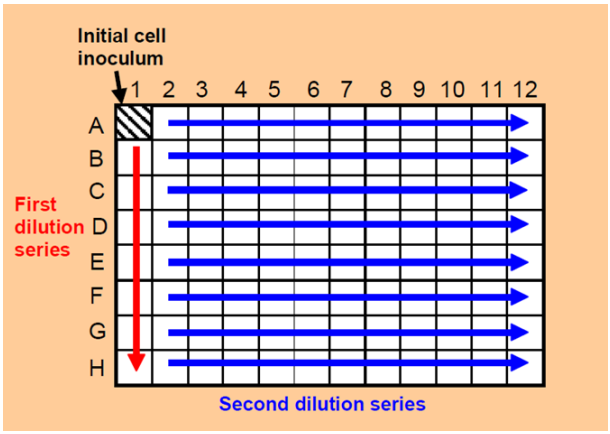

Figure 2.4 – Schematic of the dilution series used for clonal selection and expansion of luminescent cell lines on 96-well culture plates.

After 24 hours, wells were reviewed under x200 magnification and those with a single cell visible marked. After a further 72 hours marked wells were examined again and those with a single colony of wells selected for serial passage and expansion under antibiotic selection. Once a sufficient population of cells were available, luminescence was assessed using the

methods described previously and the most luminescent clone cultured for use in murine experiments.

2.2.11 Murine studies

All animal experiments were performed in accordance with criteria outlined in a Home Office UK approved project licence (PPL 70/8457) granted under the Animals (Scientific Procedures) Act 1986 and approved by the Animal Ethics Committee at the University of Liverpool. Six to eight-week-old male immune-competent (BALB/cAnNCrl) or homozygous nude (BALB/cAnN.Cg-Foxn1nu/Crl) BALB/c mice were purchased from Charles River Laboratories (Margate, UK) and housed in a licenced specified pathogen free establishment. Mice were given free access to food and water and housed at a temperature between 19°C and 23°C under a 12-hour light-dark cycle.

2.2.12 Subcutaneous injection of tumour cells

For the *sc* flank injection of CRC cell lines, non-confluent cells were detached from the flask by trypsinisation, transferred to a 15ml Falcon tube, centrifuged to remove all trypsin and the pellet resuspended in growth medium for counting. Once the cell concentration was established the required volume of cell suspension was transferred to a new 15ml Falcon tube and centrifuged at 2500 rpm for 3 minutes before resuspension in the required volume of a 1/1 (v/v) mixture of ice-cold PBS / Matrigel® (Corning, Amsterdam, The Netherlands) so that each mouse received $1x10^6$ cells in 100µl. The cell suspension was kept on ice until required. Prior to the injection of cells mice were placed into an anaesthetic chamber and general anaesthesia (GA) induced with 3% isoflurane and 1L/minute of oxygen flow before being transferred to a nose cone and GA maintained on 1.5% isoflurane. The right flank was shaved at the injection site and cells injected into the *sc* space using a 500µl insulin syringe with a 30-gauge needle after tenting the skin. Mice were ear clipped for identification and tumour growth monitored using BLI as described in section 2.2.14.

2.2.13 Orthotopic caecal injection of tumour cells

For the orthotopic injection of CRC cell lines, cells were suspended in PBS / Matrigel using the method described for *sc* injection in 2.2.12. Mice were weighed and received a *sc* preoperative dose of buprenorphine (0.1mg/kg). GA was induced and maintained as described in 2.2.12. Animals were transferred to a pre-warmed operating table and the

abdomen shaved and prepped with betadine for disinfection. Aseptic technique and meticulous draping was used to maintain sterility of the operative field.

A 1-1.5cm lower midline laparotomy was performed and moistened (sterile 0.9% saline) cotton tips used to deliver the mobile caecum from the abdomen. A 500µl insulin syringe with a 30-gauge needle was used to draw up cells after dissociation by syringing through a 21-gauge needle. $5x10^5$ cells in 50µl of the PBS / Matrigel mixture were drawn up and allowed to warm for 45-60 seconds at room temperature to ensure a relatively viscous inoculum and prevent cell leakage. The entire volume was injected into the sub-serosal plane of the caecum under direct vision, ensuring a 'bleb' of the cell suspension was formed under the serosa. Attempts were made to standardise the injection site on the caecum, aiming to inject into the anti-mesenteric side of the anterior wall of the caecum. The needle entry site was gently compressed with a moistened cotton tip to prevent the leakage of cells and ensure haemostasis before returning the caecum to the abdomen, ensuring there was no rotation of the gut which could result in volvulus and the ensuing obstruction or ischaemia. The peritoneum and muscle layer were closed with a continuous 6-0 Vicryl™ (Ethicon, subsidiary of Johnson & Johnson, Norderstedt, Germany) suture. Skin was sutured using a subcuticular continuous technique using the same suture material (figure 2.5).

Mice were ear-clipped for identification and allowed to recover in a warming chamber at 37°. They were observed closely for signs of distress and additional buprenorphine analgesia given up to 0.05mg/kg every 8 hours if required. Tumour development, growth and the formation of metastases were monitored by bioluminescent imaging.

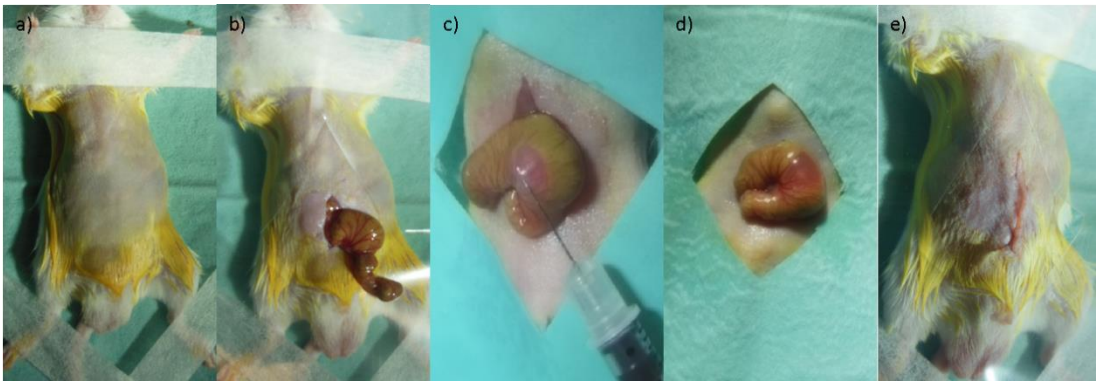

Figure 2.5 – The technique for orthotopic injection of tumour cells into the caecal wall. a) Animals were placed in the supine position and the abdomen shaved, sterilised with betadine and draped. b) A 1 cm lower midline laparotomy was performed and the caecum delivered. c) Tumour cells were injected into the subserosal plane; d) ensuring a good 'bleb' of cell suspension was achieved. e) The laparotomy wound was closed in two layers.

2.2.14 Bioluminescent in vivo imaging

Mice were imaged in the IVIS® Spectrum *in vivo* imaging system after the *ip* injection of luciferin. Animals were weighed and GA induced and maintained as described previously. The area of interest was shaved if required. Each mouse received a dose of 150mg/kg VivoGlo™ firefly luciferin by injecting 10µl/g bodyweight of the 15mg/ml stock solution prior to transfer to the IVIS® imager, where GA was maintained on the machine's nose cones. For mice flank-injected with tumour cells, imaging was conducted in the prone or left lateral position, while orthotopically-injected mice were imaged supine. Imaging was conducted with an open filter, auto-exposure and medium binning.

To attempt to establish an optimum imaging time following the *ip* injection of luciferin a kinetic imaging curve was conducted. Mice were placed in the IVIS® immediately after injection of the substrate and imaged every 2 minutes until the luminescent signal plateaued, these invariably occurred after 20 minutes in flank grafting mice and all imaging was conducted at this time-point after luciferin injection in this model. By imaging mice within this plateau period in later imaging points, or subsequent experiments, reproducibility could be maintained across replicates.

To estimate signal depth in mice and assess if luminescent signal could be approximated to the liver, consistent with the development of metastasis, 3-dimensional (3D) tomographic reconstruction imaging by Diffuse Light Imaging Tomography (DLIT) was utilised. Mice

suspected to have metastatic disease on 2-dimensional imaging could be allocated to 3D imaging for clarification and to assess if multiple foci of luminescent signal were present. Animals allocated to this technique could only be assessed in pairs, as opposed to the five mice that can be imaged simultaneously in 2D imaging, with the stage in position C. The CCD camera was used to capture an image of the animal and a 3D tomography constructed by the software. Luminescent signal was then captured in five images over a range of spectral filters from 560 to 640nm (every 20nm). Using a set of linear equations, the software calculated the depth of signal based on the different penetrance of light wavelengths through tissue. Images were reconstructed by placing a representation of the luminescence source within a 3D reconstruction of the animal based on the tomographic image. The signal was approximated to skin, bones and organs within the mice using the software's pre-saved templates.

2.2.15 Bioluminescent ex vivo imaging

To confirm that liver lesions were consistent with metastatic disease originating from the caecal implantation of luminescent CRC cell lines, organs were imaged ex-vivo. Upon sacrifice of mice by cervical dislocation, while luminescent signal was still present *in vivo*, necropsy was performed, caeca and livers with macroscopic disease were excised, placed in PBS and imaged with platform height set in position C, an open filter, auto-exposure and medium binning.

2.2.16 Histological assessment and immunohistochemistry

After schedule 1 cull of mice by cervical dislocation, tissue (livers and caeca) containing macroscopic disease were fixed in 4% paraformaldehyde (Sigma-Aldrich, Dorset, UK) and paraffin-embedded. 5um slices were cut on a rocking microtome, haematoxylin and eosin (H&E) stained and examined by the Veterinary Pathologist Dr Lorenzo Ressel to confirm the presence of adenocarcinoma.

For the assessment of T-cell infiltration into tumours sections were de-waxed in xylene rehydrated with ethanol solutions of decreasing concentrations. Antigens were retrieved by microwaving (96-98°C) for 30 minutes and slides blocked with DAKO REAL™ Peroxidase Blocking Solution (Dako UK Ltd., Cambridgeshire, UK) in 0.1% Tris-buffered saline with tween (TBST) for 10 minutes. Slides were incubated with the primary antibody for CD3 (Dako, A0452, 1:400 dilution) at 4°C overnight, washed in 0.1% TBST and Dako Envision and

System-HRP α rabbit secondary antibody added (Dako, K4003, 1:2000) for 30 minutes at room temperature. Slides were developed with diaminobenzidine tetrahydrochloride (DAB) (Fisher Scientific, Loughborough, UK) for 10 minutes and counterstained with haematoxylin (Merck, Nottingham, UK) for 1 minute.

2.2.17 Data analysis for luminescent imaging

IVIS® imaging quantifies light in photons / second. Utilising the Living Image™ software, areas of luminescent signal were marked as a region of interest (ROI). In cell-based experiments, a 96-well plate-grid was placed over the image of the plate and lined up to ensure each well was within its own square. To ensure reproducibility across time-points in animal studies the same size area was used to cover the abdominal area of each mouse for each time-point. The number of photons produced per second within each marked ROI was calculated by the software (total flux). The background luminescent signal for each image was subtracted from the ROI value. A well containing cells and medium without luciferin was used to calculate background signal for assessment of luminescence in cells. In animal studies background luminescence was calculated by placing an ROI on an area of a mouse without luminescent signal.

To allow each mouse to act as its own control luminescence within the ROI was expressed as a fold change from the initial reading by dividing the luminescence at each time-point by the value obtained on the first imaging time-point.

Graphical display and statistical analysis of data was performed using Prism® 7 (GraphPad Software, California, USA).

2.3 Results

2.3.1 Cytotoxicity of G418 in cell lines

Incubation of CT26 cells with neomycin resulted in cell death in a dose-dependent manner, as assessed by cell counting in the presence of trypan blue. Complete cell death, with no viable cells present, was achieved by 7 days at concentrations of G418 ≥ 600µg/ml. CT26 cells transfected with the vector pGL4.51 were therefore cultured with the addition of 600µg/ml G418 to medium to maintain selection pressure and therefore luminescence (figure 2.6).

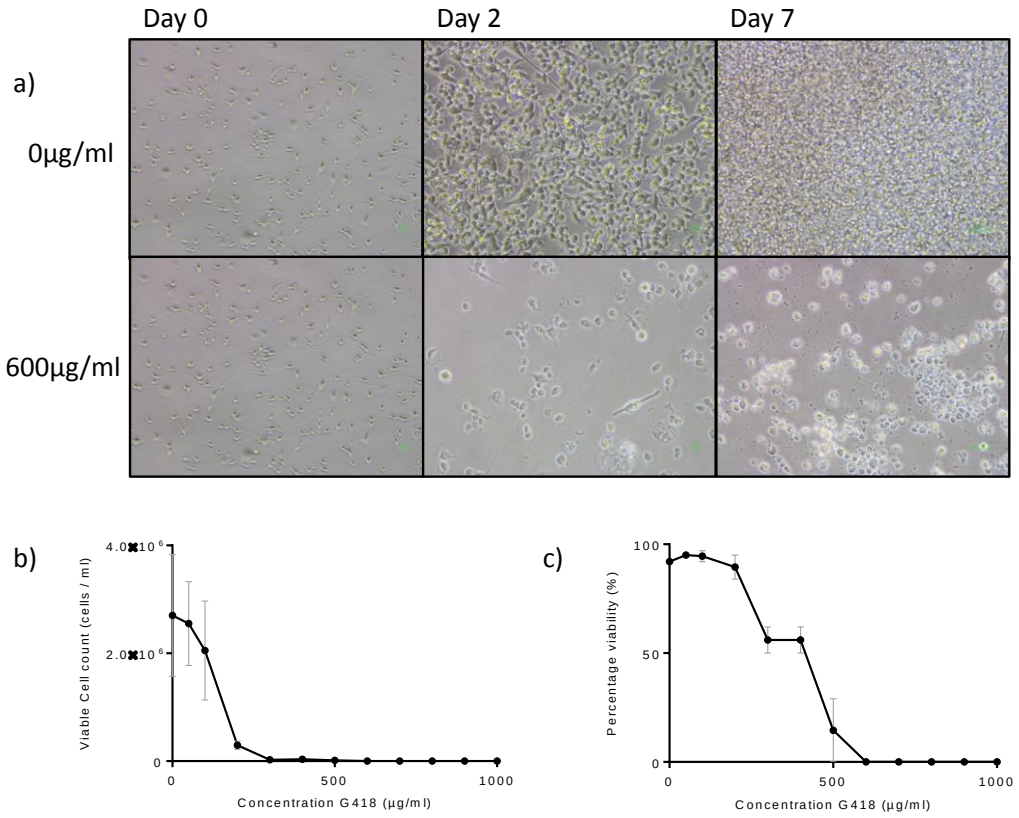

Figure 2.6 - a) Light microscopy images of CT26 cells in culture at varying magnifications (x100-x200) taken before the application of 600µg/ml G418 and 2 and 7 days after dosing in treated cells. The increasing confluence of untreated control cells is also displayed for comparison. No viable cells were visible in the treated cells by 7 days as evidenced by the change in morphology and presence of necrotic debris. These data were represented graphically, displayed as mean +/- standard deviation (SD), after a 7-day incubation with G418 using both b) the total viable cell count /ml and c) the percentage of the total cells counted that were viable for each concentration. (N=3 in duplicate)

The untransfected HCT116 cell line was relatively resistant to G418. Dosing with this antibiotic was unable to induce complete cell death in HCT116 cells up to the maximum working concentration of 1000µg/ml. Although there was a fall in the total viable cell count / ml at the higher concentrations of G418, suggesting a reduction in proliferation, there were still viable cells present even at the highest concentration. For this reason culture in G418 for selection of transfected cells was not possible in this cell line and transfection with the pGL4.51 vector not undertaken (figure 2.7).

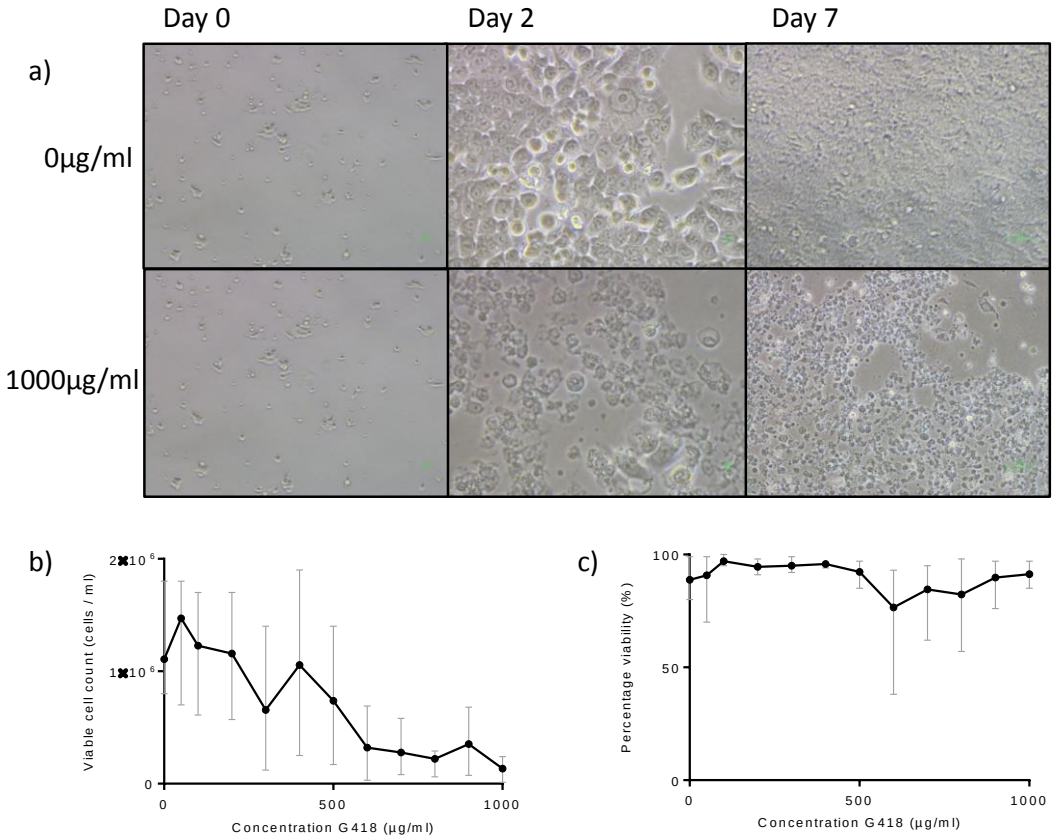

Figure 2.7 - a) Light microscopy images of HCT116 cells in culture at varying magnifications (x100-x200) taken before the application of 1000µg/ml G418 and 2 and 7 days after dosing in treated cells. The increasing confluence of untreated control cells is also displayed for comparison. Despite significant cell death, some viable cells were visible in the treated cells by 7 days, appearing brighter and with a more normal morphology than the surrounding necrotic cells. These data were represented graphically, displayed as mean +/- SD, after a 7-day incubation with G418 using both b) the total viable cell count /ml and c) the percentage of the total cells counted that were viable for each concentration. (N=3 in duplicate)

2.3.2 Cytotoxicity of zeocin in cell lines

Zeocin was cytotoxic to both the CT26 and HCT116 cell lines. Dose-response curves, using the MTS cell viability assay, were similar in both with zero percent viability reached at 400µg/ml. This concentration was subsequently used for the selection and maintenance of cells successfully transfected with the pSELECT-zeo-LucSh vector (figure 2.8).

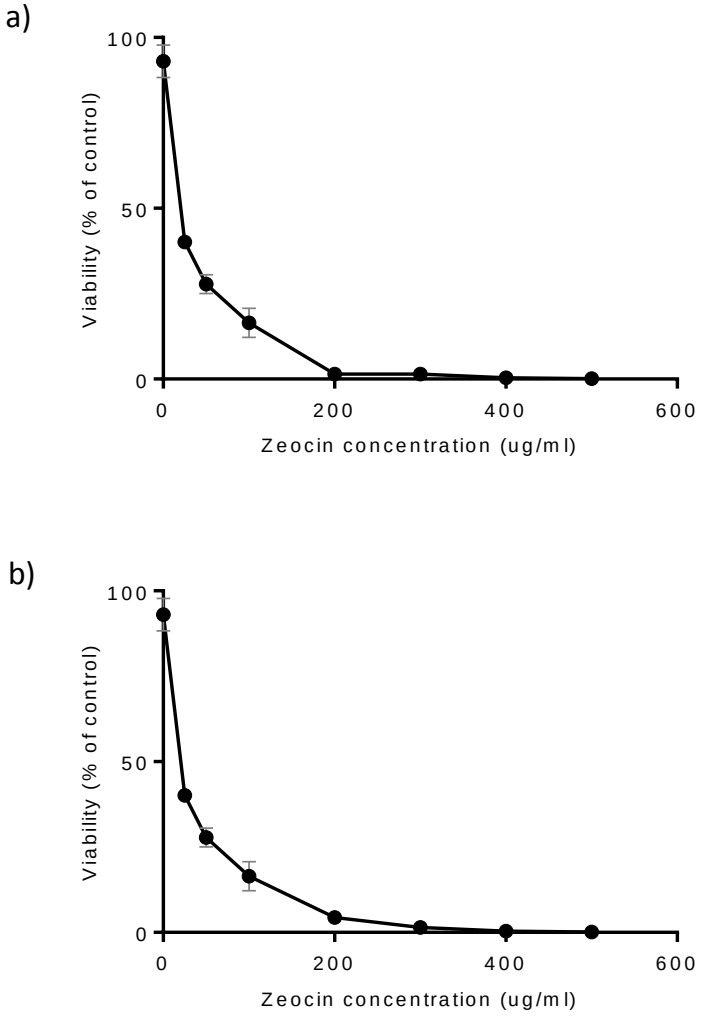

Figure 2.8 – Cytotoxicity dose-response curves, displayed as mean + SD, after a 7-day incubation with Zeocin were performed in a) CT26 and b) HCT116 cells using the MTS assay. Results are expressed as a percentage of untreated control cells left to proliferate for 7 days. There were no viable cells detectable at 7 days with 400µg/ml of zeocin in both cell lines. (N=3 in triplicate, graphs display mean +/- SD)

2.3.3 Assessing optimum transfection conditions in cell lines

Luminescence was assessed using the Bright-Glo™ Assay in the CT26 cell line 48 hours after transfection with pGL4.51 plasmid DNA and normalised to the protein content of the well. The replicate well of the transfection conditions resulting in the highest luminescent signal per µg of protein were labelled CT26luc and kept and passaged in increasing volumes to expand the population (figure 2.9). These conditions were subsequently used for the transfection of CT26 cells with the pSELECT-zeo-LucSh vector.

a)

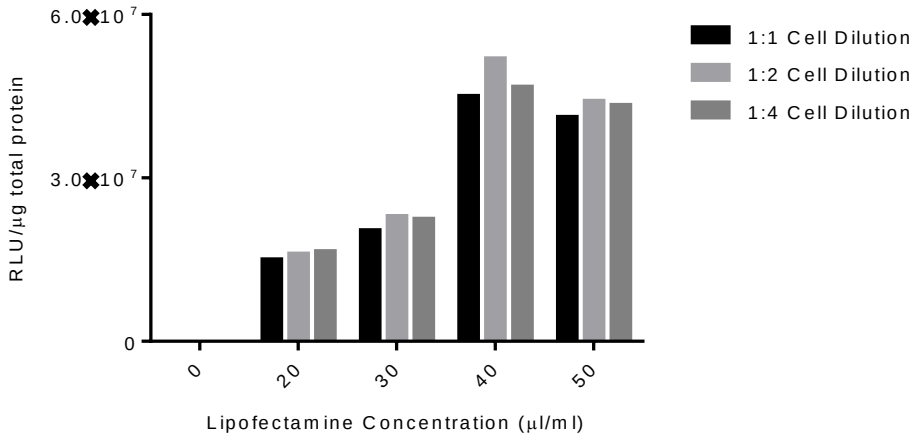

b)

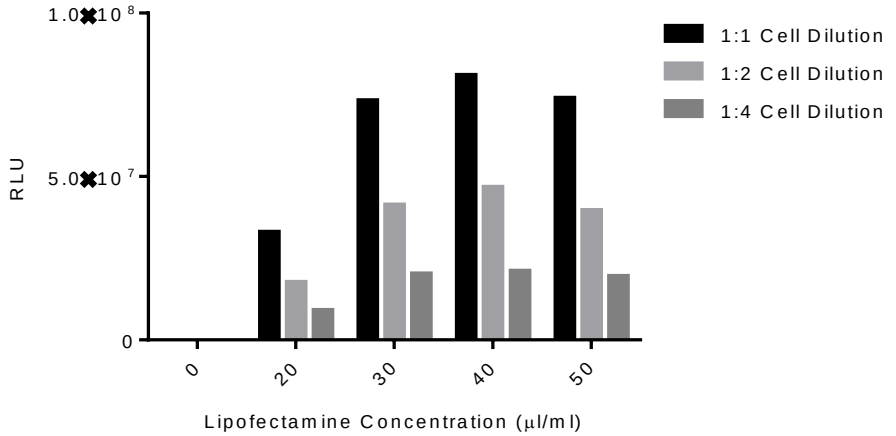

Figure 2.9 – a) Transfection in 40µl/ml of Lipofectamine® 2000 resulted in the highest luminescent signal at 48 hours, as measured by the Varioskan™ using the Bright-Glo™ Assay, in CT26 cells when normalised to the protein content of the well. b) The luminescent signal decreased proportionally with the 1 in 2 serial dilution of the 1:1 cell suspension. (RLU = relative luminescent units)

VivoGlo™ firefly Luciferin was used to assess the optimum conditions for the incorporation of the luciferase gene into HCT116 using the pSELECT-zeo-LucSh vector. Populations of transfected cells were re-plated in triplicate on to a 96-well plate for the assessment of luminescence and a 6-well plate for the continued culture. Only the most luminescent population of cells was kept and expanded in culture; labelled HCT116luc (figure 2.10).

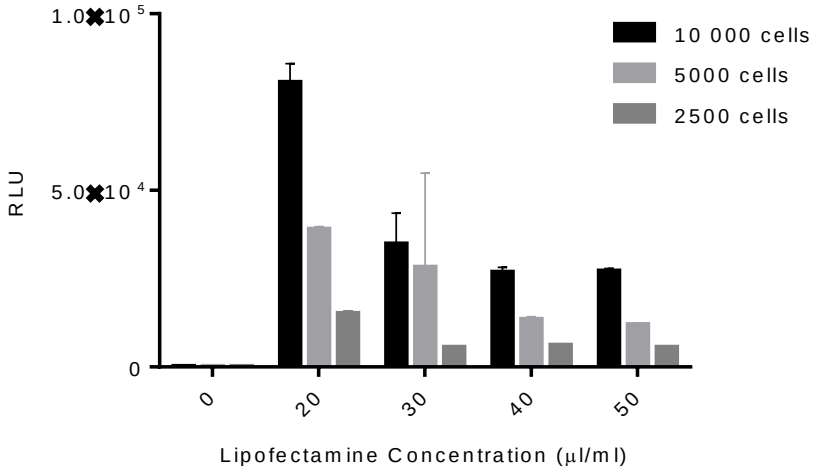

Figure 2.10 – Varioskan™ assessment of luminescence in HCT116 cells 48 hours after transfection with the pSELECT-zeo-LucSh vector. Transfection in 20µl/ml of Lipofectamine® 2000 resulted in the highest luminescent signal with this population of cells continued in culture. Luminescent signal reflected the number of cells plated, with a halving of signal for every 1 in 2 serial dilution. (Performed in triplicate with graph displaying mean +/- SD)

2.3.4 Clonal selection and expansion

After serial dilution of the CT26luc population (transfected with the pGL4.51 vector), which produced 7 photons/second/cell, and clonal expansion, analysis of luminescence in the thirteen clonal populations was performed on both the IVIS® and Varioskan™ after the application of VivoGlo™ firefly Luciferin. Only one clone (CT26lucA6) demonstrated any luminescent signal, suggesting poor initial transfection efficiency, and was expanded in culture. The CT26lucA6 clones produced 27 photons/second/cell.

This process was repeated from a population of CT26 cells transfected with the pSELECT-zeo-LucSh vector and the CT26lucA2 clone produced. This clone emitted 280 photons/second/cell (figure 2.11).

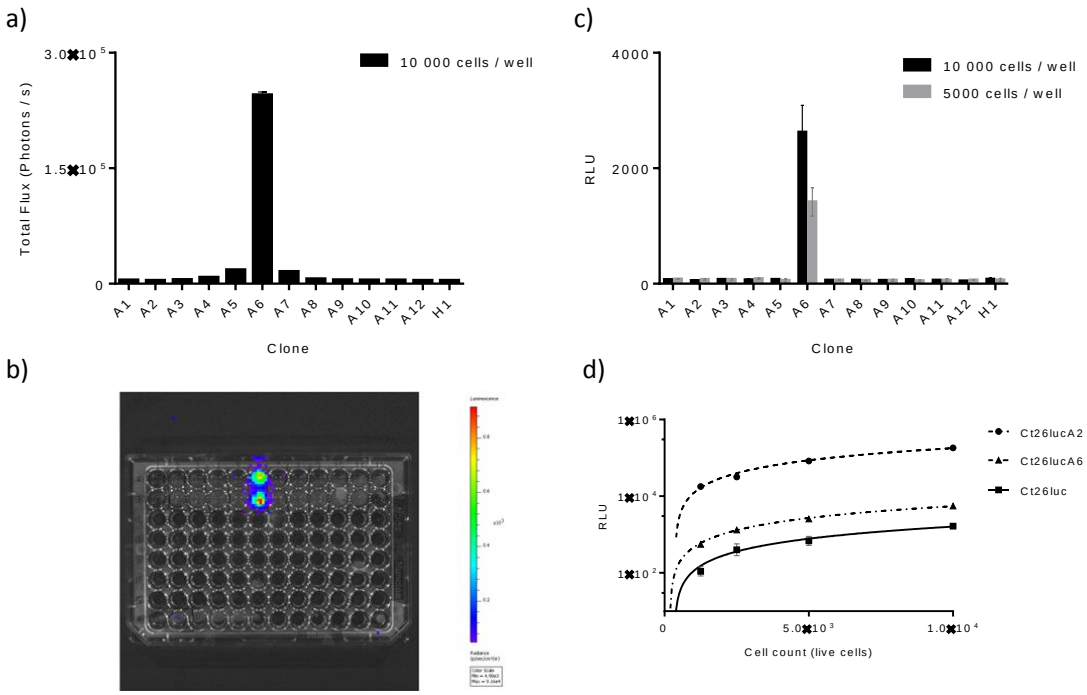

Figure 2.11 – a) IVIS® imaging demonstrated luminescent signal in only one (CT26lucA6) of the 13 clones represented by the image in b) (performed in duplicate). c) This was confirmed using Varioskan™ assessment at two cell concentrations (performed in triplicate). d) Luminescent signal was compared between clones and the CT26luc population transfected with the pGL4.51 vector using the Varioskan™ and VivoGlo™ luciferin. The CT26lucA2 clone (transfected with pSELECT-zeo-LucSh) was 10-fold more luminescent than the CT26lucA6 (performed in triplicate). (Graphs display mean +/- SD, s = seconds)

Clonal selection was also carried out from the HCT116luc population. Seventeen clones were assessed and the most luminescent of these, HCT116lucB4 (producing 120 photons/second/cell), kept and expanded in culture for future experimental work (figure 2.12).

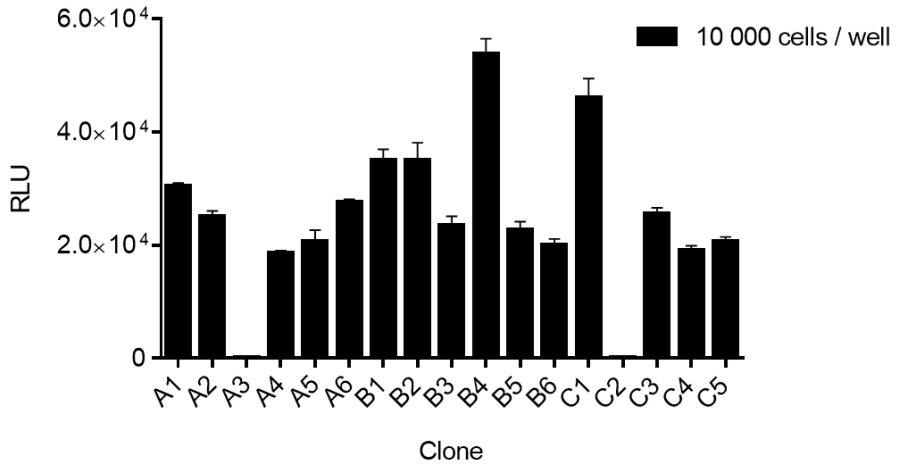

Figure 2.12 –Varioskan™ assessment with VivoGlo™ luciferin demonstrated luminescence in 15 of the 17 clones, with the HCT116lucB4 clone the most luminescent of these. (Performed in triplicate, graph displays mean +/- SD).

2.3.5 Optimum imaging time with VivoGlo™ firefly Luciferin.

In order to establish an optimum imaging time after the application of VivoGlo™ firefly Luciferin to cells, and ensure reproducibility across studies, a kinetic imaging curve was performed in both cell lines. Peak signal was achieved by 20 minutes in cell lines and remained at this level for at least a further 10 minutes, subsequent imaging with VivoGlo™ firefly Luciferin was therefore conducted at 20 minutes (figure 2.13).

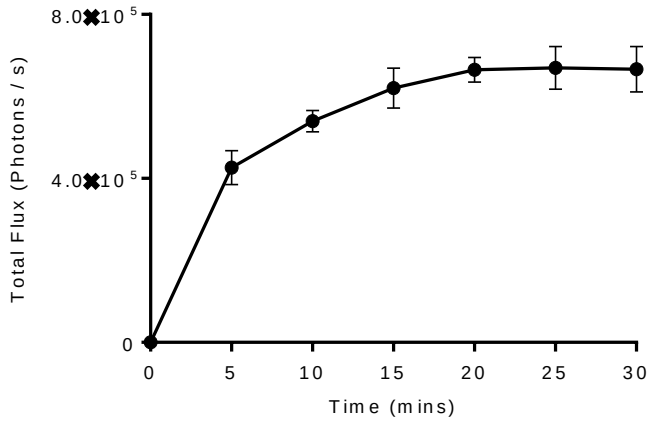

Figure 2.13 – Kinetic imaging assessment of luminescence in CT26lucA6 cells using IVIS® imaging after the application of in VivoGlo™ firefly Luciferin. This curve was generated to guide the timing of imaging after the application of luciferin in subsequent experiments. (N=3 in triplicate with graph displaying mean +/- SD, min = minutes)

2.3.6 Luminescence signal reflects the live cell count

To ensure luminescent signal was an accurate reflection of the number of viable cells present, luminescence was plotted against the number of cells seeded in a well. There was a strong positive correlation between cell count and luminescent signal in all cell lines and clones tested (figure 2.14).

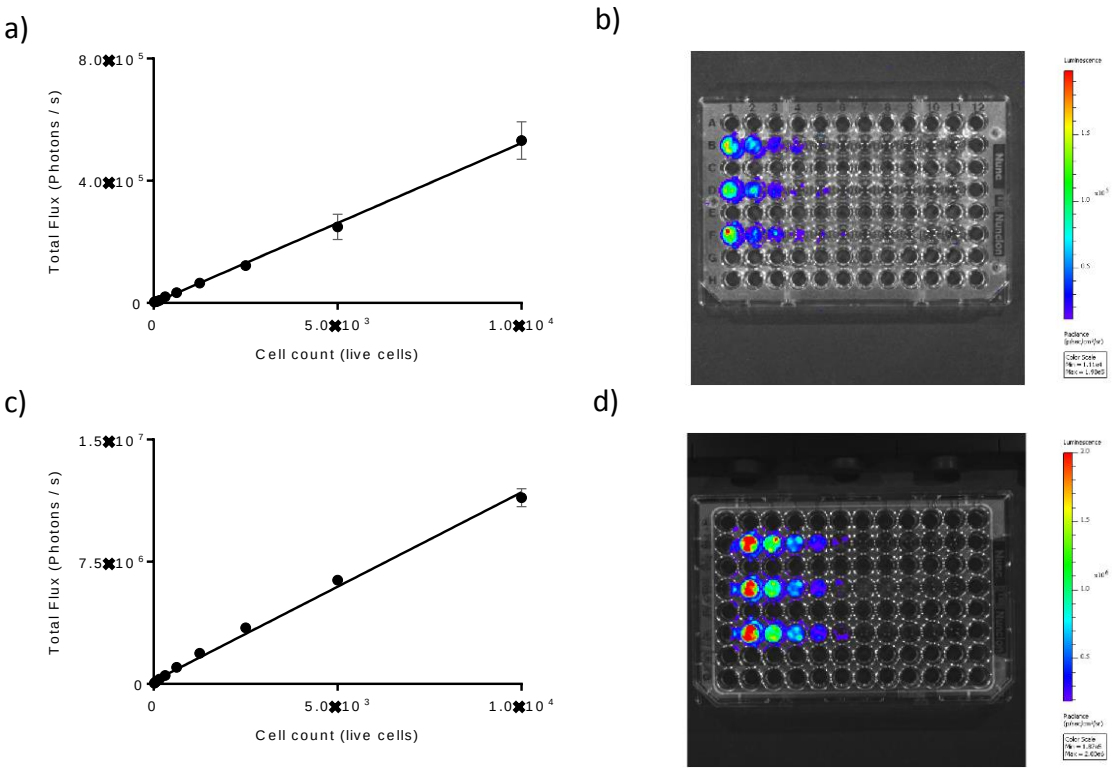

Figure 2.14 – A positive correlation was noted between luminescence and the live cell count / well in a) and b) CT26lucA6 cells (r^2 = 0.98, p<0.0001, Pearson R) and c) and d) HCT116lucB4 cells (r^2 = 0.99, p<0.0001, Pearson R). (N=3, performed in triplicate, graphs display mean +/- SD)

2.3.7 Luminescent stability in cell lines

To assess the stability of luminescence in clonal populations across passages, repeated IVIS® imaging of cell lines was undertaken using VivoGlo™ at approximately 1 month, 3 months and 6 months after the development of clones. Differences in luminescent signal were minimal in clonal cell lines across these time-points, despite increasing passage number and freeze-thawing on at least one occasion (figure 2.15).

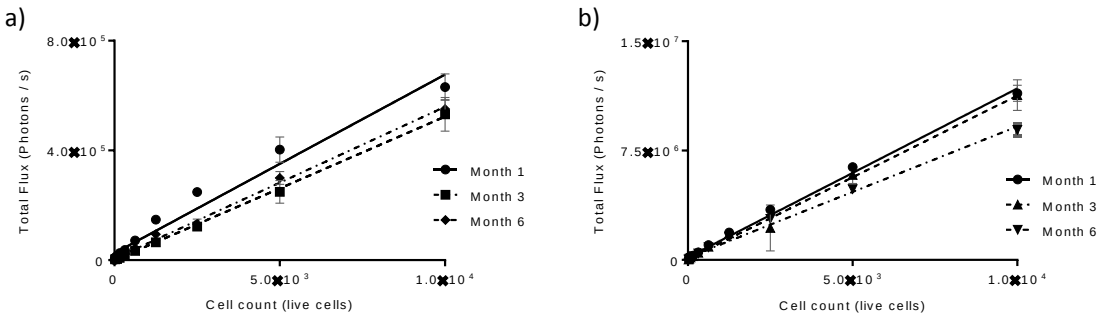

Figure 2.15 – Graphs display the minimal differences in luminescent signal in the a) CT26lucA6c and b) HCT116lucB4 clonal cell lines at increasing time-points following clonal selection.

2.3.8 Subcutaneous injection of the CT26lucA6 clone

To ensure cells would propagate *in vivo,* and assess the intensity and stability of luminescence, CT26lucA6 cells were injected in to the right flank of 6 BALB/c immune-competent mice. Mice underwent IVIS® imaging from the 3rd day after the injection of cells and then twice weekly until sacrifice. A kinetic imaging curve was performed at each imaging time-point until day 14, these consistently demonstrated a plateau in signal intensity from 20-30 minutes after the *ip* injection of luciferin, with mice imaged within this time window in subsequent studies utilising the flank grafting of cells (figure 2.16).

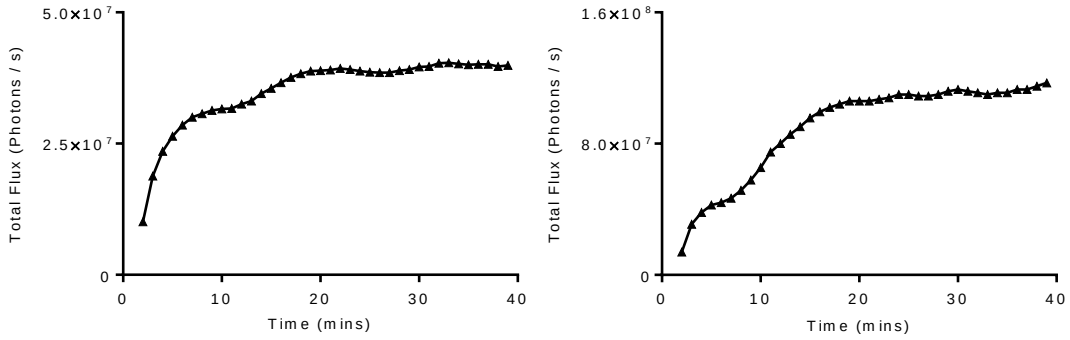

Figure 2.16 – Representative kinetic imaging curves from two individual BALB/c mice 14 days after the flank injection of CT26lucA6 cells, displaying total flux from their tumours against time after the injection of luciferin.

The tumour uptake rate was 100%, with all 6 mice developing tumours. Luminescent signal increased throughout the imaging period as the tumour increased in size. However, the increase in luminescent signal varied substantially between mice leading to a relatively wide standard error when data were combined (figure 2.17). The severity limits of the licence, due to the size of tumours, were reached by the 18th day. Due to this rapid development of tumours a lower cell count of $5x10^5$ cells in 50µl was injected in future studies using the CT26 cell line.

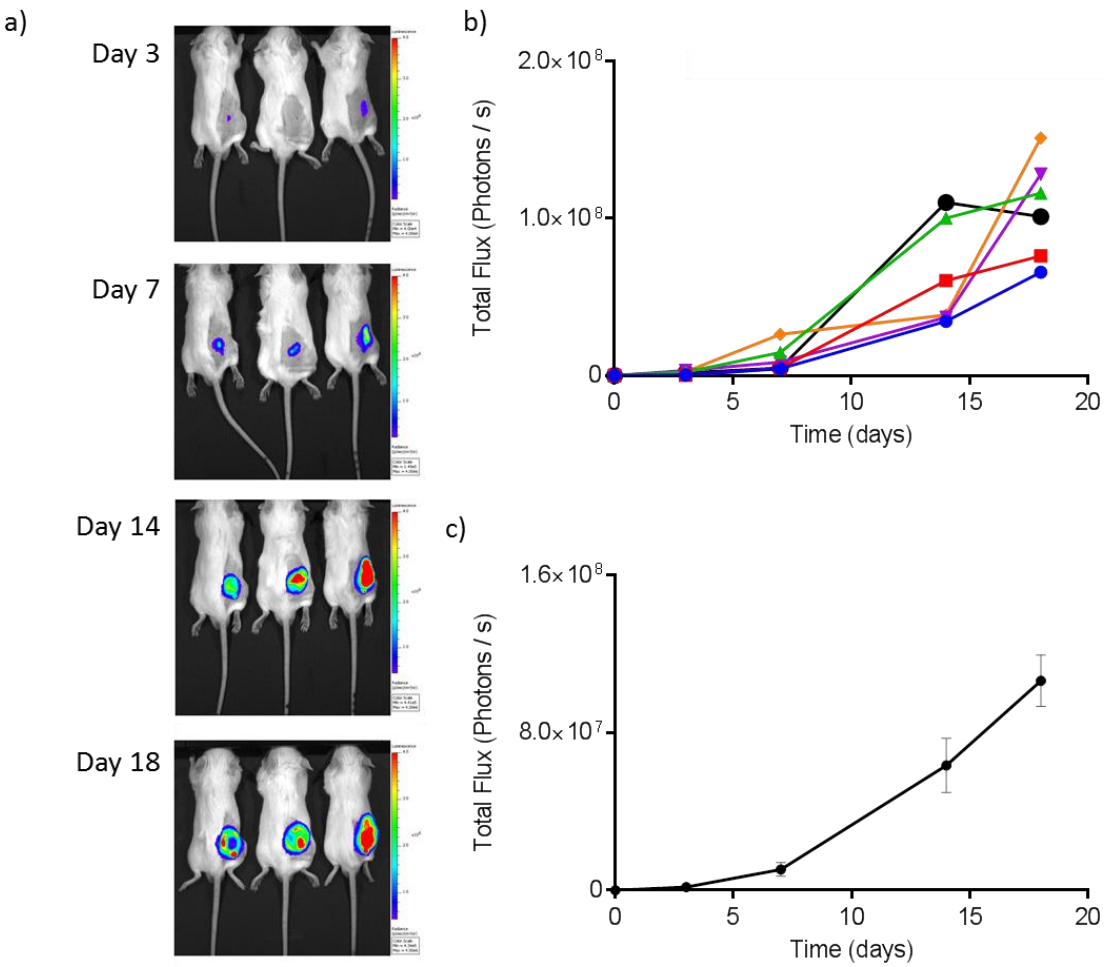

Figure 2.17 – a) Representative images of 3 BALB/c immune-competent mice serially imaged in the IVIS® after the *sc* injection of CT26A6 cells. b) Luminescence signal increased throughout the study period in a relatively exponential manner, as displayed for individual mice in a graph of time versus luminescence. c) When data were combined the standard error in the mean (SEM) was relatively wide, reflecting the variable growth rates and therefore luminescent signal in mice. (N=6, Graph displays mean +/- SEM)

At the end of the study, tumours were excised after schedule 1 cull. The largest of these was dissected with a scalpel blade and individual tumour lumps placed in wells of a 6-well culture plate. RPMI 1640 medium, with the selection antibiotic G418, was added and after 3 days the tumour lumps were removed, leaving the adherent tumour cells in culture. This allowed the development of an *in vivo*-conditioned cell line for caecal implantation, labelled CT26lucA6c.

2.3.9 Caecal implantation of the CT2lucA2 clone

The CT26lucA2 clone was developed after the *sc* injection of the CT26lucA6 clone, from the original parent cell line and not from transfected cells, in attempt to produce a more luminescent cell line for use in the orthotopic model, with increased luminescent signal allowing the early detection of primary tumours and metastatic disease. As the CT26lucA2 clone had been developed from the same parent cell line as the CT26lucA6 clone, which had developed rapidly growing flank tumours when injected *sc*, it was not-tested as a *sc* graft initially and was taken straight to orthotopic implantation.

In the first group of four immune-competent BALB/c mice orthotopically implanted with the CT26lucA2 clone, three (75%) developed detectable luminescent signal by the first imaging point (5 days after caecal injection). The total flux increased for all three mice until day 7 in one mouse and day 13 in the other two, at which point signal continued to fall until the study was abandoned on the 23rd day after orthotopic injection.

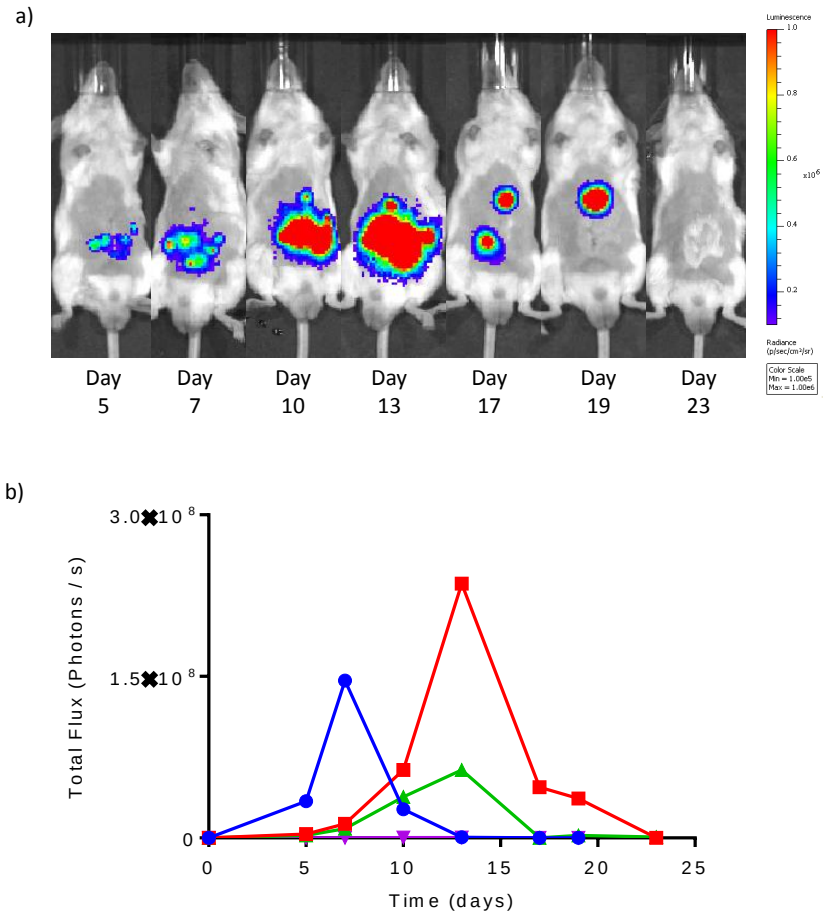

Figure 2.18 – Initial pilot study involving orthotopic implantation of the CT26lucA2 cell line into 4 BALB/c mice. a) Representative images acquired using the IVIS® demonstrate a decrease in luminescent signal from day 13. b) This occurred in all mice with detectable signal at the initial imaging point, as demonstrated graphically by plotting total flux against time for each individual mouse.

This study was repeated with a further nine mice receiving orthotopic, and one mouse flank injection, of the CT26lucA2 cell line. The inclusion of a *sc*-injected mouse allowed direct visual assessment of the tumour to confirm whether tumours were truly regressing or the cells losing their luminescent signal *in vivo*. Initial tumour uptake was similar to the first group, six (67%) of the orthotopically implanted mice developed detectable signal on day 5, but again signal had peaked by day 10 in all mice and then continued to fall until the study was terminated. The tumour in the flank-grafted mouse grew until the 10th day after the injection of cells, after which visible tumour regression and a decrease in tumour volume were noted; this change in volume was reflected by a fall in the luminescent signal (figure 2.19).

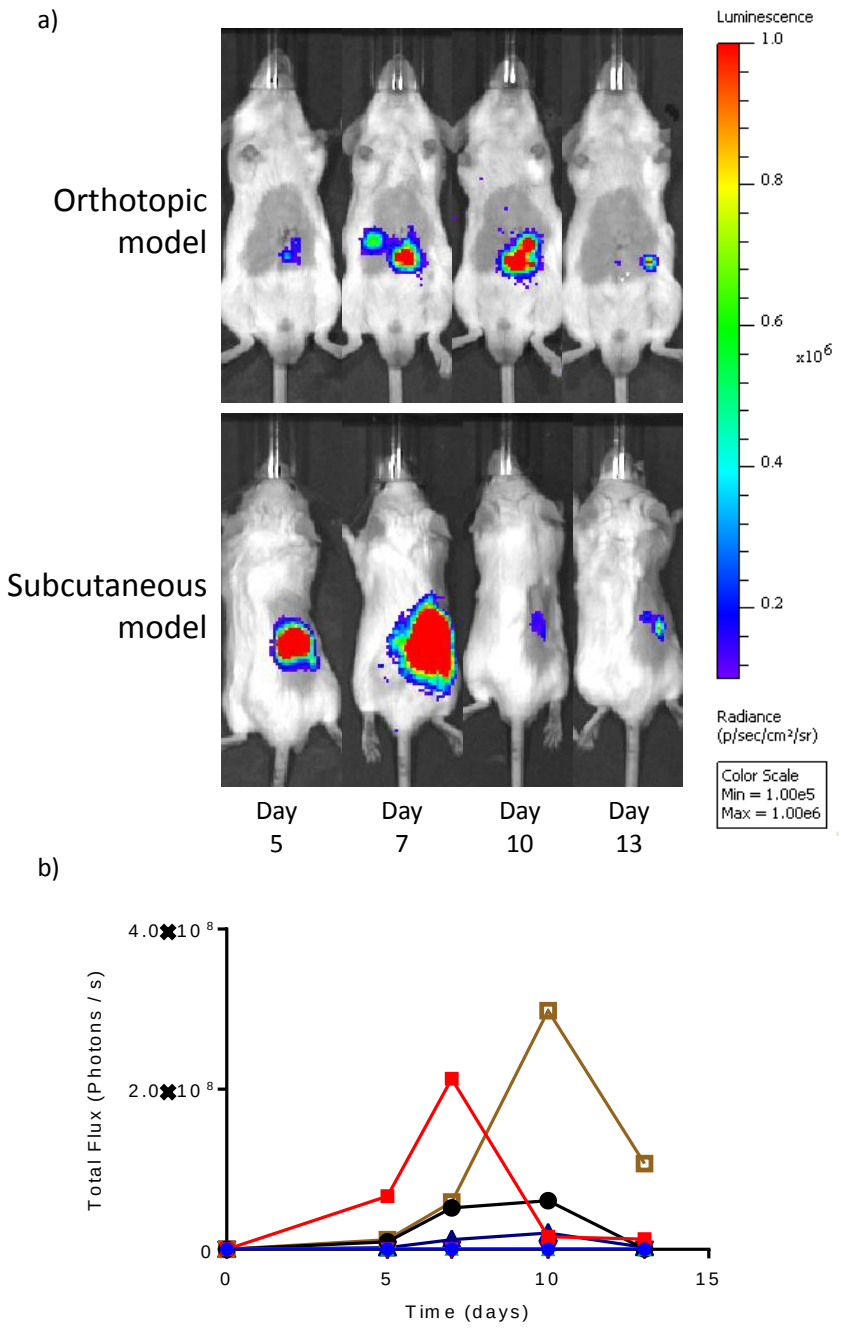

Figure 2.19 – Findings were similar in the 2nd group of 9 BALB/c mice following caecal injection of the CT26lucA2 clone, with a fall in luminescent signal, as demonstrated in a) representative images and b) graphically for each individual mouse, noted from day 7 onwards. The inclusion of a flank grafted mouse in this group allowed visual confirmation of tumour regression.

On necropsy, very small (1mm) tumour nodules were noted in the caeca of mice with detectable signal. Histology confirmed these nodules to be consistent with a poorly differentiated adenocarcinoma. However, staining for the CD3 antigen confirmed dense infiltration of T-cells into the tumour, suggesting an immune response (figure 2.20).

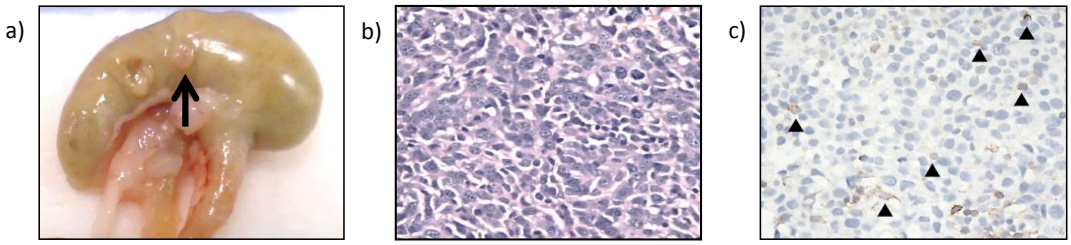

Figure 2.20 – a) Photographic image of a tiny tumour nodule (long arrow) in the caecum of a BALB/c mouse, taken 23 days after the orthotopic injection of the CT26lucA2 cell line. b) Light microscopy (x400) confirmed a poorly differentiated adenocarcinoma but with a c) dense T-cell (solid triangles) infiltrate when stained for the CD3 antigen.

2.3.10 Caecal implantation of the CT2luc6A6c clone

Due to the failure of the CT26lucA2 cell line to propagate *in vivo* the CT26lucA6c conditioned cell line was used to develop the syngeneic orthotopic murine model. To establish the optimum imaging times, growth rate of primary tumours and frequency of metastatic disease, eight immune-competent BALB/c mice underwent orthotopic injection of the CT26lucAc6 cell line in the caecal sub-serosa. There was no peri-operative morbidity or mortality up to the study end-point. Primary tumours developed in five (63%) mice, with luminescent signal continuing to increase throughout the study period, consistent with tumour growth.

Due to the large variation in signal at the first imaging point, subsequent luminescent values were expressed as the fold change in luminescence by dividing by the signal from the first imaging day. This meant each mouse was able to act as its own control, allowing standardisation and comparisons between mice by reducing the variations in signal likely to result from the operative technique and position of injection into the caecum. The study was ended on the 18th day post-implantation due to one mouse reaching the severity limits of the project licence due to symptoms of obstruction (figure 2.21).

One (20%) mouse developed ectopic signal consistent with the development of a liver metastasis and was subject to 3D imaging which suggested that signal may be originating from within the liver. This was confirmed on necropsy, ex-vivo imaging and histologically (figure 2.22).

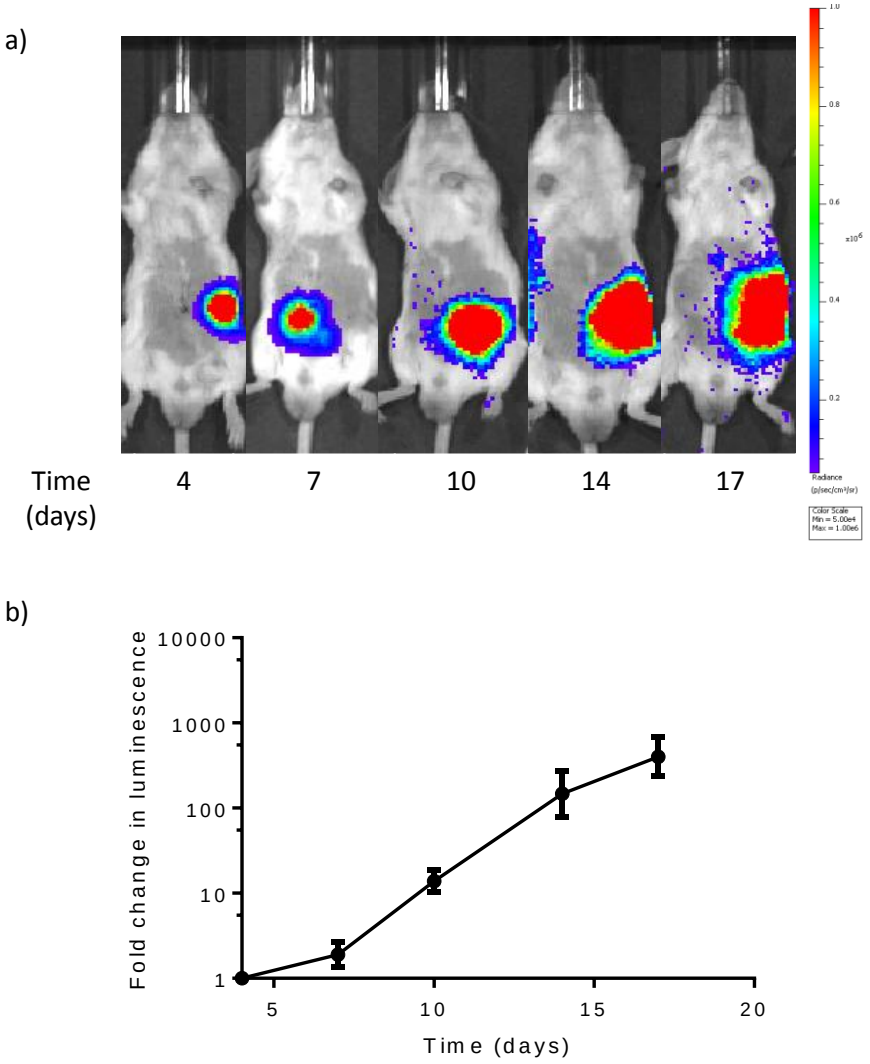

Figure 2.21 – a) Representative IVIS® images from the first attempt at caecal implantation using the CT26lucA6c clone. Imaging was consistent with development of a primary tumour in the left iliac fossa of the mouse, with ectopic signal developing on day 17 in the right upper quadrant, consistent with the development of a liver metastasis. b) Results were combined as fold change in luminescence for graphical display, confirming an increase in luminescence throughout the study period. (N=5, Graph displays mean +/- SEM)

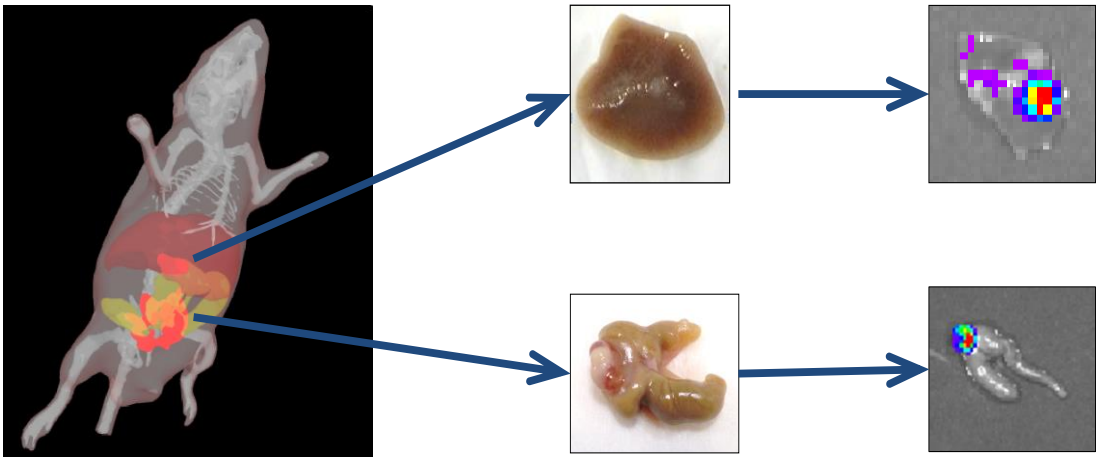

Figure 2.22 – 3D spectral un-mixing imaging can be useful for estimating the depth of luminescent signal within the mouse, suggesting luminescent signal arising from within the liver. Ex-vivo assessment confirmed the presence of a liver metastasis, with signal present in both the caecum and liver on IVIS® imaging.

Mice with luminescent signal all had macroscopic primary tumours at necropsy. One mouse was also found to have peritoneal disease and ascites. Primary tumours were confirmed to be poorly differentiated neoplastic growths of epithelial origin, displaying clear infiltrative behaviour. There was no striking evidence of lymphocytic infiltration of the tumour as noted in previous experiments with the CT26lucA2 cell line (figure 2.23).

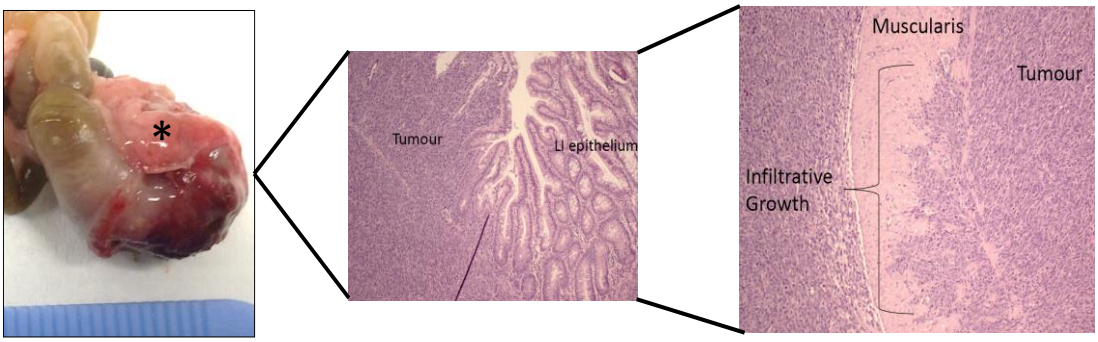

Figure 2.23 – Photograph and histology from a large caecal carcinoma (marked by *) excised 18 days after implantation. Histology confirmed tumour growth in the wall of the caecum, originating below the epithelium and invading into the muscularis.

Establishing an optimum time for imaging after the injection of luciferin was more difficult in the orthotopic model than with the *sc* injection of cells. The timing of peak signal tended to vary considerably between mice (ranging from 4-25 minutes) and the plateau period was short, perhaps reflecting variation in blood supply to the tumour. Mice were therefore imaged every 2 minutes until luminescent signal fell and the highest signal achieved used in data analysis (figure 2.24).

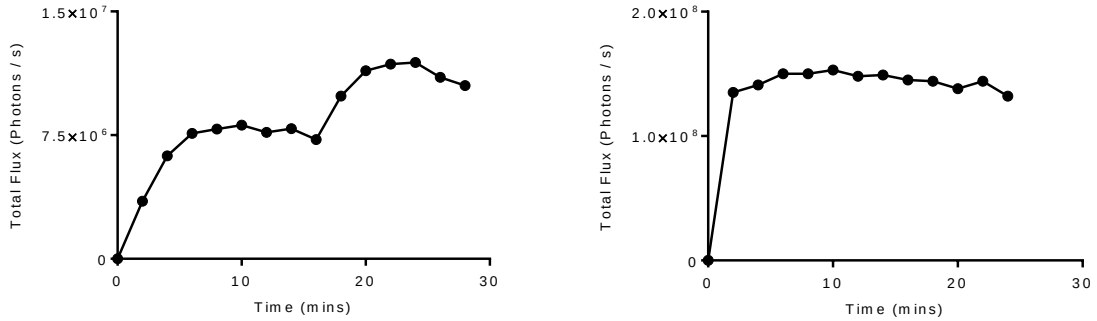

Figure 2.24 – Graphs displaying kinetic imaging curves (imaged every 2 minutes) for individual mice orthotopically implanted with the CT26lucA6c cell line. The timing of peak signal varied considerably between mice.

A total 68 immune-competent BALB/c mice have undergone caecal implantation of the CT26lucA6c cell line, with many allocated to the treatment groups described in subsequent work. There have been no complications from the procedure or peri-operative deaths in this model. Weight loss is common (occurring in all mice) in the first 3-4 days post-operatively but tends to be minimal and most mice have reached or exceeded their pre-operative weight by 7 days.

Primary tumours have developed in 44 (65%) mice and of these nine (20%) have developed liver metastases; no more than 2 metastases have been identified in a single mouse. Liver metastases are believed to have occurred through a mixture of haematological and trans-coelomic spread. Metastases via the haematological route occur within the hepatic parenchyma while those spread through the peritoneal cavity can be seen to originate on the liver capsule (figure 2.25). Gross peritoneal disease developed in seven (16%) of the mice and these were excluded from data analysis in experimental studies. One mouse in the experimental groups had to be culled prior to the study endpoint due to symptomatic colonic obstruction.

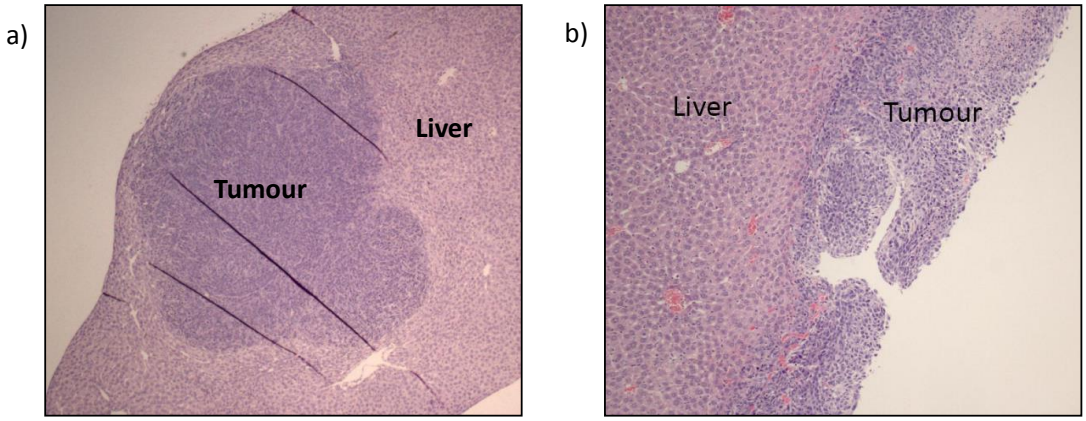

Figure 2.25 – Microscopic images of H&E stained sections of liver metastases originating from implantation of the CT26lucA6c cell line. a) Metastases originating by haematological spread occur within the hepatic parenchyma, whereas b) those resulting from trans-coelomic spread grow on the liver capsule.

2.3.11 Implantation of the HCT116lucB4 clone

An attempt was made to establish an orthotopic xenograft model of CRC by implanting the luminescent human CRC clonal cell line, HCT116lucB4 into homozygous nude BALB/c mice. Caecal injection of the cell line was performed in fifteen mice. A single mouse had a superficial dehiscence of his skin on the first post-operative day and was re-sutured. Only five (33%) mice developed detectable signal by the 7th post-operative day. Unfortunately signal fell in most mice from this imaging point and, due to the low tumour uptake rate and falling luminescent signal, the study was terminated on the 14th day post-implantation. At necropsy only very small (≤1mm) tumour nodules were visible in mice with detectable luminescent signal. No mice had macroscopic evidence of tumour formation within the peritoneal cavity or liver (figure 2.26).

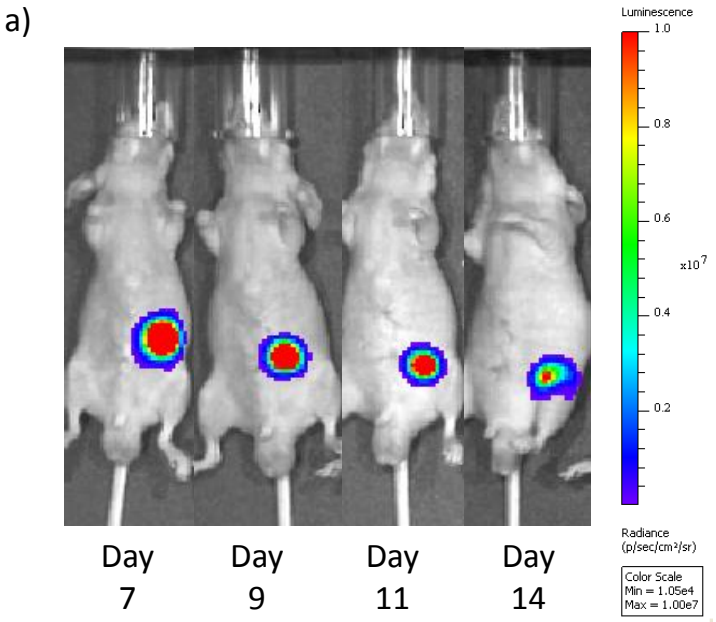

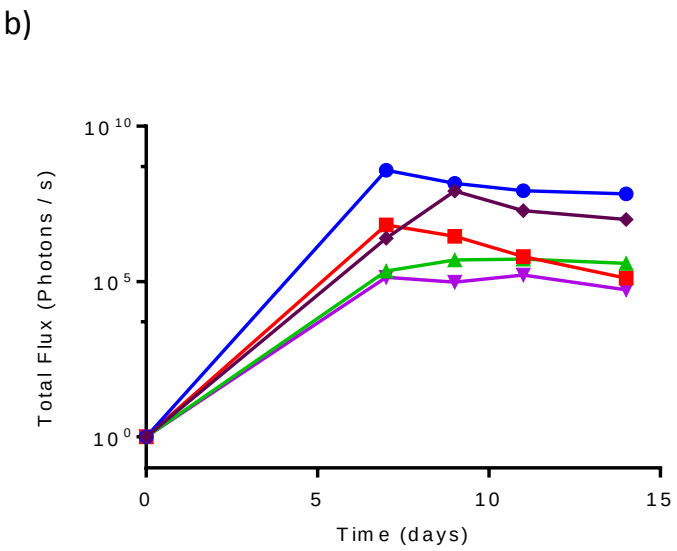

Figure 2.26 – a) Representative IVIS® images and b) data presented graphically confirm a falling luminescent signal from day 7 in the 5 out of 15 nude BALB/c mice orthotopically-injected with the HCT116lucB4 clonal cell that originally had detectable luminescence.

2.4 Discussion

This chapter describes the development of a syngeneic orthotopic metastatic murine model of CRC, from the development of luminescent populations of cell lines from a single clone, to the injection of these cell lines into the caecum of BALB/c mice and the longitudinal assessment of disease burden by IVIS® imaging.

The pilot study of this model, described in section 2.3.10, allowed improvement of the injection technique, the establishment of imaging protocols and the determination of the ideal imaging frequency, the tumour uptake rate, the frequency of metastatic disease and the likely duration of murine studies. These data were used to guide further studies applying this model to the testing of potential therapies *in vivo.* As a direct result of this pilot, future studies utilising the model followed a set protocol which included: the use of a lower cell count ($4x10^5$ cells), allowing the study period to be prolonged to 21 days after implantation before tumour-related symptoms developed; the warming of matrigel suspended cells at room temperature for up to a minute to increase the viscosity of the inoculum and prevent leakage; the use of the 7^{th} day post-implantation as the first imaging time-point, giving time for the tumour to become established, but reducing the larger variations in signal seen between mice at later imaging points; the use of kinetic imaging (every 2 minutes until peak signal) in each mouse at every time-point, improving comparisons between time-points; and the expression of data as a fold change from the initial luminescent imaging point, allowing each mouse to act as its own control and narrowing the standard deviation. Imaging frequency was also increased to three times a week for murine experiments comparing treatment groups due to the rapid growth of the tumour and resulting large changes in total flux that can occur in short time periods.

A distinct advantage of this syngeneic model is the short time-frame required for the establishment and development of primary tumours. This allows rapid screening of potential therapies *in vivo,* within a three-week window. This is in contrast to the results demonstrated in publications utilising orthotopic xenografting of human CRC cell lines. In one example $2x10^6$ cells were injected into the caecal wall and tumour growth assessed 8 weeks after implantation [410]. The use of BLI IVIS® imaging also increased through-put as up to five mice could be imaged simultaneously, permitting the relatively rapid acquisition of larger data sets. Up to 15 mice were often imaged in a single session lasting no more than two hours.

The rate of liver metastases (20%) demonstrated in the syngeneic model is similar to the incidence of synchronous liver metastasis seen in patients with CRC; recent data report metastatic disease in 21% of patients at presentation [411]. This suggests that the murine model is a reasonable representation of the presentation of CRC in patients, but limits its use in studies where liver metastases are a requirement. In this scenario, direct injection into the liver parenchyma, portal vein or the spleen is likely to be more reproducible, with take rates of 100% described in the literature [412]. Rates of metastases could potentially have been increased through the re-culturing of cells isolated from the liver metastasis that developed in mice, selecting a population of cells with the highest metastatic potential. A metastatic rate of 20% is also considerably lower than demonstrated in recent studies utilising orthotopic injection of the CT26 cell line. One study demonstrated liver metastases in 67% of mice 14 days after the caecal injection of CT26 cells. However, this study utilised MRI imaging, which could have improved detection rates, on a small number of mice (n=6) [351]. MRI imaging was considered, but BLI imaging selected due to its high-throughput and relatively low cost for the assessment of potential therapies.

Another limitation of the model is the late development of metastases, often only detectable on IVIS® imaging as a distinct area of luminescence separate from the primary tumour towards the end of the study period. Attempts were made to develop a more luminescent CT26 clone, utilising the pSELECT-zeo-LucSh vector, which could potentially have allowed the earlier detection of liver metastases or the inoculation of a lower cell count, perhaps delaying the onset of bowel obstruction and allowing more time for metastases to develop. Unfortunately, most likely as a result of a T-cell mediated immune response in the mice, this clonal population of cells were unable to propagate *in vivo.*

Other techniques could have been utilised in an attempt to develop increased luminesce in cell lines. It is possible to design vectors that allow cells to be dual-tagged with genes coding for luciferase and Green Fluorescence Protein under the control of a single promotor, permitting selection of the successfully transfected luminescent cells by Fluorescence-activated cell sorting (FACS) and removing the need for serial dilution to randomly select clones [413, 414]. Attempts were made to sort cells by flow cytometry using luminescence during this thesis (data not shown); although the wavelengths of light produced by luminescence can in theory be detected by FACS, the signal intensities were found to be too low.

Alternate transfection techniques or reagents could also have been considered. Comparisons of commercially available non-viral transfer reagents demonstrated cell line dependent variations in transfection efficiency [415]. Various transfection techniques have also been compared in the literature; in human dental follicle cells the use of electroporation resulted in a greater transfection efficiency than chemical techniques, including liposomal transfection [416]. Viral transfection methods could also have been considered; lentiviruses are particularly well studied and shown to integrate well into the host genome, resulting in stable and long-term gene expression. As with all gene transfer methods there are drawbacks; production is often labour intensive and there is the potential for the activation of latent disease, particularly with retroviral vectors [417, 418]. Clustered regularly interspaced short palindromic repeats (CRISPR) gene editing is a relatively new technique, allowing a cell's genome to be cut at a desired location and a new gene to be inserted [419]. CRISPR relies on an enzyme called Cas9 which uses a guide RNA molecule to identify its target DNA, then edits the DNA to disrupt genes or insert desired sequences. CRISPR could be used to splice the luciferase gene into the genome of a cell, removing the problems associated with poor transfection efficiencies and stability of expression.

The relatively large variations in the growth rate of tumours, as assessed by luminescent imaging, seen in the model can also present problems with data analysis as larger groups of animals may be required to achieve significance between data sets. A number of factors could contribute to this, such as the blood supply of the tumour and variations in expression of genes and proteins, such as growth factors, between individual mice. Studies have described the suturing of a small lump of tumour tissue on to the caecal wall after deliberate serosal damage, to allow implantation [420]. This technique could potentially have reduced some of the variation in signal seen at the initial imaging points, which are likely to result from the injection technique and inoculation of variable cell numbers. This effect was at least partially controlled through the expression of data in terms of fold change.

Unfortunately attempts to establish a xenograft model using the same technique were unsuccessful during the time allocated for completion of this thesis. The reasons for the poor tumour uptake rate and tumour regression demonstrated in the xenograft model were not established. The athymic development of T-cells and natural killer cells is possible in nude mice, and is more common in nudes on a BALB/c background. Athymic mice are

also able to produce B-cells and are therefore capable of mounting some humoral response. It is theoretically possible that the hEF1/HTLV promotor in the pSELECT-zeo-LucSh vector, which contains part of the human T-cell leukaemia virus gene sequence, induced an immune response. This would also explain the lack of success in the syngeneic model in cells transfected with this plasmid. Unfortunately, the size of any lesions noted at necropsy in the nude mouse study described in 2.3.11 made histological assessment of tumour tissue difficult. The use of a different mouse strain, such as SCID mice, may have improved the chances of developing a xenograft model. However, due to the success of the syngeneic model, and the greatly increased cost associated with the purchase and use of nude mice, the syngeneic model was considered to be superior.

The aim of the work presented in this chapter was to create a murine model of CRC that more accurately reflected the pattern of disease found in patients than with the *sc* flank injection of tumour cells into rodents. A murine model was created that relatively reliably developed primary colonic tumours in the correct microenvironment that were capable of metastasising to the liver. Disease also occurred in the presence of an intact immune system. The model had some distinct advantages for the testing of potential therapies: the use of BLI imaging allowed the longitudinal acquisition of data in larger numbers of mice than is achievable with other imaging modalities, with cull not required for the assessment of disease burden; the rapid development of disease meant that studies could be conducted over relatively short time periods; and the use of immune-competent mice meant the model was relatively inexpensive in comparison to immune-deficient models.

Chapter 3 – The expression and modulation of Nrf2 in colorectal cancer; application to the optimisation of irinotecan therapy.

3.1 Introduction

Chemotherapy is frequently utilised in the treatment of advanced CRC. Patients with a colonic primary and liver metastases may receive chemotherapy in an attempt to bring them to resection or to prolong life in the palliative setting. Rectal cancer may be treated with neoadjuvant LCCRT to reduce the risk of margin positivity and local recurrence following resection. Adjuvant chemotherapy may be given to any patient found to have a high-risk tumour, usually due to lymph node positivity, following resection and histopathological assessment of the primary. Unfortunately, response to chemotherapy can vary significantly due to a number of factors. These include the biology of the tumour itself, in addition to the ability of the patient to metabolise the active and toxic metabolites of the drug. Specifically, in reference to irinotecan therapy, variations in the expression of CES, CYP3A, UGT1A1 or the ABC transporters in both the patient's liver and tumour could all influence clinical response and the severity of side effects and toxicity, as discussed in section 1.8.4.

Despite the frequent utilisation of chemotherapy in the treatment of patients with stage III or IV CRC, which in the adjuvant setting is thought to confer a 10% improvement in absolute survival, outcomes for these groups remain worse than for those presenting with low risk tumours [421]. The identification and modulation of therapeutic biomarkers could potentially improve these outcomes, either through the development of novel standalone therapies or as enhancers of response to standard chemotherapy regimens. A biomarker can be defined as a molecular marker that can be obtained through analysis of mRNA, DNA or proteins to stratify patients for treatment benefit, prognosticate patient outcome or predict and modify response to therapy [422].

Nrf2 has the potential to act as a prognostic, predictive or therapeutic biomarker due to its roles in cell proliferation, cell survival, protection against ROS and drug metabolism, as discussed in section 1.10. High Nrf2 expression could theoretically confer a survival advantage to tumour cells and increase proliferation, potentially resulting in a more aggressive tumour, and a worse prognosis for patients. It could also render cells more resistant to chemotherapy through the activation of drug metabolising or cell survival pathways, predicting a worse response to therapy. A number of recent publications have correlated high Nrf2 expression in a variety of malignant tumours, including bladder, gastric and ovarian cancers, with worse absolute survivals and chemoresistance [268, 423, 424].

Inhibition of Nrf2 in cancer cells could therefore be potentially therapeutic, reducing the activation of pro-survival and chemoresistance pathways.

Nrf2 modulation could be particularly relevant to treatment with the pro-drug irinotecan. The metabolism of irinotecan and the proteins and enzymes associated with this pathway were discussed in section 1.8.4. The involvement of Nrf2 in regulation of a number of these proteins was highlighted in sections 1.10.4. To summarise these sections, irinotecan is converted to the active metabolite SN-38 by the CES and UGT1A1 detoxifies SN-38 to SN-38G for excretion. Irinotecan can also be directly metabolised to the inactive compounds APC and NPC by CYP3A. The ABC transporters aid in the active excretion of both irinotecan and SN-38 from cells. Expression of CES, UGT1A1 and a number of the ABC transporters have all been demonstrated to be inducible through activation of the Nrf2 pathway. As a result, the effect of Nrf2 modulation in CRC, particularly in reference to irinotecan therapy, is unpredictable and involves the complex interactions between drug metabolism and cell survival pathways.

A benefit to the continued investigation of Nrf2 as a therapeutic biomarker in cancer is the presence of pharmacological inducers and inhibitors. Two of the more promising and most well publicised of these, the inducer CDDO-me and inhibitor brusatol, were discussed in sections 1.10.5 and 1.10.6 respectively. These compounds potentially allow Nrf2 modulation to be translated into clinical practice without the need for complex gene based therapies.

The work in this chapter describes the expression of Nrf2 in CRC patient samples and cell lines, demonstrates modulation of Nrf2 expression *in vitro* both genetically and pharmacologically, examining the effect this has on cell proliferation and survival in isolation and when combined with irinotecan based chemotherapy, before translating these findings *in vivo* utilising the murine model described in chapter 2.

3.2 Methods

3.2.1 Tissue microarray construction

NHS Research Ethics Committee and Research and Development approval was obtained for all work on patient samples (12/NW/0011). Only patients with metastatic CRC were included in the study. Archived samples of formalin-fixed paraffin embedded patient primary and metastatic colorectal cancer tissue were obtained from contributing research sites within the Merseyside and Cheshire cancer network. Normal adjacent colonic mucosa was also obtained where available. Blocks and corresponding H&E stained slides were reviewed and marked to identify representative areas of both tumour and normal tissue.

Tissue Microarrays (TMAs) were constructed using a tissue microarrayer (Beecher Instruments Incorporated, Wisconsin, USA) with 0.6mm cores retrieved from donor blocks and transferred into the recipient master paraffin block in triplicate as described in the literature [425]. Normal liver tissue was also transferred to each TMA in triplicate to act as a control. Samples of primary tumour, normal colon and liver metastases were randomised across 3 TMAs. To allow inter-array comparisons, a sample set containing all three tissue types from a single patient was placed on each of the TMAs. TMAs were incubated at 37°C overnight, placed on ice and 5µm sections were cut on a rocking microtome and placed onto coated glass slides.

3.2.2 IHC analysis of Nrf2 expression in patient samples

To establish optimal conditions, 3 dilutions of the primary antibody for Nrf2 were used on a series of test slides with concentrations spanning those suggested by the manufacturer (1:20, 1:50, 1:200, 1:500). Nrf2 is ubiquitously expressed, but examination of Protein Atlas (www.proteinatlas.org) suggested a high intensity staining would be expected in normal liver tissue, and this was included on each of the test slides to guide staining protocols. Antibody diluent only and a mouse IgG1 isotype control (Abcam, ab91353, Cambridge, UK) were used as negative control for background staining.

Sections were de-waxed in xylene and rehydrated with ethanol solutions of decreasing concentrations. After blocking with 3% hydrogen peroxide in 100% methanol, antigens were retrieved by microwaving for 20 minutes in 10mM citrate buffer and further blocked with 10% goat serum in 0.1% TBST. Slides were incubated with a 1:50 dilution of the primary antibody for Nrf2 (Santa Cruz, SC-722, California, USA) for 2 hours followed by a

1:200 horseradish peroxidase conjugated secondary antibody for 30 minutes (Dako UK Ltd, E0433, Cambridgeshire, UK). Following incubation with the Vectastain Elite® ABC reporter system (Vectorlabs, Burlingame, USA), slides were developed with DAB and counterstained with haematoxylin.

Stained sections of the TMA were reviewed by light microscopy and scanned using the Aperio Scanscope (Leica Biosystems, Wetzlar, Germany) and semi-quantification of protein expression performed using Tissue Studio v.2.0 (Definiens AG, Munich, Germany). Software training was required prior to scoring. In brief this consisted of nuclear and cell membrane identification to enable cellular recognition, followed by the setting of intensity thresholds for weak, moderate and intense staining. Minor adjustments within the software were made until concordance with a 10% sample similarly scored by eye was achieved.

Staining intensities from the automated system allowed the generation of H-scores for cores as described by Shousha [426]. This involved assigning scoring intensities of negative, weak (1), moderate (2) or high (3) to cells with the H-score calculated utilising the equation: H-score = (1 x percentage of cells scored 1) + (2 x percentage of cells scored 2) + (3 x percentage of cells scored 3).

3.2.3 Cell culture

General cell culture, cell counting and details specific to the culturing of the HCT116 and CT26 cell lines were described in section 2.2.4. The benign human colonic cell line, CCD-33CO, was also purchased from the American Type Culture Collection and cultured in Eagle's Minimum Essential Medium (EMEM) (Sigma-Aldrich, Dorset, UK) supplanted with 10% fetal bovine serum and antibiotics (100 units/ml penicillin G and 100 µg/ml streptomycin).

3.2.4 siRNA modulation of the Nrf2 pathway

siRNA silencing was utilised to modulate Nrf2 in CRC cell lines. Cell were plated out and left to adhere overnight at 5000 cells/well in 100µl of medium on 96-well plates for viability experiments, or $3x10^5$ cells/well in 1ml of medium on 12-well plates (Nalge-Nuc international, C/O VWR International, Lutterworth, UK) for western immunoblotting. siRNA targeting human or murine Nrf2 or Keap1 (see table 3.1 for details of siRNA sequences and manufacturers) were purchased from Dharmacon or Qiagen and prepared as per the

manufacturer's instruction. A non-targeting scrambled siRNA (referred to as siRNA control) was used as a control in all experiments.

Species	Target	Company	Name	Target Sequence
Human	Nrf2	Dharmacon	siGenome D-003755-05-0020 NFE2L2 NM_001145413	5'-UGACAGAAGUUGACAAUUA-3'
Human	Keap1	Dharmacon	siGenome D-012453-03-0020 Nm_012289	5'-GGGCGUGGCUGUCCUCAAU-3'
Human	Control	Dharmacon	siGenome D-001210-03-20 Non-targeting siRNA	Proprietary
Murine	Nrf2	Dharmacon	siGenome MQ-040766-00-0002 NM_010902	5'-AAAGACTCAAATCCCACCTTA-3'
Murine	Keap1	Qiagen	FlexiTube Mm_Keap1_7 NM_001110305	5'-TTCCTGCAACTCGGTGATCAA-3'
Murine	Control	Qiagen	xiTube siRNA AllStars Negative Control siRNA (SI03650318)	Proprietary

Table 3.1 – siRNA used for transfection of cell lines and modulation of the Nrf2 pathway.

For the transfection of cells plated out on a 12-well plate, a mixture of Lipofectamine® RNAiMAX (Invitrogen, Paisley, UK), siRNA stock and Opti-MEM was prepared in a nuclease free Eppendorf and incubated at room temperature for 15 minutes as per the manufacturer's instructions (Invitrogen). 135µl of this mixture was added drop-wise to 1ml of medium in each cell-containing well and plates incubated at 37°C for 48 hours, ensuring modulation of protein expression before confirmation by western immunoblotting. The same protocol was used for the siRNA transfection of cells in the 96-well format with 10µl of the RNA / transfection reagent mixture added to 90µl of medium in each cell containing-well 48 hours before the application of chemotherapeutics in viability experiments. The volume of Lipofectamine® RNAiMAX applied per well was 0.5ul or 1uL and the quantity of RNA 1.5pmol or 20pmol RNA in the 96 or 12-well formats respectively after optimisation.

3.2.5 Treatment of cells with chemicals and compounds

Stock concentrations of all drugs, including irinotecan (80mM, J&H Chemical, Shanghai, China), 5-FU (Sigma-Aldrich, Dorset, UK), CDDO-me (90µM, Cayman chemicals, Michigan, USA) and brusatol (270µM, kind gift from Zhi-Xiu Lin), were prepared in dimethyl sulfoxide (DMSO) (Fisher Scientific, Loughborough, UK) for dose-response experiments. A 1 in 3 serial dilution of drug stocks was performed in DMSO and these added to medium to produce the final concentrations required for application to cells, ensuring a maximum of 0.5% (v/v) DMSO. For the co-dosing of chemotherapeutics with CDDO-me or brusatol on HCT116 cells,

stock solutions of 60µM or 200µM and 30µM or 200µM respectively were produced in DMSO and diluted x2000-fold in medium for application to cells, in combination with irinotecan or 5-FU. This resulted in final concentrations of 30nM or 100nM for CDDO-me and 15nM or 100nM for brusatol. For CT26 cells a stock solution of 600µM brusatol was created and diluted as above to produce a final concentration of 300nM for application to cells.

For the MTS viability assay cells were plated out at 5000 cells/well and left overnight to adhere. They were then dosed in triplicate with either irinotecan, 5FU, CDDO-me, brusatol or combinations of these across a range of concentrations. To assess the effect of Nrf2 modulation on chemosensitivity cells were either pre-transfected with siRNA as described in section 3.2.4, and chemotherapeutics applied after 48 hours, or were co-dosed with CDDO-me or brusatol. All results were calculated as a percentage of a vehicle control (0.5% DMSO in medium or control siRNA) treated cells after 48 hour incubations with chemotherapeutics.

For western immunoblot analysis cells were plated out on 12-well plates at $3x10^5$ cells/well and treated with siRNA, CDDO-me or brusatol prepared in DMSO as described and added to medium to produce the desired concentrations for application to cells. Cells were subsequently incubated at 37°C and lysed at 48 hours for assessment of siRNA, increasing time-points for time-course experiments or after three hours for dose-response analysis of drugs. All experiments described in this section were performed in triplicate on at least three occasions.

3.2.6 Preparation of cell lysates

After the required period of incubation with drugs or siRNA, medium was aspirated from cells and wells washed twice with ice-cold PBS. 50µl of radioimmunoprecipitation RIPA buffer (150mM NaCl, 1.0% IGEPAL® CA-630, 0.5% sodium deoxycholate, 0.1% sodium dodecyl sulphate (SDS), 50 mM Tris, pH 8.0, Sigma-Aldrich, Dorset, UK) containing x100 diluted protease inhibitor cocktail (Sigma-Aldrich, Dorset, UK) was added to each well of a 12-well plate and left for 5 minutes on ice. Cells were then scraped off wells and pipetted into an Eppendorf. Eppendorfs were spun at 15 000 rpm for 15 minutes at 4°C and the supernatant collected and stored at -80°C prior to determination of the protein content and western immunoblotting.

3.2.6 Western immunoblotting

Prior to western immunoblotting the bicinchoninic acid (BCA) assay, utilising the Pierce™ BCA Protein Assay Kit (ThermoFisher Scientific), was used for protein quantification of samples as described in the literature [409]. 40µg of total protein was loaded in 4x Laemmli buffer (BioRad, California, USA) in each well of a Mini-PROTEAN® TGX™ Precast Gel (BioRad, California, USA) after denaturing proteins by heating for 5 minutes at 100°C. 4µl of the PrecisionPlus kaleidoscope molecular weight marker (BioRad, California, USA) was added to one well on every gel as a reference.

Gels were subjected to electrophoresis in running buffer (25mM Tris, 190nM glycine, 20% methanol and 0.01% SDS) at 90 volts until resolved and then 150 volts until the blue dye front reached the bottom of the gel. Following electrophoresis gels were transferred to a Hybond nitrocellulose sheet (GE Lifesciences, Pittsburgh, USA) using a blotting sandwich in a transfer unit containing transfer buffer at 230 mA for 2 hours. Membranes were washed briefly in TBST and the quality of transfer assessed using a Ponceau S stain (Sigma-Aldrich, Dorset, UK). The stain was removed by washing with TBST and the membrane blocked in non-fat milk (Biorad, California, USA) in TBST on an orbital shaker before addition of the primary antibody. The optimal conditions for antibody incubations were determined by experimentation and the final conditions used displayed in table 3.2.

Primary antibody	Primary Manufacturer	Blocking	Primary Dilution	Secondary antibody	Secondary Manufacturer	Secondary Dilution	TBST Washes
Nrf2 16396-1-AP	Proteintech, Illinois, USA	5% milk 2 hours	x1000 in 5% milk overnight	Anti-rabbit HRPA9169	Sigma-Aldrich, Dorset, UK	x5000 dilution 5% milk 1hour	3x20 mins.
Keap1 10503-2-AP	Proteintech, Illinois, USA	5% milk 2 hours	x2000 in 5% milk overnight	Anti-rabbit HRPA9169	Sigma-Aldrich, Dorset, UK	x5000 dilution 5% milk 1hour	3x20 mins.
CES1 AF7929	R&D Systems, Minneapolis, USA	10% milk 1 hour	x400 in 2% milk overnight	Anti-sheep HRP A3145	Sigma-Aldrich, Dorset, UK	x10 000 2% milk 1hour	3x5 mins.
NQO1 ab28947	Abcam, Cambridge, UK	10% milk 30 mins.	x2000 in 2% milk overnight	Anti-goat HRP P0449	Dako, Cambridge, UK	x2000 dilution 2% milk 1hour	3x5 mins.
HO-1 ab13243	Abcam, Cambridge, UK	10% milk 30 mins.	x10 000 in 2% milk	Anti-rabbit HRP A9169	Sigma-Aldrich, Dorset, UK	x10 000 2% milk 1hour	3x5 mins.
Actin ab6726	Abcam, Cambridge, UK	10% milk overnight	x10 000 in 2% milk	Anti-mouse HRP A9044	Abcam, Cambridge, UK	x10 000 2% milk 1hour	3x5 mins.

Table 3.2 – Antibodies and conditions used in western blotting experiments

Following incubation with the primary antibody and secondary antibodies, membranes were washed in TBST and chemiluminescence visualised in the dark by addition of the Enhanced Western Lightening reagents (Hyperfill ECL; Perkin Elmer, Massachusetts, USA). A film placed over the membrane was subsequently developed in Kodak developer and fixer solution and densitometry performed on bands of interest utilising Image-J (National Institutes of Health, Maryland, USA); each sample was normalised to actin as a loading control.

3.2.7 MTS cell viability assay

The MTS cell viability assay was utilised for the generation of dose-response curves as described in section 2.2.6.

3.2.8 Colony forming (clonogenic assay)

The reproductive integrity of cells following treatment with brusatol was assessed in both cancer cell lines using a colony forming assay. Cells were plated out on 24-well plates at $2x10^4$ cells/well and left to adhere and then exposed to treatment regimens including a 24-hour exposure to a vehicle (0.5% DMSO) control or brusatol across a range of concentrations. Cells were then re-plated on 6-well plates at 200 live cells/well and left for 7-10 days to allow the formation of colonies. Growth medium was aspirated, wells washed

with PBS, fixed with methanol for 15 minutes, stained for 30 minutes with 0.5% crystal violet in methanol and colonies counted using GelCount™ (Oxford Optronix, Oxford, UK). The surviving fraction (SF) for each treatment was then calculated as a percentage of the vehicle control using the method described by Franken *et al.* [427].

To ensure the accurate counting of colony numbers, settings on the GelCount™ were adjusted until concordance was reached with manual counting by eye. The final settings for the CT26 and HCT116 lines are displayed in table 1.16.

	CT26	HCT116
Edge detection sensitivity	96	70
Detection mode	dark in light	dark in light
Centre detection send	15	80.4
Colony diameter range	400-3000um	250-1700um
Centre to centre separation	200um	250um
Smoothing	3	3
Circulatory factor	64	34
Edge distance threshold	0.95	0.9
Number of spokes	32	32
Good edge factor	0.7	0.25
Overlap threshold	0.5	0.5
Shape filtering	Gaussian smooth filter 4	Gaussian smooth filter 3
Shape processing	best fit circle	best fit circle
Colony intensity	0.1-1.5	0.1-1.5

Table 3.3 – Settings utilised on the GelCount™ for the determination of surviving fractions of colonies.

3.2.9 Murine studies

The housing conditions of mice, in addition to the ethical and legal considerations of the animal work covered in this thesis are described in section 2.2.11. Both *sc* flank injection and the orthotopic syngeneic caecal implantation murine model described in chapter 2 were used in the experiments described in this chapter using the CT26lucA6c cell line.

3.2.10 Assessment of brusatol efficacy in a subcutaneous tumour model

A pilot study was conducted in 6 male 6-8 week old BALB/c mice comparing brusatol treatment (2mg/kg via *ip* injection) to vehicle control (1% DMSO in PBS). This study was designed to assess the safety of chronic dosing with brusatol and ensure Nrf2 inhibition in tumour tissue before confirming findings in the more complex orthotopic model. Mice received a *sc* injection of $5x10^5$ CT26lucA6c cells into the right flank as described in 2.2.12 and, after a 7-day period to allow establishment of tumours, mice (n=3) were randomised to treatment groups. For *ip* injection of brusatol 20mg/ml was dissolved in DMSO and then diluted x100 in PBS, with each mouse receiving 10µl/g of bodyweight. The same volume to weight ratio was used for the *ip* dosing of mice with the vehicle control.

Mice were dosed and imaged according to the schedule laid out in figure 3.1. Tumour growth was monitored by simultaneous luminescent IVIS® imaging and caliper measurement. Tumour volume was calculated from caliper measurements using the equation; tumour volume = maximum width^2 x maximum length x ½, as described in the literature [428]. IVIS® imaging was conducted as described in 2.2.14. After 21 days (14 days of dosing) mice were culled by cervical dislocation and tumours excised and snap frozen in liquid nitrogen for use in subsequent experiments and confirmation of Nrf2 inhibition by western blotting.

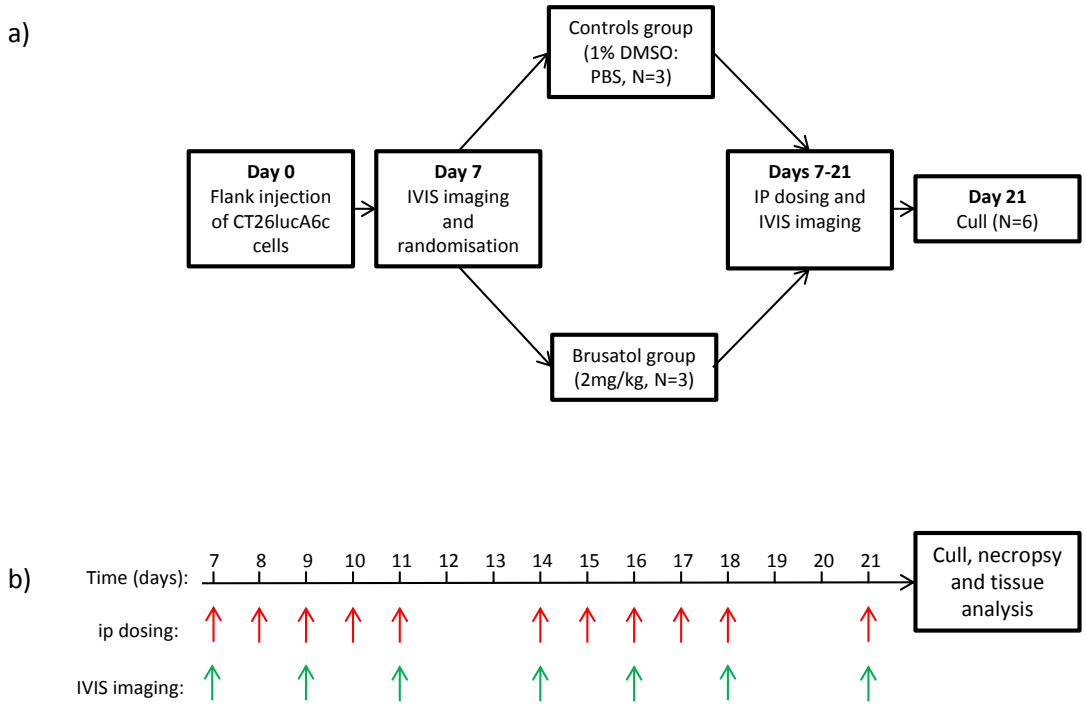

Figure 3.1 – a) Study plan and b) dosing regimens used in the pilot study comparing brusatol treatment to a vehicle control following the flank grafting of CT26lucA6c cells.

3.2.11 In vivo assessment in the syngeneic orthotopic model

This study utilised the orthotopic syngeneic murine model developed in chapter 2 and the method is described in section 2.2.13. In brief, 6-8 week old immune-competent male BALB/c mice were injected with $4x10^5$ CT26lucA6c into caecal sub-serosa following laparotomy and delivery of the caecum. Bioluminescent imaging of mice using the IVIS® was commenced on the seventh post-operative day and mice with detectable signal randomised to treatment regimens including: vehicle control, brusatol alone (2mg/kg *ip*), irinotecan alone (20mg/kg *ip*) or irinotecan plus brusatol (for dosing regimens see figure 3.2). For dosing with irinotecan the drug was dissolved at 2mg/ml in PBS and each mouse received 10µl/g of bodyweight. Brusatol dosing is described in 3.2.10.

Imaging was conducted thrice weekly until the study end-point. Three mice initially treated with brusatol were imaged for a further seven days after cessation of treatment to ensure the effect could be attributed to the drug.

Luminescent signals were quantified in photons/second and tumour growth expressed as the fold change in luminescence signal from the first imaging day (pre-treatment), with

each mouse acting as its own control. At the study end-point mice were sacrificed and tumour tissue stored in 4% paraformaldehyde prior to paraffin embedding for histological assessment and immunohistochemical staining.

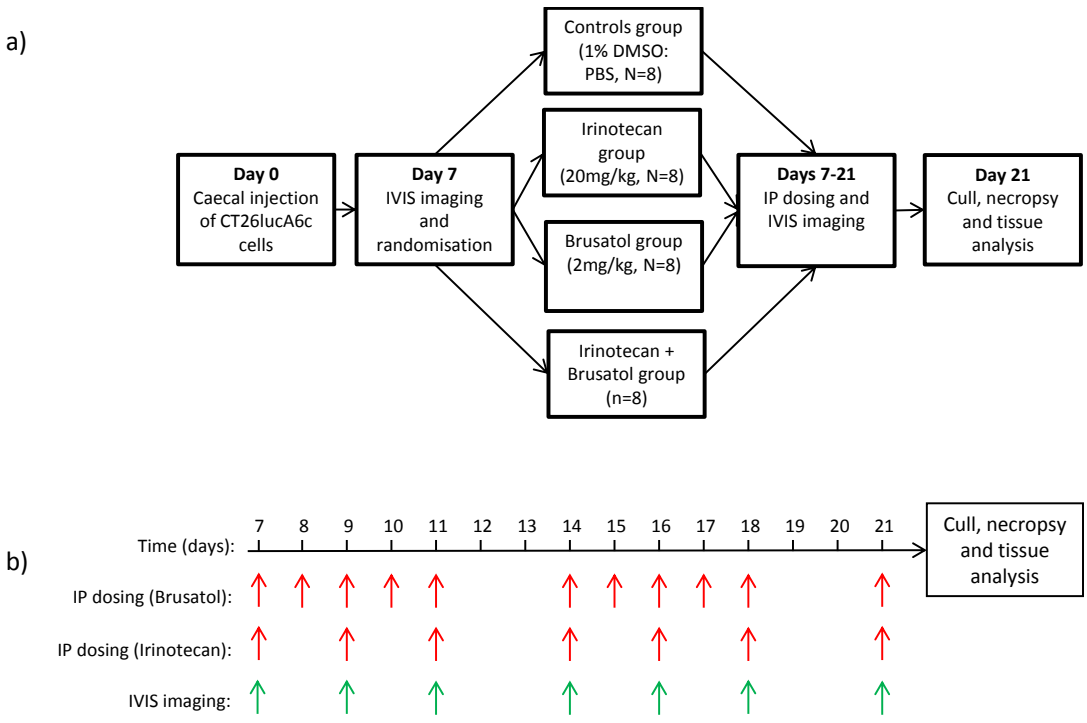

Figure 3.2 – a) Study plan and b) dosing regimens for the study comparing brusatol, irinotecan and irinotecan with brusatol to a vehicle control following the orthotopic injection of CT26lucA6c cells.

3.2.12 Homogenisation of flank tumours

Sections of tumours (50mg) from the mice flank-grafted with the CT26A6c cell line in the study described in section 3.2.10 were homogenised in 250µl of ice-cold 0.5M triethylammonium bicarbonate (TEAB) / 0.1% SDS buffer using a MM400 oscillating bead mill (Retsch, Haan, Germany). Samples were subjected to a freeze-thaw cycle (-80°C for 1 hour) and sonicated 3 times for 10 seconds each at an amplitude of 5µm. The homogenate was centrifuged at 14 000rpm for 10 minutes at 4°C and the supernatant retained. The supernatant was centrifuged again at the same rpm for a further 5 minutes. The protein concentration of the supernatant was determined using the BCA assay as described in section 2.2.8 and stored until required for proteomic analysis. Western blotting of tumour homogenates was conducted as described in section 3.2.6.

3.2.13 Histology, IHC staining and analysis of murine tumours

From paraffin-embedded tumour blocks, consecutive 4-microns thick sections were obtained and stained with haematoxylin eosin (HE) for morphological confirmation of the neoplastic process. Representative sections of the lesions were selected for IHC. All tissue sections were placed in an automated staining system (Link 48 Immunostainer; Dako, Germany), within which samples were deparaffinised, rehydrated and processed for epitope retrieval using computer-controlled antigen retrieval system (PT Link-Low pH; Dako, Germany) according to the manufacturer's recommendations. Primary anti-Nrf2 antibody (16396-1-AP, Proteintech, UK 1:100 dilution for 30 minutes) was applied and the anti-mouse/rabbit EnVision FLEX (Dako, Germany) detection system used. Upon completion of the immunostaining, sections were counterstained with Mayer's haematoxylin. BALB/c mice livers treated with CDDO-me were used as a positive control, while livers from Nrf2 knockout mice were employed as a negative control. Consecutive tumour sections incubated with non-immune rabbit serum served as technical negative control. Morphological evaluation and confirmation of tumour formation was performed by a board certified veterinary pathologist (LR) upon brightfield microscope examination of HE sections. Evaluation of Nrf2 expression was semiquantitative, using the methods described for the calculation of H-scores in section 3.2.1. Scoring was performed blinded to the experimental conditions.

3.2.14 Statistical analysis

GraphPad Prism® 6 statistical software was used for the generation of dose-response curves, the calculation of IC50 values and for comparisons of statistical significance. Statistical significance was assumed at $p<0.05$ (*$p<0.05$, **$p<0.01$, ***$p<0.001$, ****$p<0.0001$). IC50 values were calculated by fitting a four parameter log-concentration versus response curve to the data. Drug combinations were assessed for synergy by calculation of combination indexes (CI) using the Chou-Talalay method and the software package Compusyn® (CI < 1 indicates synergy) [429]. For mouse studies the slope of a line of best fit for each individual mouse was calculated as a surrogate marker of tumour growth rate. Growth rates for treatment groups were then compared with those in untreated controls with significance assessed by one-way ANOVA. SPSS statistics 21® was used to analyse patient data. In all data a Shapiro-Wilk normality test was used to guide appropriate statistical test selection. Tests used in each analysis are included with the presented data.

3.3 Results

3.3.1 Nrf2 expression in CRC patient samples

Fifty-nine patients with metastatic CRC were included in the TMA, 50 (85%) with cores of primary CRC, 43 (73%) with cores of liver metastases and 34 (58%) with normal colon available. Matched primary and metastatic samples were available for 34 (58%) patients. Available clinicopathological variables for patients, divided by tissue type, are displayed in table 3.4.

A moderate positive correlation was seen in Nrf2 H-scores between matched primary and metastatic samples ($r=0.4$, $p=0.03$, Pearson R), implying that Nrf2 expression in the metastasis reflects that of the primary (figure 3.3). Mean Nrf2 expression was significantly higher in primary (H-score = 30) and metastatic (H-score = 43) tumour tissue than normal colon (H-score 6, Kruskal-Wallis with Dunn's multiple comparisons test), highlighting an increased expression of Nrf2 in CRC (figure 3.4). Nrf2 expression did not vary significantly with T stage or nodal status (table 3.5).

There was no difference in Nrf2 expression in the primary or metastatic samples of chemo-naïve patients when compared with those who received neoadjuvant chemotherapy, suggesting overexpression of Nrf2 is not simply a marker of the increased cellular stress associated with chemotherapy, but that Nrf2 is constitutively activated (figure 3.5).

Variable		Primary Tumour	Liver Metastases	Normal Colon	P value
Median age (range)		78 (40-98)	78 (40-98)	79 (40-98)	p = 0.834 (ANOVA)
Gender (%)	Male	35 (70)	29 (67)	23 (68)	p = 0.958 (Chi-Square)
	Female	15 (30)	14 (33)	11 (32)	
T stage (%)	1	0	0	0	p = 0.911 (Chi-Square)
	2	8 (16)	4 (9)	4 (13)	
	3	33 (66)	31 (72)	24 (71)	
	4	9 (18)	8 (19)	6 (18)	
N stage (%)	0	14 (28)	11 (26)	11 (23)	p = 0.486 (Chi-Square)
	1	26 (52)	25 (58)	21 (62)	
	2	10 (20)	7 (16)	2 (6)	
Chemotherapy (%)	Yes	31 (62)	22 (51)	22 (65)	p = 0.597 (Chi-Square)
	No	17 (34)	17 (40)	11 (32)	
	Unknown	2 (4)	4 (9)	1 (3)	
Total		50	43	34	

Table 3.4 – There were no statistically significant differences in clinicopathological variables between patients included in the analysis of tissue cores on the TMA when grouped by tissue type.

		Primary-tumour		Liver metastases		Normal colon	
Variable		Mean H-score (95% CI)	P value	Mean H-score (95% CI)	P value	Mean H-score (95% CI)	P value
Gender	Male	27 (20-36)	p = 0.265 (ANOVA)	39 (34-72)	p = 0.07 (ANOVA)	5 (2-9)	p = 0.403 (ANOVA)
	Female	36 (21-51)		53 (28-46)		8 (3-14)	
T stage	1	NA	p = 0.442 (ANOVA)	NA	p = 0.673 (ANOVA)	NA	p = 0.269 (ANOVA)
	2	39 (14-65)		54 (25-82)		2 (0-11)	
	3	27 (19-36)		43 (33-52)		6 (2-9)	
	4	33 (19-46)		41 (22-59)		11 (4-18)	
N stage	0	32 (16-49)	p = 0.556 (ANOVA)	50 (34-66)	p = 0.334 (ANOVA)	6 (0.2-12)	p = 0.986 (ANOVA)
	1	27 (18-36)		39 (29-49)		6 (2-10)	
	2	36 (19-54)		28 (24-75)		7 (0-20)	
Totals		30 (24-36)		43 (37-50)		6 (0-13)	

Table 3.5 – Nrf2 expression did not vary significantly with gender, T stage or N stage in any of the available tissue types.

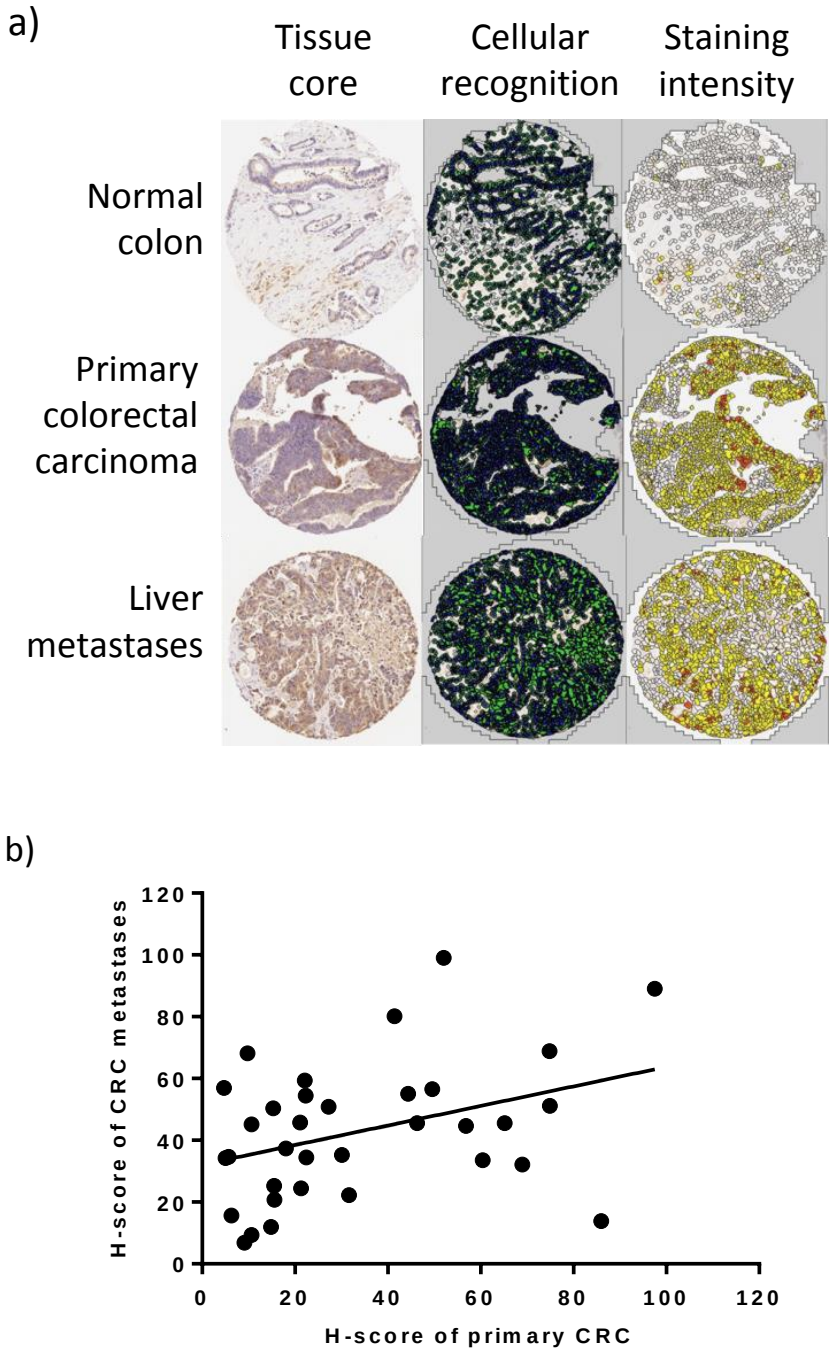

Figure 3.3 – a) Representative tissue cores displaying cellular recognition (green for cytoplasm and blue for nucleus) and Nrf2 staining intensity as assigned by the software; white represents negative, yellow weakly positive, orange moderately positive and red strongly positive cells. b) Nrf2 expression, measured by the calculation of H-scores, confirmed a positive correlation between matched primary tumour and liver metastases in patient samples (r=0.4, p=0.03, Pearson R). Analysed by Tissue Studio v.2.0

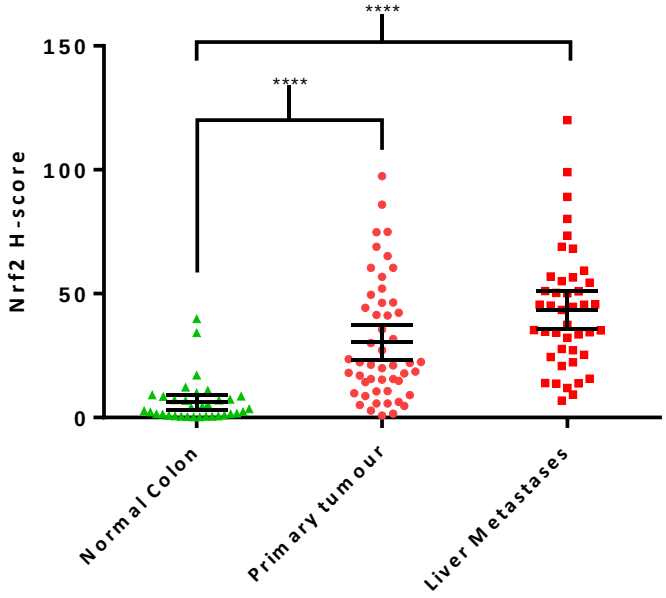

Figure 3.4 – Mean Nrf2 expression was significantly higher in primary (H-score = 30) and metastatic (H-score = 43) tumour tissue than normal colon (H-score = 6, Kruskal-Wallis with Dunn's multiple comparisons test). (Graphs displays mean with 95% confidence interval with each data point representing an individual patient)

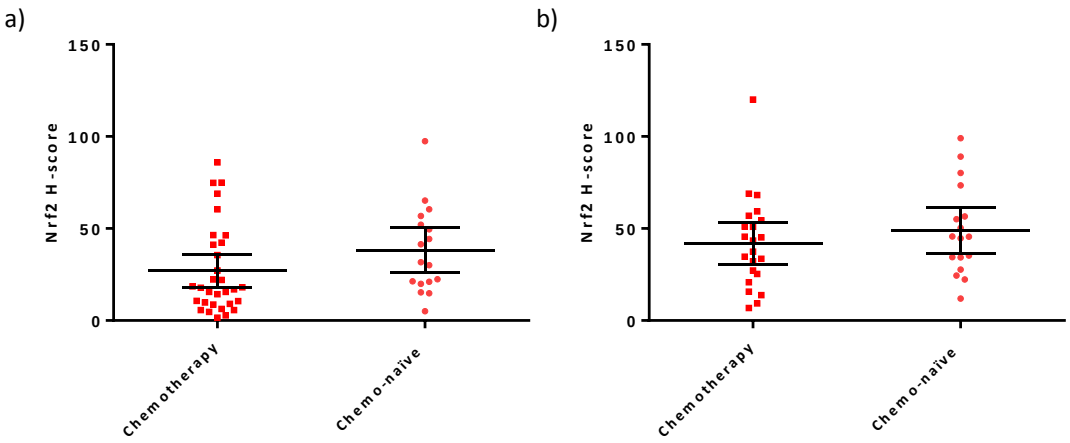

Figure 3.5 - Comparison of H-scores in chemo-naïve and treated patients found no significant differences in Nrf2 expression in a) primary or b) metastatic tissue (Mann-Whitney test). (Graphs display mean with 95% confidence interval)

3.3.2 Western blot confirmation of Nrf2 modulation in cell lines

Confirmation of Nrf2 modulation was demonstrated by western immunoblotting in response to genetic silencing of Nrf2 or Keap1 utilising siRNA (figure 3.6), or to pharmacological induction of Nrf2 with CDDO-me or inhibition with brusatol in the HCT116 and CT26 cell lines.

siRNA inhibition of Nrf2 achieved an 11-fold reduction in expression of the protein in the CT26 cell line and a 4-fold reduction in the HCT116 cell line, as assessed by western immunoblotting and densitometry. Nrf2 protein expression was increased by 4-fold in the CT26 cells and 3-fold in the HCT116 cells following inhibition of Keap1 by siRNA.

A higher concentration of brusatol was required to significantly inhibit Nrf2 in CT26 (300nM) than HCT116 (100nM) cells (figure 3.7). In both cell lines brusatol mediated inhibition of Nrf2 was transient, with maximum inhibition seen at three hours (figure 3.8). A rebound in Nrf2 expression was also observed in both cell lines between 12 and 24 hours. CDDO-me was a potent Nrf2 inducer with significantly higher expression noted with concentrations ≥30nM in both cell lines (figure 3.7). The induction of Nrf2 by CDDO-me peaked between 1-3 hours after dosing but persisted for up to 24 hours (figure 3.8).

In the CT26 cells a concentration of 300nM of brusatol resulted in a 10-fold reduction in Nrf2 expression, while in HCT116 100nM of brusatol decreased Nrf2 expression by 13-fold after 3 hours. Conversely, a 12-fold increase in Nrf2 expression was noted in the CT26 cell and a 3-fold increase in the HCT116 cell on western immunoblotting following a 3-hour incubation with CDDO-me.

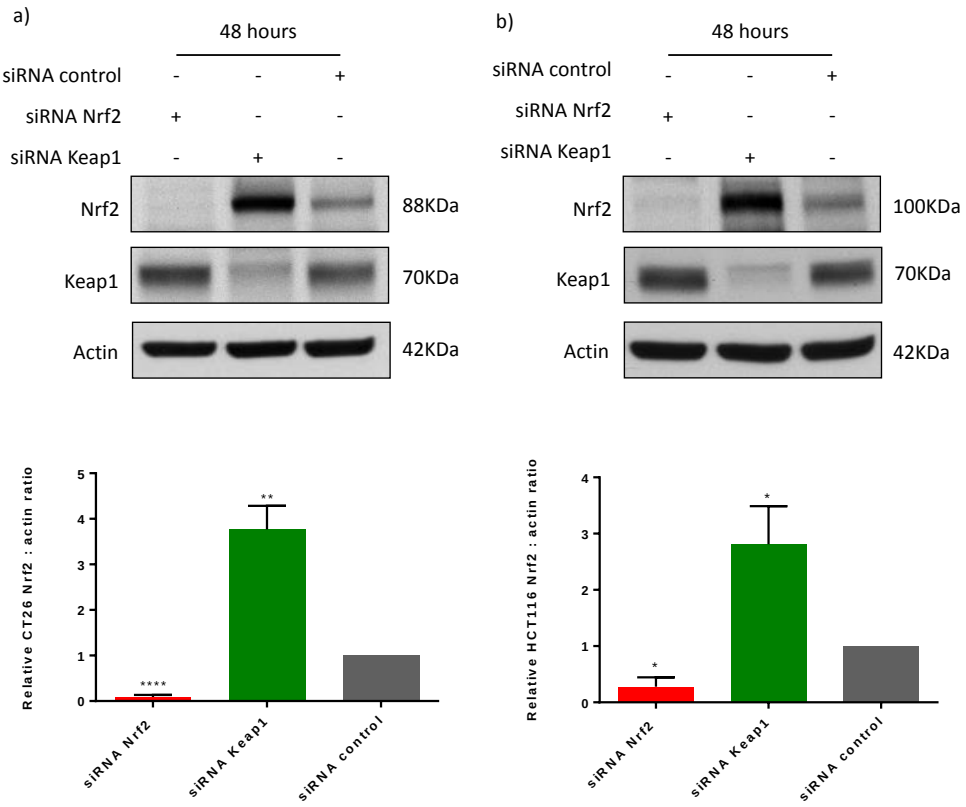

Figure 3.6 – Confirmation of significant inhibition of Nrf2 48 hours after transfection with siRNA targeting Nrf2; representative western blot images and relative expression are displayed for the a) CT26 and b) HCT116 cell lines. Inhibition of Keap1 with siRNA resulted in significant induction of Nrf2. (one-way ANOVA with Holm-Sidak's multiple comparison test, N=4, bar charts display mean +/- SD)

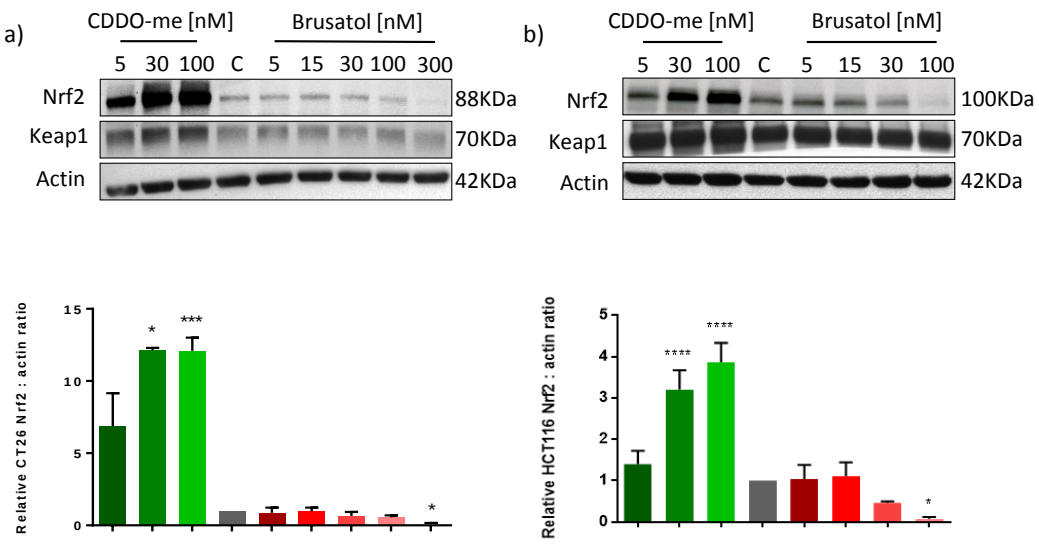

Figure 3.7 – Representative western blot images and bar charts displaying significant Nrf2 inhibition at 100nM and 300nM of brusatol as assessed by densitometry in the a) CT26 and b) HCT116 cell lines respectively. Significant induction was demonstrated at 30nM of CDDO-me in both. (one-way ANOVA with Holm-Sidak's multiple comparison test, N=4, bar charts display mean +/- SD, C= 0.5% DMSO vehicle control)

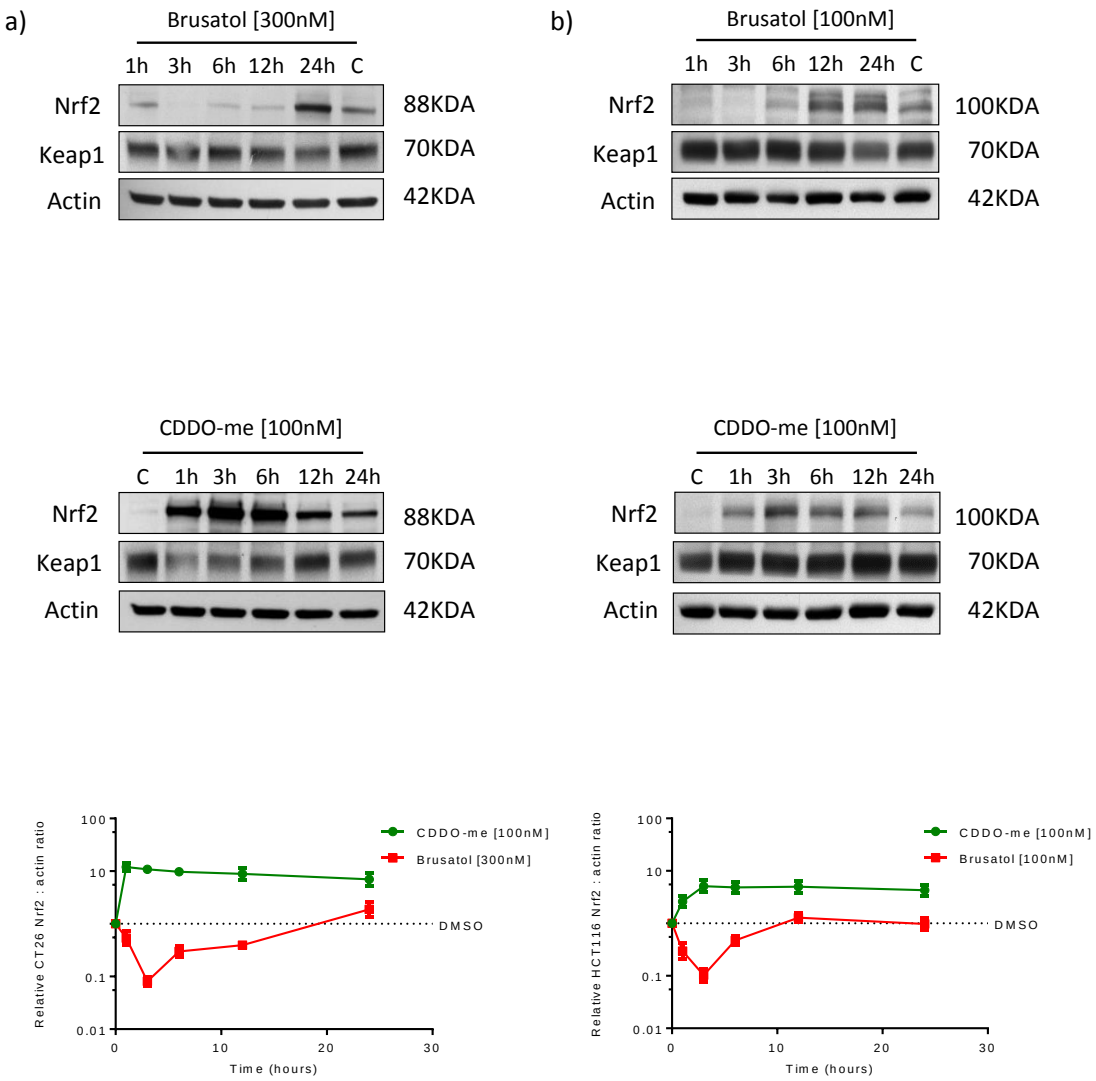

Figure 3.8 – Representative western blot images and graphs displaying the transient inhibition of Nrf2 by brusatol as assessed by densitometry in a) CT26 and b) HCT116 cell lines respectively. CDDO-me induction resulted in upregulation of Nrf2 for greater than 24 hours. (N=3, graphs display mean +/- SD, C= 0.5% DMSO vehicle control)

3.3.3 Western blotting for Nrf2 downstream proteins in cell lines

Western immunoblotting of CRC cell lines was undertaken to examine the effects of genetic (using siRNA) or pharmacological (using CDDO-me or brusatol) Nrf2 modulation on downstream effector proteins of the Nrf2 pathway. Cells were lysed 48 hours after siRNA transfection or 24 hours after treatment with CDDO-me or brusatol for western immunoblotting. Increased expression of CES1, NQO1 and HO-1 was noted in response to induction of Nrf2. The effects of Nrf2 inhibition on downstream effectors were less obvious, with the exception being NQO1 expression in the CT26 cell line 48 hours after transfection with a siRNA targeting Nrf2. As demonstrated in figure 3.8, the inhibition of Nrf2 by brusatol is transient and therefore chronic application to cells over a period of time may be required to decrease the expression of downstream effector proteins in response to this.

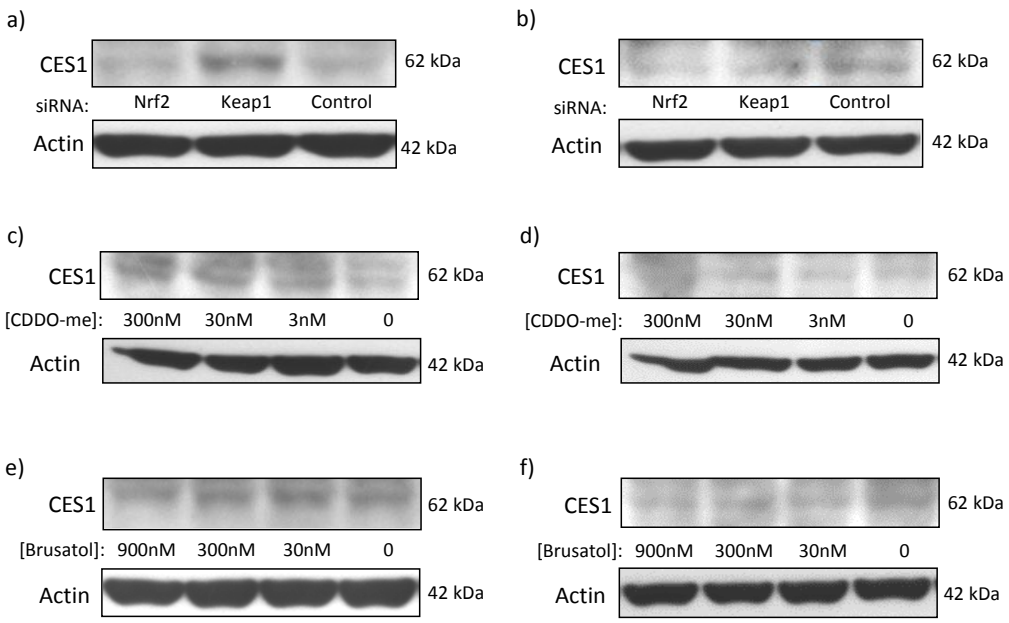

Figure 3.9 – Representative western immunoblotting images of CRC cell lines confirmed induction of CES1 expression following overexpression of Nrf2 using siRNA to inhibit Keap1 in a) CT26 and b) HCT116 cells. The effect of siRNA inhibition of Nrf2 on CES1 expression was minimal. Nrf2 induction by CDDO-me in c) CT26 and d) HCT116 cells also increased the expression of CES1. The effects of Nrf2 inhibition with brusatol on CES1 expression in e) CT26 and b) HCT116 were minimal.

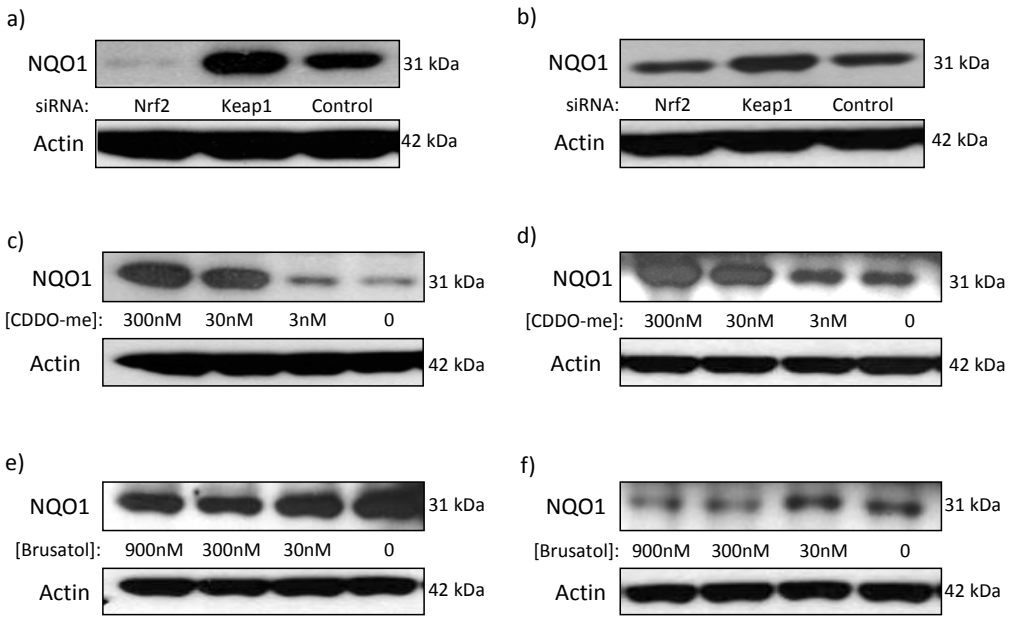

Figure 3.10 – Representative western immunoblotting images of CRC cell lines confirmed induction of NQO1 expression following overexpression of Nrf2 using siRNA to inhibit Keap1 in a) CT26 and b) HCT116 cells. siRNA inhibition of Nrf2 did inhibit NQO1 expression in the a) CT26 but not in the b) HCT116 cell lines. Nrf2 induction by CDDO-me in c) CT26 and d) HCT116 cells also increased the expression of NQO1. The effects of Nrf2 inhibition with brusatol on NQO1 expression in e) CT26 and b) HCT116 were minimal.

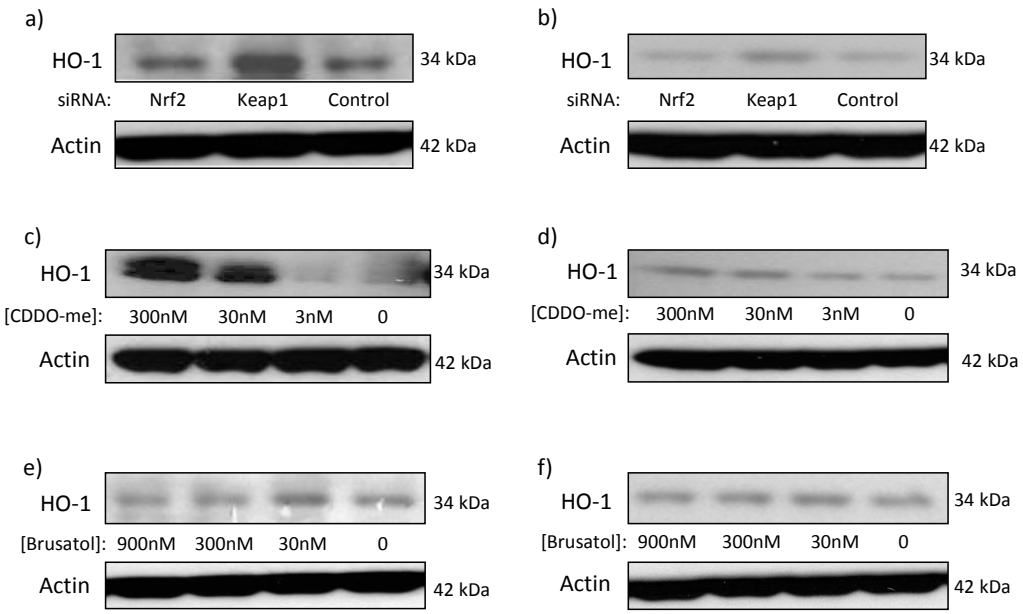

Figure 3.11 – Representative western immunoblotting images of CRC cell lines confirmed induction of HO-1 expression following overexpression of Nrf2 using siRNA to inhibit Keap1 in a) CT26 and b) HCT116 cells. siRNA inhibition of Nrf2 did not inhibit HO-1 expression in either CRC cell line. Nrf2 induction by CDDO-me in c) CT26 and d) HCT116 cells also increased the expression of HO-1. The effects of Nrf2 inhibition with brusatol on HO-1 expression in e) CT26 and b) HCT116 were minimal.

3.3.4 The effect of Nrf2 modulation on cell viability

siRNA inhibition of Nrf2 resulted in a 14% and 23% reduction in cell viability in HCT116 and CT26 cells respectively. The opposite trend was seen for overexpression of Nrf2 through Keap1 inhibition in HCT116 cells, with an increase in viability of 21%. There was a non-significant 7% increase in the viability of CT26 cells with Keap1 inhibition (figure 3.12).

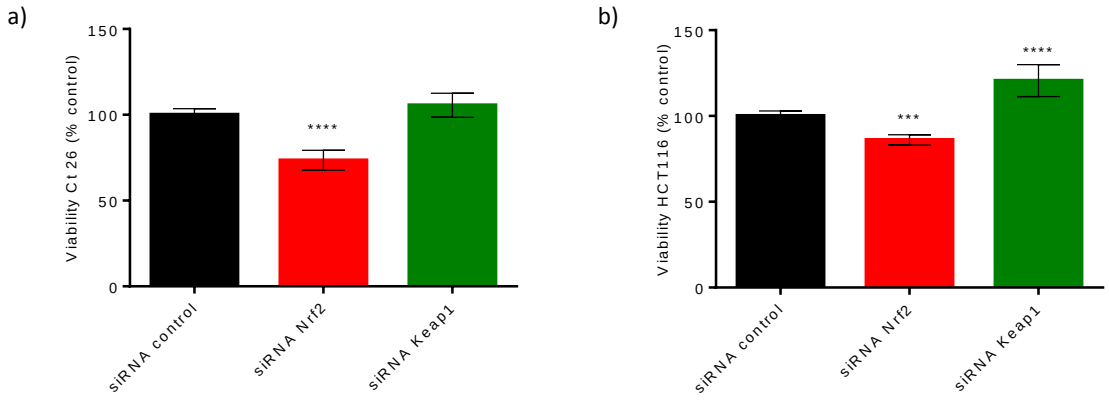

Figure 3.12 – Bar charts displaying the significant decrease in cell viability noted with siRNA inhibition of Nrf2 in a) CT26 and b) HCT116 cells as assessed using the MTS assay 96 hours after transfection and compared with the siRNA control. siRNA inhibition of Keap1 only produced an increase in proliferation / viability in the HCT116 cell line. (one-way ANOVA with Holm-Sidak's multiple comparison test, N=6 in triplicate, graphs display mean +/-SD)

Dosing of cells with brusatol also caused reductions in cell viability in both cancer cell lines in a dose-dependent manner. The brusatol IC50 value for the CT26 cell line was higher than in the HCT116 cell line, reflecting the fact that a higher concentration of brusatol was required to achieve Nrf2 inhibition in this cell line. In HCT116 cells CDDO-me caused slight increases in cell viability in a dose-dependent manner. This effect was not noted in the CT26 cells, which have higher basal expression of Nrf2 as assessed by western blotting.

The safety of brusatol treatment was assessed in the benign cell line CCD-33Co, with a reduced fall in viability noted at the highest concentration of brusatol (300nM) compared with that seen in the cancer cell lines. The IC50 value for the benign cell line was nearly 2-fold higher than seen in the CT26 cell line, perhaps suggesting a decreased dependence on Nrf2 in benign tissue (figure 3.13).

a)

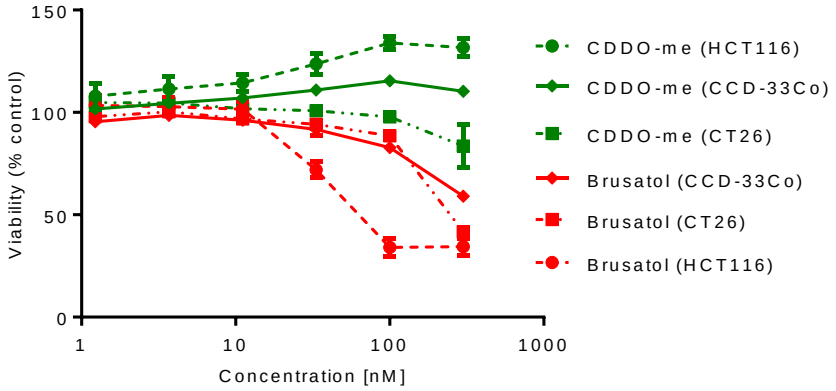

b)

Cell line	IC50 Brusatol (nM)	95% confidence interval (uM)	Significance (F test)
CCD-33Co	453.8	377.9 to 544.8	****
CT26	256.1	240.6 to 272.5	****
HCT116	87.4	63.1 to 121.2	****

Figure 3.13 – a) Graph displaying dose-response curves for the CT26, HCT116 and benign colonic cell line CCD-33Co, as assessed using the MTS assay 48 hours after the application of CDDO-me or brusatol. (N=3 in triplicate, graphs display mean +/-SD, results expressed as a percentage of cells treated with the vehicle 0.5% DMSO control). b) Table demonstrating the significantly different IC50 values between cell lines, as assessed by the sum-of-squares F test.

Having noted a fall in cell viability with brusatol treatment the ability of both CRC cell lines to form colonies was evaluated to determine the effect of brusatol treatment on cellular reproductive potential. Brusatol treatment significantly reduced the surviving fraction in both cancer cell lines in a dose-response manner, similar to seen with the MTS assay. The IC50 values were 21nM (95% CI, 19-23nM) and 373nM (95% CI, 277-502nM) in HCT116 and CT26 cells respectively, suggesting a reduction in reproductive integrity following brusatol treatment (figure 3.14).

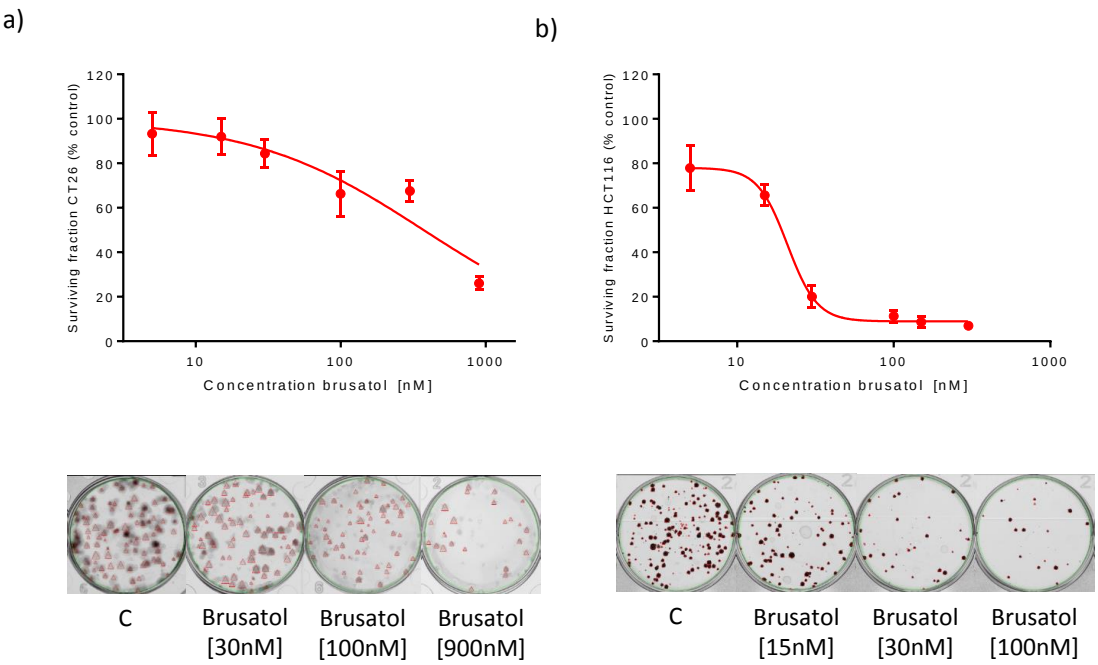

Figure 3.14 – Assessment of reproductive integrity following exposure to brusatol confirmed inhibition of colony formation, represented graphically by calculation of surviving fractions expressed as a percentage of untreated cells, and as representative images of wells, in a) CT26 and b) HCT116 cells. (N=5 in triplicate, graphs display mean +/-SD, * C= 0.5% DMSO vehicle control)

3.3.5 The effect of Nrf2 modulation on irinotecan chemosensitivity

Having established an effect with Nrf2 modulation in cell lines, the effect of siRNA or pharmacological Nrf2 modulation was assessed in combination with irinotecan.

Inhibition of Nrf2 with siRNA (figure 3.15) or brusatol (figure 3.16) significantly decreased the IC50 value of irinotecan in both CRC cell lines, signifying an increased sensitivity to irinotecan therapy following Nrf2 depletion. A non-cytotoxic dose of brusatol (15nM) significantly enhanced irinotecan response but with the effect on IC50 more marked with the higher brusatol concentrations (100nM in HCT116 and 300nM in CT26 cells), known to significantly inhibit Nrf2 expression on western immunoblotting.

The cyto-protective effect of Nrf2 overexpression was again more marked in the HCT116 cell line than CT26 (figures 3.15 and 3.16). Combinations of irinotecan with high-dose (100nM) CDDO-me in the CT26 cell line only just increased the IC50 value for irinotecan significantly, this was in contrast to the HCT116 cell line where even a low dose of CDDO-me reached significance. This perhaps signifies a biological limit to the protective effect of activation of the Nrf2 pathway in the CT26 cell line.

a)

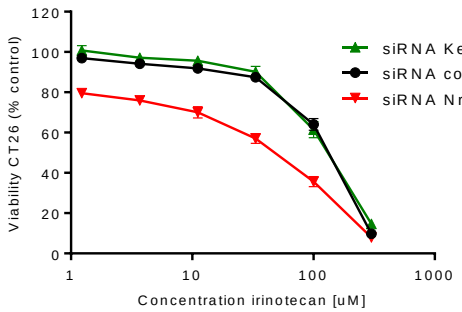

b)

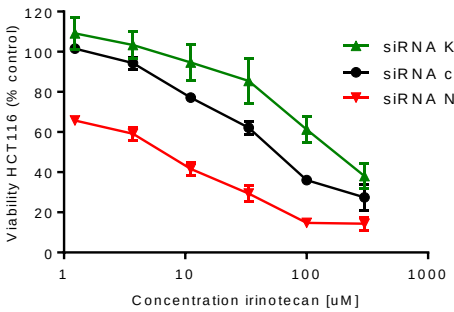

c)

Drug combination	IC50 (uM)	95% confidence interval (uM)	Significance (F test)
IR + siRNA Keap1	124	115.5 to 133.1	NS
IR + siRNA cont	122.5	108.0 to 139.0	NA
IR + siRNA Nrf2	32.36	23.2 to 44.8	****

d)

Drug combination	IC50 (uM)	95% confidence interval (uM)	Significance (F test)
IR + siRNA Keap1	173.6	128.8 to 234.1	****
IR + siRNA cont	61.7	50.8 to 74.9	NA
IR + siRNA Nrf2	5.7	4.7 to 7.0	****

Figure 3.15 – Graphs display the effect of siRNA modulation of Nrf2 on cell lines dosed with irinotecan as measured by the MTS assay. siRNA inhibition of Nrf2 significantly increased the cytotoxicity of irinotecan in a) CT26 and c) HCT116 cells as reflected by the decreased IC50 values when compared with treatment with irinotecan alone, displayed in tables b) for CT26 cells and d) for HCT116 cells (extra sum-of-squares F test). The cytoprotective effect of overexpression of Nrf2 by Keap1 inhibition was non-significant in the CT26 but reached significance in the HCT116 cell line. (IR = irinotecan, siRNA cont = siRNA control, N=3 in triplicate, graphs display mean +/-SD, NS = non-significant, NA = not applicable)

a)

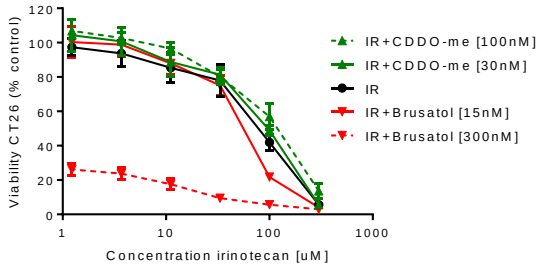

b)

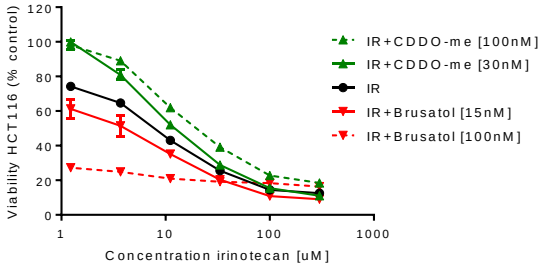

c)

Drug combination	IC50 (uM)	95% confidence interval (uM)	Significance (F test)
IR + CDDO-me [100nM]	106.5	90.84 to 124.7	*
IR + CDDO-me [30nM]	87.3	72.3 to 105.4	NS
IR alone	72.8	62.75 to 84.47	NA
IR + brusatol [15nM]	54.3	47.0 to 62.8	***
IR + brusatol [300nM]	0.1	0.04 to 0.3	****

d)

Drug combination	IC50 (uM)	95% confidence interval (uM)	Significance (F test)
IR + CDDO-me [100nM]	24.1	20.0 to 29.1	****
IR + CDDO-me [30nM]	14.4	12.2 to 17.0	****
IR alone	7.5	6.7 to 8.5	NA
IR + brusatol [15nM]	3.4	2.8 to 4.1	****
IR + brusatol [100nM]	3.1E-04	4.2E-05 to 2.2E-03	****

Figure 3.16 – Graphs display the effect of pharmacological modulation of Nrf2 with brusatol and CDDO-me in combination with irinotecan dosing of cell lines using the MTS assay. The same trends were noted as observed with siRNA in both the a) CT26 and b) HCT116 cell lines. Tables c) and d) demonstrate the change in the irinotecan IC50 values with the pharmacological modulation of Nrf2 in the CT26 and HCT116 cell lines respectively (extra sum-of-squares F test). (IR = irinotecan, N=3 in triplicate, graphs display mean +/-SD, NS = non-significant, NA = not applicable)

CIs for irinotecan combined with brusatol confirmed drug synergy in both cancer cell lines (figures 3.17) across a range of irinotecan concentrations, implying brusatol enhances the cytotoxicity of irinotecan in CRC cell lines.

a)

		[Irinotecan]					
[Brusatol]	uM	300.0	100.0	33.0	11.1	3.7	1.23
	0.015	0.65	0.75	1.24	0.93	2.03	NA
	0.3	0.60	0.40	0.32	0.17	0.47	0.49

b)

		[Irinotecan]					
[Brusatol]	uM	300.0	100.0	33.0	11.1	3.7	1.23
	0.015	0.96	0.39	0.49	0.60	0.69	0.65
	0.1	2.84	1.28	0.58	0.37	0.34	0.34

Figure 3.17 – Heat map tables displaying calculated combination indices for treatment with varying concentrations of irinotecan and brusatol. These confirm drug synergy in a) CT26 and b) HCT116 cells across a range of concentrations. Red, yellow and orange signify decreasing degrees of synergy, with cells highlighted in green demonstrating an antagonistic effect. (Synergy assumed at CI<1)

3.3.6 The effect of Nrf2 modulation on 5-FU chemosensitivity

To assess whether the effects of Nrf2 modulation on chemosensitivity were limited to the use of irinotecan the same experiments undertaken in section 3.3.5 were repeated with 5-FU. Trends were the same as noted with irinotecan dosing; Nrf2 inhibition by siRNA (figure 3.18) or brusatol treatment (figure 3.19) significantly decreased the IC50 of 5-FU. Only the higher brusatol dose (300nM) significantly decreased the IC50 of 5-FU in the CT26 cell line.

a)

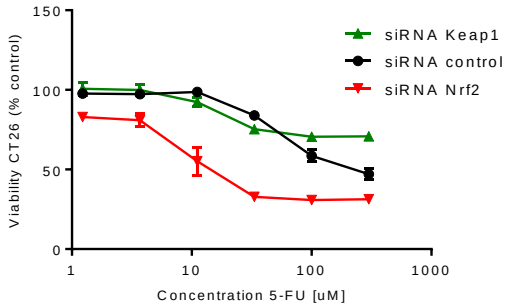

c)

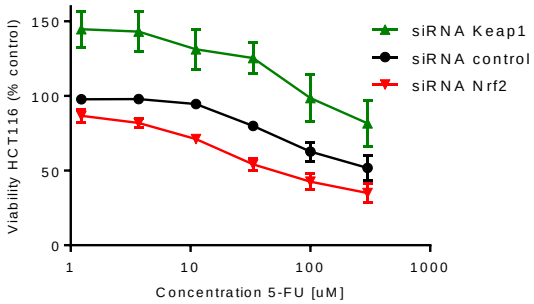

b)

Drug combination	IC50 (uM)	95% confidence interval (uM)	Significance (F test)
5-FU + siRNA Keap1	NC	Not converged	NA
5-FU + siRNA cont	214.3	171.5 to 267.7	NA
5-FU + siRNA Nrf2	21.9	14.5 to 33.3	****

d)

Drug combination	IC50 (uM)	95% confidence interval (uM)	Significance (F test)
5-FU + siRNA Keap1	NC	Not converged	NA
5-FU + siRNA cont	278.6	204.8 to 379.2	NA
5-FU + siRNA Nrf2	62.6	49.3 to 79.5	***

Figure 3.18 – Graphs display the effect of siRNA modulation of Nrf2 on cell lines dosed with 5-FU as measured by the MTS assay. siRNA inhibition of Nrf2 significantly increased the cytotoxicity of 5-FU in a) CT26 and c) HCT116 cells, as reflected by the decrease IC50 values, when compared with treatment with 5-FU alone as displayed in tables b) for CT26 cells and d) for HCT116 cells (extra sum-of-squares F test). The cytoprotective effect of overexpression of Nrf2 by Keap1 inhibition meant IC50 values could not be calculated. (siRNA cont = siRNA control, N=3 in triplicate, graphs display mean +/-SD)

a)

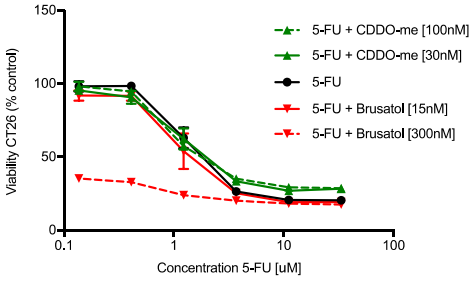

b)

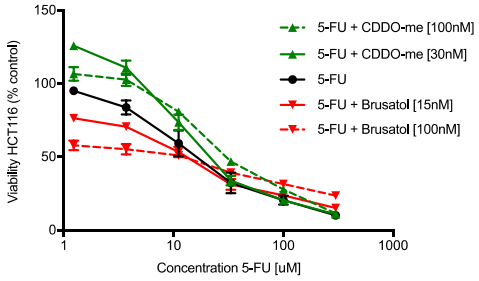

c)

Drug combination	IC50 (uM)	95% confidence interval (uM)	Significance (F test)
5-FU + CDDO-me [100nM]	3.0	2.0 to 4.5	NS
5-FU + CDDO-me [30nM]	2.8	2.0 to 4.1	NS
5-FU alone	2.2	1.795 to 2.704	NA
5-FU + brusatol [15nM]	1.8	1.3 to 2.4	NS
5-FU + brusatol [300nM]	6E-03	3E-03 to 2E-03	****

d)

Drug combination	IC50 (uM)	95% confidence interval (uM)	Significance (F test)
5-FU + CDDO-me [100nM]	37.3	30.6 to 45.4	****
5-FU + CDDO-me [30nM]	25.1	17.1 to 36.7	*
5-FU alone	17.9	15.7 to 20.4	NA
5-FU + brusatol [15nM]	12.3	10.4 to 14.7	**
5-FU + brusatol [100nM]	6.7	5.0 to 9.0	****

Figure 3.19 – Graphs display the effect of pharmacological modulation of Nrf2 with brusatol and CDDO-me in combination with 5-FU dosing of cell lines using the MTS assay. The same trends were noted as observed with irinotecan in both the a) CT26 and b) HCT116 cell lines, although to a lesser extent. Tables c) and d) demonstrate the change in the 5-FU IC50 values with the pharmacological modulation of Nrf2 in the CT26 and HCT116 cell lines respectively (extra sum-of-squares F test). (N=3 in triplicate, graphs display mean +/-SD, NS = non-significant, NA = not applicable)

Although the trend was the same as noted with irinotecan, drug synergy was achieved at fewer concentrations than noted with irinotecan, particularly in the HCT116 cell line. Additionally, the degree of synergy, as described by a lower CI value, never reached those noted with irinotecan (figure 3.20). This could suggest that the effects of combining Nrf2 inhibition with irinotecan may be due to alterations in drug metabolism and cellular survival; Nrf2 modulation is not known to have any effect on 5-FU metabolism and therefore the observed effect may be solely due to the loss of cellular protection.

a)

[Brusatol]	[5-FU] uM	33.0	11.1	3.7	1.23	0.41	0.137
	0.015	2.31	0.83	0.37	0.41	1.10	ND
	0.3	2.35	1.05	0.63	0.45	0.68	0.69

b)

[Brusatol]	[5-FU] uM	300.0	100.0	33.0	11.1	3.7	1.23
	0.015	2.58	1.61	0.84	0.91	1.16	1.12
	0.1	4.75	2.73	1.78	1.90	1.82	1.95

Figure 3.20 – Heat map tables displaying calculated combination indexes for treatment with varying concentrations of 5-FU and brusatol. Drug synergy was seen at fewer concentrations and to a lesser extent in a) CT26 and b) HCT116 cells than noted with irinotecan. Red and orange signify a degree of drug synergy, with cells highlighted in yellow and green demonstrating an antagonistic effect. (Synergy assumed at CI<1)

3.3.7 Assessment of brusatol therapy in a subcutaneous murine tumour model

Based on the *in vitro* findings, with both CRC cell lines displaying the same trend towards reduced proliferation and viability following brusatol treatment, *in vivo* investigation was first completed in six immune-competent BALB/c mice *sc* injected with the CT26lucA6c cell line. Prior to *in vivo* investigation, brusatol dose-response curves and growth rates were compared between the CT26 parent population and CT26ucA6c cell line to ensure phenotypic equivalence prior to *in vivo* investigation (see Appendix 1 for data).

Mice were randomised to treatment with brusatol or a vehicle control on the 7th day post-tumour injection (N=3/group), according to the dosing regimen described in figure 3.1. Tumour growth was monitored using both caliper measurements and luminescence to ensure luminescence was an accurate reflection of tumour size. Tumour growth was significantly inhibited in brusatol-treated mice over the 14-day study period. No adverse effects were noted in either group of mice (figure 3.21). To ensure luminescence accurately reflected tumour volume, data points were individually plotted for each mouse at each time-point with a significant positive correlation achieved (figure 3.22).

Western immunoblotting confirmed successful Nrf2 inhibition by brusatol at the study end-point (figure 3.23), indicating that brusatol was able to reach the tumour tissue. Nrf2 protein expression was reduced by 74%, as assessed by western immunoblotting and densitometry, in biological replicates treated with brusatol compared with the saline-treated controls.

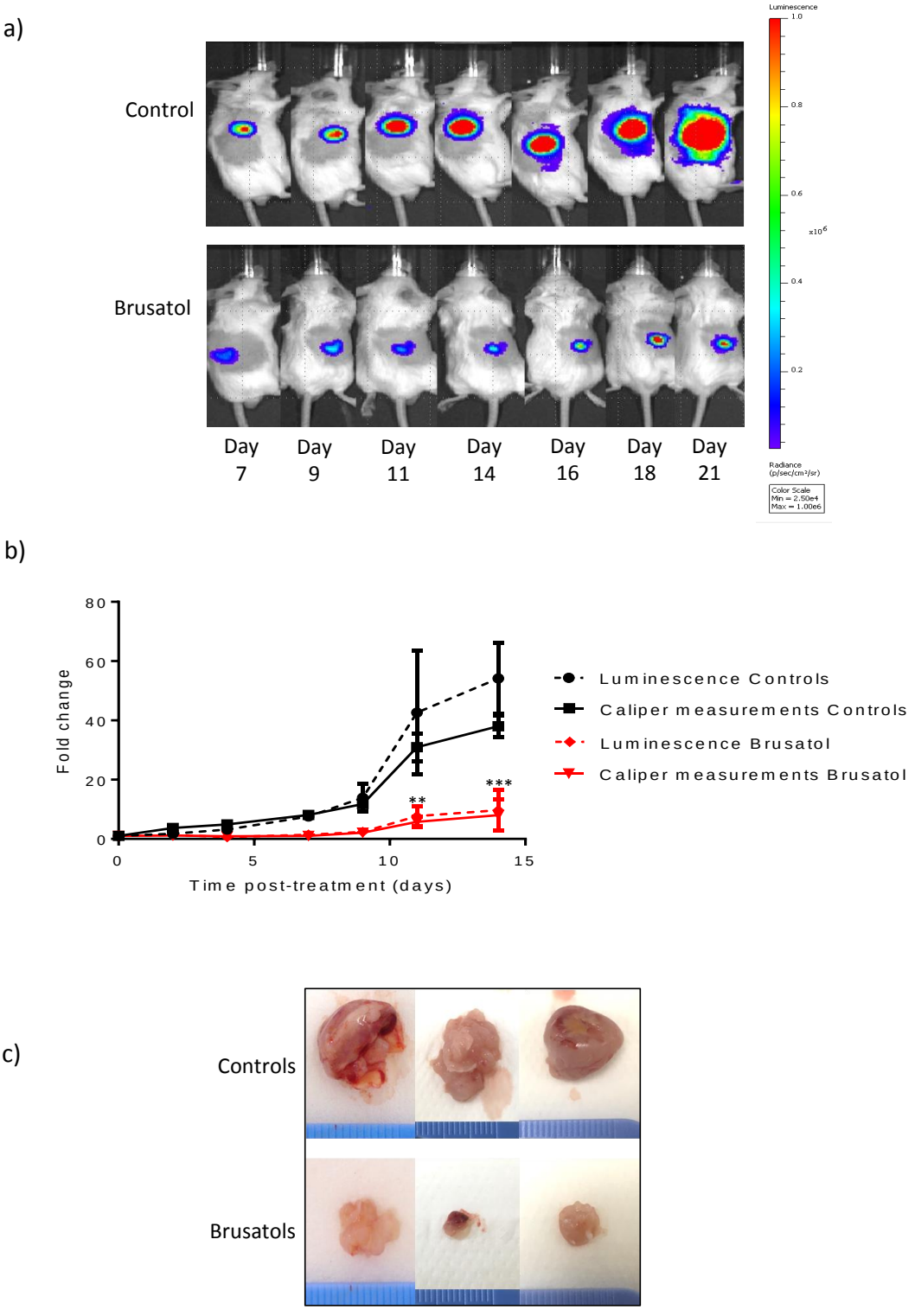

Figure 3.21 – a) Representative IVIS® images of a BALB/c mouse from the brusatol--treated and control group after *sc* flank injection of the CT26lucA6c cell line. b) Graph displays the significant inhibition of tumour growth in mice treated with brusatol in comparison with vehicle-treated controls (multiple t-tests, N=3/group, mean +/-SEM). c) Photographs of the flank tumours excised from mice (scale in 1mm increments) 21 days after implantation.

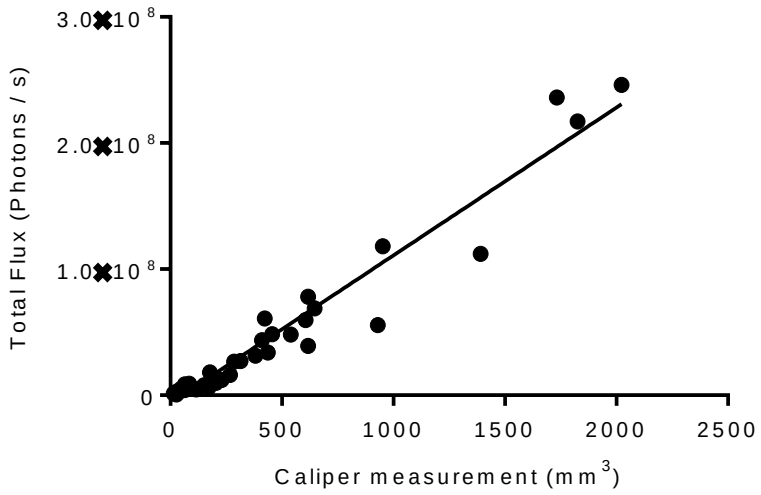

Figure 3.22 – A significant positive correlation was observed between caliper measurements and luminescence for brusatol-treated and untreated mice *sc* injected with the CT26lucA6c cell line (r^2 = 0.94, p < 0.0001, Pearson R).

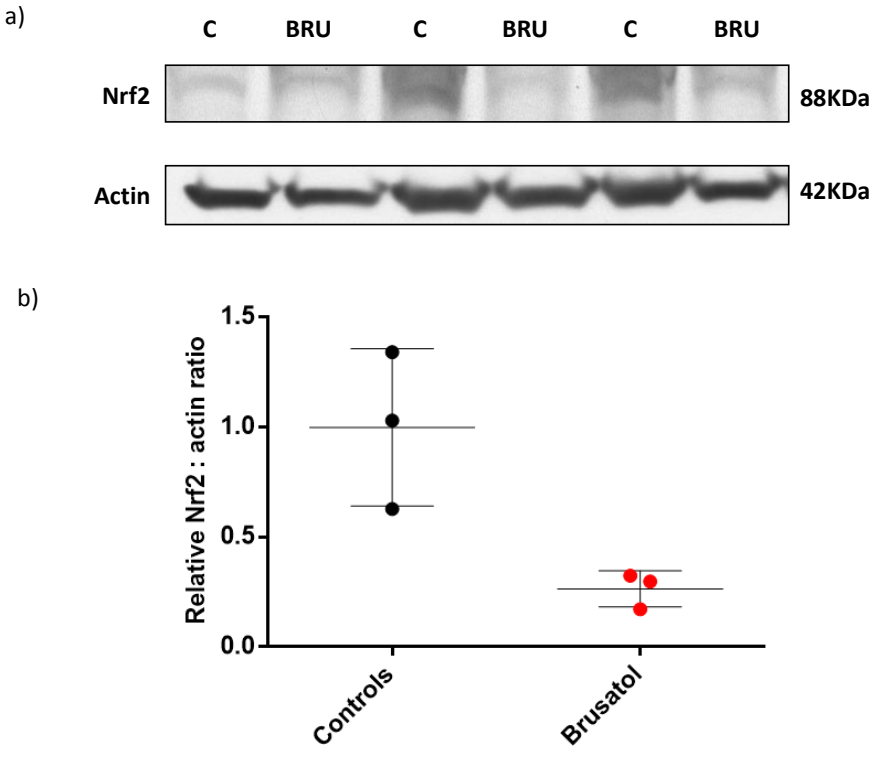

Figure 3.23 – a) Western blotting and b) densitometry confirmed significant inhibition of Nrf2 in the flank tumours excised from mice treated with brusatol (p=0.03, unpaired t-test). (Bar chart displays mean +/- SD, C = control, BRU = brusatol)

3.3.8 Assessment in the syngeneic orthotopic model

The effects of treatment with brusatol, irinotecan or a combination of irinotecan and brusatol on tumour growth in the syngeneic orthotopic model (N=8 per group) were compared with tumour growth in vehicle controls. Dosing and imaging regimens are described in figure 3.2.

A significant reduction in tumour growth rate (as represented by the fold change in luminescence) was noted over the study period ($p<0.01$, one-way ANOVA) in mice treated with brusatol. No detrimental effects were noted in mice receiving brusatol. In contrast, a number of mice in the control group began to exhibit tumour-related symptoms, including ascites, weight loss and obstruction, limiting the study end-point to ensure severity limits were not exceeded.

There was a trend towards improved irinotecan efficacy in mice treated with a combination of brusatol and irinotecan as evidenced by a reduced rate of growth. In comparison to the control group, greater significance was achieved for combination therapy ($p<0.001$, one-way ANOVA) than with each treatment in isolation ($p<0.01$, one-way ANOVA). However, a significant inhibition of tumour growth rate was not achieved between treatment groups (figure 3.24). Lines of best fit and slope comparisons (representative of tumour growth) are displayed in appendix 2). When the fold change in luminescence between treatment groups was compared on the 14^{th} and final day of treatment there was a significant difference between mice who received irinotecan alone compared with those on a combination of irinotecan and brusatol ($p<0.05$, t-test).

A continuation study was carried out in three mice from the brusatol-treated group to ensure the effect was attributable to therapy. Cessation of brusatol resulted in an increase in luminescence with mice reaching the humane end-point of the study one week later, at which point the fold change in luminescence was similar to that seen in controls one week earlier (figure 3.25).

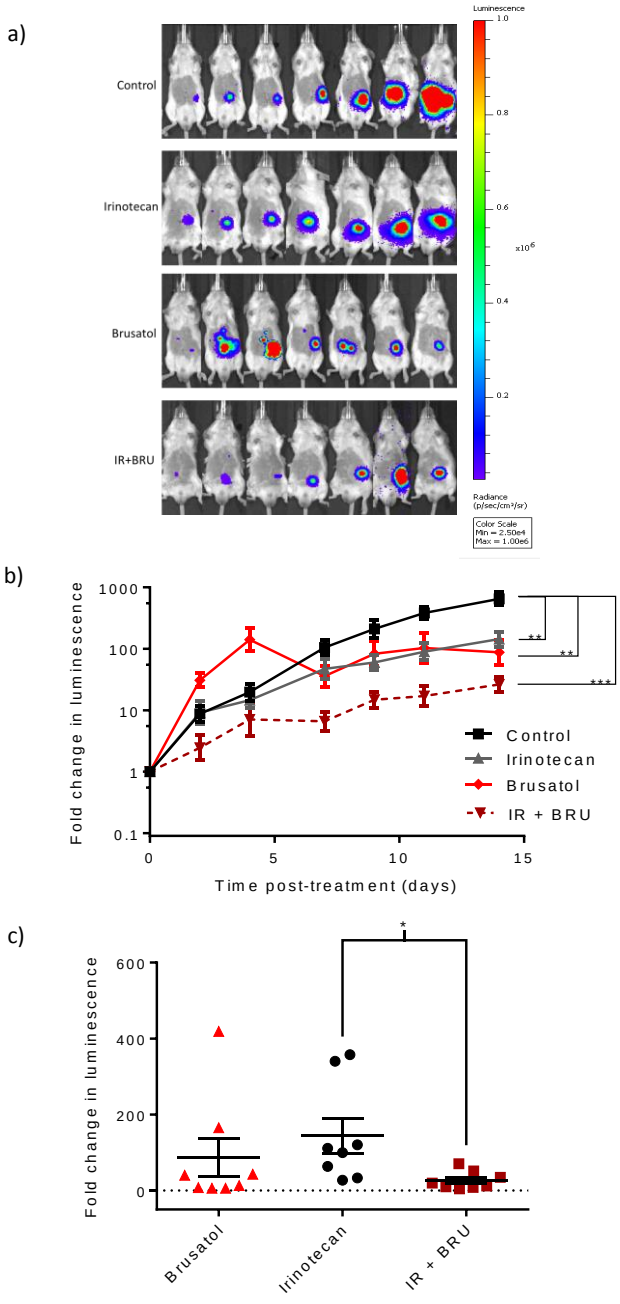

Figure 3.24 – a) Representative serial IVIS® images from BALB/c mice orthotopically implanted with CT26lucA6c cells and randomised to treatment groups. b) Data displayed graphically as fold change in luminescence from the first day of treatment. All treatments inhibited tumour growth significantly when compared with the control group (one-way ANOVA comparing tumour growth rate calculated from lines of best fit). c) Fold change in luminescence on the 14th day post-treatment was significantly different in mice on the combination therapy rather than irinotecan alone (Mean fold change = 144.1, SEM 46.34 versus 26.4, SEM 8.4 unpaired t-test with welch correction). (N=8, IR = irinotecan, BRU = brusatol, graphs display mean +/- SEM)

a)

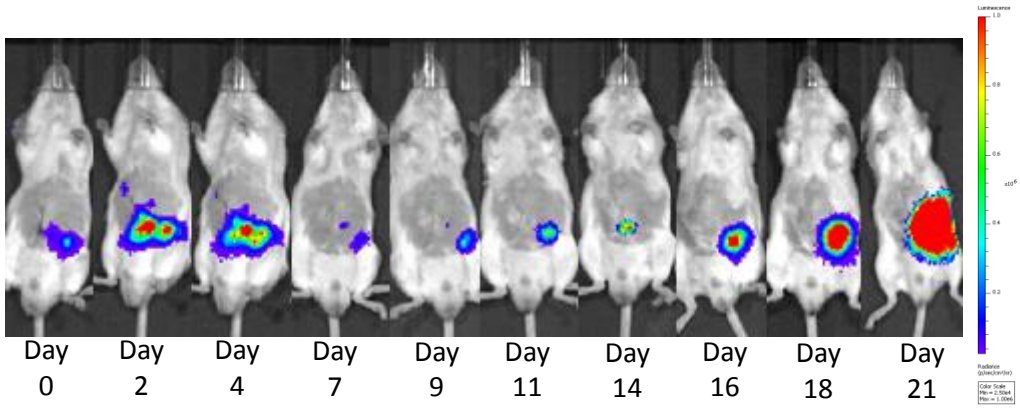

b)

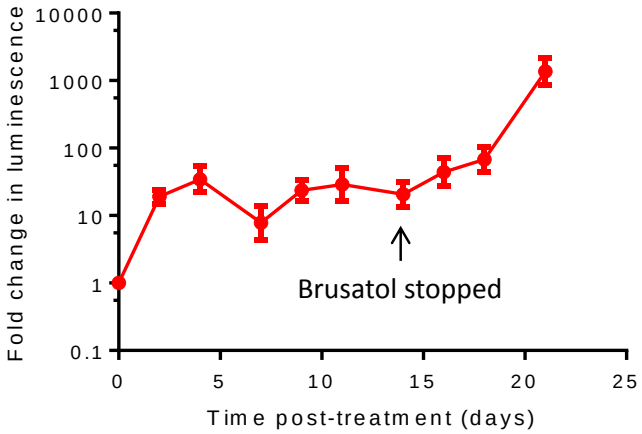

Figure 3.25 – a) Representative serial IVIS® images from BALB/c mice from the onset of treatment with brusatol (day 0). Treatment was stopped after 14 days and imaging continued for a week. b) Data displayed graphically as fold change in luminescence from the first day of treatment with the signal increasing exponentially after the cessation of therapy. (N=3, graph displays mean +/- SEM)

Weight loss was common in all groups for the first week post-operatively, but never approached the 20% limit stipulated in the project licence. Most mice in treatment groups gained weight from this point with no significant weight loss. Some weight loss was noted

in control mice leading up to the study end-point: this was attributed to malignant burden. Several mice in the control group began to exhibit tumour-related symptoms including ascites, weight loss and obstruction, limiting the study end-point to ensure severity limits were not exceeded. Animal weights for treatment groups are displayed graphically in figure 3.26. No additional detrimental effects were noted in mice receiving brusatol therapy in isolation. Acute diarrhoea was common in mice receiving irinotecan or combination therapy: a single mouse receiving combination therapy experienced prolonged diarrhoea (lasting greater than 48 hours) resulting in early cull (data excluded from analysis). No mice underwent early cull due to tumour-related symptoms in the treatment groups.

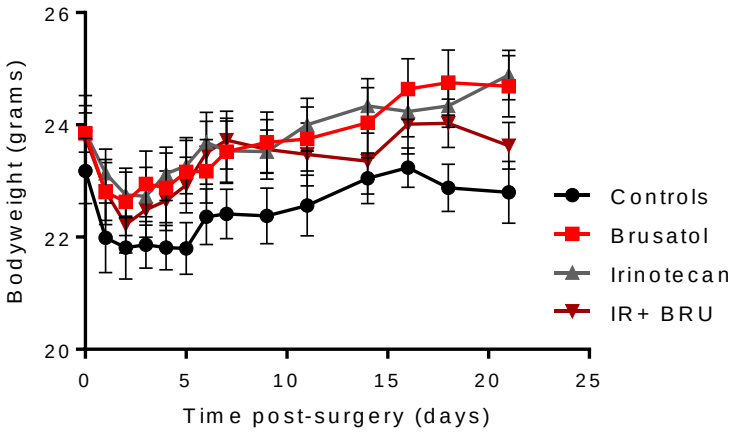

Figure 3.26 – Graph displaying the bodyweight of BALB/c mice orthotopically implanted with the CT26lucA6c cell line over time. Treatment was initiated on day 7 post-surgery. (Graph displays mean +/- SEM, IR = irinotecan, BRU = brusatol).

IHC staining for Nrf2 of three randomly selected caecal tumours excised from orthotopically implanted BALB/c mice at the end of the study period demonstrated reduced staining in the mice treated with brusatol (mean Nrf2 H-score = 53.3, SD 40.1) when compared with the saline-treated controls (mean Nrf2 H-score = 190, SD 63) (figure 3.27).

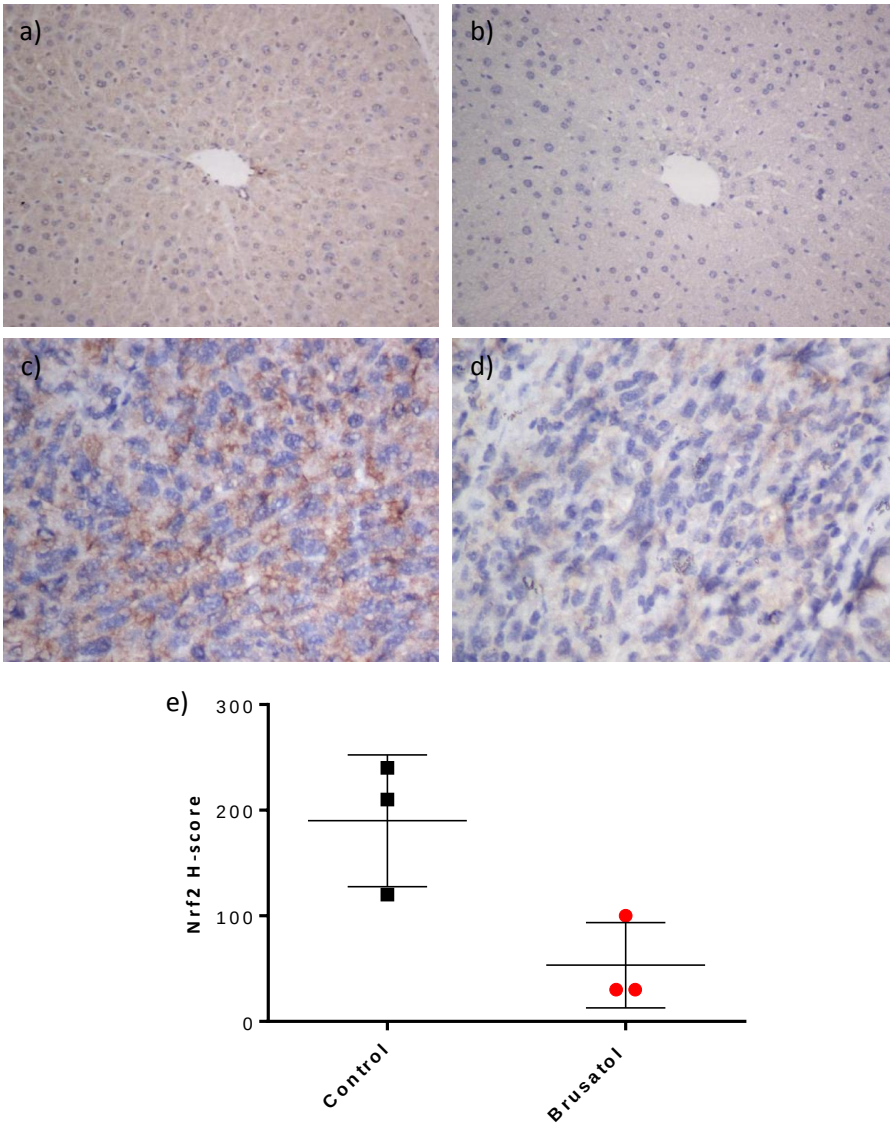

Figure 3.27 – Light microscopy representative images from tissue stained for Nrf2 by IHC. Strong staining is demonstrated in the a) positive control of liver from BALB/c mice treated with CDDO-me. b) Livers from Nrf2 knockout mice were used as a negative control and displayed weak staining. There was strong staining demonstrated in caecal tumours excised from mice in the c) control group and staining was reduced in the tumours from mice treated with d) brusatol. e) Graphical display of data reveals significantly (p=0.04 unpaired t-test with Welch's correction) reduced Nrf2 H-scores in brusatol-treated mice (N=3, graph displays mean +/- SD)

3.4 Discussion

The TMA analysis of normal colon, primary CRC and liver metastases from patients with advanced disease confirmed increased expression of Nrf2 in CRC tissue. Nrf2 expression in matched liver metastases reflected that in the primary tumour, suggesting that information on expression of the protein can be obtained from the primary lesion without the need for biopsy of the liver lesion. This is beneficial given the risks of track seeding and poor outcomes associated with biopsy of liver metastases, as highlighted in section 1.5.5.

The analyses reported in this chapter consistently suggest reduced proliferation and survival of CRC cells when Nrf2 is inhibited. The effect of Nrf2 modulation on irinotecan efficacy was also explored, with data suggesting drug synergy for combinations of brusatol with irinotecan *in vitro*. Several mechanisms could account for this. For example, Nrf2 activation stimulates transcription of antioxidant proteins including glutathione S-transferases, NQO1, thioredoxin and thioredoxin reductase, reducing the production of ROS and protecting the cell from chemotherapy-induced cell death [430]. Additionally, inhibition of Nrf2 may decrease UGT1A1 expression, preventing glucuronidation and therefore excretion of SN-38 [280]. These multiple Nrf2-mediated mechanisms involved in irinotecan metabolism could explain the reduced drug synergy noted with 5-FU when combined with brusatol, where the only benefit to inhibition of Nrf2 is the impairment of cell survival pathways.

These findings were, for the first time, translated into a robust pre-clinical murine model of CRC, confirming the effectiveness and safety of prolonged brusatol treatment in early animal testing, and demonstrating the reduced expression of Nrf2 in tumour tissue *in vivo* with brusatol treatment. Although tumour growth was slowed by the combination of irinotecan with brusatol, in comparison to each treatment in isolation, significance was not reached between treatment arms in tumour growth rates, and the high degree drug synergy noted *in vitro* perhaps not achieved. This may be due to the large variation in tumour growth rates between mice in each treatment group, in addition to the effectiveness of both brusatol and irinotecan treatment in isolation. It also highlights the importance of assessing the effect of Nrf2 inhibition *in vivo,* where the role of the CES enzymes in converting irinotecan to SN-38 in the liver becomes relevant. With the liver potentially responsible for 50% of the conversion of irinotecan to SN-38, it is possible that brusatol inhibited inducible CES expression in the liver by targeting Nrf2 and subsequently

reduced irinotecan activation. Further work examining this effect could be achieved by utilising liquid chromatography–mass spectrometry (LC-MS) to measure irinotecan and its metabolites in the serum or liver homogenates of animals dosed with irinotecan following pharmacological modulation of Nrf2. A reliable LC-MS assay has been developed in-house to Food and Drug Administration standards and used within the context of a clinical trial investigating the use of irinotecan releasing beads [173].

Data presented in this chapter agree with those in the published literature, with higher Nrf2 expression contributing to chemoresistance in CRC cell lines in a number of published studies [272, 273, 431]. Additionally, clinico-pathological data have correlated high Nrf2 expression in human CRC samples to poor clinical outcomes [271] and advanced disease [432], implying Nrf2 may have a role as a prognostic biomarker. However, this is the first study to demonstrate the effects of brusatol on CRC tumour cells *in vitro* and *in vivo*, utilising a robust murine model of the disease process, with the tumour growing in the correct microenvironment with an intact immune system.

Brusatol allows the potential for Nrf2 inhibition to be translated into the clinical setting. The mechanism by which brusatol achieves Nrf2 inhibition is undetermined. Studies on a lymphocytic leukaemia tumour cell line were some of the first to report the anti-neoplastic effect of an ester of brusatol *in vivo*, demonstrating that protein and nucleic acid metabolism were inhibited in a manner which correlated positively with their antileukemic activity [433]. It was postulated that quassanoids bound to the 80s ribosome, inhibiting protein elongation [434]. Recently published data acquired on a *Keap1* mutant lung cancer (A549) cell line, through whole proteomic analysis by mass spectrometry (MS), postulated that brusatol inhibits the translation of a number of short half-life proteins. However, these proteins showed only minimal changes on western immunoblotting, with no reporting of statistical significance in the data. Additionally, the doses of brusatol used in this study were far higher than those demonstrated to cause Nrf2 inhibition both in the data presented in this thesis and in the majority of the published literature [435].

The pattern of Nrf2 inhibition by brusatol in cell lines described in this chapter is similar to data presented by Olayanju *et al.* in Hepa-1c1c7 cells and primary human hepatocytes, with rapid transient depletion of Nrf2 seen on western immunoblotting [436]. It is possible that brusatol achieves such significant inhibition of Nrf2 as a result of the proteins extremely short half-life. However, it is difficult to examine the effect of brusatol on protein

translation in cancer cells, with doses causing significant Nrf2 inhibition invariably associated with cytotoxicity, which in itself may alter expression of a number of proteins. As a result of this uncertainty around the specificity of brusatol as an inhibitor of Nrf2 the next chapter of this thesis will attempt to examine the effects of brusatol treatment on protein expression *in vivo*, using the livers excised from brusatol-treated mice.

The main limitation of the data in this chapter could be the reliance on luminescence as a marker of tumour growth in the orthotopic model. Starting luminescent signal can vary substantially between mice in the same treatment group as a result of the caecal injection technique, resulting in varying cell inoculums and injection sites on the caecum. Attempts were made to ensure cells were injected into the same point of the caecum, but this was not always possible, and the mobility of the murine caecum mean the depth of tumours between mice can vary substantially. With a 10-fold loss of signal for every 1cm of tissue, this can cause significant differences in total flux between animals. These large variations are likely to have reduced the chance of finding significant differences between treatment arms although this effect was partially negated by the expression of data as a fold change in luminescence; this allowed each animal to act as its own control.

Given the lack of knowledge of the mechanism of action of brusatol, there were concerns regarding the effects it could have on luminescence. One reason for conducting the flank tumour study described in section 3.3.7. was to ensure that luminescence remained an accurate reflection of tumour volume *in vivo* and that brusatol therapy was not reducing luminescent signals. Given the findings of the flank study in BALB/c mice, with the luminescent data mirroring that obtained from callper measurement, in combination with data from the orthotopic model, it was felt luminescence accurately reflected disease burden and data were a reliable reflection of tumour growth. It was in fact noted in the orthotopic model that brusatol treatment actually resulted in a more rapid increase in luminescence in the first 3-5 days after initiation of treatment when compared with administration of a vehicle control, as demonstrated in figure 3.22 b). This could possibly be explained by Nrf2-mediated inhibition of the ABC transporters, responsible for the efflux of luciferin from cells, by brusatol [437]. This effect would subsequently be lost as cell viability fell and luminescence began to reflect this.

This chapter provides an extensive overview of the role of Nrf2 in CRC, highlighting a potential role as a therapeutic biomarker. The presented data also suggest brusatol acts as

a potent anti-tumorigenic agent in its own right. Further work is needed to clarify the effect Nrf2 modulation has on irinotecan metabolism and not just on the therapeutic effect. Investigation into the mechanism by which brusatol achieves Nrf2 inhibition is also essential before considering its use in clinical trials.

Chapter 4 – Exploring the effects of brusatol *in vivo*

4.1 Introduction

The controversy surrounding the mechanism of action of brusatol treatment and its specificity as an Nrf2 inhibitor were highlighted in the discussion of chapter three. There are relatively few studies involving the use of brusatol to date, with most of these focusing on the therapeutic effect of the compound in malignancy. Even fewer have sought to investigate its mechanism of action or specificity towards Nrf2 inhibition, with none having examined this *in vivo*.

In 1981 Willingham *et al.* attempted to clarify the effects of brusatol on protein synthesis in rabbit reticulocytes by comparing its effects to a number of protein inhibitors with known mechanisms of action. They suggested that brusatol was inhibiting peptide bond formation during translation by preventing the peptidyl transferase reaction, resulting in the rapid inhibition of protein synthesis. However, endogenous protein inhibition was only achieved at high (micromolar) concentrations of brusatol in reticulocyte lysates rather than the nanomolar concentrations noted to cause inhibition of Nrf2 [438]. In 1983 similar findings were reported with brusatol and another quassinoid bruceantin. The authors suggested both compounds bound reversibly to the 80S ribosome in reticulocytes at concentrations of 100μM, temporarily preventing protein synthesis [439]. At a similar time to these studies bruceantin was being investigated in phase II clinical trials. Phase I trials in patients with a variety of solid tumours reported minor but frequent side effects including hypotension, nausea and vomiting at high concentrations of bruceantin but only minor haematological toxicity in the form of thrombocytopenia [440, 441]. Phase II trials were subsequently conducted in metastatic breast cancer [442] and malignant melanoma [443]; both trials were terminated due to lack of objective tumour regression. Patient numbers in both trials were however very small, with only 15 and 22 patients recruited in the studies of breast cancer and melanoma respectively. No published studies to date report the use of brusatol in treating patients.

More recent publications have attempted to clarify the effect of brusatol on the expression of a number of short half-life proteins. Ren *et al.* demonstrated that, out of a panel of proteins, only c-Myc was depleted in response to brusatol on western immunoblotting of the A549 cell line, albeit to a lesser extent than Nrf2. They concluded that brusatol selectively inhibited the Nrf2 pathway through enhanced ubiquitination and degradation of Nrf2 [294]. Olayanju *et al.* examined the effect of brusatol on a number of short half-life

proteins in Hepa-1c1c7 cells, including cyclin A, HIF-1α, p53 and survivin. They concluded that the inhibitory effect of brusatol was specific, and not a consequence of a broader effect on protein synthesis, at the nanomolar concentrations required to deplete Nrf2 [436].

The application of mass spectrometric profiling to study the effects of brusatol in the A549 cell line was briefly mentioned in section 3.4. The method utilised in this study combined multiplexed mass spectrometry (MS) with a cellular thermal shift assay (CESTA). CESTA relies on detection of the conformational changes and alterations in thermal stability that occur in proteins due to the binding of small molecules. Using this method on lysates from the lung cancer A549 cell line, following a four-hour incubation with 500nM brusatol, Vartanian *et al.* reported lower abundance of the majority of identified proteins. There were 37 proteins found to be upregulated, of which half were associated with ribosomal assembly and protein translation. As a result of these findings the authors suggested that the modulation of protein translation could be the mechanism whereby brusatol decreases Nrf2. However, the study also reported a loss in viability of nearly 100% in A549 cells treated with 500nM of brusatol for 48 hours. It is feasible that the decrease in short half-life proteins seen with brusatol are the result of functional disruption to the cells due to the profound cytotoxicity associated with the inhibition of Nrf2 induced by brusatol [435]. Separating the loss of viability observed in cancer cell lines with brusatol treatment from the effects of the compound on protein expression is challenging, as concentrations associated with Nrf2 depletion invariably result in a loss of cellular viability. No studies to date have examined the effect of brusatol treatment on the proteome *in vivo*.

Isobaric tagging for relative and absolute quantification (iTRAQ) is a proteomic technique designed to determine the protein profile of a number of different samples within a single experiment, often comparing this to a control sample included in each experimental run. Cysteine residues in the samples are reduced and alkylated prior to tryptic digestion, whereby proteins are cleaved at the carboxyl side of the amino acids lysine and arginine (except where either is followed by proline). This produces peptides that are subsequently labelled by incubating samples with a specific isotope-labelled molecule which covalently binds to the N-terminus and side-chains within each sample. This iTRAQ isotope tag contains a reporter moiety, which allows quantification during analysis, and a balance moiety. All tags have the same 1450Da mass but the reporter moieties in each tag have

differing masses. When each tag binds to a peptide which is present in all samples then all labelled peptides should have an identical mass.

Prior to MS, peptides are separated into fractions of certain ionic charges by cation exchange. Fractions are then subject to nano LC-MS/MS, where they are ionised and separated by mass, producing parent ion molecules. Each parent ion, represented by a single peak, is isolated and directed to a collision chamber, where tagged peptides are fragmented by a collision gas. During this process, reporter and balance moieties are cleaved from each other and the peptide they are bound to. The peptide itself is also broken into fragment ions, which are cross-referenced with a database of known proteins, allowing identification. The reported molecules, with their differing masses, are used to quantify the relative abundance of the peptides they were originally bound to by calculating ratios of the reporter molecules (figure 4.1). The abundance of each protein is normalised to a common 'pool' of the samples which can be used across multiple runs to ensure consistency of analysis [444].

iTRAQ analysis offers the potential to examine the relative expression of proteins in tissue excised from mice treated with brusatol. The work presented in this chapter aims to examine the protein profile and Nrf2-related gene expression in tissues excised from mice following chronic treatment with brusatol.

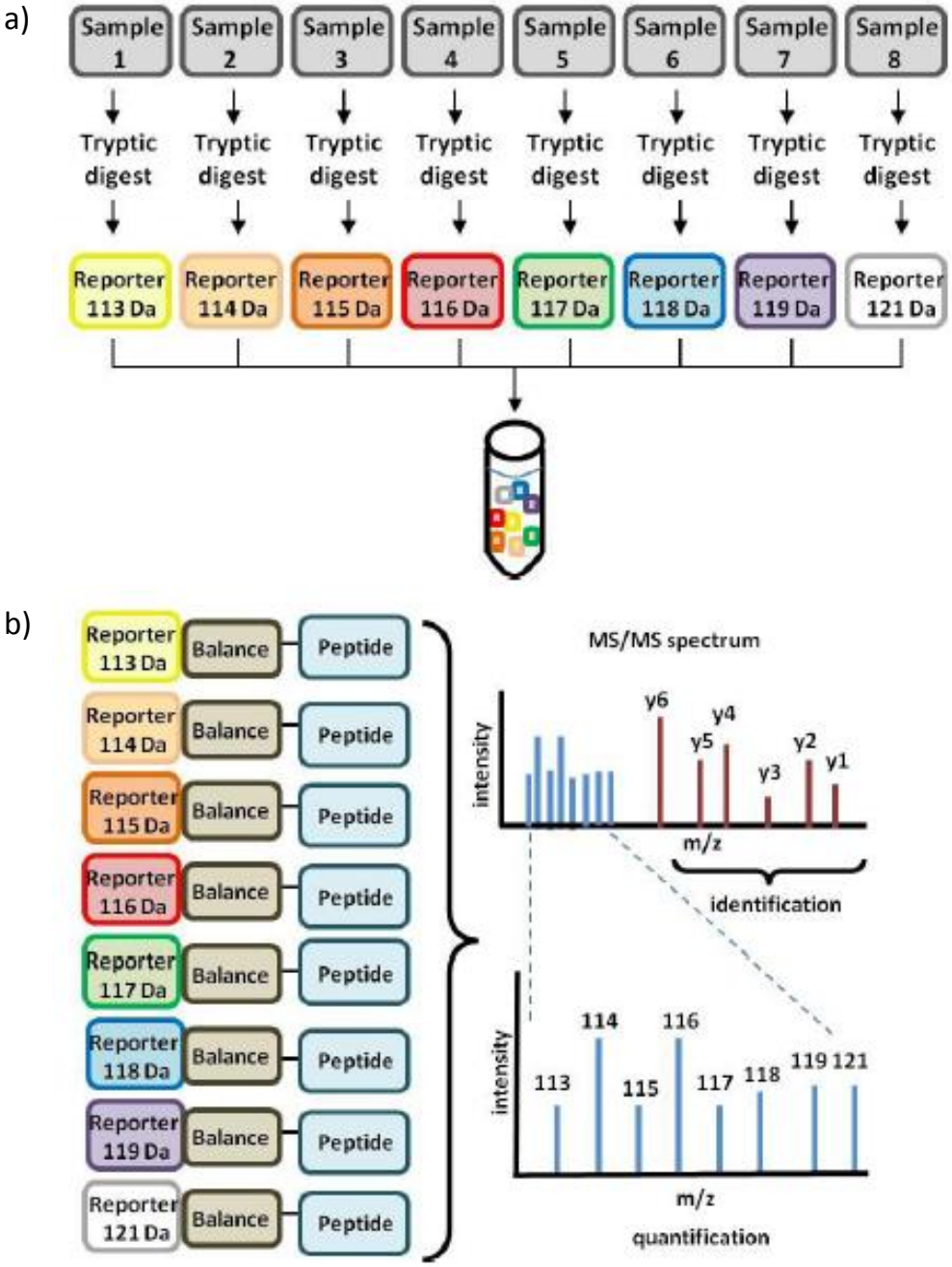

Figure 4.1 – Schematic of the labelling and analysis of iTRAQ samples. iTRAQ allows the simultaneous quantification of up to eight samples. a) Proteins in each sample undergo tryptic digestion prior to labelling of peptides with a reporter tag. b) Each reporter tag is associated with a balance to ensure all tags have the same mass. The balance and reporter tags separate during MS with analysis permitting the relative quantification of peptides in each sample after proteins are identified through comparison to a database.

4.2 Methods

4.2.1 Animal Studies

Details of animal husbandry, in addition to the ethical and legal considerations of the animal work covered in this thesis, are described in section 2.2.11. Male 6-8 week old immune-competent BALB/c mice chronically dosed with brusatol over a two-week period as part of the tumour-based experiments presented in chapter three were utilised in the work described in this section.

To assess the effects of brusatol on normal tissue including liver and colon (where available) from mice exposed to brusatol over a two-week period, within the study described in section 3.2.11, was excised following cull by cervical dislocation. Cull was undertaken three hours following the final dose of brusatol. Tissue was immediately excised and snap frozen in liquid nitrogen before storage at -80°C until required.

4.2.2 Tissue homogenisation

Sections of colon (50mg) or liver (100mg) were homogenised in ice-cold iTRAQ buffer [0.5M triethylammonium bicarbonate (TEAB) / 0.1% SDS] using a MM400 oscillating bead mill (Retsch, Haan, Germany). Colons were homogenised in 250µl and livers in 500µl of iTRAQ buffer. Samples were subjected to a freeze-thaw cycle (-80°C for 1 hour) and sonicated three times for 10 seconds each at an amplitude of 5µm. The homogenate was centrifuged at 14 000rpm for 10 minutes at 4°C and the supernatant retained. The supernatant was centrifuged again at the same rpm for 5 minutes. The protein concentration of the supernatant was determined at multiple dilutions (x100, x200 and x400) using the well-established method of Bradford [445].

4.2.3 Coomassie staining

To ensure accurate quantification of samples, and as an assessment of protein quality, a Coomassie stain of liver tissue was undertaken prior to iTRAQ analysis. 10µg of total protein was loaded in 4x Laemmli buffer in each well of a Mini-PROTEAN® TGX™ Precast Gel after denaturing proteins by heating for 5 minutes at 100°C. 4µl of the PrecisionPlus kaleidoscope molecular weight marker was added to one well on every gel as a reference. Gels were subjected to electrophoresis in running buffer (25mM Tris, 190nM glycine, 20%

methanol and 0.01% SDS) at 90 volts until resolved and then 150 volts until the blue dye front reached the bottom of the gel after which a Coomassie stain was performed.

Gels were placed in 7% glacial acid with 40% methanol for one hour to fix proteins and then stained with one-part Brilliant Blue G 250 (Sigma-Aldrich, Dorset, UK) in four parts methanol for one hour. Gels were then rinsed in 10% acetic acid in methanol for 60 seconds and destained in 25% methanol for approximately 24 hours until bands appeared.

4.2.4 Western immunoblotting

Western immunoblotting of tissue homogenates was conducted for Nrf2 relative expression as described in section 3.3.2. Tissue samples from brusatol-treated or vehicle control mice were run on a single 10 or 15 well gel to allow comparison of Nrf2 expression across samples.

4.2.5 iTRAQ labelling

For iTRAQ analysis, 100µg of total protein from each liver sample was suspended in 20µl of iTRAQ buffer. A pooled reference sample with the same total protein content was created from all samples for inclusion in duplicate on all iTRAQ runs. iTRAQ reagents are available in an 8-plex format, restricting samples to six per run and two pooled samples. A random selection of liver samples, including three from brusatol-treated and three from control mice, were included in the run. Labelling with iTRAQ reagents was carried out according to the Applied Biosystems protocol for an 8-plex procedure (Life Technologies, Paisley, UK). In brief, samples were reduced with Tris (2-carboxyethyl) phosphine hydrochloride (TCEP) and sulphydryl groups capped with methylmethanethiosulfate (MMTS), before overnight digestion with trypsin (Promega, Southampton, UK). Peptides were then labelled with isobaric tags, pooled and diluted to 5ml with 10mM potassium dihydrogen phosphate/25% acetonitrile (ACN: w/v) and acidified to a pH of <3 with phosphoric acid.

4.2.6 Cation exchange

Samples were fractionated on a Polysulfoethyl A strong cation-exchange column (200 × 4.6mm, 5µm, 300Å; Poly LC, Columbia, MD) at 2ml/minute using a gradient from 10mM potassium dihydrogen phosphate/25% ACN (w/v) to 0.5M potassium chloride/10mM potassium dihydrogen phosphate/25% ACN (w/w/v) in 75 minutes. Fractions of 2ml were collected and dried by centrifugation under vacuum (SpeedVac, Eppendorf UK Ltd,

Stevenage, UK) before reconstitution in 1ml of 0.1% trifluoroacetic acid (TFA) and desalting using a mRP Hi Recovery protein 4.6 x 50mm column (Agilent, Berkshire UK) on a Vision Workstation (Applied Biosystems/Life Technologies, Paisley, UK) prior to mass spectrometric analysis.

4.2.7 Mass spectrometry

Desalted fractions were reconstituted in 40µl of 0.1% formic acid and 5µl aliquots were delivered into a Triple TOF 6600 (AB Sciex, Warrington, UK) via an Eksigent NanoUltra cHiPLC System (AB Sciex) mounted with a microfluidic trap and analytical column (15 cm × 75 µm) packed with ChromXP C18−CL 3µm. A NanoSpray III source was fitted with a 10µm inner diameter PicoTip emitter (New Objective, Woburn, USA). The trap column was washed with 2% ACN/0.1% (v/v) formic acid for 10 minutes at 2µL/minute before switching in-line with the analytical column. A gradient of 2−50% ACN/0.1% formic acid (v/v) over 90 minutes was applied to the column at a flow rate of 300nl/min.

Spectra were acquired automatically in positive ion mode using information-dependent acquisition powered by Analyst TF 1.5.1. software (AB Sciex, Massachusetts, USA). Up to 25 MS/MS spectra were acquired per cycle (approximately 10Hz) using a threshold of 100 counts per second and with dynamic exclusion for 12 seconds. The rolling collision energy was increased automatically by selecting the iTRAQ check box in Analyst, and manually by increasing the collision energy intercepts by 5.

4.2.8 iTRAQ protein identification and data analysis

Acquired data were searched using ProteinPilot 4.2 and the Paragon algorithm (AB Sciex, Massachusetts, USA) against the latest version of the SwissProt database, with MMTS as a fixed modification of cysteine residues and biological modifications allowed. The data were also searched against a reversed decoy database and only proteins lying within a 1% global false discovery rate (FDR) were taken forward for analysis. Quantitation of proteins was relative to the common pool sample present in the iTRAQ-MS experiment. iTRAQ data for proteins identified with at least 95% confidence of correct sequence assignment, or by a single peptide with at least 99% confidence were $\log_2$ transformed, batch corrected and included in subsequent analyses. Proteins present in all samples were taken forward for further analysis.

Mean fold changes in protein expression were calculated and analysis conducted on the logged fold-change values. Brusatol dependent protein expression was defined by comparing the proteome in the vehicle (1% DMSO in x1 PBS) treated control mice livers to those dosed with the drug over a period of 2 weeks.

4.2.9 Pathway analysis

The accession numbers of proteins identified as significantly differentially expressed were subjected to analysis with Ingenuity Pathway Analysis (Redwood City, USA) to identify pathways altered by treatment with brusatol. Ingenuity Pathways Analysis computes a score for each network according to the fit of that network with the identified proteins of interest (referred to as the focus proteins). The score is derived from a p-value and indicates the probability of the focus proteins in a network being found together due to random chance. A score of 2 indicates that there is a 1 in 100 chance that the focus proteins are together in a network due to random chance, therefore scores greater than 2 have at least a 99% confidence of not being generated by random chance alone. Analysis must also take into account both the number of focus proteins identified and total known proteins in each network. Significant canonical pathways were identified with a threshold p value of <0.05 (after correction). If there are *n* proteins in a pathway, and *f* have been identified through iTRAQ, the p-value is the probability of finding *f* or more proteins in a set of *n* proteins randomly selected from the global molecular network.

4.2.10 RNA isolation

RNA isolation was performed using the RNeasy Mini-kit (QIAGEN, Manchester, UK) according to the manufacturer's instructions. Approximately 30mg of liver tissue was weighed out and 600µl of buffer RLT added. Tissue was homogenised using the MM400 oscillating mill (Retsch, Haan, Germany) and centrifuged at 18 000g for 3 minutes. The supernatant was retained and 600µl of 70% ethanol added. The solution was passed through an RNeasy spin column by centrifugation at 10 000g for 15 seconds and the RNA, which had bound to the spin column, washed in three subsequent centrifugation steps using the buffers provided. RNA was eluted in RNase-free dH_2O and the concentration determined using a Nanodrop™ ND-1000 UV spectrophotometer (Labtech International, East Sussex, UK).

4.2.11 cDNA synthesis (Reverse Transcription)

cDNA synthesis was carried out using the GoScript™ Reverse Transcription System (Promega, Southampton, UK) according to the manufacturer's instructions with some minor modifications. 0.5µg of RNA were combined with 1µl of oligo and 1µl of random primers and made up to a total volume of 10µl with RNase-free dH_2O. The solution was incubated at 70°C for 5 minutes and then cooled on ice. A master mix containing 8µl of 5x R buffer, 4µl of 25nM $MgCl_2$, 2µl dNTPs, 2µl reverse transcriptase and 14µl of RNase-free dH_2O was added to each RNA sample. Strands were annealed (25°C; 5 minutes) and extended (42°C; 1 hour), before the reverse transcriptase was inactivated (70°C; 15 minutes). cDNA concentration was subsequently determined using the Nanodrop™ ND-1000 UV spectrophotometer as described in section 2.2.3.

4.2.12 Microfluidic TaqMan low density array cards

Custom TaqMan® low density gene expression array cards (TLDA, ThermoFisher Scientific, Paisley, UK) were designed to include well established Nrf2-regulated genes, as identified from in-house data and the literature. In addition to the 18S gene, used as a housekeeper to correct loading errors, 47 Nrf2 genes were included on each plate. The represented genes and plate layout are detailed in figure 4.1 and table 4.2. Eight samples could be run on each card, which included a pool of cDNA from all samples to allow data comparison across plates and a negative control (nuclease-free dH_2O). Samples were randomised across plates by group so that an equal number of samples from control or brusatol-treated mice were run on each. All samples were run in duplicate and the average values used for comparisons between brusatol-treated and control groups of mice.

The previously synthesised cDNA was diluted in nuclease-free dH_2O to a concentration of 20ng/µl. This cDNA solution was subsequently mixed with 50µl of TaqMan® Gene Expression Master Mix (ThermoFisher Scientific, Paisley, UK) to give 1000ng of total cDNA. Samples were vortexed and transferred by pipette to the appropriate well of the TaqMan array card. Pooled cDNA samples were prepared in the same way. Once loaded, cards were centrifuged twice at 331g for 1 min, sealed and wells removed. Cards were run on the 7900HT Fast Real-Time Polymerase Chain Reaction (PCR) System (Applied Biosystems, California, USA) with a 10-minute denaturation at 95°C followed by 40 amplification cycles (15 seconds at 95°C and 1 minute at 60°C) and a final cooling period of 5 minutes at 70°C.

4.2.13 Microfluidic card data analysis

Data were analysed using the comparative C_T method ($\Delta\Delta C_T$) to allow relative quantification [446]. C_T values were determined using the RQ manager 1.2 component of the 7900HT Fast System software. The threshold was manually set to a value of 0.3 for all plates. Gene expression was quantified relative to the sample pool run on the same plate and normalised to 18S gene expression. Statistical analysis was performed to compare relative expression of genes in brusatol-treated and control mice where C_T values were available for ≥3 animals in each group. A Shapiro-Wilk test was used to assess the normality of the data with normal data analysed using an unpaired t-test and non-normal data analysed using a Mann-Whitney U test. Statistical significance was assumed at $p<0.05$.

Gene symbol	Gene ID	Gene Name
Abcc1	Mm00456156_m1	ATP-binding cassette, sub-family C (CFTR/MRP), member 1
Abcc2	Mm00496899_m1	ATP-binding cassette, sub-family C (CFTR/MRP), member 2
Abcc3	Mm00551550_m1	ATP-binding cassette, sub-family C (CFTR/MRP), member 3
Abcc4	Mm01226381_m1	ATP-binding cassette, sub-family C (CFTR/MRP), member 4
Abcc5	Mm01343626_m1	ATP-binding cassette, sub-family C (CFTR/MRP), member 5
Aox1	Mm00437482_m1	aldehyde oxidase 1
Cat	Mm00437992_m1	catalase
Cbr1	Mm04207333_g1	carbonyl reductase 1
Cbr3	Mm00557339_m1	carbonyl reductase 3
Ces1g	Mm00491334_m1	carboxylesterase 1G
18S	18S-Hs99999901_s1	Eukaryotic 18S rRNA
Ces2c	Mm01250994_m1	carboxylesterase 2C
Cyp2a4	Mm00487248_g1	cytochrome P450, family 2, subfamily a, polypeptide 4
Entpd5	Mm00514245_m1	ectonucleoside triphosphate diphosphohydrolase 5
Ephx1	Mm00468752_m1	epoxide hydrolase 1, microsomal
Ephx2	Mm01313813_m1	epoxide hydrolase 2, cytoplasmic
Fth1	Mm00850707_g1	ferritin heavy chain 1
Ftl1	Mm03030144_g1	ferritin light chain 1
G6pdx	Mm00656735_g1	glucose-6-phosphate dehydrogenase X-linked
Gclc	Mm00802655_m1	glutamate-cysteine ligase, catalytic subunit
Gclm	Mm00514996_m1	glutamate-cysteine ligase, modifier subunit
Gsr	Mm00439154_m1	glutathione reductase
Gss	Mm00515065_m1	glutathione synthetase
Gsta2	Mm03019257_g1	glutathione S-transferase, alpha 2 (Yc2)
Gsta3	Mm00494798_m1	glutathione S-transferase, alpha 3
Gsta4	Mm00494803_m1	glutathione S-transferase, alpha 4
Gstm1	Mm00833915_g1	glutathione S-transferase, mu 1
Gstm2	Mm00725711_s1	glutathione S-transferase, mu 2
Gstm3	Mm00833923_m1	glutathione S-transferase, mu 3
Gstm4	Mm00728197_s1	glutathione S-transferase, mu 4
Gstp1	Mm04213618_gH	glutathione S-transferase, pi 1
Hmox1	Mm00516005_m1	heme oxygenase 1
Keap1	Mm00497268_m1	kelch-like ECH-associated protein 1
Me1	Mm00782380_s1	malic enzyme 1, NADP(+)-dependent, cytosolic
Mgst1	Mm00498294_m1	microsomal glutathione S-transferase 1
Nampt	Mm00451938_m1	nicotinamide phosphoribosyltransferase
Nfe2l2	Mm00477784_m1	nuclear factor, erythroid derived 2, like 2
Nqo1	Mm01253561_m1	NAD(P)H dehydrogenase, quinone 1
Prdx1	Mm01621996_s1	peroxiredoxin 1
Prdx6	Mm00725435_s1	peroxiredoxin 6
Slc22a12	Mm01236822_m1	solute carrier family 22 (organic anion/cation transporter), member 12
Srxn1	Mm00769566_m1	sulfiredoxin 1 homolog (S. cerevisiae)
Txn1	Mm00726847_s1	thioredoxin 1
Txnrd1	Mm00443675_m1	thioredoxin reductase 1
Ugdh	Mm00447643_m11	UDP-glucose dehydrogenase
Ugt1a1	Mm02603337_m1	UDP glucuronosyltransferase 1 family, polypeptide A1
Ugt2b5	Mm01623253_s1	UDP glucuronosyltransferase 2 family, polypeptide B5
PGD	Mm00503037_m1	phosphogluconate dehydrogenase

Table 4.1 – Gene symbols and names represented on the Microfluidic TaqMan low density array card.

Sample number	Gene symbols																						
1	Abcc1	Abcc2	Abcc3	Abcc4	Abcc5	Aox1	Cat	Cbr1	Cbr3	Ces1g	18S	Ces2c	Cyp2a5	Entpd5	Ephx1	Ephx2	Fth1	Ftl1	G6pdx	Gclc	Gclm	Gsr	Gss	Gsta2
	Gsta3	Gsta4	Gstm1	Gstm2	Gstm3	Gstm4	Gstp1	Hmox1	Keap1	Me1	Mgst1	Nampt	Nfe2l2	Nqo1	Prdx1	Prdx6	Slc22a12	Srxn1	Txn1	Txnrd1	Ugdh	Ugt1a1	Ugt2b5	Pgd
2	Abcc1	Abcc2	Abcc3	Abcc4	Abcc5	Aox1	Cat	Cbr1	Cbr3	Ces1g	18S	Ces2c	Cyp2a5	Entpd5	Ephx1	Ephx2	Fth1	Ftl1	G6pdx	Gclc	Gclm	Gsr	Gss	Gsta2
	Gsta3	Gsta4	Gstm1	Gstm2	Gstm3	Gstm4	Gstp1	Hmox1	Keap1	Me1	Mgst1	Nampt	Nfe2l2	Nqo1	Prdx1	Prdx6	Slc22a12	Srxn1	Txn1	Txnrd1	Ugdh	Ugt1a1	Ugt2b5	Pgd
3	Abcc1	Abcc2	Abcc3	Abcc4	Abcc5	Aox1	Cat	Cbr1	Cbr3	Ces1g	18S	Ces2c	Cyp2a5	Entpd5	Ephx1	Ephx2	Fth1	Ftl1	G6pdx	Gclc	Gclm	Gsr	Gss	Gsta2
	Gsta3	Gsta4	Gstm1	Gstm2	Gstm3	Gstm4	Gstp1	Hmox1	Keap1	Me1	Mgst1	Nampt	Nfe2l2	Nqo1	Prdx1	Prdx6	Slc22a12	Srxn1	Txn1	Txnrd1	Ugdh	Ugt1a1	Ugt2b5	Pgd
4	Abcc1	Abcc2	Abcc3	Abcc4	Abcc5	Aox1	Cat	Cbr1	Cbr3	Ces1g	18S	Ces2c	Cyp2a5	Entpd5	Ephx1	Ephx2	Fth1	Ftl1	G6pdx	Gclc	Gclm	Gsr	Gss	Gsta2
	Gsta3	Gsta4	Gstm1	Gstm2	Gstm3	Gstm4	Gstp1	Hmox1	Keap1	Me1	Mgst1	Nampt	Nfe2l2	Nqo1	Prdx1	Prdx6	Slc22a12	Srxn1	Txn1	Txnrd1	Ugdh	Ugt1a1	Ugt2b5	Pgd
5	Abcc1	Abcc2	Abcc3	Abcc4	Abcc5	Aox1	Cat	Cbr1	Cbr3	Ces1g	18S	Ces2c	Cyp2a5	Entpd5	Ephx1	Ephx2	Fth1	Ftl1	G6pdx	Gclc	Gclm	Gsr	Gss	Gsta2
	Gsta3	Gsta4	Gstm1	Gstm2	Gstm3	Gstm4	Gstp1	Hmox1	Keap1	Me1	Mgst1	Nampt	Nfe2l2	Nqo1	Prdx1	Prdx6	Slc22a12	Srxn1	Txn1	Txnrd1	Ugdh	Ugt1a1	Ugt2b5	Pgd
6	Abcc1	Abcc2	Abcc3	Abcc4	Abcc5	Aox1	Cat	Cbr1	Cbr3	Ces1g	18S	Ces2c	Cyp2a5	Entpd5	Ephx1	Ephx2	Fth1	Ftl1	G6pdx	Gclc	Gclm	Gsr	Gss	Gsta2
	Gsta3	Gsta4	Gstm1	Gstm2	Gstm3	Gstm4	Gstp1	Hmox1	Keap1	Me1	Mgst1	Nampt	Nfe2l2	Nqo1	Prdx1	Prdx6	Slc22a12	Srxn1	Txn1	Txnrd1	Ugdh	Ugt1a1	Ugt2b5	Pgd
7	Abcc1	Abcc2	Abcc3	Abcc4	Abcc5	Aox1	Cat	Cbr1	Cbr3	Ces1g	18S	Ces2c	Cyp2a5	Entpd5	Ephx1	Ephx2	Fth1	Ftl1	G6pdx	Gclc	Gclm	Gsr	Gss	Gsta2
	Gsta3	Gsta4	Gstm1	Gstm2	Gstm3	Gstm4	Gstp1	Hmox1	Keap1	Me1	Mgst1	Nampt	Nfe2l2	Nqo1	Prdx1	Prdx6	Slc22a12	Srxn1	Txn1	Txnrd1	Ugdh	Ugt1a1	Ugt2b5	Pgd
8	Abcc1	Abcc2	Abcc3	Abcc4	Abcc5	Aox1	Cat	Cbr1	Cbr3	Ces1g	18S	Ces2c	Cyp2a5	Entpd5	Ephx1	Ephx2	Fth1	Ftl1	G6pdx	Gclc	Gclm	Gsr	Gss	Gsta2
	Gsta3	Gsta4	Gstm1	Gstm2	Gstm3	Gstm4	Gstp1	Hmox1	Keap1	Me1	Mgst1	Nampt	Nfe2l2	Nqo1	Prdx1	Prdx6	Slc22a12	Srxn1	Txn1	Txnrd1	Ugdh	Ugt1a1	Ugt2b5	Pgd

Table 4.2 – Microfluidic TaqMan low density array card layout. Eight samples were run on each plate. Each loading well corresponds to two adjacent rows of the plate. The gene names for each gene code are detailed in table 4.1

4.3 Results

4.3.1 Effect of brusatol on Nrf2 expression in vivo

Brusatol caused a significant reduction in the level of Nrf2, as assessed by western immunoblotting, in flank tumours (data displayed in figure 3.23), normal colon (figure 4.2) and normal liver tissue (figure 4.3) excised from BALB/c mice repeatedly dosed with the compound over two weeks. Nrf2 protein expression, as assessed by western immunoblotting and densitometry, was reduced by 74%, 95% and 97% in the flank tumours, normal colon and normal liver tissue excised from brusatol-treated mice in comparison to the saline-treated controls respectively.

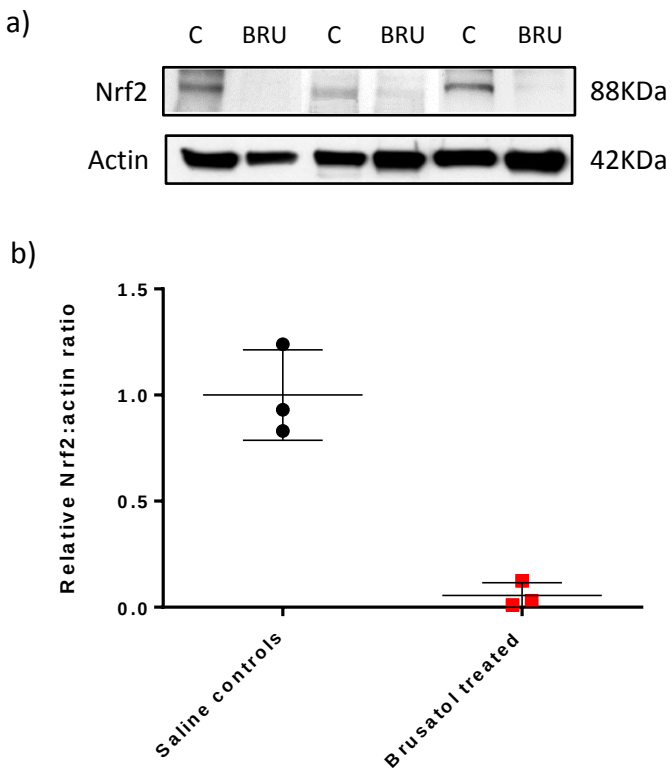

Figure 4.2 – a) Western immunoblot image displaying inhibition of Nrf2 in colon tissue excised from BALB/c mice after dosing with brusatol for two weeks. b) Graphical display of densitometry confirmed significant inhibition of Nrf2 (p = 0.01 unpaired t-test with Welch's correction). (N=3, graph displays mean +/- SD, c = saline control, BRU = brusatol)

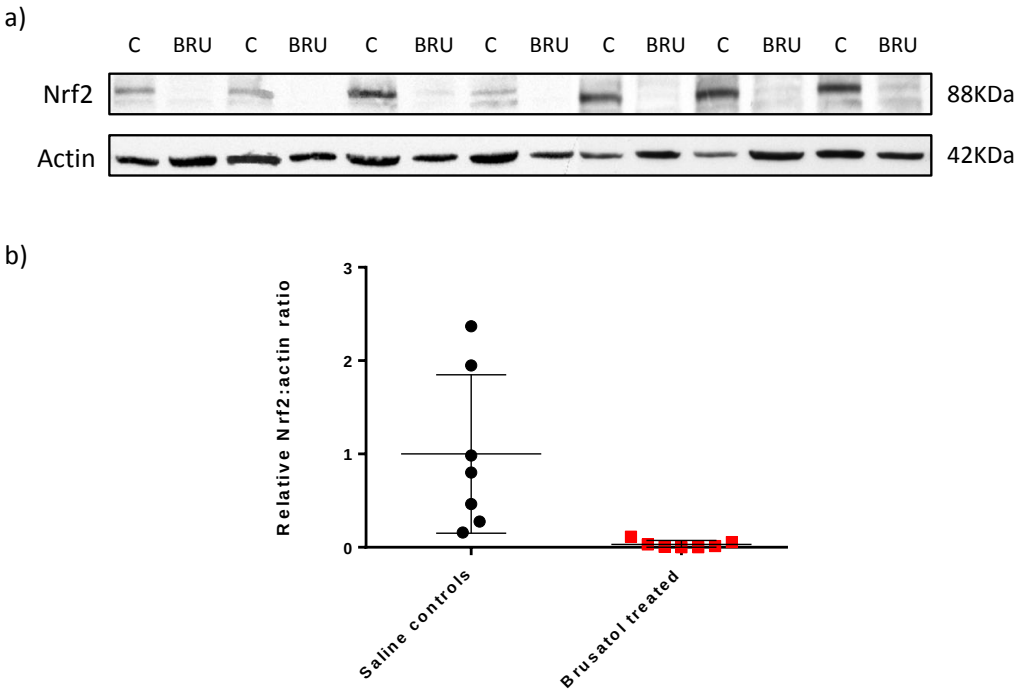

Figure 4.3 – a) Western immunoblot image displaying inhibition of Nrf2 in liver tissue excised from BALB/c mice after dosing with brusatol. b) Graphical display of densitometry confirmed significant inhibition of Nrf2 (p = 0.02 unpaired t-test with Welch's correction). (N=7, graph displays mean +/- SD, C = saline control, BRU = brusatol)

4.3.2 Coomaissie staining of samples

Prior to running iTRAQ analysis, protein electrophoresis and Coomaisse blue staining was completed to verify accurate quantification of the total protein content of samples and ensure adequate sample quality. iTRAQ analysis was only undertaken on normal liver excised from mice either treated with brusatol or a saline control. The quantity and quality of colonic and tumour tissue was considered inadequate for proteomic assessment.

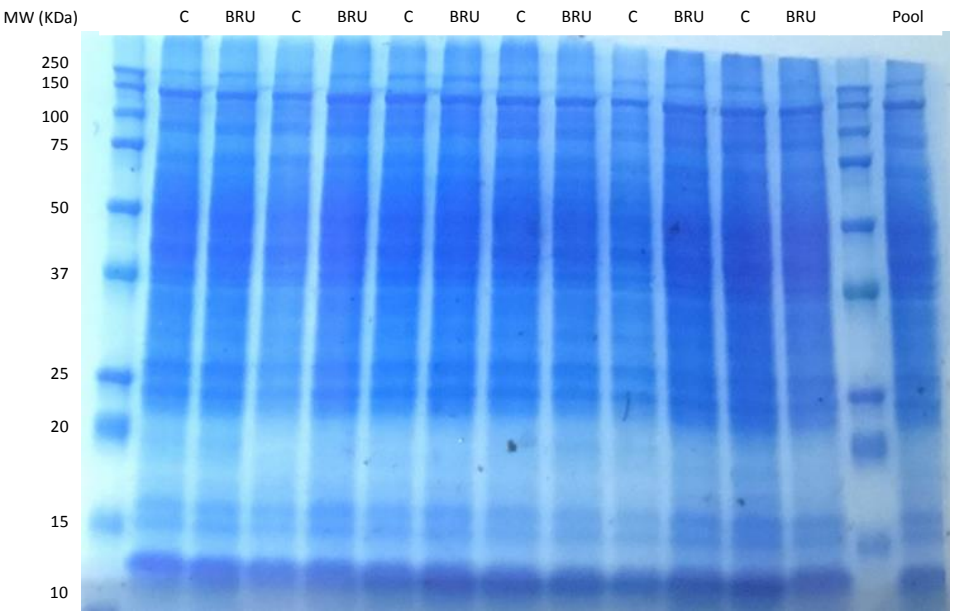

Figure 4.4 – Image of a Coomaissie stain of normal liver tissue samples used in the iTRAQ analysis excised from BALB/c mice treated with either brusatol or a saline control. (C = saline control, BRU = brusatol, MW = molecular weight)

4.3.3 iTRAQ analysis of mouse liver tissue

Liver samples from three mice treated with brusatol and three mice receiving vehicle alone were subject to iTRAQ analysis in a single run and compared with the average of a common pooled sample, which was run in duplicate. A fold-change value for each detected protein in each sample was obtained, relative to the pooled samples, and utilised to compare the fold-change in protein expression between brusatol-treated and control liver tissue.

A total of 3515 proteins were identified in the iTRAQ run. An unpaired t-test was used to identify proteins with significantly different expression between mouse groups. Significance was assumed at two-tailed p value of <0.05. By applying a relatively non-stringent statistical analysis, the expression of 262 liver proteins were deemed statistically different between brusatol-treated and control mice. Brusatol exposure significantly increased the expression of 137 proteins (Table 4.3) and decreased the expression of 125 (Table 4.4) in murine liver. Differences in protein expression between control mouse liver tissue and that taken from mice treated with brusatol were generally subtle, which could be considered advantageous in the context of a potential therapeutic compound.

Whilst this level of statistical analysis is insufficient for unequivocal designation of brusatol associated proteins, it provides a sufficient number of potentially regulated proteins to allow meaningful pathway analysis. As noted by Subramanian *et al.*[447], the application of stringent multiple testing correction algorithms (such as Bonferroni or Benjamini Hochberg analyses) to large scale global analysis data can preclude the identification of modest expression changes that can collectively modulate a specific pathway.

					Relative expression to pool											
SwissProt. Acc No.	Name	Avg. percentage coverage (%)	Avg. number of Peptides	Mean Pool	Mouse C1	Mouse C2	Mouse C3	Mean Control	Control SD	Mouse Bru1	Mouse Bru2	Mouse Bru3	Mean Brusatol	Brusatol SD	Fold-change Bru/C	p value
O08547	Vesicle-trafficking protein SEC22b	45.50	30	1.34	0.62	0.76	0.15	0.51	0.32	4.13	2.70	3.87	3.57	0.76	6.99	0.00301
Q9CPQ3	Mitochondrial import receptor subunit TOM22 homolog	2.42	1	0.19	0.25	0.04	0.04	0.11	0.12	0.69	0.89	0.67	0.75	0.12	6.80	0.00281
Q3TW96	UDP-N-acetylhexosamine pyrophosphorylase-like protein 1	8.50	1	2.09	0.06	0.08	0.34	0.16	0.15	0.87	0.79	1.05	0.90	0.13	5.63	0.00319
Q9CZS1	Aldehyde dehydrogenase X, mitochondrial	4.39	1	0.86	0.15	0.42	0.09	0.22	0.18	0.93	0.47	1.06	0.82	0.31	3.68	0.04410
Q61733	28S ribosomal protein S31, mitochondrial	3.70	2	0.32	0.16	0.24	0.23	0.21	0.04	0.64	0.74	0.86	0.75	0.11	3.61	0.00136
Q8R035	Peptidyl-tRNA hydrolase ICT1, mitochondrial	2.43	3	0.09	0.21	0.67	1.49	0.79	0.65	3.34	1.94	2.19	2.49	0.75	3.16	0.04073
P48036	Annexin A5	62.70	30	1.34	0.70	1.16	0.81	0.89	0.24	2.54	2.49	3.02	2.68	0.29	3.01	0.00121
Q3TC93	HCLS1-binding protein 3	37.31	17	0.74	0.59	0.72	0.50	0.60	0.11	2.33	1.69	1.14	1.72	0.60	2.86	0.03360
Q5F2F2	Abhydrolase domain-containing protein 15	3.77	1	0.43	0.34	0.04	0.42	0.26	0.20	0.64	0.77	0.81	0.74	0.09	2.80	0.01905
P63330	Serine/threonine-protein phosphatase 2A catalytic subunit alpha isoform	16.19	2	1.03	0.56	0.95	0.68	0.73	0.20	2.09	2.44	1.47	2.00	0.49	2.75	0.01411
Q8BRK8	5'-AMP-activated protein kinase catalytic subunit alpha-2	51.91	15	0.86	0.68	0.70	0.21	0.53	0.28	1.63	1.16	1.49	1.42	0.24	2.69	0.01388
P34022	Ran-specific GTPase-activating protein	9.11	2	1.31	0.41	0.32	0.57	0.43	0.13	1.08	1.21	1.10	1.13	0.07	2.62	0.00124
P49312	Heterogeneous nuclear ribonucleoprotein A1	2.36	2	0.70	0.62	0.39	0.29	0.43	0.17	1.02	1.14	1.10	1.08	0.06	2.51	0.00331
Q9ET01	Glycogen phosphorylase, liver form	10.26	4	0.94	0.48	0.49	0.46	0.48	0.02	1.07	1.25	1.27	1.19	0.11	2.50	0.00039
Q9QXA5	U6 snRNA-associated Sm-like protein LSm4	5.76	2	1.64	0.65	0.70	1.10	0.81	0.25	2.05	1.71	2.25	2.00	0.27	2.46	0.00505
Q9DB27	Malignant T-cell-amplified sequence 1	61.26	42	1.25	1.02	1.10	0.21	0.77	0.49	2.13	1.89	1.58	1.87	0.27	2.41	0.02811
O70493	Sorting nexin-12	56.47	56	0.90	0.86	0.70	0.17	0.57	0.36	1.57	1.31	1.21	1.36	0.19	2.38	0.02800
Q8CBE3	WD repeat-containing protein 37	24.68	10	1.00	0.46	0.49	0.51	0.48	0.02	0.90	1.21	1.29	1.14	0.21	2.35	0.00550
P10648	Glutathione S-transferase A2	7.72	4	2.78	0.83	2.83	2.25	1.97	1.03	3.87	5.20	4.83	4.63	0.69	2.35	0.02024
Q9CPU4	Microsomal glutathione S-transferase 3	66.09	40	0.76	0.66	0.69	0.54	0.63	0.08	1.64	1.66	1.13	1.48	0.30	2.34	0.00947
Q8R1I1	Cytochrome b-c1 complex subunit 9	21.96	11	1.11	0.58	0.54	0.28	0.47	0.16	0.75	1.13	1.39	1.09	0.32	2.33	0.04075
Q99PU5	Long-chain-fatty-acid--CoA ligase ACSBG1	52.41	42	1.67	0.85	0.94	0.60	0.80	0.17	1.89	1.77	1.89	1.85	0.07	2.32	0.00061
Q91W43	Glycine dehydrogenase (decarboxylating), mitochondrial	30.88	5	0.20	0.37	0.28	0.38	0.35	0.06	0.71	0.72	0.95	0.80	0.14	2.30	0.00623
Q9CZ91	Serum response factor-binding protein 1	29.30	27	0.68	0.44	0.53	0.47	0.48	0.05	1.25	0.96	0.91	1.04	0.18	2.16	0.00658
Q91Y97	Fructose-bisphosphate aldolase B	21.91	3	1.32	0.69	1.13	1.22	1.01	0.28	2.11	2.56	1.82	2.16	0.37	2.13	0.01319
P58389	Serine/threonine-protein phosphatase 2A activator	61.29	112	1.96	0.76	1.22	1.13	1.04	0.25	2.19	2.05	2.38	2.21	0.16	2.13	0.00237
Q60649	Caseinolytic peptidase B protein homolog	3.74	1	0.60	0.92	0.49	0.21	0.54	0.36	1.21	1.03	1.20	1.15	0.10	2.12	0.04707

Q9DBJ1	Phosphoglycerate mutase 1	3.42	1	0.95	0.98	0.48	0.35	0.60	0.33	1.41	1.16	1.20	1.26	0.13	2.08	0.03463
P45376	Aldose reductase	44.56	15	1.57	0.95	1.25	0.60	0.93	0.32	2.09	1.61	2.11	1.94	0.28	2.08	0.01514
Q8R081	Heterogeneous nuclear ribonucleoprotein L	75.49	18	1.72	1.00	1.54	1.00	1.18	0.31	2.81	2.03	2.49	2.44	0.39	2.07	0.01187
Q8VC30	Triokinase/FMN cyclase	68.90	56	1.61	1.10	1.21	1.13	1.15	0.06	2.49	1.82	2.75	2.35	0.48	2.05	0.01252
Q80UU9	Membrane-associated progesterone receptor component 2	19.27	7	0.69	0.69	0.65	0.52	0.62	0.09	1.18	1.33	1.26	1.26	0.08	2.03	0.00068
Q8CI94	Glycogen phosphorylase, brain form	22.32	7	0.76	0.84	1.05	0.52	0.80	0.27	1.46	1.72	1.67	1.62	0.14	2.02	0.00943
Q61081	Hsp90 co-chaperone Cdc37	48.80	23	1.96	1.42	1.32	1.24	1.32	0.09	3.25	2.33	2.40	2.66	0.51	2.01	0.01123
P10605	Cathepsin B	39.17	4	0.67	0.62	0.60	0.23	0.48	0.22	1.00	0.82	1.05	0.95	0.12	1.98	0.03119
P56656	Cytochrome P450 2C39	34.69	15	1.31	0.95	0.65	0.85	0.82	0.16	1.50	1.57	1.74	1.60	0.12	1.96	0.00234
Q9EPB5	Serine hydrolase-like protein	29.41	2	1.58	1.18	2.33	1.10	1.54	0.69	3.44	2.96	2.63	3.01	0.40	1.96	0.03333
Q9DC70	NADH dehydrogenase [ubiquinone] iron-sulfur protein 7, mitochondrial	23.51	11	1.06	0.41	0.86	0.90	0.72	0.27	1.47	1.57	1.18	1.41	0.20	1.94	0.02481
Q6ZPJ0	Testis-expressed sequence 2 protein	46.41	23	1.32	0.55	0.89	0.61	0.68	0.18	1.45	1.16	1.37	1.32	0.15	1.94	0.00877
Q99KY4	Cyclin-G-associated kinase	1.99	1	1.60	1.15	1.14	1.85	1.38	0.41	2.70	2.05	3.22	2.66	0.59	1.93	0.03637
P51855	Glutathione synthetase	36.57	9	1.80	1.10	1.37	1.08	1.18	0.16	2.44	2.23	2.09	2.25	0.18	1.91	0.00153
Q9QZ23	NFU1 iron-sulfur cluster scaffold homolog, mitochondrial	17.66	6	0.73	0.60	0.64	0.23	0.49	0.23	1.03	0.79	0.99	0.94	0.13	1.91	0.04313
P28650	Adenylosuccinate synthetase isozyme 1	7.38	6	1.13	0.52	0.69	0.64	0.61	0.09	1.12	1.42	0.97	1.17	0.23	1.90	0.01704
P34884	Macrophage migration inhibitory factor	49.71	22	0.95	0.64	0.79	0.37	0.60	0.21	1.34	1.15	0.92	1.14	0.21	1.90	0.03512
Q7TMF3	NADH dehydrogenase [ubiquinone] 1 alpha subcomplex subunit 12	36.46	5	1.45	1.34	1.38	1.12	1.28	0.14	2.13	2.61	2.51	2.42	0.25	1.89	0.00249
P46061	Ran GTPase-activating protein 1	1.61	1	0.82	0.52	0.37	0.29	0.39	0.12	0.86	0.58	0.74	0.73	0.14	1.86	0.03325
Q921S7	39S ribosomal protein L37, mitochondrial	56.40	69	1.45	1.15	0.98	1.18	1.10	0.11	2.00	2.36	1.79	2.05	0.29	1.85	0.00600
P52840	Sulfotransferase 1A1	64.80	90	1.72	1.13	1.85	0.86	1.28	0.51	2.65	2.27	2.19	2.37	0.25	1.85	0.02968
Q64433	10 kDa heat shock protein, mitochondrial	42.99	51	1.18	1.04	0.77	0.36	0.72	0.34	1.28	1.50	1.22	1.34	0.15	1.85	0.04605
P17751	Triosephosphate isomerase	4.13	1	0.79	0.63	0.73	0.45	0.60	0.14	1.00	1.34	0.98	1.11	0.20	1.84	0.02402
P62774	Myotrophin	24.74	12	0.56	0.53	0.69	0.58	0.60	0.08	0.88	1.43	1.01	1.11	0.29	1.84	0.04370
Q9D1P0	39S ribosomal protein L13, mitochondrial	8.56	3	0.74	1.05	0.87	0.67	0.86	0.19	1.89	1.54	1.32	1.58	0.29	1.84	0.02224
Q9DCD0	6-phosphogluconate dehydrogenase, decarboxylating	13.36	2	2.05	1.87	1.80	1.80	1.83	0.04	2.88	4.21	2.88	3.33	0.76	1.82	0.02740
Q61133	Glutathione S-transferase theta-2	34.17	7	0.82	0.32	0.75	0.67	0.58	0.23	1.17	1.02	0.95	1.04	0.11	1.80	0.03539
P29391	Ferritin light chain 1	32.87	19	1.49	1.03	1.22	0.80	1.02	0.21	2.19	1.64	1.64	1.83	0.31	1.79	0.02092
Q9CPU2	NADH dehydrogenase [ubiquinone] 1 beta subcomplex subunit 2, mitochondrial	27.02	27	0.72	0.64	0.79	0.87	0.77	0.12	1.46	1.36	1.24	1.35	0.11	1.75	0.00335
Q9CWS0	N(G),N(G)-dimethylarginine dimethylaminohydrolase 1	22.37	7	1.60	0.85	0.80	0.81	0.82	0.02	1.13	1.79	1.38	1.43	0.33	1.75	0.03358

Q60855	Receptor-interacting serine/threonine-protein kinase 1	39.76	15	0.54	0.52	0.55	0.63	0.57	0.05	1.06	0.77	1.11	0.98	0.18	1.72	0.01980
Q920B9	FACT complex subunit SPT16	1.92	2	0.65	0.51	0.72	0.73	0.65	0.13	1.22	1.02	1.12	1.12	0.10	1.71	0.00799
P48758	Carbonyl reductase [NADPH] 1	14.58	8	0.89	0.69	0.66	1.17	0.84	0.29	1.36	1.58	1.37	1.44	0.13	1.71	0.03025
P35123	Ubiquitin carboxyl-terminal hydrolase 4	33.88	39	1.01	0.83	0.79	0.77	0.80	0.03	1.46	1.13	1.43	1.34	0.18	1.68	0.00741
P80314	T-complex protein 1 subunit beta	74.02	43	1.36	1.25	1.33	1.17	1.25	0.08	2.17	1.80	2.29	2.09	0.25	1.67	0.00549
P63147	Ubiquitin-conjugating enzyme E2 B	67.47	30	1.41	1.09	1.29	0.93	1.10	0.18	2.15	1.51	1.80	1.82	0.32	1.65	0.02744
Q8R1T1	Charged multivesicular body protein 7	8.79	2	0.90	0.77	0.93	0.76	0.82	0.10	1.69	1.15	1.20	1.35	0.30	1.65	0.04322
Q9WV55	Vesicle-associated membrane protein-associated protein A	32.30	20	1.12	0.76	0.94	0.82	0.84	0.09	1.46	1.53	1.15	1.38	0.20	1.65	0.01346
Q80UG5	Septin-9	5.30	2	0.49	0.92	0.51	0.98	0.80	0.26	1.15	1.33	1.47	1.32	0.16	1.64	0.04294
O55071	Cytochrome P450 2B19	25.85	7	1.08	0.97	1.03	0.57	0.86	0.25	1.31	1.63	1.27	1.40	0.20	1.64	0.04144
P24549	Retinal dehydrogenase 1	25.45	7	1.21	0.76	1.00	0.76	0.84	0.14	1.50	1.28	1.31	1.36	0.12	1.62	0.00779
P42125	Enoyl-CoA delta isomerase 1, mitochondrial	25.56	10	1.27	1.24	1.34	0.63	1.07	0.38	1.72	1.64	1.79	1.72	0.07	1.61	0.04531
Q9CR59	Growth arrest and DNA damage-inducible proteins-interacting protein 1	56.41	94	1.04	0.63	0.86	0.53	0.67	0.17	1.04	0.97	1.22	1.08	0.13	1.60	0.02926
Q9WVL3	Solute carrier family 12 member 7	6.97	2	1.08	1.28	0.98	0.82	1.03	0.23	1.75	1.79	1.39	1.64	0.22	1.60	0.02888
Q8C196	Carbamoyl-phosphate synthase [ammonia], mitochondrial	29.10	7	1.09	0.89	0.80	1.14	0.94	0.17	1.57	1.61	1.33	1.51	0.15	1.60	0.01367
Q8C142	Low density lipoprotein receptor adapter protein 1	24.57	17	0.65	0.59	0.44	0.59	0.54	0.08	0.86	0.81	0.92	0.86	0.06	1.59	0.00556
Q9CY18	Sorting nexin-7	5.20	1	0.88	0.78	0.52	0.58	0.63	0.14	1.06	1.06	0.86	0.99	0.11	1.59	0.02317
Q6DFW4	Nucleolar protein 58	2.66	3	1.08	0.67	0.95	0.76	0.79	0.14	1.18	1.32	1.22	1.24	0.07	1.57	0.00798
Q8BX90	Fibronectin type-III domain-containing protein 3A	13.11	4	0.96	0.84	0.53	0.58	0.65	0.17	1.17	0.93	0.95	1.02	0.13	1.57	0.03981
Q9ESY9	Gamma-interferon-inducible lysosomal thiol reductase	3.54	1	1.21	1.12	1.07	1.25	1.14	0.09	1.85	1.94	1.56	1.78	0.20	1.56	0.00757
P97478	5-demethoxyubiquinone hydroxylase, mitochondrial	79.38	91	2.91	2.11	3.02	2.78	2.64	0.47	4.66	3.34	4.29	4.09	0.68	1.55	0.03771
P97371	Proteasome activator complex subunit 1	24.11	98	0.92	0.82	0.57	0.48	0.62	0.17	0.99	0.88	1.00	0.96	0.07	1.54	0.03636
P97872	Dimethylaniline monooxygenase [N-oxide-forming] 5	46.52	62	1.06	1.26	1.14	0.70	1.03	0.30	1.75	1.50	1.47	1.58	0.16	1.53	0.04759
O70475	UDP-glucose 6-dehydrogenase	41.97	15	0.91	0.92	0.90	0.65	0.82	0.15	1.21	1.08	1.45	1.25	0.19	1.52	0.03752
O54774	AP-3 complex subunit delta-1	36.28	21	1.36	1.24	1.43	1.53	1.40	0.15	2.33	1.96	2.05	2.11	0.20	1.51	0.00721
Q3TYX3	SET and MYND domain-containing protein 5	72.56	29	1.04	1.28	1.28	1.01	1.19	0.16	2.01	1.60	1.75	1.79	0.21	1.50	0.01680
P61164	Alpha-centractin	10.66	4	1.16	0.86	0.58	0.82	0.75	0.16	1.27	1.00	1.13	1.13	0.14	1.50	0.03376
Q99KI0	Aconitate hydratase, mitochondrial	15.29	3	0.90	0.70	0.79	0.55	0.68	0.12	1.02	1.04	1.01	1.02	0.01	1.50	0.00892
Q91X78	Erlin-1	6.16	4	1.53	1.82	1.42	1.72	1.65	0.21	2.27	2.21	2.96	2.48	0.42	1.50	0.03789

P38647	Stress-70 protein, mitochondrial	4.43	1	1.77	1.77	1.47	1.56	1.60	0.15	2.56	2.56	1.96	2.36	0.35	1.47	0.02555
Q61823	Programmed cell death protein 4	14.63	4	1.05	0.55	0.70	0.55	0.60	0.09	0.93	0.75	0.97	0.88	0.12	1.47	0.02919
P50427	Steryl-sulfatase	11.18	1	0.50	0.45	0.57	0.39	0.47	0.09	0.65	0.73	0.69	0.69	0.04	1.47	0.01835
Q9CQE3	28S ribosomal protein S17, mitochondrial	7.00	1	0.64	0.52	0.64	0.50	0.55	0.08	0.67	0.93	0.81	0.80	0.13	1.45	0.04458
Q9DCA2	28S ribosomal protein S11, mitochondrial	12.62	2	0.99	0.54	0.59	0.61	0.58	0.04	0.84	0.86	0.80	0.83	0.03	1.44	0.00071
Q924T2	28S ribosomal protein S2, mitochondrial	31.68	23	0.87	1.01	0.90	0.68	0.86	0.17	1.08	1.34	1.21	1.21	0.13	1.41	0.04743
Q8BZS9	Putative pre-mRNA-splicing factor ATP-dependent RNA helicase DHX32	16.62	5	1.50	0.95	1.17	0.99	1.04	0.12	1.50	1.37	1.43	1.43	0.07	1.38	0.00703
Q9CY02	Alpha-hemoglobin-stabilizing protein	21.10	4	0.77	0.67	0.65	0.65	0.65	0.01	1.06	0.79	0.85	0.90	0.14	1.37	0.04172
P46664	Adenylosuccinate synthetase isozyme 2	7.59	2	1.33	1.21	1.10	0.98	1.10	0.12	1.61	1.25	1.64	1.50	0.22	1.37	0.04833
Q9QYR9	Acyl-coenzyme A thioesterase 2, mitochondrial	1.37	1	0.89	0.88	0.88	0.98	0.91	0.06	1.14	1.39	1.21	1.25	0.13	1.37	0.01578
Q921F4	Heterogeneous nuclear ribonucleoprotein L-like	42.96	3	1.08	0.68	0.75	0.73	0.72	0.04	0.98	0.99	0.96	0.98	0.01	1.36	0.00036
Q8K2M0	39S ribosomal protein L38, mitochondrial	43.22	5	1.37	1.26	1.42	1.43	1.37	0.10	1.85	1.66	1.98	1.83	0.16	1.34	0.01301
Q9QYY8	Spastin	26.76	15	1.37	1.08	0.90	1.18	1.05	0.14	1.32	1.46	1.43	1.40	0.07	1.34	0.01980
Q9CW42	Mitochondrial amidoxime-reducing component 1	14.85	14	2.23	1.39	1.58	1.21	1.40	0.19	2.00	1.77	1.75	1.84	0.13	1.32	0.02887
Q9WVA4	Transgelin-2	54.48	10	0.93	0.86	0.74	0.70	0.77	0.09	1.03	0.98	1.01	1.01	0.02	1.31	0.00955
A6H8H2	DENN domain-containing protein 4C	28.13	6	0.84	1.07	1.16	0.86	1.03	0.16	1.32	1.45	1.24	1.33	0.11	1.30	0.04777
Q9QXS1	Plectin	5.24	1	1.01	1.12	1.04	1.03	1.06	0.05	1.54	1.22	1.36	1.37	0.16	1.30	0.03128
Q9R0M4	Podocalyxin	3.09	3	0.73	1.01	0.79	0.92	0.91	0.11	1.11	1.24	1.15	1.16	0.07	1.28	0.02497
Q61151	Serine/threonine-protein phosphatase 2A 56 kDa regulatory subunit epsilon isoform	1.99	2	0.64	0.77	0.67	0.81	0.75	0.07	0.94	1.06	0.88	0.96	0.09	1.27	0.03581
Q5SWD9	Pre-rRNA-processing protein TSR1 homolog	62.41	40	1.63	1.58	1.69	1.41	1.56	0.14	1.96	1.77	2.19	1.97	0.21	1.26	0.04830
Q99LC3	NADH dehydrogenase [ubiquinone] 1 alpha subcomplex subunit 10, mitochondrial	1.34	4	0.92	0.84	0.82	0.95	0.87	0.07	0.97	1.21	1.11	1.10	0.12	1.26	0.04578
P09411	Phosphoglycerate kinase 1	17.87	3	1.18	0.88	0.86	0.93	0.89	0.03	1.05	1.26	1.06	1.12	0.12	1.26	0.03258
Q62351	Transferrin receptor protein 1	16.98	8	1.47	1.28	1.32	1.28	1.29	0.02	1.61	1.50	1.74	1.62	0.12	1.25	0.00982
O88811	Signal transducing adapter molecule 2	38.14	11	0.81	0.78	0.78	0.80	0.79	0.01	0.97	0.99	0.98	0.98	0.01	1.25	0.00003
Q8K4H1	Kynurenine formamidase	7.59	4	0.70	0.82	0.64	0.84	0.77	0.11	0.94	1.00	0.92	0.95	0.04	1.24	0.04899
Q4VA53	Sister chromatid cohesion protein PDS5 homolog B	17.57	10	1.03	0.93	0.93	0.86	0.90	0.04	1.15	1.12	1.10	1.12	0.03	1.24	0.00170
Q99M87	DnaJ homolog subfamily A member 3, mitochondrial	57.94	29	1.54	1.14	1.25	1.26	1.21	0.07	1.58	1.53	1.38	1.50	0.11	1.23	0.01721
Q8K114	Integrator complex subunit 9	50.00	5	1.01	1.06	1.05	1.00	1.03	0.03	1.25	1.34	1.24	1.28	0.06	1.23	0.00322
P31001	Desmin	2.43	1	0.99	0.87	0.99	1.11	0.99	0.12	1.19	1.16	1.28	1.21	0.06	1.22	0.04602
O08600	Endonuclease G, mitochondrial	11.76	4	0.94	0.95	1.07	0.96	0.99	0.07	1.19	1.22	1.21	1.21	0.02	1.22	0.00497
Q9JKX6	ADP-sugar pyrophosphatase	3.85	2	1.04	0.76	0.96	0.86	0.86	0.10	1.07	1.04	1.04	1.05	0.02	1.22	0.03664

Q8R2K1	Fucose mutarotase	6.22	2	1.00	0.82	0.92	0.79	0.84	0.07	1.10	0.94	1.03	1.02	0.08	1.21	0.04380
Q923D5	WW domain-binding protein 11	12.41	3	0.99	0.91	0.98	0.91	0.94	0.04	1.10	1.14	1.15	1.13	0.03	1.21	0.00239
P28653	Biglycan	66.07	157	1.02	0.99	1.04	0.93	0.99	0.05	1.26	1.13	1.15	1.18	0.07	1.20	0.02030
Q8R104	NAD-dependent protein deacetylase sirtuin-3	22.29	9	0.95	1.01	0.97	0.85	0.94	0.08	1.18	1.14	1.06	1.12	0.06	1.19	0.04067
P97470	Serine/threonine-protein phosphatase 4 catalytic subunit	2.21	4	0.89	0.86	0.89	0.82	0.86	0.04	0.92	1.05	1.09	1.02	0.09	1.19	0.04004
Q9R0N0	Galactokinase	3.74	2	0.81	0.97	1.01	0.85	0.94	0.08	1.14	1.12	1.07	1.11	0.04	1.17	0.03730
Q8K1J6	CCA tRNA nucleotidyltransferase 1, mitochondrial	4.78	4	1.32	1.33	1.27	1.21	1.27	0.06	1.45	1.45	1.57	1.49	0.07	1.17	0.01586
Q8BWY7	Zinc transporter ZIP11	10.69	4	0.97	1.01	1.02	1.00	1.01	0.01	1.08	1.24	1.20	1.17	0.08	1.16	0.02928
Q9D1H9	Microfibril-associated glycoprotein 4	13.28	3	1.11	0.88	0.80	0.83	0.84	0.04	0.95	1.05	0.91	0.97	0.07	1.16	0.04303
Q8K1Z0	Ubiquinone biosynthesis protein COQ9, mitochondrial	1.72	1	2.07	1.34	1.25	1.41	1.33	0.08	1.47	1.64	1.51	1.54	0.09	1.16	0.03820
Q6VNB8	WD repeat and FYVE domain-containing protein 3	3.86	1	0.91	1.08	1.15	1.12	1.11	0.04	1.25	1.29	1.32	1.29	0.04	1.16	0.00418
Q8K2T8	RNA polymerase II-associated factor 1 homolog	24.09	10	1.22	1.12	1.08	0.96	1.05	0.08	1.19	1.20	1.24	1.21	0.02	1.15	0.02996
P17879	Heat shock 70 kDa protein 1B	33.33	7	0.87	0.75	0.76	0.74	0.75	0.01	0.85	0.87	0.82	0.85	0.02	1.13	0.00270
Q8BIW1	Protein prune homolog	22.17	3	1.08	1.05	1.00	1.03	1.03	0.02	1.13	1.14	1.13	1.13	0.01	1.10	0.00171
Q8VCB3	Glycogen [starch] synthase, liver	4.25	4	0.86	0.87	0.86	0.91	0.88	0.03	0.97	0.93	0.97	0.96	0.03	1.09	0.02243
P07901	Heat shock protein HSP 90-alpha	82.42	173	1.00	0.99	0.98	0.98	0.98	0.01	1.05	1.09	1.05	1.06	0.02	1.08	0.00495
Q8BJZ4	28S ribosomal protein S35, mitochondrial	33.33	3	1.13	1.02	0.97	0.95	0.98	0.04	1.06	1.06	1.03	1.05	0.02	1.07	0.04279
Q9R0P3	S-formylglutathione hydrolase	11.32	3	1.06	0.93	0.94	0.92	0.93	0.01	0.97	1.02	0.96	0.99	0.03	1.06	0.03376
Q9DC16	Endoplasmic reticulum-Golgi intermediate compartment protein 1	28.37	12	1.07	1.01	1.01	0.97	1.00	0.02	1.06	1.05	1.07	1.06	0.01	1.06	0.01117
Q8VEH5	EPM2A-interacting protein 1	80.53	785	1.01	1.01	0.99	0.99	1.00	0.01	1.07	1.04	1.03	1.04	0.02	1.05	0.02305

Table 4.3 – The 137 proteins significantly upregulated in the livers of BALB/c mice following chronic dosing with brusatol in comparison to the vehicle-treated controls. All values are expressed relative to the common pooled sample included in duplicate on the iTRAQ run. An unpaired t-test was utilised to compare between treatment groups. Proteins are listed according to their expression in brusatol-treated mice relative to control animals in descending order of the fold-change value. (Acc. = accession, Avg. = average, C = control, Bru = brusatol).

					Relative expression to pool											
SwissProt. Acc. No.	Name	Avg. percentage coverage (%)	Avg. number of Peptides	Mean Pool	Mouse C1	Mouse C2	Mouse C3	Mean Control	Control SD	Mouse Bru1	Mouse Bru2	Mouse Bru3	Mean Brusatol	Brusatol SD	Fold-change Bru/C	p value
P08226	Apolipoprotein E	43.09	29	1.18	2.03	1.80	0.82	1.55	0.64	0.69	0.34	0.08	0.37	0.31	0.24	0.04496
P58044	Isopentenyl-diphosphate Delta-isomerase 1	31.28	7	1.24	1.53	1.51	2.70	1.92	0.68	0.67	0.61	0.21	0.50	0.25	0.26	0.02788
Q8JZK9	Hydroxymethylglutaryl-CoA synthase, cytoplasmic	29.23	13	1.47	2.56	1.79	3.77	2.70	1.00	0.78	0.49	0.90	0.73	0.21	0.27	0.02833
Q9JKX3	Transferrin receptor protein 2	9.15	6	2.15	2.42	2.36	1.53	2.10	0.50	0.42	0.74	0.70	0.62	0.17	0.30	0.00835
P40936	Indolethylamine N-methyltransferase	42.80	26	1.16	2.51	2.75	1.33	2.20	0.76	0.44	0.60	0.95	0.67	0.26	0.30	0.03009
P22599	Alpha-1-antitrypsin 1-2	52.06	77	1.34	1.74	1.92	2.75	2.14	0.54	0.27	0.67	1.07	0.67	0.40	0.31	0.01933
P29788	Vitronectin	12.34	4	0.89	1.58	0.82	1.66	1.36	0.46	0.23	0.62	0.42	0.42	0.20	0.31	0.03226
Q9DBE0	Cysteine sulfinic acid decarboxylase	33.27	25	1.08	1.54	2.51	1.43	1.83	0.59	0.89	0.52	0.40	0.60	0.25	0.33	0.03032
P11725	Ornithine carbamoyltransferase, mitochondrial	70.62	70	1.16	1.66	1.50	0.91	1.36	0.39	0.45	0.41	0.49	0.45	0.04	0.33	0.01659
E9Q414	Apolipoprotein B-100	5.62	19	0.86	0.98	1.05	0.95	0.99	0.05	0.55	0.28	0.19	0.34	0.19	0.34	0.00419
P11881	Inositol 1,4,5-trisphosphate receptor type 1	2.55	9	0.92	0.95	0.66	0.71	0.78	0.16	0.33	0.33	0.16	0.28	0.10	0.35	0.00989
Q8QZT1	Acetyl-CoA acetyltransferase, mitochondrial	70.52	73	1.29	1.56	2.61	2.03	2.06	0.53	1.10	0.38	0.74	0.74	0.36	0.36	0.02265
Q8R086	Sulfite oxidase, mitochondrial	49.82	32	1.13	1.34	1.50	0.90	1.25	0.31	0.36	0.50	0.50	0.45	0.08	0.36	0.01321
P21614	Vitamin D-binding protein	43.49	19	0.91	1.47	1.72	1.84	1.68	0.19	0.97	0.35	0.56	0.63	0.32	0.38	0.00780
Q8R1J9	Torsin-2A	8.72	2	1.26	1.96	1.72	2.91	2.20	0.63	1.03	0.90	0.56	0.83	0.24	0.38	0.02446
G5E870	E3 ubiquitin-protein ligase TRIP12	2.47	4	1.61	2.17	1.75	1.98	1.97	0.21	1.22	0.77	0.26	0.75	0.48	0.38	0.01599
Q8CIM7	Cytochrome P450 2D26	45.20	47	1.34	1.36	1.43	1.34	1.38	0.05	0.71	0.60	0.38	0.56	0.17	0.41	0.00132
O54749	Cytochrome P450 2J5	41.92	48	1.28	1.31	1.51	1.34	1.39	0.11	0.73	0.56	0.44	0.58	0.15	0.41	0.00160
Q63836	Selenium-binding protein 2	87.71	207	1.24	1.45	1.39	0.98	1.27	0.25	0.69	0.46	0.45	0.53	0.13	0.42	0.01099
Q8VCU1	Carboxylesterase 3B	43.08	42	1.42	2.19	2.11	1.60	1.97	0.32	1.04	0.38	1.05	0.82	0.38	0.42	0.01632
Q06890	Clusterin	14.06	6	1.79	2.38	1.32	2.05	1.92	0.54	0.84	0.49	1.11	0.81	0.31	0.42	0.03762
Q8BWQ1	UDP-glucuronosyltransferase 2A3	35.02	29	1.14	1.39	1.50	0.77	1.22	0.39	0.46	0.41	0.69	0.52	0.15	0.42	0.04387
P48776	Tryptophan 2,3-dioxygenase	13.05	6	1.05	1.64	1.03	1.07	1.25	0.35	0.69	0.48	0.42	0.53	0.14	0.43	0.02943
Q921X9	Protein disulfide-isomerase A5	24.76	16	1.16	1.02	0.92	1.46	1.13	0.29	0.48	0.38	0.61	0.49	0.12	0.43	0.02315
Q8CF02	Protein FAM25C	43.82	2	1.38	1.13	1.77	1.13	1.34	0.37	0.68	0.45	0.64	0.59	0.12	0.44	0.02922
Q78XF5	Oligosaccharyltransferase complex subunit OSTC	8.05	2	1.89	1.29	1.91	2.33	1.84	0.52	1.06	0.42	0.97	0.82	0.34	0.44	0.04668
O55242	Sigma non-opioid intracellular receptor 1	8.52	3	1.08	1.49	1.08	0.80	1.12	0.34	0.45	0.64	0.42	0.50	0.12	0.45	0.04205
P11352	Glutathione peroxidase 1	83.08	73	1.16	1.26	1.46	0.91	1.21	0.28	0.61	0.63	0.42	0.55	0.11	0.46	0.01915
P50247	Adenosylhomocysteinase	70.83	109	2.38	2.68	2.25	1.94	2.29	0.37	0.76	0.86	1.64	1.09	0.48	0.48	0.02699
Q8BZW8	NHL repeat-containing protein 2	5.52	3	1.27	1.71	1.60	2.07	1.79	0.25	0.56	0.60	1.41	0.86	0.48	0.48	0.03918

Q3UNX5	Acyl-coenzyme A synthetase ACSM3, mitochondrial	22.59	11	0.81	0.85	1.37	1.37	1.19	0.30	0.64	0.45	0.69	0.59	0.13	0.50	0.03307
P60229	Eukaryotic translation initiation factor 3 subunit E	19.55	9	1.39	1.60	1.84	2.70	2.05	0.58	1.14	1.06	0.87	1.02	0.14	0.50	0.04106
Q9QXD6	Fructose-1,6-bisphosphatase 1	72.49	118	1.60	1.67	2.38	2.99	2.35	0.66	1.31	0.96	1.28	1.18	0.19	0.50	0.04250
P42225	Signal transducer and activator of transcription 1	9.88	8	0.92	1.34	1.03	1.00	1.12	0.19	0.81	0.44	0.45	0.57	0.21	0.51	0.02716
Q8VCH6	Delta(24)-sterol reductase	6.01	4	1.18	1.53	1.79	2.09	1.80	0.28	1.45	0.76	0.54	0.92	0.47	0.51	0.04903
P01029	Complement C4-B	26.24	36	1.01	1.19	1.06	1.31	1.18	0.12	0.61	0.77	0.44	0.61	0.17	0.51	0.00871
Q64464	Cytochrome P450 3A13	14.12	9	0.99	0.50	0.58	0.82	0.63	0.17	0.24	0.41	0.32	0.32	0.08	0.51	0.04639
P55050	Fatty acid-binding protein, intestinal	45.45	10	1.11	1.47	1.82	1.37	1.55	0.24	0.78	0.76	0.88	0.81	0.06	0.52	0.00617
Q9D051	Pyruvate dehydrogenase E1 component subunit beta, mitochondrial	36.21	19	2.40	2.25	2.05	2.33	2.21	0.14	0.87	1.31	1.27	1.15	0.24	0.52	0.00284
Q00896	Alpha-1-antitrypsin 1-3	55.83	79	1.01	1.66	1.22	1.66	1.51	0.25	0.79	0.63	1.00	0.81	0.19	0.53	0.01706
P97290	Plasma protease C1 inhibitor	13.89	5	0.77	1.02	0.89	1.18	1.03	0.15	0.70	0.55	0.39	0.55	0.15	0.53	0.01730
Q9DBT9	Dimethylglycine dehydrogenase, mitochondrial	63.18	98	1.64	1.58	1.66	1.43	1.56	0.12	0.80	0.63	1.07	0.83	0.22	0.53	0.00733
Q8BWP5	Alpha-tocopherol transfer protein	54.32	21	0.95	0.95	1.21	1.26	1.14	0.17	0.77	0.72	0.41	0.63	0.20	0.55	0.02684
Q9JIF0	Protein arginine N-methyltransferase 1	5.39	2	1.18	0.82	0.86	0.92	0.87	0.05	0.47	0.29	0.70	0.49	0.21	0.56	0.03763
Q9Z1G3	V-type proton ATPase subunit C 1	11.26	3	1.39	0.97	1.01	1.27	1.08	0.16	0.60	0.47	0.76	0.61	0.14	0.56	0.01931
Q7TNE1	Succinate--hydroxymethylglutarate CoA-transferase	18.35	7	1.12	1.07	1.03	0.85	0.98	0.12	0.29	0.69	0.68	0.55	0.22	0.56	0.04292
Q01339	Beta-2-glycoprotein 1	20.58	6	1.77	2.40	1.71	2.38	2.16	0.39	1.26	0.98	1.42	1.22	0.22	0.56	0.02261
Q9QZ73	DCN1-like protein 1	6.56	2	0.84	0.60	0.63	0.45	0.56	0.10	0.35	0.39	0.22	0.32	0.09	0.57	0.03396
Q6PAM1	Alpha-taxilin	5.78	2	0.71	0.79	0.64	0.59	0.67	0.10	0.53	0.27	0.36	0.39	0.13	0.58	0.04322
Q91VA0	Acyl-coenzyme A synthetase ACSM1, mitochondrial	52.01	39	1.92	1.53	2.07	1.41	1.67	0.35	0.98	0.72	1.19	0.96	0.24	0.58	0.04570
Q8JZQ2	AFG3-like protein 2	3.62	4	1.98	2.03	1.77	1.54	1.78	0.25	0.82	1.05	1.26	1.04	0.22	0.58	0.01783
Q9DBG1	Sterol 26-hydroxylase, mitochondrial	47.84	39	1.29	1.41	1.77	1.12	1.43	0.33	1.00	0.71	0.80	0.84	0.15	0.59	0.04584
Q99MN9	Propionyl-CoA carboxylase beta chain, mitochondrial	56.38	36	1.47	1.24	1.18	0.86	1.09	0.20	0.75	0.65	0.54	0.65	0.11	0.59	0.02768
Q01853	Transitional endoplasmic reticulum ATPase	68.49	110	1.42	1.41	1.77	1.98	1.72	0.29	1.15	0.87	1.05	1.02	0.14	0.60	0.01995
P27612	Phospholipase A-2-activating protein	11.34	7	0.98	1.11	1.46	1.11	1.22	0.20	0.97	0.63	0.59	0.73	0.21	0.60	0.04321
P70302	Stromal interaction molecule 1	7.88	4	1.07	1.16	1.26	1.14	1.19	0.06	0.76	0.53	0.83	0.71	0.16	0.60	0.00826
P52633	Signal transducer and transcription activator 6	2.87	3	1.29	1.51	1.36	1.71	1.52	0.18	0.90	1.10	0.74	0.91	0.18	0.60	0.01345
Q8K182	Complement component C8 alpha chain	12.10	7	0.64	1.00	1.53	1.49	1.34	0.29	0.93	0.78	0.72	0.81	0.11	0.60	0.04283
Q9R112	Sulfide:quinone oxidoreductase, mitochondrial	49.56	23	1.18	1.12	1.46	1.11	1.23	0.20	0.95	0.72	0.58	0.75	0.19	0.61	0.04095
Q8VC97	Beta-ureidopropionase	29.52	10	1.31	1.41	1.34	1.39	1.38	0.03	0.71	0.86	0.97	0.85	0.13	0.61	0.00245

Q9D0R2	Threonine--tRNA ligase, cytoplasmic	41.55	33	1.17	1.09	1.03	1.08	1.06	0.03	0.83	0.74	0.41	0.66	0.22	0.62	0.03474
Q8CCJ3	E3 UFM1-protein ligase 1	18.92	12	0.67	0.81	0.90	1.00	0.90	0.10	0.67	0.65	0.38	0.56	0.16	0.62	0.03530
P55302	Alpha-2-macroglobulin receptor-associated protein	11.39	7	1.00	1.03	0.85	1.17	1.01	0.16	0.63	0.53	0.74	0.63	0.11	0.62	0.02715
P70362	Ubiquitin fusion degradation protein 1 homolog	15.64	5	1.00	1.05	1.36	1.26	1.22	0.16	0.90	0.66	0.74	0.76	0.12	0.63	0.01626
Q9QXT0	Protein canopy homolog 2	37.36	7	1.10	0.98	0.89	1.12	1.00	0.12	0.57	0.63	0.68	0.62	0.05	0.63	0.00736
P58021	Transmembrane 9 superfamily member 2	11.33	6	1.11	1.25	1.10	1.56	1.30	0.23	0.79	0.67	1.02	0.83	0.18	0.64	0.04930
P14576	Signal recognition particle 54 kDa protein	25.79	12	1.47	1.27	1.51	1.87	1.55	0.30	1.11	0.82	1.05	0.99	0.15	0.64	0.04533
Q91X34	Bile acid-CoA:amino acid N-acyltransferase	47.14	38	1.19	1.37	1.47	1.13	1.32	0.18	0.89	0.82	0.92	0.87	0.05	0.66	0.01373
Q9CQA5	Mediator of RNA polymerase II transcription subunit 4	4.81	1	0.77	1.75	1.53	1.45	1.58	0.16	0.81	1.34	1.01	1.05	0.27	0.67	0.04480
Q61183	Poly(A) polymerase alpha	3.25	2	1.02	1.04	1.00	1.09	1.04	0.04	0.74	0.63	0.73	0.70	0.06	0.67	0.00149
Q8C1B7	Septin-11	7.66	3	1.39	1.42	1.20	1.57	1.40	0.19	1.08	0.72	1.04	0.94	0.20	0.68	0.04382
Q91ZA3	Propionyl-CoA carboxylase alpha chain, mitochondrial	35.50	36	1.16	1.14	1.15	0.98	1.09	0.09	0.75	0.72	0.74	0.74	0.01	0.68	0.00304
Q9Z2I8	Succinyl-CoA ligase [GDP-forming] subunit beta, mitochondrial	59.82	54	1.56	1.66	2.07	1.57	1.77	0.27	1.38	1.00	1.28	1.22	0.20	0.69	0.04641
O55029	Coatomer subunit beta'	27.96	24	1.22	1.15	1.26	1.49	1.30	0.17	0.88	0.86	0.98	0.91	0.07	0.70	0.02127
Q9D5T0	ATPase family AAA domain-containing protein 1	17.17	5	0.97	1.19	0.93	0.90	1.01	0.16	0.72	0.77	0.64	0.71	0.07	0.71	0.04449
P54823	Probable ATP-dependent RNA helicase DDX6	28.16	10	1.07	1.17	1.05	1.25	1.15	0.10	0.85	0.78	0.83	0.82	0.04	0.71	0.00559
Q9R1P0	Proteasome subunit alpha type-4	27.97	6	1.22	1.39	1.31	1.25	1.32	0.07	1.15	0.93	0.72	0.93	0.21	0.71	0.04203
Q9ER72	Cysteine--tRNA ligase, cytoplasmic	19.25	12	0.96	1.06	1.36	1.26	1.22	0.15	0.74	0.88	0.99	0.87	0.12	0.71	0.03576
P58281	Dynamin-like 120 kDa protein, mitochondrial	20.52	23	1.25	1.29	1.14	1.20	1.21	0.08	0.75	1.00	0.84	0.86	0.13	0.71	0.01541
P48024	Eukaryotic translation initiation factor 1	63.72	12	1.09	0.86	0.95	0.95	0.92	0.05	0.62	0.72	0.64	0.66	0.06	0.72	0.00396
Q9Z2W0	Aspartyl aminopeptidase	28.54	14	0.95	1.10	1.15	1.34	1.20	0.13	0.89	0.95	0.74	0.86	0.11	0.72	0.02532
Q6P5E4	UDP-glucose:glycoprotein glucosyltransferase 1	18.96	19	1.08	1.08	1.06	1.22	1.12	0.09	0.72	0.77	0.92	0.80	0.10	0.72	0.01717
Q8BGQ7	Alanine--tRNA ligase, cytoplasmic	45.45	44	1.49	1.42	1.69	1.67	1.59	0.15	1.13	0.98	1.33	1.15	0.18	0.72	0.02871
O55060	Thiopurine S-methyltransferase	67.08	21	1.77	1.43	1.82	1.79	1.68	0.21	1.18	1.17	1.28	1.21	0.06	0.72	0.02215
Q8BVE3	V-type proton ATPase subunit H	9.11	3	1.12	1.41	1.27	1.42	1.37	0.08	0.95	0.92	1.10	0.99	0.10	0.72	0.00651
Q9Z2U1	Proteasome subunit alpha type-5	52.28	24	1.51	1.60	1.67	1.69	1.65	0.05	1.20	1.29	1.12	1.20	0.09	0.73	0.00152
Q9D662	Protein transport protein Sec23B	20.08	16	2.23	2.17	2.38	2.83	2.46	0.34	1.82	1.75	1.80	1.79	0.03	0.73	0.02767
Q8R0F9	SEC14-like protein 4	42.18	28	1.17	1.75	1.72	1.50	1.66	0.14	1.31	1.29	1.03	1.21	0.16	0.73	0.02062
P70195	Proteasome subunit beta type-7	22.02	7	2.25	1.64	2.00	2.05	1.90	0.22	1.49	1.36	1.36	1.40	0.08	0.74	0.02080
O08807	Peroxiredoxin-4	38.32	13	1.11	1.45	1.31	1.46	1.40	0.08	0.87	1.07	1.17	1.04	0.15	0.74	0.02141
Q9EQ32	Phosphoinositide 3-kinase adapter protein 1	2.96	2	0.56	0.69	0.66	0.77	0.71	0.05	0.49	0.63	0.48	0.53	0.08	0.75	0.03637

P09055	Integrin beta-1	9.90	8	0.87	0.79	0.81	0.95	0.85	0.09	0.64	0.59	0.68	0.64	0.04	0.75	0.01995
Q9EPU4	Cleavage and polyadenylation specificity factor subunit 1	1.11	2	1.17	1.10	1.15	1.11	1.12	0.03	0.81	0.93	0.84	0.86	0.06	0.77	0.00279
Q9D8V0	Minor histocompatibility antigen H13	8.47	4	1.08	1.20	1.01	1.21	1.14	0.11	0.88	0.90	0.86	0.88	0.02	0.77	0.01721
Q80YQ8	Protein RMD5 homolog A	6.39	2	1.31	1.38	1.34	1.37	1.36	0.02	1.25	0.97	0.95	1.06	0.17	0.77	0.03353
Q6P2B1	Transportin-3	3.79	3	0.97	0.95	1.04	0.95	0.98	0.05	0.77	0.72	0.79	0.76	0.04	0.78	0.00413
Q99M96	Suppressor of tumorigenicity 7 protein	4.16	3	1.19	1.19	1.22	1.29	1.24	0.05	1.06	0.96	0.89	0.97	0.08	0.78	0.00976
P32921	Tryptophan--tRNA ligase, cytoplasmic	7.07	3	0.79	0.82	0.78	0.81	0.80	0.02	0.67	0.65	0.58	0.63	0.05	0.79	0.00468
Q8VHG0	Dimethylaniline monooxygenase [N-oxide-forming] 4	6.43	4	1.13	1.17	0.95	1.04	1.05	0.11	0.86	0.86	0.78	0.83	0.04	0.79	0.03348
Q9Z0J0	Epididymal secretory protein E1	6.04	1	1.33	1.46	1.27	1.43	1.39	0.10	1.16	1.04	1.10	1.10	0.06	0.79	0.01336
Q9D2R6	Cytochrome c oxidase assembly factor 3 homolog, mitochondrial	9.26	1	0.88	1.33	1.31	1.20	1.28	0.07	1.01	1.08	0.98	1.02	0.05	0.80	0.00601
Q4U4S6	Xin actin-binding repeat-containing protein 2	1.08	8	0.83	0.95	0.98	0.98	0.97	0.02	0.73	0.82	0.77	0.78	0.05	0.80	0.00273
Q9JM93	ADP-ribosylation factor-like protein 6-interacting protein 4	8.73	1	0.63	0.79	0.86	0.90	0.85	0.05	0.65	0.72	0.70	0.69	0.04	0.81	0.01208
O54833	Casein kinase II subunit alpha'	7.14	3	1.01	1.14	1.18	1.14	1.15	0.02	0.89	0.87	1.09	0.95	0.12	0.82	0.04502
Q8R121	Protein Z-dependent protease inhibitor	9.82	3	0.99	1.26	1.18	1.29	1.24	0.06	1.04	1.06	1.00	1.03	0.03	0.83	0.00477
B2RY56	RNA-binding protein 25	6.80	4	0.96	0.96	0.90	1.04	0.97	0.07	0.89	0.74	0.79	0.81	0.08	0.83	0.04985
P35922	Fragile X mental retardation protein 1 homolog	3.26	2	1.03	1.13	1.12	1.02	1.09	0.06	0.86	1.00	0.89	0.91	0.08	0.84	0.03618
Q8CC86	Nicotinate phosphoribosyltransferase	47.21	22	1.32	1.10	1.09	0.93	1.04	0.09	0.87	0.86	0.90	0.87	0.02	0.84	0.04213
Q9ES74	Serine/threonine-protein kinase Nek7	8.28	3	0.92	0.98	1.11	1.11	1.06	0.07	0.97	0.82	0.90	0.90	0.07	0.84	0.04866
O35744	Chitinase-like protein 3	3.77	1	0.48	0.59	0.53	0.61	0.58	0.04	0.49	0.49	0.49	0.49	0.00	0.84	0.02259
P63085	Mitogen-activated protein kinase 1	22.07	5	0.97	1.10	1.11	1.03	1.08	0.04	0.93	0.85	0.99	0.92	0.07	0.86	0.03294
P16301	Phosphatidylcholine-sterol acyltransferase	3.20	1	0.96	0.96	0.94	0.95	0.95	0.01	0.84	0.79	0.84	0.82	0.03	0.87	0.00264
Q8VCR2	17-beta-hydroxysteroid dehydrogenase 13	60.86	24	1.03	1.06	1.05	1.11	1.07	0.03	0.92	0.92	0.99	0.94	0.04	0.88	0.01334
P48760	Folylpolyglutamate synthase, mitochondrial	4.94	2	1.13	1.34	1.24	1.25	1.28	0.06	1.16	1.17	1.10	1.14	0.04	0.90	0.03054
Q8C7X2	ER membrane protein complex subunit 1	15.35	12	0.94	1.00	0.95	1.01	0.99	0.03	0.86	0.93	0.86	0.88	0.04	0.90	0.02822
P24547	Inosine-5'-monophosphate dehydrogenase 2	18.29	8	1.01	1.08	1.10	1.11	1.09	0.02	0.96	1.01	0.97	0.98	0.02	0.90	0.00251
Q60749	KH domain-containing, RNA-binding, signal transduction-associated protein 1	6.55	2	1.08	1.05	1.07	1.00	1.04	0.03	0.95	0.97	0.90	0.94	0.04	0.91	0.03412
Q9CY62	E3 ubiquitin-protein ligase RNF181	4.85	1	0.91	0.86	0.80	0.82	0.83	0.03	0.74	0.77	0.75	0.75	0.01	0.91	0.01184
O54984	ATPase Asna1	14.08	4	0.98	1.06	1.06	1.04	1.05	0.01	0.99	0.94	0.95	0.96	0.03	0.92	0.00623
Q61702	Inter-alpha-trypsin inhibitor heavy chain H1	9.70	5	0.91	1.08	1.03	1.06	1.05	0.02	0.91	0.98	1.00	0.96	0.05	0.92	0.04216
Q9QYC7	Vitamin K-dependent gamma-carboxylase	10.57	6	0.96	1.03	1.11	1.04	1.06	0.04	1.00	0.96	0.97	0.98	0.02	0.93	0.04400
P12367	cAMP-dependent protein kinase type II-alpha regulatory subunit	31.92	10	1.04	1.08	1.06	1.12	1.08	0.03	1.01	1.02	1.00	1.01	0.01	0.93	0.01598

Q9JIG7	Coiled-coil domain-containing protein 22	13.88	5	0.89	0.93	0.91	0.93	0.92	0.01	0.87	0.85	0.88	0.87	0.02	0.94	0.00656
P46735	Unconventional myosin-Ib	22.94	25	1.04	1.05	1.02	1.07	1.04	0.02	0.99	1.00	1.00	1.00	0.01	0.95	0.02980
Q6PD26	GPI transamidase component PIG-S	10.09	4	0.97	0.93	0.95	0.91	0.93	0.02	0.90	0.88	0.88	0.89	0.01	0.95	0.03116

Table 4.4 – The 125 proteins with significantly lower expression in the livers of BALB/c mice following chronic dosing with brusatol in comparison to the vehicle-treated controls. All values are expressed relative to a common pooled sample included in duplicate on the iTRAQ run. An unpaired t-test was utilised to compare between treatment groups. Proteins are listed according to their expression in brusatol-treated mice relative to control animals in ascending order of the fold-change value. (Acc. = accession, Avg. = average, C = control, Bru = brusatol).

4.3.4 Pathway analysis of iTRAQ data

Ingenuity core pathway analysis of proteins with significantly different expression in the livers of mice following administration of brusatol identified the *Nrf2-mediated Oxidative Stress Response* pathway in the top 40 most likely pathways to be associated with brusatol therapy (Table 4.5, p=0.002, Ingenuity Analysis). It is important to note that many of the pathways more significantly associated with brusatol therapy are linked to drug metabolism and detoxification (e.g. Xenobiotic Metabolism Signaling) or oxidative stress response (e.g. Production of Nitric Oxide and Reactive Oxygen Species in Macrophages pathway), and therefore may be involved in the metabolism of the compound itself, or modified by the Nrf2 pathway. Additionally, many of the pathways, including those linked to lipid metabolism, have been associated with the Nrf2 pathway in the published literature as discussed in the conclusion to this chapter. The 40 most significantly altered pathways are displayed in table 4.5.

Ingenuity Canonical Pathways	p value	Ratio	Molecules
FXR/RXR Activation	0.00000004	2/21	C4A/C4B, BAAT, APOE, APOB, APOH, LCAT, CYP27A1, VTN, FBP1, SERPINA1, GC, CLU
Xenobiotic Metabolism Signaling	0.00000044	1/18	CYP3A7, ALDH1B1, MAPK1, PPP2CA, GSTA5, FMO5, ESD, GSTT2/GSTT2B, FTL, ALDH1A1, PPP2R4, HSP90AA1, PPP2R5E, FMO4, MGST3, CYP2C8
LPS/IL-1 Mediated Inhibition of RXR Function	0.00000309	1/17	GSTT2/GSTT2B, ALDH1B1, APOE, CYP3A7, FABP2, ACSBG1, ALDH1A1, GSTA5, FMO5, FMO4, HMGCS1, MGST3, CYP2C8
Glycolysis I	0.00001072	1/5	PGK1, ALDOB, TPI1, PGAM1, FBP1
LXR/RXR Activation	0.00001660	7/94	C4A/C4B, APOE, APOB, APOH, LCAT, VTN, SERPINA1, GC, CLU
Superpathway of Methionine Degradation	0.00003236	14/87	PCCA, PCCB, SUOX, PRMT1, AHCY
Nicotine Degradation II	0.00011220	2/21	CYP3A7, UGT2A3, INMT, FMO5, FMO4, CYP2C8
PI3K/AKT Signaling	0.00013490	2/31	ITGB1, CDC37, MAPK1, PPP2CA, PPP2R4, HSP90AA1, PPP2R5E, GYS2
Sucrose Degradation V (Mammalian)	0.00013804	1/3	ALDOB, TPI1, TKFC
Gluconeogenesis I	0.00021380	4/25	PGK1, ALDOB, PGAM1, FBP1
Purine Nucleotides De Novo Biosynthesis II	0.00026915	3/11	ADSS, ADSSL1, IMPDH2
Superpathway of Cholesterol Biosynthesis	0.00033884	1/7	DHCR24, IDI1, ACAT1, HMGCS1
Mevalonate Pathway I	0.00045709	3/13	IDI1, ACAT1, HMGCS1

Production of Nitric Oxide and Reactive Oxygen Species in Macrophages	0.00058884	2/43	APOE, APOB, MAPK1, PPP2CA, PPP2R4, SERPINA1, PPP2R5E, STAT1, CLU
α-Adrenergic Signaling	0.00066069	2/29	MAPK1, PRKAR2A, PYGB, PYGL, ITPR1, GYS2
Clathrin-mediated Endocytosis Signaling	0.00067608	1/22	ITGB1, APOE, CSNK2A2, APOB, GAK, TFRC, SERPINA1, LDLRAP1, CLU
Cell Cycle Regulation by BTG Family Proteins	0.00081283	9/79	PPP2CA, PPP2R4, PPP2R5E, PRMT1
Methylmalonyl Pathway	0.00085114	1/2	PCCA, PCCB
Superpathway of Geranylgeranyldiphosphate Biosynthesis I (via Mevalonate)	0.00104713	3/17	IDI1, ACAT1, HMGCS1
PXR/RXR Activation	0.00112202	1/13	CYP3A7, ALDH1A1, CES3, PRKAR2A, CYP2C8
tRNA Charging	0.00123027	7/68	CARS, WARS, TARS, AARS
CDK5 Signaling	0.00128825	2/33	ITGB1, MAPK1, PPP2CA, PPP2R4, PRKAR2A, PPP2R5E
2-oxobutanoate Degradation I	0.00141254	2/5	PCCA, PCCB
Glutathione Redox Reactions I	0.00147911	3/19	GSTT2/GSTT2B, GPX1, MGST3
Aryl Hydrocarbon Receptor Signaling	0.00158489	1/20	GSTT2/GSTT2B, ALDH1B1, ALDH1A1, MAPK1, GSTA5, HSP90AA1, MGST3
Tryptophan Degradation III (Eukaryotic)	0.00199526	1/7	AFMID, TDO2, ACAT1
IL-12 Signaling and Production in Macrophages	0.00204174	1/21	STAT6, APOE, APOB, MAPK1, SERPINA1, STAT1, CLU
Urea Cycle	0.00208930	1/3	OTC, CPS1
NRF2-mediated Oxidative Stress Response	0.00245471	1/24	GSTT2/GSTT2B, FTL, MAPK1, GSTA5, VCP, DNAJA3, CBR1, MGST3
Tryptophan Degradation to 2-amino-3-carboxymuconate Semialdehyde	0.00389045	1/4	AFMID, TDO2
Protein Ubiquitination Pathway	0.00398107	3/85	PSMB7, PSME1, UBE2B, USP4, HSPE1, HSPA9, PSMA5, PSMA4, HSP90AA1
Acute Phase Response Signaling	0.00457088	1/24	C4A/C4B, SERPING1, FTL, RIPK1, APOH, MAPK1, SERPINA1
Glutathione-mediated Detoxification	0.00501187	7/68	GSTT2/GSTT2B, GSTA5, MGST3
Ketogenesis	0.00616595	1/5	ACAT1, HMGCS1
Melatonin Degradation I	0.00676083	2/31	CYP3A7, UGT2A3, Sult1a1, CYP2C8
Glycogen Degradation II	0.00741310	2/11	PYGB, PYGL
AMPK Signaling	0.00831764	1/27	MAPK1, PPP2CA, PPP2R4, PRKAA2, PRKAR2A, PPP2R5E, GYS2
Mitotic Roles of Polo-Like Kinase	0.00831764	2/33	PPP2CA, PPP2R4, HSP90AA1, PPP2R5E
Dopamine Degradation	0.00851138	3/35	ALDH1B1, ALDH1A1, Sult1a1
Synaptic Long Term Depression	0.00870964	3/73	LCAT, MAPK1, PPP2CA, PPP2R4, ITPR1, PPP2R5E

Table 4.5 – Pathway analysis for proteins both upregulated and downregulated in the in the livers of BALB/c mice following chronic dosing with brusatol. The ratio identifies the number of focus molecules identified (numerator) in the pathway (denominator).

4.3.5 TLDA analysis of Nrf2 related gene expression

In order to determine the effects of brusatol on the gene expression of Nrf2 and downstream effectors, cDNA reverse transcribed from RNA extracted from the livers (N=6) of brusatol-treated and saline control BALB/c mice was amplified by real-time PCR using the TLDA cards. A common pooled sample was run on each plate, with gene expression of all other samples expressed relative to the pool and normalised to expression of the 18s house-keeper gene.

Mean relative gene expression was calculated and compared between animals form the two treatment arms. Two genes (*Slc22a12* and *Txn1*) were excluded from the analysis due to incomplete data sets, with gene expression only available for less than three out of the six samples.

There was a generalised decrease in gene expression across the panel of Nrf2-regulated genes, as shown in figure 4.5. 35 of the 44 Nrf2-dependent genes analysed in the excised murine liver tissue demonstrated a numerical decrease in expression, although none of these achieved statistical significance, possibly due to the low number of replicates and the variability in gene expression noted in both the treatment and control groups. mRNA expression of Nrf2 was slightly increased in mice treated with brusatol, indicating that the inhibition of Nrf2 by brusatol occurs at the post-transcriptional level. The levels of Keap1 mRNA were unchanged by brusatol treatment. In relation to the metabolism of irinotecan, Ces1g and Ces2g gene expression was decreased in the livers of mice dosed with brusatol, which could affect conversion to SN-38 if this is reflected at the protein level. Ugt1a1 expression was very similar in treatment arms, suggesting the glucuronidation of SN-38 may not be affected by brusatol, and that co-administration with irinotecan may not alter the safety profile of the chemotherapeutic.

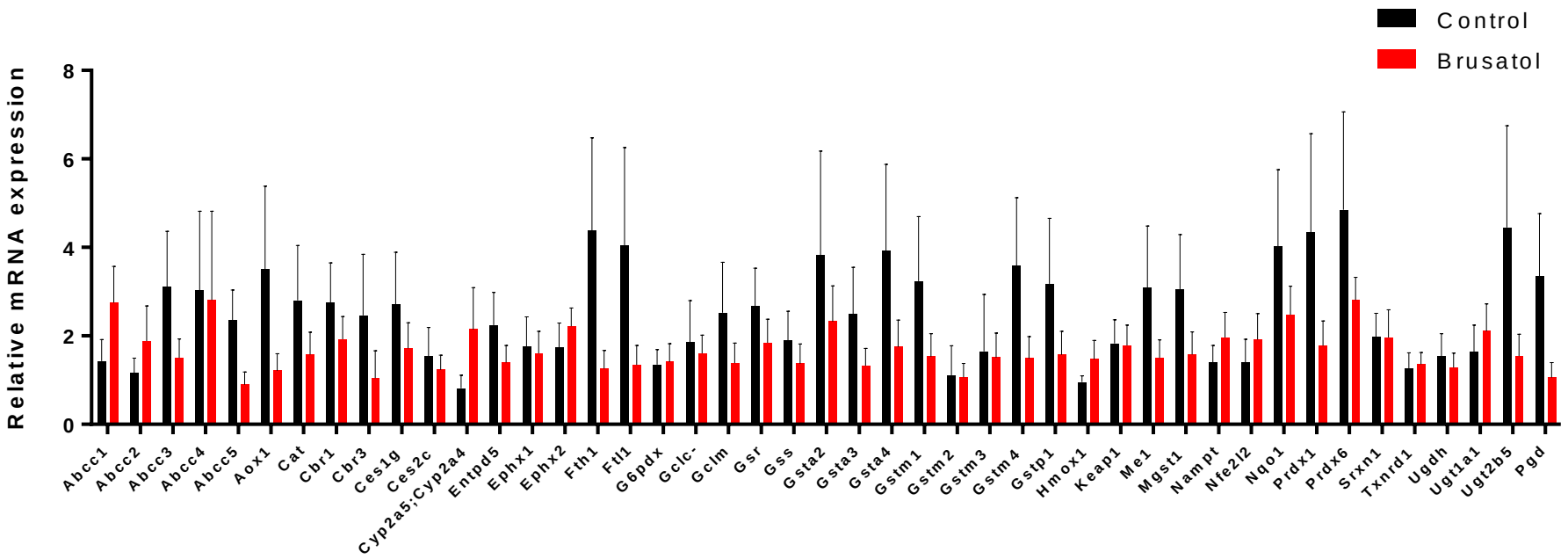

Figure 4.5 - Relative levels of mRNA expression in livers of control and brusatol-treated BALB/c mice as detected by Microfluidic TaqMan low density array analysis. Decreased mRNA expression was noted in 35 of the 45 Nrf2 related genes measured. (Bar chart displays mean +/- SEM)

4.4 Discussion

The inhibition of Nrf2 in murine liver and colon by brusatol, as demonstrated in this chapter, has not previously been documented by western immunoblotting in the published literature, with studies to date focusing on the effects of brusatol in tumour tissue and cell lines. Verifying the profound inhibition of Nrf2 by brusatol in murine liver allowed proteomic analysis, with confidence that the dose of brusatol utilised was effective. The inhibition of a number of Nf2-related downstream effector genes, although not reaching significance, also allowed reassurance that the pathway was being inhibited by brusatol. Interestingly, Nrf2 was not inhibited at the mRNA level by brusatol, reinforcing the belief that brusatol inhibits Nrf2 at the post-transcriptional level [294, 436].

The Ingenuity core pathway analysis of iTRAQ data identified a number of pathways associated with lipid and drug metabolism and cellular stress response. The *Farnesoid X receptor (FXR) / retinoid X receptor (RXR)* pathway, identified as most likely to be associated with brusatol therapy, is linked to the control of lipid, fatty acid and bile acid metabolism. Chen *et al.* recently demonstrated that induction of Nrf2 by oleanolic acid in mice acted as a direct antagonist to FXR, reducing bile acid production, highlighting a possible association between the Nrf2 and FXR pathways [448]. Further evidence of a link between Nrf2 and lipid metabolism has been demonstrated in the proteomic data from two animal studies. These noted that many of the differentially regulated proteins in either Nrf2 knockout mice, compared with their wild type counterparts, or following Nrf2 induction in wild type mice were associated with lipid metabolism [278, 279]. It is therefore feasible that the FXR / RXR pathway acts as the link between the Nrf2 pathway and the control of lipid metabolism. The link between lipid metabolism and brusatol therapy continues throughout the pathway analysis, both the *Superpathway of Cholesterol Biosynthesis* [449] and the *AMPK Signaling* pathways [450] are associated with lipid metabolism. Interestingly, the RXR nuclear receptor featured in the *FXR / RXR* pathway also acts as a key link in four of the forty pathways included in this analysis, and is reportedly required for the activation of many phase II metabolising enzymes [451].

Drug metabolising and detoxification protein families feature repeatedly in the pathway analysis of the iTRAQ data. The phase-I drug metabolising cytochrome P450s CYP27A1, CYP3A7 and CYP2C8 are included in seven of the top forty pathways associated with brusatol therapy, while the glutathione S-transferases (GSTs), a major group of detoxifying

enzymes, GSTT2 and GSTA5 are involved in six of the top forty pathways. The *Glutathione Redox Reactions I* and *Glutathione-mediated Detoxification* pathways both feature in the pathway analysis. Previously published proteomic data from murine liver tissue demonstrated that the proteins found to be down-regulated in Nrf2 knockout mice were predominantly phase-II drug metabolising enzymes, or those involved in the glutathione system [279]. More recently Lin *et al.* demonstrated that Nrf2 was required for the upregulation of GSTs in rat primary hepatocytes [452], again highlighting a link between Nrf2 and many of the pathways associated with brusatol administration.

The mitogen-activated protein kinase (MAPK) family are involved in directing cellular responses to an array of stimuli, including mitogens, oxidative stress, osmotic stress, heat shock and proinflammatory cytokines, through the regulation of cell adhesion, cell cycle progression, cell migration, cell survival, differentiation, metabolism, proliferation and transcription [453]. MAPK1, also known as Extracellular signal Regulated Kinase 2 (ERK2), appears in eleven of the forty brusatol associated pathways. Studies have linked the control of Nrf2 to the ERK and PI3K (also significantly altered in the pathway analysis) signaling cascades [454]; in human glioblastoma cells inhibition of ERK and PI3K suppressed the nuclear accumulation of Nrf2 and decreased cellular expression of the protein [455]. These findings were replicated by Choi *et al.*, who demonstrated that ERK2 inhibitors prevented phosphorylation of Nrf2, reducing its protective effect in HepG2 cells and in the murine liver *in vivo* [456].

There are some limitations to the data presented in this chapter. Firstly, the brusatol dosing study in mice was not designed to allow the assessment of this compound on the liver proteome, but rather as a study of the effects of brusatol on CRC burden. As a result, a dosing time-course study was not completed to assess when the maximum inhibition of Nrf2 and its downstream effector proteins was achieved after administration. However, the multiple dosing regimens the mice received over a period of two weeks should have allowed alteration of downstream proteins, despite the transient nature of Nrf2 inhibition by brusatol noted *in vitro*. Secondly, the mice included in the study had undergone the caecal implantation of tumour cells and had varying degrees of disease burden at the time of cull. This variation in disease burden, and therefore the health status of each mouse, could also be reflected at the genetic and proteomic level in murine liver tissue. This could perhaps explain the relatively large variations noted between individual mice in both the control and brusatol-treated groups, preventing the mRNA data from reaching statistical

significance. Thirdly, the proteomic data and pathway analysis may have picked up changes not related to the effects of brusatol but due to metabolism of the drug itself. It is therefore possible that a number of the significantly altered proteins and pathways are involved in the metabolism and excretion of brusatol, rather than the direct result of Nrf2 inhibition.

Although many of the pathways presented in the analysis of proteomic data may be linked to Nrf2 directly or indirectly, through cellular stress response signalling and drug metabolism molecules and pathways, the limitations discussed above and the small numbers of mice included in the study mean it is not possible to state definitively that brusatol is a specific Nrf2 inhibitor *in vivo*. However, the relatively subtle changes in protein expression noted in the murine liver following the repeated administration of brusatol, perhaps as a result of its transient effect on Nrf2, hint at its potential safety and help to explain why it is perceived to be so well tolerated in the animal studies presented in this thesis and the published literature[294].

Chapter 5 – Concluding discussion

5.1 Summary of aims and major findings

The neoadjuvant and adjuvant treatment of CRC with chemotherapy currently relies on standardised regimens based on data from clinical trials, without taking into account the tumour biology or metabolic profile of each individual patient; the only exception to this being the use of KRAS in predicting response to EGFR inhibitors. Response to standard therapy can vary substantially, with a number of patients experiencing potentially life-threatening complications and side effects yet deriving no clinical benefit due to tumour resistance. The identification of biomarkers, in the tumour or normal tissue, capable of predicting or modifying the response to therapy could revolutionise the use of chemotherapy in the management of CRC.

Irinotecan is a pro-drug converted to the activate metabolite SN-38, which acts as a topoisomerase I inhibitor, preventing cell division and replication. Its metabolism is complex, relying on the CESs, predominantly in the liver and tumour, for conversion to SN-38, UGT1A1 for glucuronidation to SN-38G and the ABC transporters for excretion into bile. Nrf2 is a transcription factor bound to the regulatory protein Keap1 in the quiescent state. Under conditions of cellular stress, Keap1 is no longer able to target Nrf2 for degradation and it accumulates in the nucleus, where it binds to the ARE in a range of genes, thus activating their expression. The expression of the CES [277, 278], UGT1A1 [280] and the ABC transporters [283] have all been demonstrated to be regulated either basally or in an inducible manner by Nrf2. Nrf2 is also responsible for the activation of cell survival pathways and proteins such as NQO1 and HO-1, which confer protection against ROS induced DNA damage and apoptosis. These effects of Nrf2 activation have been noted to be exploited by malignant tissue to confer a survival advantage and resistance to chemotherapy, as discussed in chapter 1.

Given the multiple roles of Nrf2, this transcription factor has the potential to act as a predictive or therapeutic biomarker, particularly in relation to irinotecan-based therapy, and the effects of Nrf2 modulation in this context are difficult to predict.

The overall aim of this thesis was to develop a murine model of CRC capable of testing the hypothesis that Nrf2 modulation could alter the efficacy of irinotecan chemotherapy. *In vivo* testing is essential when investigating the effects of potential modulators of irinotecan efficacy. A complete system is required due to the complex interaction between normal

tissue, such as the liver, and the tumour in the activation and excretion of the pro-drug. Although Nrf2 inhibition may be beneficial in tumour tissue, where it may reduce the activity of cell defence mechanisms, it may inhibit SN-38 production in the liver and subsequently drug efficacy.

Chapter 2 describes the development of a syngeneic orthotopic murine model of CRC, required for testing the effects of Nrf2 modulation on irinotecan efficacy *in vivo.* Luminescent populations of cells were developed by transfection with plasmids containing luciferase DNA. Clonal selection and expansion was carried out from a single luminescent cell and this clone implanted, initially in the flank of an immune-competent mouse, before caecal injection and assessment of disease burden by BLI.

This model had several distinct advantages, including: the rapid development of primary tumours, allowing high throughput assessment of potential therapies; the growth of tumours in the correct microenvironment, ensuring drug delivery was possible to the required site; the potential to develop liver metastases, accurately replicating the disease process in humans; and the use of BLI for the longitudinal assessment of disease burden, allowing continual monitoring of tumour progression in the same animal and reducing the number of animals required in experiments. Additionally, the use of immune-competent animals significantly reduced costs and would allow the testing of immune-therapies if required. Unfortunately, attempts to develop an immune-deficient model were unsuccessful, as was the implantation of more luminescent clones, reliant on a different vector for expression of luciferase, in the syngeneic model.

In chapter 3 the murine model was applied to the *in vivo* assessment of data generated in a human and murine CRC cell line. Significantly higher expression of Nrf2 was demonstrated by IHC in sections from primary tumours and liver metastases in comparison to normal colon taken from patients, suggesting a benefit to overexpression of Nrf2 in cancer. *In vitro* findings consistently demonstrated reduced CRC cellular proliferation and viability in response to Nrf2 inhibition using siRNA or the pharmacological inhibitor brusatol. The cytotoxicity of irinotecan was also enhanced, as evidenced by a decrease in IC50 values, following genetic or pharmacological inhibition of Nrf2. When irinotecan was combined with brusatol, drug synergy was achieved across a number of concentration combinations. Translation of these findings into the murine model again demonstrated a significant reduction in tumour growth, as assessed by BLI, following treatment with the Nrf2 inhibitor

brusatol. The degree of synergy noted when combining irinotecan and brusatol *in vitro* was perhaps not replicated *in vivo*, although a trend towards increased efficacy was noted with combination therapy. It is possible that statistical significance for the combination of brusatol with irinotecan may not have been reached due to the effectiveness of each treatment in isolation. However, the data generated in this chapter consistently demonstrate that brusatol acts as a potent anti-tumorigenic agent, capable of significantly inhibiting Nrf2 in malignant cells or tumour tissue both *in vitro* and *in vivo.*

In an attempt to explore the specificity of brusatol as an Nrf2 inhibitor, investigate its safety profile and improve understanding of its mechanism of action, the work described in chapter 4 utilised liver tissue excised from mice chronically exposed to the compound over two weeks to investigate protein and mRNA expression in comparison with mice receiving a vehicle control; this is the first study to investigate this. The ability of brusatol to inhibit Nrf2 in normal liver and colon was first demonstrated by western immunoblotting before iTRAQ proteomic analysis was conducted on the liver tissue. Although multiple pathways were significantly altered in the livers of mice administered brusatol, many of these could be linked to the Nrf2 pathway or were involved in drug metabolism. The data in this chapter does have to be regarded with a degree of caution given the relatively small number of animals included in the proteomic assessment and the varying degrees of tumour burden the mice had a cull. Although all macroscopic disease was excluded from the analysis, mice with advanced disease or bowel obstruction may have an altered protein profile due to their disease state.

Nrf2 mRNA expression did not decrease in liver tissue taken from mice following treatment with brusatol, a non-significant increase was noted, agreeing with findings in the published literature demonstrating that brusatol works at a post-transcriptional level [294, 436]. The slight increase in Nrf2 mRNA is likely to be in compensation to the decrease in the Nrf2 noted at the protein level.

5.2 Advances in the animal modelling of CRC

Many of the recent publications surrounding each topic covered in this thesis are included in the discussion sections of each chapter. However, some notable advances have been made in the murine modelling of CRC for the investigation of potential chemotherapeutic agents.

Significant advances have been made in small animal endoscopy with a recent publication describing the development of metastatic CRC in mice using a minimally invasive endoscopic technique to inject tumour cells into the colonic submucosa. Interestingly, this technique failed to induce tumours in CD-1 nude mice but had a high uptake rate in SCID mice (5 out of 6 mice), with many developing liver metastases [457]. This technique is less invasive than surgical orthotopic implantation and could have reduced the stress response in mice following laparotomy and surgical implantation. However, specialist equipment and expertise is required, further increasing costs and training time. Selective portal vein injection of CRC tumour cells has also been used to generate syngeneic murine models of CRC liver metastases. This technique relies on portal vein injection with selective clamping of liver lobes to induce liver metastases in the required liver segment. This method could have removed the need for primary tumour pre-growth, reduced the incidence of extra-hepatic metastases and prolonged the survival time in untreated mice due to complications from the primary tumour, while still allowing investigation of the effects of therapies on liver localised disease. However, the lack of a primary colonic tumour reduces the accuracy of the model in replicating the disease process in humans [412].

BLI imaging was recently validated in comparison to MRI for the imaging of CRC liver metastases in mice. A strong positive correlation between disease burden, as assessed by MRI, and luminescent signal was noted, supporting the use of BLI in pre-clinical studies. They did however note that BLI may overestimate tumour growth rates at earlier imaging points and smaller variations in tumour growth may not be detected, making it more difficult to reach significance between treatments arms, as noted in the data presented in this thesis. Significant variations in tumour doubling time were also noted between untreated animals, far greater than noted with traditional ectopic models, which is again in concordance with the data presented in this thesis [458].

5.3 The role of Nrf2 in CRC

Data continues to be published examining the role of Nrf2 in CRC. Po-Lin *et al.* recently demonstrated that in 160 patients with CRC, cytoplasmic overexpression of Nrf2 was associated with poor overall survival. Nrf2 knockdown, using a short-hairpin RNA, was subsequently found to decrease CRC cell invasion and growth, with the opposite being true for Nrf2 induction. The mechanism for the decreased invasive potential following Nrf2 inhibition was believed to be via activation of PSMD4, a proteasomal gene overexpressed on induction of Nrf2, which in turn activated β-catenin and promoted cellular invasion. These findings were verified *in vivo* in a model of CRC lung metastases, with no tumours developing in mice injected with the Nrf2 knockout cell line [459]. This highlighted the potential for Nrf2 to act as a prognostic biomarker, with increased expression of the protein associated with an aggressive tumour type.

Zhao *et al.* attempted to establish a link between Nrf2 expression and resistance to 5-FU. They found increased Nrf2 and HO-1 expression in CRC cells with induced resistance to 5-FU in comparison to the parent cell line. Bisulphate DNA sequencing of the Nrf2 promoter region revealed significant demethylation in 5-FU resistant cells compared with the parent population [460]. This study highlighted the role of Nrf2 in chemoresistance and its ability to act as a predictive biomarker, with increased expression resulting from promotor demethylation leading to drug resistance.

In contrast, Yokoo *et al.* sought to define the role of Nrf2 in the chemoprevention of CRC. This study explored the risk of developing neoplastic small bowel lesions in Nrf2 knockout mice, in comparison to their wild type counterparts, following exposure to the carcinogen potassium bromate. A significant increase in the number of pre-neoplastic and neoplastic lesions was noted in the Nrf2 knockout mice [461].

The role of Nrf2 in the development and treatment of CRC is yet to be fully appreciated. The data presented in this thesis is the first time Nrf2 inhibition has been explored in relation to the cytotoxicity of irinotecan and utilising the Nrf2 inhibitor brusatol in the treatment of CRC, both *in vitro* and in a complex murine model of CRC.

5.4 Advances in irinotecan therapy

No major changes have been made to the treatment of patients with irinotecan since the commencement of the work reported in this thesis, however the possibility of direct delivery of SN-38 has been explored in pre-clinical experiments. Preliminary data comparing the cytotoxicity of SN-38 loaded into three different nanoparticle formulations on CRC cell lines was undertaken during the research time for this thesis (data not shown) in conjunction with the Chemistry Department at the University of Liverpool. These data have been included in a successful grant application to Cancer Research UK to explore the possibility of nano-particle delivery of SN-38 further. Funding was obtained for three PhD students and two post-doctoral researchers across the Departments of Pharmacology and Chemistry at the University. Using co-nanoprecipitation of branched hydrophobic Copolymers and A–B amphiphilic block copolymers rapid formation of sterically stabilised nanoparticles in aqueous medium was possible. These were capable of encapsulating SN-38 in the hydrophobic core of the nanoparticle, while the outer hydrophilic copolymers improved solubility [462]. Cytotoxicity of SN-38 encapsulated in nanoparticles was not significantly different to SN-38 dissolved in DMSO in the CT26 and HCT116 cell lines and provided a more sustained release of the drug *in vivo* as assessed by LC-MS.

These findings are similar to those seen in a number of recent publications investigating the use of nanoparticles for the direct delivery of SN-38. Mosallaei *et al.* demonstrated significant cytotoxicity in the CT26 and HCT116 CRC cell lines using SN-38 encapsulated in solid lipid nanoparticles and PEGylated solid lipid nanoparticles *in vitro.* The ability of the SN-38 loaded nano-particles to inhibit tumour growth *in vivo* was also explored in a syngeneic flank injection model using the CT26 cell line. Tumour growth was significantly inhibited by the SN-38 nanoparticles formulations when compared with irinotecan dissolved in 5% dextrose [463]. This study demonstrated not only the efficacy of nano-particle delivery of SN-38 but also its safety in the pre-clinical setting.

Similar findings were reported by Essa *et al.* with SN-38 encapsulated in poly(D,L-lactide-co-glycolide) nanoparticles enhancing solubility, stability and cellular uptake of the drug. Nanoparticles were also able to protect the active lactone ring of SN-38 against inactivation under physiological conditions, with significant cytotoxicity demonstrated against the COLO-205 CRC cell line [464].

Nanoparticle drug delivery offers the potential to improve drug pharmacokinetics, by allowing a sustained release, rapid increases in the serum and tissue concentrations of drugs can be avoided, which may reduce toxicity and improve efficacy. Specifically in the context of SN-38 delivery, nanoparticles avoid the problems associated with variable conversion of irinotecan to SN-38 by the CES and allow the drug to be delivered in a pharmacologically acceptable solution. Their use warrants further investigation.

5.5 Advances in the understanding of brusatol

It is clear from the recent increase in the number of publications examining the pharmacokinetics, method of action and cytotoxicity of brusatol that interest in the compound is increasing. Many of the recently published studies have already been discussed but recent attempts have been made to understand the pharmacokinetics of brusatol. Zhang *et al.* developed an ultra-performance liquid chromatography tandem mass-spectrometry technique capable of quantifying brusatol in rat plasma with high accuracy at concentrations down to 1ng/ml. They demonstrated rapid clearance of brusatol in rat plasma in the first two hours, with half the drug cleared within an hour after i.v. dosing at three different concentrations up to 2mg/kg rat bodyweight [465]. The rapid excretion of brusatol may contribute to its apparent safety in murine studies, with rapid clearance preventing accumulation and toxicity, despite the profound effects on tumour growth.

The debate over the specificity of brusatol as an Nrf2 inhibitor, and not a global inhibitor of short half-life proteins, in relation to the paper by Vartanian *et al.*, has been discussed [435]. A recent publication by Chio *et al.* may offer a possible explanation for the inhibition of a number of short half-life proteins noted by Vartanian. Chio demonstrated that in pancreatic cancer tumour organoids, Nrf2 regulated the activity of the translational machinery, with Nrf2 deficiency impairing protein synthesis. The mechanism for this was postulated to be through impaired redox homeostasis, with Nrf2 exercising redox-dependent control over multiple aspects of the translational machinery. Global cysteine proteomics, using a selectively cleavable cysteine-reactive reagent followed by iTRAQ analysis of pancreatic tumour organoids, revealed that Nrf2 depletion induced cysteine oxidation of components of the translational machinery. The functional role of Nrf2 in mRNA translation was then examined in pancreatic cancer cells, demonstrating that deletion of Nrf2 led to a measurable decrease in polysomes, with a corresponding increase

in monosomes, suggesting a decrease in translation efficiency in cancer cells when Nrf2 is absent. The authors also noted that Nrf2 knockdown by shRNA adversely affected tumour organoid development, with little effect noted in organoids developed from normal pancreatic tissue. *In vivo* tumour growth rate of the Suit2 cell line flank grafted in to nude mice was also inhibited following Nrf2 deletion. These data again highlight the role of Nrf2 in tumour survival and proliferation [466].

The findings by Chio *et al.* could explain the conclusions postulated by Vartanian *et al.*; it is feasible that the inhibition of Nrf2 by brusatol results in the decreased expression of a number of short half-life proteins following brusatol application, rather than it being a direct action of brusatol itself.

5.6 Future work

This thesis has provided data on the effect of Nrf2 inhibition in reducing tumour CRC cell line proliferation and *in vivo* growth, and in enhancing chemosenstivity to irinotecan. It has not established the mechanisms by which Nrf2 exerts these effects or how Nrf2 modulation alters the metabolism of irinotecan; further work should concentrate on these aspects.

A logical approach to the assessment of the effect of Nrf2 modulation on irinotecan metabolism would involve the modulation of Nrf2 in cell lines using siRNA targeting Nrf2 or Keap1, followed by the measurement of irinotecan and its metabolites in media and cell lysates using LC-MS. This would allow quantification of the conversion of irinotecan to SN-38 and its subsequent deactivation by glucuronidation, in addition to assessing drug uptake and excretion through comparisons of the concentrations of metabolites in media and lysates. Positive findings could subsequently be validated *in vivo.* The quantification of irinotecan and its metabolites in serum and tissue taken at necropsy from mice dosed with irinotecan following pharmacological modulation of Nrf2 expression could allow assessment of the effect of this on irinotecan metabolism. Significant work is likely to be required to ensure that alteration of Nrf2 expression, and that of the downstream proteins involved in irinotecan metabolism, has been achieved before dosing cells or mice with irinotecan.

The work in this thesis also established brusatol as a potent Nrf2 inhibitor and anti-tumorigenic agent in CRC both in *vitro* and *in vivo*, with no published literature currently

available on the effect of brusatol on Nrf2 expression in normal tissue excised from mice. However, it was not established whether brusatol's chemotherapeutic effects are purely mediated through its effects on the Nrf2 pathway.

CRISPR gene editing technology, as described in the discussion of chapter 2, could allow the creation of stable Nrf2 deleted CRC cell lines which could be utilised in exploring whether the effects of brusatol are Nrf2 specific. If the effects of brusatol on CRC cell lines are Nrf2 mediated, then the compound should exert little additional cytotoxicity or alteration in chemosensitivity in a Nrf2 depleted cell line. The use of CRISPR could also allow *in vivo* assessment of tumour growth following Nrf2 inhibition in its own right and in response to brusatol therapy. This work could be limited if the Nrf2 knockout cell lines fail to propagate *in vitro* and *in vivo*, although this would demonstrate the profound effect Nrf2 inhibition on CRC cell viability.

The ultimate aim would be to translate the use of brusatol to the treatment of patients with CRC, either as a standalone chemotherapeutic or as addition to current standardised chemotherapy regimens to enhance their efficacy by overcoming chemoresistance. It could be delivered to patients with advanced disease in attempt to bring them to resection, or given as an adjuvant therapy post-resection to improve outcomes. Establishing the variation in tumour response to treatment with brusatol in patients could allow selection to therapy by relative Nrf2 expression or KEAP1 function, it would be logical that tumours with higher Nrf2 expression, possibly through KEAP1 mutations, are likely to be more dependent on the protein and therefore may demonstrate a greater response to treatment.

Although brusatol was well tolerated in the murine studies presented in this thesis, there are as yet unanswered questions on its mechanism of action, which raise concerns about its use in humans. One approach to limiting possible systemic off-target effects of brusatol is direct drug-delivery techniques, such as nano-particle formulations or chemo-embolisation, allowing more targeted delivery and enhancing its safety.

5.7 Final conclusions

In the introduction to this thesis a number of hypotheses were generated for assessment, these included:

1. Is Nrf2 a relevant target for therapy in CRC?

Proven – Nrf2 expression was demonstrated to be 5-fold higher in primary CRC tumours and 7-fold higher in liver metastases than in normal colon, suggesting a survival advantage to tumour cells with increased Nrf2 expression in CRC tissue.

2. Is it possible to modulate Nrf2 expression in CRC cell lines either genetically (using siRNA) or pharmacologically (using CDDO-me and brusatol)?

Proven – Significant upregulation of Nrf2 was achieved in two CRC (human and murine) cell lines by targeting Keap1 with siRNA or following the application of CDDO-me. Both siRNA targeting Nrf2 and brusatol caused significant inhibition of Nrf2. The effects of brusatol were transient, with maximum inhibition achieved at 3 hours and with baseline expression returning between 8-12 hours following application to cells.

3. Does genetic or pharmacological modulation of Nrf2 in CRC cell lines effect cell viability and proliferation?

Proven – Both siRNA and brusatol inhibition of Nrf2 resulted in a significant decrease in the viability of the two CRC cell lines.

4. Does modulation of Nrf2 in CRC cell lines alter their response to irinotecan-based therapy?

Proven – *In vitro* inhibition of Nrf2 significantly decreased the IC50 of irinotecan, with drug synergy noted across a number of concentration combinations when irinotecan was combined with brusatol.

5. Can in vitro findings be replicated in a murine model of CRC that more accurately represents the development of the disease in humans?

Partially proven – A murine model was created that accurately reflects the metastatic rates reported at presentation in patients with tumours occurring in the presence of an intact immune system and developing in the correct microenvironment. This model was utilised to evaluate *in vitro* findings in the presence of a complete system. This was essential in relation to irinotecan therapy, with a large proportion of conversion of the pro-drug to SN-38 occurring in the liver.

As demonstrated *in vitro,* brusatol acted as a potent anti-tumourigenic agent *in vivo,* significantly inhibiting tumour growth. When combined with irinotecan there was a trend towards increased efficacy, but this did not significantly decrease the tumour growth rate when compared with irinotecan alone. However, at the final time-point the fold change in luminescence noted in the mice on the combination regimen was significantly different from the mice treated with irinotecan monotherapy.

6. Can pharmacological modulation be achieved in vivo?

Proven – Significant inhibition of Nrf2, as assessed by western immunoblotting or IHC, was achieved in tumour tissue, normal colon and normal liver excised from mice treated with brusatol over the study period.

7. Is Nrf2 modulation safe in vivo?

Partially proven – Although no obvious side-effects or significant toxicity was noted in mice treated with brusatol for up to two weeks the longer term effects of brusatol therapy are unknown.

8. Is brusatol a specific Nrf2 inhibitor?

Unknown – although brusatol is a potent inhibitor of Nrf2 both *in vitro* and *in vivo* at nanomolar concentration, and many of the pathways altered in the proteomic data could be under basal or inducible Nrf2 control, the data limitations and the number of altered pathways mean a definitive answer cannot be given.

Bibliography

1. O'Connell, J.B., M.A. Maggard, and C.Y. Ko, *Colon cancer survival rates with the new American Joint Committee on Cancer sixth edition staging.* J Natl Cancer Inst, 2004. **96**(19): p. 1420-5.

2. Garden, O.J., *et al.*, *Guidelines for resection of colorectal cancer liver metastases.* Gut, 2006. **55 Suppl 3**: p. iii1-8.

3. Van Cutsem, E., *et al.*, *Towards a pan-European consensus on the treatment of patients with colorectal liver metastases.* Eur J Cancer, 2006. **42**(14): p. 2212-21.

4. Chan, D.S., *et al.*, *Red and processed meat and colorectal cancer incidence: meta-analysis of prospective studies.* PLoS One, 2011. **6**(6): p. e20456.

5. Sandhu, M.S., I.R. White, and K. McPherson, *Systematic review of the prospective cohort studies on meat consumption and colorectal cancer risk: a meta-analytical approach.* Cancer Epidemiol Biomarkers Prev, 2001. **10**(5): p. 439-46.

6. Norat, T., *et al.*, *Meat consumption and colorectal cancer risk: dose-response meta-analysis of epidemiological studies.* Int J Cancer, 2002. **98**(2): p. 241-56.

7. Larsson, S.C. and A. Wolk, *Meat consumption and risk of colorectal cancer: a meta-analysis of prospective studies.* Int J Cancer, 2006. **119**(11): p. 2657-64.

8. Aune, D., *et al.*, *Dietary fibre, whole grains, and risk of colorectal cancer: systematic review and dose-response meta-analysis of prospective studies.* Bmj, 2011. **343**: p. d6617.

9. Ngo, S.N., *et al.*, *Does garlic reduce risk of colorectal cancer? A systematic review.* J Nutr, 2007. **137**(10): p. 2264-9.

10. Aune, D., *et al.*, *Dairy products and colorectal cancer risk: a systematic review and meta-analysis of cohort studies.* Ann Oncol, 2012. **23**(1): p. 37-45.

11. Aune, D., *et al.*, *Nonlinear reduction in risk for colorectal cancer by fruit and vegetable intake based on meta-analysis of prospective studies.* Gastroenterology, 2011. **141**(1): p. 106-18.

12. Gnagnarella, P., *et al.*, *Glycemic index, glycemic load, and cancer risk: a meta-analysis.* Am J Clin Nutr, 2008. **87**(6): p. 1793-801.

13. Mulholland, H.G., *et al.*, *Glycemic index, glycemic load, and risk of digestive tract neoplasms: a systematic review and meta-analysis.* Am J Clin Nutr, 2009. **89**(2): p. 568-76.

14. Carroll, C., *et al.*, *Supplemental calcium in the chemoprevention of colorectal cancer: a systematic review and meta-analysis.* Clin Ther, 2010. **32**(5): p. 789-803.

15. Weingarten, M.A., A. Zalmanovici, and J. Yaphe, *Dietary calcium supplementation for preventing colorectal cancer and adenomatous polyps.* Cochrane Database Syst Rev, 2008(1): p. Cd003548.

16. Cole, B.F., *et al.*, *Folic acid for the prevention of colorectal adenomas: a randomized clinical trial.* Jama, 2007. **297**(21): p. 2351-9.

17. Carroll, C., *et al.*, *Meta-analysis: folic acid in the chemoprevention of colorectal adenomas and colorectal cancer.* Aliment Pharmacol Ther, 2010. **31**(7): p. 708-18.

18. Kennedy, D.A., *et al.*, *Folate intake and the risk of colorectal cancer: a systematic review and meta-analysis.* Cancer Epidemiol, 2011. **35**(1): p. 2-10.

19. Fife, J., *et al.*, *Folic acid supplementation and colorectal cancer risk: a meta-analysis.* Colorectal Dis, 2011. **13**(2): p. 132-7.

20. Larsson, S.C., N. Orsini, and A. Wolk, *Vitamin B6 and risk of colorectal cancer: a meta-analysis of prospective studies.* Jama, 2010. **303**(11): p. 1077-83.

21. Key, T.J., *et al.*, *Vitamins, minerals, essential fatty acids and colorectal cancer risk in the United Kingdom Dietary Cohort Consortium.* Int J Cancer, 2012. **131**(3): p. E320-5.

22. Dahlin, A.M., *et al.*, *Plasma vitamin B12 concentrations and the risk of colorectal cancer: a nested case-referent study.* Int J Cancer, 2008. **122**(9): p. 2057-61.

23. Fedirko, V., *et al.*, *Alcohol drinking and colorectal cancer risk: an overall and dose-response meta-analysis of published studies.* Ann Oncol, 2011. **22**(9): p. 1958-72.

24. Moskal, A., *et al.*, *Alcohol intake and colorectal cancer risk: a dose-response meta-analysis of published cohort studies.* Int J Cancer, 2007. **120**(3): p. 664-71.

25. Wang, J., *et al.*, *Alcohol ingestion and colorectal neoplasia: a meta-analysis based on a Mendelian randomization approach.* Colorectal Dis, 2011. **13**(5): p. e71-8.

26. Liang, P.S., T.Y. Chen, and E. Giovannucci, *Cigarette smoking and colorectal cancer incidence and mortality: systematic review and meta-analysis.* Int J Cancer, 2009. **124**(10): p. 2406-15.

27. Tsoi, K.K., *et al.*, *Cigarette smoking and the risk of colorectal cancer: a meta-analysis of prospective cohort studies.* Clin Gastroenterol Hepatol, 2009. **7**(6): p. 682-688.e1-5.

28. Botteri, E., *et al.*, *Smoking and colorectal cancer: a meta-analysis.* Jama, 2008. **300**(23): p. 2765-78.

29. Ning, Y., L. Wang, and E.L. Giovannucci, *A quantitative analysis of body mass index and colorectal cancer: findings from 56 observational studies.* Obes Rev, 2010. **11**(1): p. 19-30.

30. Larsson, S.C. and A. Wolk, *Obesity and colon and rectal cancer risk: a meta-analysis of prospective studies.* Am J Clin Nutr, 2007. **86**(3): p. 556-65.

31. Huxley, R.R., *et al.*, *The impact of dietary and lifestyle risk factors on risk of colorectal cancer: A quantitative overview of the epidemiological evidence.* International Journal of Cancer, 2009. **125**(1): p. 171-180.

32. Harriss, D.J., *et al.*, *Lifestyle factors and colorectal cancer risk (2): a systematic review and meta-analysis of associations with leisure-time physical activity.* Colorectal Dis, 2009. **11**(7): p. 689-701.

33. Wolin, K.Y., *et al.*, *Physical activity and colon cancer prevention: a meta-analysis.* Br J Cancer, 2009. **100**(4): p. 611-6.

34. Rothwell, P.M., *et al.*, *Long-term effect of aspirin on colorectal cancer incidence and mortality: 20-year follow-up of five randomised trials.* Lancet, 2010. **376**(9754): p. 1741-50.

35. Bardou, M., A. Barkun, and M. Martel, *Effect of statin therapy on colorectal cancer.* Gut, 2010. **59**(11): p. 1572-1585.

36. Grodstein, F., P.A. Newcomb, and M.J. Stampfer, *Postmenopausal hormone therapy and the risk of colorectal cancer: a review and meta-analysis.* Am J Med, 1999. **106**(5): p. 574-82.

37. Anderson, G.L., *et al.*, *Effects of conjugated equine estrogen in postmenopausal women with hysterectomy: the Women's Health Initiative randomized controlled trial.* Jama, 2004. **291**(14): p. 1701-12.

38. Csizmadi, I., *et al.*, *The effects of transdermal and oral oestrogen replacement therapy on colorectal cancer risk in postmenopausal women.* Br J Cancer, 2004. **90**(1): p. 76-81.

39. Tsilidis, K.K., *et al.*, *Menopausal hormone therapy and risk of colorectal cancer in the European Prospective Investigation into Cancer and Nutrition.* Int J Cancer, 2011. **128**(8): p. 1881-9.

40. Hildebrand, J.S., *et al.*, *Colorectal cancer incidence and postmenopausal hormone use by type, recency, and duration in cancer prevention study II.* Cancer Epidemiol Biomarkers Prev, 2009. **18**(11): p. 2835-41.

41. Hulley, S., *et al.*, *Noncardiovascular disease outcomes during 6.8 years of hormone therapy: Heart and Estrogen/progestin Replacement Study follow-up (HERS II).* Jama, 2002. **288**(1): p. 58-66.

42. Chlebowski, R.T., *et al.*, *Estrogen plus progestin and colorectal cancer in postmenopausal women.* N Engl J Med, 2004. **350**(10): p. 991-1004.

43. Eaden, J.A., K.R. Abrams, and J.F. Mayberry, *The risk of colorectal cancer in ulcerative colitis: a meta-analysis.* Gut, 2001. **48**(4): p. 526-35.

44. Lutgens, M.W., *et al.*, *Declining risk of colorectal cancer in inflammatory bowel disease: an updated meta-analysis of population-based cohort studies.* Inflamm Bowel Dis, 2013. **19**(4): p. 789-99.

45. Fearon, E.R. and B. Vogelstein, *A genetic model for colorectal tumorigenesis.* Cell, 1990. **61**(5): p. 759-67.

46. Sjoblom, T., *et al.*, *The consensus coding sequences of human breast and colorectal cancers.* Science, 2006. **314**(5797): p. 268-74.

47. Network, T.C.G.A., *Comprehensive molecular characterization of human colon and rectal cancer.* Nature, 2012. **487**(7407): p. 330-7.

48. Armaghany, T., *et al.*, *Genetic alterations in colorectal cancer.* Gastrointest Cancer Res, 2012. **5**(1): p. 19-27.

49. Boland, C.R., *et al.*, *A National Cancer Institute Workshop on Microsatellite Instability for cancer detection and familial predisposition: development of international criteria for the determination of microsatellite instability in colorectal cancer.* Cancer Res, 1998. **58**(22): p. 5248-57.

50. Rajagopalan, H., *et al.*, *The significance of unstable chromosomes in colorectal cancer.* Nat Rev Cancer, 2003. **3**(9): p. 695-701.

51. Tsang, A.H., *et al.*, *Current and future molecular diagnostics in colorectal cancer and colorectal adenoma.* World J Gastroenterol, 2014. **20**(14): p. 3847-57.

52. Pino, M.S. and D.C. Chung, *Microsatellite instability in the management of colorectal cancer.* Expert Rev Gastroenterol Hepatol, 2011. **5**(3): p. 385-99.

53. Pino, M.S. and D.C. Chung, *The chromosomal instability pathway in colon cancer.* Gastroenterology, 2010. **138**(6): p. 2059-72.

54. Sinicrope, F.A., *et al.*, *Prognostic impact of microsatellite instability and DNA ploidy in human colon carcinoma patients.* Gastroenterology, 2006. **131**(3): p. 729-37.

55. Walther, A., R. Houlston, and I. Tomlinson, *Association between chromosomal instability and prognosis in colorectal cancer: a meta-analysis.* Gut, 2008. **57**(7): p. 941-50.

56. Lao, V.V. and W.M. Grady, *Epigenetics and colorectal cancer.* Nat Rev Gastroenterol Hepatol, 2011. **8**(12): p. 686-700.

57. Juo, Y.Y., *et al.*, *Prognostic value of CpG island methylator phenotype among colorectal cancer patients: a systematic review and meta-analysis.* Ann Oncol, 2014. **25**(12): p. 2314-27.

58. Iacopetta, B., K. Kawakami, and T. Watanabe, *Predicting clinical outcome of 5-fluorouracil-based chemotherapy for colon cancer patients: is the CpG island methylator phenotype the 5-fluorouracil-responsive subgroup?* Int J Clin Oncol, 2008. **13**(6): p. 498-503.

59. Powell, S.M., *et al.*, *APC mutations occur early during colorectal tumorigenesis.* Nature, 1992. **359**(6392): p. 235-7.

60. De Filippo, C., *et al.*, *Mutations of the APC gene in human sporadic colorectal cancers.* Scand J Gastroenterol, 2002. **37**(9): p. 1048-53.

61. Polakis, P., *The adenomatous polyposis coli (APC) tumor suppressor.* Biochim Biophys Acta, 1997. **1332**(3): p. F127-47.

62. Fearon, E.R., *Molecular genetics of colorectal cancer.* Annu Rev Pathol, 2011. **6**: p. 479-507.

63. Castagnola, P. and W. Giaretti, *Mutant KRAS, chromosomal instability and prognosis in colorectal cancer.* Biochim Biophys Acta, 2005. **1756**(2): p. 115-25.

64. Lochhead, P., *et al.*, *Microsatellite instability and BRAF mutation testing in colorectal cancer prognostication.* J Natl Cancer Inst, 2013. **105**(15): p. 1151-6.

65. Tejpar, S., *et al.*, *Prognostic and predictive biomarkers in resected colon cancer: current status and future perspectives for integrating genomics into biomarker discovery.* Oncologist, 2010. **15**(4): p. 390-404.

66. Vogelstein, B., D. Lane, and A.J. Levine, *Surfing the p53 network.* Nature, 2000. **408**(6810): p. 307-10.

67. Baker, S.J., *et al.*, *p53 gene mutations occur in combination with 17p allelic deletions as late events in colorectal tumorigenesis.* Cancer Res, 1990. **50**(23): p. 7717-22.

68. Leslie, A., *et al.*, *The colorectal adenoma-carcinoma sequence.* Br J Surg, 2002. **89**(7): p. 845-60.

69. Lopez, I., *et al.*, *Different mutation profiles associated to P53 accumulation in colorectal cancer.* Gene, 2012. **499**(1): p. 81-7.

70. Duman-Scheel, M., *Deleted in Colorectal Cancer (DCC) pathfinding: axon guidance gene finally turned tumor suppressor.* Curr Drug Targets, 2012. **13**(11): p. 1445-53.

71. Moran, A., *et al.*, *Differential colorectal carcinogenesis: Molecular basis and clinical relevance.* World J Gastrointest Oncol, 2010. **2**(3): p. 151-8.

72. Takayama, T., *et al.*, *Colorectal cancer: genetics of development and metastasis.* J Gastroenterol, 2006. **41**(3): p. 185-92.

73. Cho, K.R., *et al.*, *The DCC gene: structural analysis and mutations in colorectal carcinomas.* Genomics, 1994. **19**(3): p. 525-31.

74. Miyaki, M., *et al.*, *Higher frequency of Smad4 gene mutation in human colorectal cancer with distant metastasis.* Oncogene, 1999. **18**(20): p. 3098-103.

75. Valle, L., *Genetic predisposition to colorectal cancer: where we stand and future perspectives.* World J Gastroenterol, 2014. **20**(29): p. 9828-49.

76. Syngal, S., *et al.*, *ACG clinical guideline: Genetic testing and management of hereditary gastrointestinal cancer syndromes.* Am J Gastroenterol, 2015. **110**(2): p. 223-62; quiz 263.

77. Novelli, M., *The pathology of hereditary polyposis syndromes.* Histopathology, 2015. **66**(1): p. 78-87.

78. de la Chapelle, A., *The incidence of Lynch syndrome.* Fam Cancer, 2005. **4**(3): p. 233-7.

79. Lynch, H.T., *et al.*, *Review of the Lynch syndrome: history, molecular genetics, screening, differential diagnosis, and medicolegal ramifications.* Clin Genet, 2009. **76**(1): p. 1-18.

80. Half, E., D. Bercovich, and P. Rozen, *Familial adenomatous polyposis.* Orphanet J Rare Dis, 2009. **4**: p. 22.

81. Al-Tassan, N., *et al.*, *Inherited variants of MYH associated with somatic G:C-->T:A mutations in colorectal tumors.* Nat Genet, 2002. **30**(2): p. 227-32.

82. Aretz, S., *et al.*, *High proportion of large genomic STK11 deletions in Peutz-Jeghers syndrome.* Hum Mutat, 2005. **26**(6): p. 513-9.

83. Jass, J.R., *Colorectal polyposes: from phenotype to diagnosis.* Pathol Res Pract, 2008. **204**(7): p. 431-47.

84. Mester, J. and C. Eng, *Estimate of de novo mutation frequency in probands with PTEN hamartoma tumor syndrome.* Genet Med, 2012. **14**(9): p. 819-22.

85. Orlowska, J., *Hyperplastic polyposis syndrome and the risk of colorectal cancer.* Gut, 2012. **61**(3): p. 470-1; author reply 471-2.

86. Zauber, A.G., *et al.*, *Colonoscopic polypectomy and long-term prevention of colorectal-cancer deaths.* N Engl J Med, 2012. **366**(8): p. 687-96.

87. Armaroli, P., *et al.*, *European Code against Cancer, 4th Edition: Cancer screening.* Cancer Epidemiol, 2015. **39 Suppl 1**: p. S139-52.

88. Hewitson, P., *et al.*, *Screening for colorectal cancer using the faecal occult blood test, Hemoccult.* Cochrane Database Syst Rev, 2007(1): p. Cd001216.

89. Hamza, S., *et al.*, *Long-term effect of faecal occult blood screening on incidence and mortality from colorectal cancer.* Dig Liver Dis, 2014. **46**(12): p. 1121-5.

90. McGregor, L.M., *et al.*, *Uptake of Bowel Scope (Flexible Sigmoidoscopy) Screening in the English National Programme: the first 14 months.* J Med Screen, 2015.

91. Elmunzer, B.J., *et al.*, *Effect of flexible sigmoidoscopy-based screening on incidence and mortality of colorectal cancer: a systematic review and meta-analysis of randomized controlled trials.* PLoS Med, 2012. **9**(12): p. e1001352.

92. Langevin, J.M. and S. Nivatvongs, *The true incidence of synchronous cancer of the large bowel. A prospective study.* Am J Surg, 1984. **147**(3): p. 330-3.

93. Robinson, M.H., *et al.*, *The risks of screening: data from the Nottingham randomised controlled trial of faecal occult blood screening for colorectal cancer.* Gut, 1999. **45**(4): p. 588-92.

94. van Rijn, J.C., *et al.*, *Polyp miss rate determined by tandem colonoscopy: a systematic review.* Am J Gastroenterol, 2006. **101**(2): p. 343-50.

95. Lahaye, M.J., *et al.*, *Imaging for predicting the risk factors--the circumferential resection margin and nodal disease--of local recurrence in rectal cancer: a meta-analysis.* Semin Ultrasound CT MR, 2005. **26**(4): p. 259-68.

96. Dighe, S., *et al.*, *Diagnostic precision of CT in local staging of colon cancers: a meta-analysis.* Clin Radiol, 2010. **65**(9): p. 708-19.

97. Floriani, I., *et al.*, *Performance of imaging modalities in diagnosis of liver metastases from colorectal cancer: a systematic review and meta-analysis.* J Magn Reson Imaging, 2010. **31**(1): p. 19-31.

98. Kekelidze, M., *et al.*, *Colorectal cancer: current imaging methods and future perspectives for the diagnosis, staging and therapeutic response evaluation.* World J Gastroenterol, 2013. **19**(46): p. 8502-14.

99. Maffione, A.M., *et al.*, *Diagnostic accuracy and impact on management of (18)F-FDG PET and PET/CT in colorectal liver metastasis: a meta-analysis and systematic review.* Eur J Nucl Med Mol Imaging, 2015. **42**(1): p. 152-63.

100. Taylor, F.G., *et al.*, *A systematic approach to the interpretation of preoperative staging MRI for rectal cancer.* AJR Am J Roentgenol, 2008. **191**(6): p. 1827-35.

101. *Diagnostic accuracy of preoperative magnetic resonance imaging in predicting curative resection of rectal cancer: prospective observational study.* Bmj, 2006. **333**(7572): p. 779.

102. Niekel, M.C., S. Bipat, and J. Stoker, *Diagnostic imaging of colorectal liver metastases with CT, MR imaging, FDG PET, and/or FDG PET/CT: a meta-analysis of prospective studies including patients who have not previously undergone treatment.* Radiology, 2010. **257**(3): p. 674-84.

103. Cresswell, A.B., F.K. Welsh, and M. Rees, *A diagnostic paradigm for resectable liver lesions: to biopsy or not to biopsy?* HPB (Oxford), 2009. **11**(7): p. 533-40.

104. Barresi, V., *et al.*, *Histological grading in colorectal cancer: new insights and perspectives.* Histol Histopathol, 2015. **30**(9): p. 1059-67.

105. Dukes, C., *The classification of cancer of the rectum.* Journal of Pathology and Bacteriology, 1932. **35**: p. 323-332.

106. Dukes, C.E. and H.J. Bussey, *The spread of rectal cancer and its effect on prognosis.* Br J Cancer, 1958. **12**(3): p. 309-20.

107. Turnbull, R.B., Jr., *et al.*, *Cancer of the colon: the influence of the no-touch isolation technic on survival rates.* Ann Surg, 1967. **166**(3): p. 420-7.

108. Edge, S.B. and C.C. Compton, *The American Joint Committee on Cancer: the 7th edition of the AJCC cancer staging manual and the future of TNM.* Ann Surg Oncol, 2010. **17**(6): p. 1471-4.

109. Barresi, V., *et al.*, *Histologic prognostic markers in stage IIA colorectal cancer: a comparative study.* Scand J Gastroenterol, 2016. **51**(3): p. 314-20.

110. Jass, J.R., *Classification of colorectal cancer based on correlation of clinical, morphological and molecular features.* Histopathology, 2007. **50**(1): p. 113-30.

111. Wang, J., *et al.*, *Endoscopic submucosal dissection vs endoscopic mucosal resection for colorectal tumors: a meta-analysis.* World J Gastroenterol, 2014. **20**(25): p. 8282-7.

112. Sajid, M.S., *et al.*, *Systematic review and meta-analysis of published trials comparing the effectiveness of transanal endoscopic microsurgery and radical resection in the management of early rectal cancer.* Colorectal Dis, 2014. **16**(1): p. 2-14.

113. Kidane, B., *et al.*, *Local resection compared with radical resection in the treatment of T1N0M0 rectal adenocarcinoma: a systematic review and meta-analysis.* Dis Colon Rectum, 2015. **58**(1): p. 122-40.

114. Hong, K.D., *et al.*, *Transanal Minimally Invasive Surgery (TAMIS) for Rectal Lesions: A Systematic Review.* Hepatogastroenterology, 2015. **62**(140): p. 863-7.

115. Yamamoto, S., *et al.*, *The risk of lymph node metastasis in T1 colorectal carcinoma.* Hepatogastroenterology, 2004. **51**(58): p. 998-1000.

116. Beaton, C., *et al.*, *Systematic review and meta-analysis of histopathological factors influencing the risk of lymph node metastasis in early colorectal cancer.* Colorectal Dis, 2013. **15**(7): p. 788-97.

117. Frasson, M., *et al.*, *Risk Factors for Anastomotic Leak After Colon Resection for Cancer: Multivariate Analysis and Nomogram From a Multicentric, Prospective, National Study With 3193 Patients.* Ann Surg, 2015. **262**(2): p. 321-30.

118. Nelson, H., *et al.*, *Guidelines 2000 for colon and rectal cancer surgery.* J Natl Cancer Inst, 2001. **93**(8): p. 583-96.

119. Heald, R.J., *The 'Holy Plane' of rectal surgery.* J R Soc Med, 1988. **81**(9): p. 503-8.

120. Heald, R.J., *et al.*, *Rectal cancer: the Basingstoke experience of total mesorectal excision, 1978-1997.* Arch Surg, 1998. **133**(8): p. 894-9.

121. Nagtegaal, I.D. and P. Quirke, *What is the role for the circumferential margin in the modern treatment of rectal cancer?* J Clin Oncol, 2008. **26**(2): p. 303-12.

122. Bordeianou, L., *et al.*, *Sphincter-sparing surgery in patients with low-lying rectal cancer: techniques, oncologic outcomes, and functional results.* J Gastrointest Surg, 2014. **18**(7): p. 1358-72.

123. Veldkamp, R., *et al.*, *Laparoscopic surgery versus open surgery for colon cancer: short-term outcomes of a randomised trial.* Lancet Oncol, 2005. **6**(7): p. 477-84.

124. Guillou, P.J., *et al.*, *Short-term endpoints of conventional versus laparoscopic-assisted surgery in patients with colorectal cancer (MRC CLASICC trial): multicentre, randomised controlled trial.* Lancet, 2005. **365**(9472): p. 1718-26.

125. Buunen, M., *et al.*, *Survival after laparoscopic surgery versus open surgery for colon cancer: long-term outcome of a randomised clinical trial.* Lancet Oncol, 2009. **10**(1): p. 44-52.

126. Liao, G., *et al.*, *Robotic-assisted versus laparoscopic colorectal surgery: a meta-analysis of four randomized controlled trials.* World J Surg Oncol, 2014. **12**: p. 122.

127. Trastulli, S., *et al.*, *Robotic resection compared with laparoscopic rectal resection for cancer: systematic review and meta-analysis of short-term outcome.* Colorectal Dis, 2012. **14**(4): p. e134-56.

128. Collinson, F.J., *et al.*, *An international, multicentre, prospective, randomised, controlled, unblinded, parallel-group trial of robotic-assisted versus standard laparoscopic surgery for the curative treatment of rectal cancer.* Int J Colorectal Dis, 2012. **27**(2): p. 233-41.

129. Kanas, G.P., *et al.*, *Survival after liver resection in metastatic colorectal cancer: review and meta-analysis of prognostic factors.* Clin Epidemiol, 2012. **4**: p. 283-301.

130. Poston, G.J., *Staging of advanced colorectal cancer.* Surg Oncol Clin N Am, 2008. **17**(3): p. 503-17, viii.

131. Mattar, R.E., *et al.*, *Preoperative selection of patients with colorectal cancer liver metastasis for hepatic resection.* World J Gastroenterol, 2016. **22**(2): p. 567-81.

132. Vogl, T.J., *et al.*, *Thermal ablation of liver metastases from colorectal cancer: radiofrequency, microwave and laser ablation therapies.* Radiol Med, 2014. **119**(7): p. 451-61.

133. Pfannschmidt, J., H. Dienemann, and H. Hoffmann, *Surgical resection of pulmonary metastases from colorectal cancer: a systematic review of published series.* Ann Thorac Surg, 2007. **84**(1): p. 324-38.

134. Treasure, T., *et al.*, *Pulmonary metastasectomy in colorectal cancer: the PulMiCC trial.* Thorax, 2012. **67**(2): p. 185-7.

135. Lykoudis, P.M., *et al.*, *Systematic review of surgical management of synchronous colorectal liver metastases.* Br J Surg, 2014. **101**(6): p. 605-12.

136. Kelly, M.E., *et al.*, *Synchronous colorectal liver metastasis: a network meta-analysis review comparing classical, combined, and liver-first surgical strategies.* J Surg Oncol, 2015. **111**(3): p. 341-51.

137. Harrison, L. and K. Blackwell, *Hypoxia and anemia: factors in decreased sensitivity to radiation therapy and chemotherapy?* Oncologist, 2004. **9 Suppl 5**: p. 31-40.

138. Vens, C. and A.C. Begg, *Targeting base excision repair as a sensitization strategy in radiotherapy.* Semin Radiat Oncol, 2010. **20**(4): p. 241-9.

139. Barker, H.E., *et al.*, *The tumour microenvironment after radiotherapy: mechanisms of resistance and recurrence.* Nat Rev Cancer, 2015. **15**(7): p. 409-25.

140. Lu, J.Y., *et al.*, *Clinical outcome of neoadjuvant chemoradiation therapy with oxaliplatin and capecitabine or 5-fluorouracil for locally advanced rectal cancer.* J Surg Oncol, 2013. **108**(4): p. 213-9.

141. *Local recurrence rate in a randomised multicentre trial of preoperative radiotherapy compared with operation alone in resectable rectal carcinoma. Swedish Rectal Cancer Trial.* Eur J Surg, 1996. **162**(5): p. 397-402.

142. Folkesson, J., *et al.*, *Swedish Rectal Cancer Trial: long lasting benefits from radiotherapy on survival and local recurrence rate.* J Clin Oncol, 2005. **23**(24): p. 5644-50.

143. Kapiteijn, E., *et al.*, *Preoperative radiotherapy combined with total mesorectal excision for resectable rectal cancer.* N Engl J Med, 2001. **345**(9): p. 638-46.

144. Sebag-Montefiore, D., *et al.*, *Preoperative radiotherapy versus selective postoperative chemoradiotherapy in patients with rectal cancer (MRC CR07 and NCIC-CTG C016): a multicentre, randomised trial.* Lancet, 2009. **373**(9666): p. 811-20.

145. Ngan, S.Y., *et al.*, *Randomized trial of short-course radiotherapy versus long-course chemoradiation comparing rates of local recurrence in patients with T3 rectal cancer: Trans-Tasman Radiation Oncology Group trial 01.04.* J Clin Oncol, 2012. **30**(31): p. 3827-33.

146. Pettersson, D., *et al.*, *Tumour regression in the randomized Stockholm III Trial of radiotherapy regimens for rectal cancer.* Br J Surg, 2015. **102**(8): p. 972-8; discussion 978.

147. Gerard, J.P., *et al.*, *Preoperative radiotherapy with or without concurrent fluorouracil and leucovorin in T3-4 rectal cancers: results of FFCD 9203.* J Clin Oncol, 2006. **24**(28): p. 4620-5.

148. Bosset, J.F., *et al.*, *Fluorouracil-based adjuvant chemotherapy after preoperative chemoradiotherapy in rectal cancer: long-term results of the EORTC 22921 randomised study.* Lancet Oncol, 2014. **15**(2): p. 184-90.

149. Bujko, K., *et al.*, *Long-term results of a randomized trial comparing preoperative short-course radiotherapy with preoperative conventionally fractionated chemoradiation for rectal cancer.* Br J Surg, 2006. **93**(10): p. 1215-23.

150. Rodel, C., *et al.*, *Oxaliplatin added to fluorouracil-based preoperative chemoradiotherapy and postoperative chemotherapy of locally advanced rectal cancer (the German CAO/ARO/AIO-04 study): final results of the multicentre, open-label, randomised, phase 3 trial.* Lancet Oncol, 2015. **16**(8): p. 979-89.

151. Sauer, R., *et al.*, *Preoperative versus postoperative chemoradiotherapy for locally advanced rectal cancer: results of the German CAO/ARO/AIO-94 randomized phase III trial after a median follow-up of 11 years.* J Clin Oncol, 2012. **30**(16): p. 1926-33.

152. Taylor, F.G., *et al.*, *One millimetre is the safe cut-off for magnetic resonance imaging prediction of surgical margin status in rectal cancer.* Br J Surg, 2011. **98**(6): p. 872-9.

153. Taylor, F.G., *et al.*, *Preoperative high-resolution magnetic resonance imaging can identify good prognosis stage I, II, and III rectal cancer best managed by surgery alone: a prospective, multicenter, European study.* Ann Surg, 2011. **253**(4): p. 711-9.

154. Sun Myint, A., *et al.*, *Combined modality treatment of early rectal cancer: the UK experience.* Clin Oncol (R Coll Radiol), 2007. **19**(9): p. 674-81.

155. Saltz, L.B., *Palliative management of rectal cancer: the roles of chemotherapy and radiation therapy.* J Gastrointest Surg, 2004. **8**(3): p. 274-6.

156. Gustavsson, B., *et al.*, *A review of the evolution of systemic chemotherapy in the management of colorectal cancer.* Clin Colorectal Cancer, 2015. **14**(1): p. 1-10.

157. Longley, D.B., D.P. Harkin, and P.G. Johnston, *5-fluorouracil: mechanisms of action and clinical strategies.* Nat Rev Cancer, 2003. **3**(5): p. 330-8.

158. Project, A.C.C.M.-A., *Modulation of fluorouracil by leucovorin in patients with advanced colorectal cancer: evidence in terms of response rate. .* J Clin Oncol, 1992. **10**(6): p. 896-903.

159. Perego, P. and J. Robert, *Oxaliplatin in the era of personalized medicine: from mechanistic studies to clinical efficacy.* Cancer Chemother Pharmacol, 2016. **77**(1): p. 5-18.

160. Zedan, A.H., *et al.*, *Oxaliplatin-induced neuropathy in colorectal cancer: many questions with few answers.* Clin Colorectal Cancer, 2014. **13**(2): p. 73-80.

161. Rubbia-Brandt, L., *et al.*, *Severe hepatic sinusoidal obstruction associated with oxaliplatin-based chemotherapy in patients with metastatic colorectal cancer.* Ann Oncol, 2004. **15**(3): p. 460-6.

162. Kunimoto, T., *et al.*, *Antitumor activity of 7-ethyl-10-[4-(1-piperidino)-1-piperidino]carbonyloxy-camptothec in, a novel water-soluble derivative of camptothecin, against murine tumors.* Cancer Res, 1987. **47**(22): p. 5944-7.

163. Kawato, Y., *et al.*, *Antitumor activity of a camptothecin derivative, CPT-11, against human tumor xenografts in nude mice.* Cancer Chemother Pharmacol, 1991. **28**(3): p. 192-8.

164. Mathijssen, R.H., *et al.*, *Clinical pharmacokinetics and metabolism of irinotecan (CPT-11).* Clin Cancer Res, 2001. **7**(8): p. 2182-94.

165. Hsiang, Y.H. and L.F. Liu, *Identification of mammalian DNA topoisomerase I as an intracellular target of the anticancer drug camptothecin.* Cancer Res, 1988. **48**(7): p. 1722-6.

166. Liu, L.F., *et al.*, *Mechanism of action of camptothecin.* Ann N Y Acad Sci, 2000. **922**: p. 1-10.

167. Cao, Y., *et al.*, *Synergistic effects of topoisomerase I inhibitor, SN38, on Fas-mediated apoptosis.* Anticancer Res, 2010. **30**(10): p. 3911-7.

168. Sanghani, S.P., *et al.*, *Carboxylesterases expressed in human colon tumor tissue and their role in CPT-11 hydrolysis.* Clin Cancer Res, 2003. **9**(13): p. 4983-91.

169. Robinson, S.M., *et al.*, *Chemotherapy-associated liver injury in patients with colorectal liver metastases: a systematic review and meta-analysis.* Ann Surg Oncol, 2012. **19**(13): p. 4287-99.

170. Humerickhouse, R., *et al.*, *Characterization of CPT-11 hydrolysis by human liver carboxylesterase isoforms hCE-1 and hCE-2.* Cancer Res, 2000. **60**(5): p. 1189-92.

171. Guichard, S., *et al.*, *CPT-11 converting carboxylesterase and topoisomerase activities in tumour and normal colon and liver tissues.* Br J Cancer, 1999. **80**(3-4): p. 364-70.

172. Hatfield, M.J., *et al.*, *Organ-specific carboxylesterase profiling identifies the small intestine and kidney as major contributors of activation of the anticancer prodrug CPT-11.* Biochem Pharmacol, 2011. **81**(1): p. 24-31.

173. Jones, R.P., *et al.*, *Hepatic activation of irinotecan predicts tumour response in patients with colorectal liver metastases treated with DEBIRI: exploratory findings from a phase II study.* Cancer Chemother Pharmacol, 2013. **72**(2): p. 359-68.

174. Cecchin, E., *et al.*, *Carboxylesterase isoform 2 mRNA expression in peripheral blood mononuclear cells is a predictive marker of the irinotecan to SN38 activation step in colorectal cancer patients.* Clin Cancer Res, 2005. **11**(19 Pt 1): p. 6901-7.

175. Matzow, T., *et al.*, *Hypoxia-targeted over-expression of carboxylesterase as a means of increasing tumour sensitivity to irinotecan (CPT-11).* J Gene Med, 2007. **9**(4): p. 244-52.

176. Haaz, M.C., *et al.*, *Metabolism of irinotecan (CPT-11) by human hepatic microsomes: participation of cytochrome P-450 3A and drug interactions.* Cancer Res, 1998. **58**(3): p. 468-72.

177. Smith, N.F., W.D. Figg, and A. Sparreboom, *Pharmacogenetics of irinotecan metabolism and transport: an update.* Toxicol In Vitro, 2006. **20**(2): p. 163-75.

178. Santos, A., *et al.*, *Metabolism of irinotecan (CPT-11) by CYP3A4 and CYP3A5 in humans.* Clin Cancer Res, 2000. **6**(5): p. 2012-20.

179. Watanabe, M., *et al.*, *Expression of CYP3A4 mRNA is correlated with CYP3A4 protein level and metabolic activity in human liver.* J Pharmacol Sci, 2004. **94**(4): p. 459-62.

180. Massaad, L., *et al.*, *Comparison of mouse and human colon tumors with regard to phase I and phase II drug-metabolizing enzyme systems.* Cancer Res, 1992. **52**(23): p. 6567-75.

181. van der Bol, J.M., *et al.*, *A CYP3A4 phenotype-based dosing algorithm for individualized treatment of irinotecan.* Clin Cancer Res, 2010. **16**(2): p. 736-42.

182. Iyer, L., *et al.*, *Genetic predisposition to the metabolism of irinotecan (CPT-11). Role of uridine diphosphate glucuronosyltransferase isoform 1A1 in the glucuronidation of its active metabolite (SN-38) in human liver microsomes.* J Clin Invest, 1998. **101**(4): p. 847-54.

183. Iyer, L., *et al.*, *UGT1A1*28 polymorphism as a determinant of irinotecan disposition and toxicity.* Pharmacogenomics J, 2002. **2**(1): p. 43-7.

184. Liu, X., *et al.*, *Association of UGT1A1*28 polymorphisms with irinotecan-induced toxicities in colorectal cancer: a meta-analysis in Caucasians.* Pharmacogenomics J, 2014. **14**(2): p. 120-9.

185. Dias, M.M., R.A. McKinnon, and M.J. Sorich, *Impact of the UGT1A1*28 allele on response to irinotecan: a systematic review and meta-analysis.* Pharmacogenomics, 2012. **13**(8): p. 889-99.

186. Slatter, J.G., *et al.*, *Pharmacokinetics, metabolism, and excretion of irinotecan (CPT-11) following I.V. infusion of [(14)C]CPT-11 in cancer patients.* Drug Metab Dispos, 2000. **28**(4): p. 423-33.

187. de Jong, F.A., *et al.*, *Role of pharmacogenetics in irinotecan therapy.* Cancer Lett, 2006. **234**(1): p. 90-106.

188. Paulik, A., J. Grim, and S. Filip, *Predictors of irinotecan toxicity and efficacy in treatment of metastatic colorectal cancer.* Acta Medica (Hradec Kralove), 2012. **55**(4): p. 153-9.

189. Chen, S., *et al.*, *ABCC5 and ABCG1 polymorphisms predict irinotecan-induced severe toxicity in metastatic colorectal cancer patients.* Pharmacogenet Genomics, 2015. **25**(12): p. 573-83.

190. De Mattia, E., *et al.*, *Pharmacogenetics of ABC and SLC transporters in metastatic colorectal cancer patients receiving first-line FOLFIRI treatment.* Pharmacogenet Genomics, 2013. **23**(10): p. 549-57.

191. Trumpi, K., *et al.*, *ABC-Transporter Expression Does Not Correlate with Response to Irinotecan in Patients with Metastatic Colorectal Cancer.* J Cancer, 2015. **6**(11): p. 1079-86.

192. Bosslet, K., *et al.*, *Elucidation of the mechanism enabling tumor selective prodrug monotherapy.* Cancer Res, 1998. **58**(6): p. 1195-201.

193. Huang, P.T., *et al.*, *Enhancement of CPT-11 antitumor activity by adenovirus-mediated expression of beta-glucuronidase in tumors.* Cancer Gene Ther, 2011. **18**(6): p. 381-9.

194. Takakura, A., *et al.*, *Rapid deconjugation of SN-38 glucuronide and adsorption of released free SN-38 by intestinal microorganisms in rat.* Oncol Lett, 2012. **3**(3): p. 520-524.

195. Saliba, F., *et al.*, *Pathophysiology and therapy of irinotecan-induced delayed-onset diarrhea in patients with advanced colorectal cancer: a prospective assessment.* J Clin Oncol, 1998. **16**(8): p. 2745-51.

196. Chabot, G.G., *et al.*, *Population pharmacokinetics and pharmacodynamics of irinotecan (CPT-11) and active metabolite SN-38 during phase I trials.* Ann Oncol, 1995. **6**(2): p. 141-51.

197. Allegra, C.J., *et al.*, *American Society of Clinical Oncology provisional clinical opinion: testing for KRAS gene mutations in patients with metastatic colorectal carcinoma to predict response to anti-epidermal growth factor receptor monoclonal antibody therapy.* J Clin Oncol, 2009. **27**(12): p. 2091-6.

198. Lievre, A., *et al.*, *KRAS mutation status is predictive of response to cetuximab therapy in colorectal cancer.* Cancer Res, 2006. **66**(8): p. 3992-5.

199. Chau, I., *et al.*, *Gefitinib and irinotecan in patients with fluoropyrimidine-refractory, irinotecan-naive advanced colorectal cancer: a phase I-II study.* Ann Oncol, 2007. **18**(4): p. 730-7.

200. Bajetta, E., *et al.*, *Dose finding study of erlotinib combined to capecitabine and irinotecan in pretreated advanced colorectal cancer patients.* Cancer Chemother Pharmacol, 2009. **64**(1): p. 67-72.

201. Martins, S.F., *et al.*, *Clinicopathological correlation and prognostic significance of VEGF-A, VEGF-C, VEGFR-2 and VEGFR-3 expression in colorectal cancer.* Cancer Genomics Proteomics, 2013. **10**(2): p. 55-67.

202. Wilkinson, N.W., *et al.*, *Long-term survival results of surgery alone versus surgery plus 5-fluorouracil and leucovorin for stage II and stage III colon cancer: pooled analysis of NSABP C-01 through C-05. A baseline from which to compare modern adjuvant trials.* Ann Surg Oncol, 2010. **17**(4): p. 959-66.

203. Kopetz, S., *et al.*, *Improved survival in metastatic colorectal cancer is associated with adoption of hepatic resection and improved chemotherapy.* J Clin Oncol, 2009. **27**(22): p. 3677-83.

204. Wolmark, N., *et al.*, *The benefit of leucovorin-modulated fluorouracil as postoperative adjuvant therapy for primary colon cancer: results from National Surgical Adjuvant Breast and Bowel Project protocol C-03.* J Clin Oncol, 1993. **11**(10): p. 1879-87.

205. Trials, I.M.P.A.o.C.C., *Efficacy of adjuvant fluorouracil and folinic acid in colon cancer. International Multicentre Pooled Analysis of Colon Cancer Trials (IMPACT) investigators.* Lancet, 1995. **345**(8955): p. 939-44.

206. Haller, D.G., *et al.*, *Phase III study of fluorouracil, leucovorin, and levamisole in high-risk stage II and III colon cancer: final report of Intergroup 0089.* J Clin Oncol, 2005. **23**(34): p. 8671-8.

207. Andre, T., *et al.*, *Phase III study comparing a semimonthly with a monthly regimen of fluorouracil and leucovorin as adjuvant treatment for stage II and III colon cancer patients: final results of GERCOR C96.1.* J Clin Oncol, 2007. **25**(24): p. 3732-8.

208. Andre, T., *et al.*, *Improved overall survival with oxaliplatin, fluorouracil, and leucovorin as adjuvant treatment in stage II or III colon cancer in the MOSAIC trial.* J Clin Oncol, 2009. **27**(19): p. 3109-16.

209. Kuebler, J.P., *et al.*, *Oxaliplatin combined with weekly bolus fluorouracil and leucovorin as surgical adjuvant chemotherapy for stage II and III colon cancer: results from NSABP C-07.* J Clin Oncol, 2007. **25**(16): p. 2198-204.

210. Van Cutsem, E., *et al.*, *Randomized phase III trial comparing biweekly infusional fluorouracil/leucovorin alone or with irinotecan in the adjuvant treatment of stage III colon cancer: PETACC-3.* J Clin Oncol, 2009. **27**(19): p. 3117-25.

211. Saltz, L.B., *et al.*, *Irinotecan fluorouracil plus leucovorin is not superior to fluorouracil plus leucovorin alone as adjuvant treatment for stage III colon cancer: results of CALGB 89803.* J Clin Oncol, 2007. **25**(23): p. 3456-61.

212. Ychou, M., *et al.*, *A phase III randomised trial of LV5FU2 + irinotecan versus LV5FU2 alone in adjuvant high-risk colon cancer (FNCLCC Accord02/FFCD9802).* Ann Oncol, 2009. **20**(4): p. 674-80.

213. Saltz, L.B., *et al.*, *Irinotecan plus fluorouracil and leucovorin for metastatic colorectal cancer. Irinotecan Study Group.* N Engl J Med, 2000. **343**(13): p. 905-14.

214. Foxtrot Collaborative, G., *Feasibility of preoperative chemotherapy for locally advanced, operable colon cancer: the pilot phase of a randomised controlled trial.* Lancet Oncol, 2012. **13**(11): p. 1152-60.

215. Portier, G., *et al.*, *Multicenter randomized trial of adjuvant fluorouracil and folinic acid compared with surgery alone after resection of colorectal liver metastases: FFCD ACHBTH AURC 9002 trial.* J Clin Oncol, 2006. **24**(31): p. 4976-82.

216. Mitry, E., *et al.*, *Adjuvant chemotherapy after potentially curative resection of metastases from colorectal cancer: a pooled analysis of two randomized trials.* J Clin Oncol, 2008. **26**(30): p. 4906-11.

217. Ychou, M., *et al.*, *A randomized phase III study comparing adjuvant 5-fluorouracil/folinic acid with FOLFIRI in patients following complete resection of liver metastases from colorectal cancer.* Ann Oncol, 2009. **20**(12): p. 1964-70.

218. Wein, A., *et al.*, *Neoadjuvant treatment with weekly high-dose 5-Fluorouracil as 24-hour infusion, folinic acid and oxaliplatin in patients with primary resectable liver metastases of colorectal cancer.* Oncology, 2003. **64**(2): p. 131-8.

219. Taieb, J., *et al.*, *Intensive systemic chemotherapy combined with surgery for metastatic colorectal cancer: results of a phase II study.* J Clin Oncol, 2005. **23**(3): p. 502-9.

220. Adam, R., *et al.*, *Is perioperative chemotherapy useful for solitary, metachronous, colorectal liver metastases?* Ann Surg, 2010. **252**(5): p. 774-87.

221. Nordlinger, B., *et al.*, *Perioperative chemotherapy with FOLFOX4 and surgery versus surgery alone for resectable liver metastases from colorectal cancer (EORTC Intergroup trial 40983): a randomised controlled trial.* Lancet, 2008. **371**(9617): p. 1007-16.

222. Nordlinger, B., *et al.*, *Perioperative FOLFOX4 chemotherapy and surgery versus surgery alone for resectable liver metastases from colorectal cancer (EORTC 40983): long-term results of a randomised, controlled, phase 3 trial.* Lancet Oncol, 2013. **14**(12): p. 1208-15.

223. Adam, R., *et al.*, *Five-year survival following hepatic resection after neoadjuvant therapy for nonresectable colorectal.* Ann Surg Oncol, 2001. **8**(4): p. 347-53.

224. Folprecht, G., *et al.*, *Survival of patients with initially unresectable colorectal liver metastases treated with FOLFOX/cetuximab or FOLFIRI/cetuximab in a multidisciplinary concept (CELIM study).* Ann Oncol, 2014. **25**(5): p. 1018-25.

225. Capussotti, L., *et al.*, *Neoadjuvant chemotherapy and resection for initially irresectable colorectal liver metastases.* Br J Surg, 2006. **93**(8): p. 1001-6.

226. Tournigand, C., *et al.*, *FOLFIRI followed by FOLFOX6 or the reverse sequence in advanced colorectal cancer: a randomized GERCOR study.* J Clin Oncol, 2004. **22**(2): p. 229-37.

227. Sobrero, A.F., *et al.*, *EPIC: phase III trial of cetuximab plus irinotecan after fluoropyrimidine and oxaliplatin failure in patients with metastatic colorectal cancer.* J Clin Oncol, 2008. **26**(14): p. 2311-9.

228. Bokemeyer, C., *et al.*, *Efficacy according to biomarker status of cetuximab plus FOLFOX-4 as first-line treatment for metastatic colorectal cancer: the OPUS study.* Ann Oncol, 2011. **22**(7): p. 1535-46.

229. Van Cutsem, E., *et al.*, *Cetuximab and chemotherapy as initial treatment for metastatic colorectal cancer.* N Engl J Med, 2009. **360**(14): p. 1408-17.

230. Van Cutsem, E., *et al.*, *Cetuximab plus irinotecan, fluorouracil, and leucovorin as first-line treatment for metastatic colorectal cancer: updated analysis of overall survival according to tumor KRAS and BRAF mutation status.* J Clin Oncol, 2011. **29**(15): p. 2011-9.

231. Bokemeyer, C., *et al.*, *Addition of cetuximab to chemotherapy as first-line treatment for KRAS wild-type metastatic colorectal cancer: pooled analysis of the CRYSTAL and OPUS randomised clinical trials.* Eur J Cancer, 2012. **48**(10): p. 1466-75.

232. Grothey, A., *et al.*, *Bevacizumab beyond first progression is associated with prolonged overall survival in metastatic colorectal cancer: results from a large observational cohort study (BRiTE).* J Clin Oncol, 2008. **26**(33): p. 5326-34.

233. Hurwitz, H., *et al.*, *Bevacizumab plus irinotecan, fluorouracil, and leucovorin for metastatic colorectal cancer.* N Engl J Med, 2004. **350**(23): p. 2335-42.

234. Heinemann, V., *et al.*, *FOLFIRI plus cetuximab versus FOLFIRI plus bevacizumab as first-line treatment for patients with metastatic colorectal cancer (FIRE-3): a randomised, open-label, phase 3 trial.* Lancet Oncol, 2014. **15**(10): p. 1065-75.

235. Geiger-Gritsch, S., *et al.*, *Safety of bevacizumab in patients with advanced cancer: a meta-analysis of randomized controlled trials.* Oncologist, 2010. **15**(11): p. 1179-91.

236. Braun, M.S., *et al.*, *Predictive biomarkers of chemotherapy efficacy in colorectal cancer: results from the UK MRC FOCUS trial.* J Clin Oncol, 2008. **26**(16): p. 2690-8.

237. Sargent, D.J., *et al.*, *Defective mismatch repair as a predictive marker for lack of efficacy of fluorouracil-based adjuvant therapy in colon cancer.* J Clin Oncol, 2010. **28**(20): p. 3219-26.

238. Marin, J.J., *et al.*, *Chemoprevention, chemotherapy, and chemoresistance in colorectal cancer.* Drug Metab Rev, 2012. **44**(2): p. 148-72.

239. Jaiswal, A.K., *Nrf2 signaling in coordinated activation of antioxidant gene expression.* Free Radic Biol Med, 2004. **36**(10): p. 1199-207.

240. Reddy, N.M., *et al.*, *Genetic dissection of the Nrf2-dependent redox signaling-regulated transcriptional programs of cell proliferation and cytoprotection.* Physiol Genomics, 2007. **32**(1): p. 74-81.

241. Tong, K.I., *et al.*, *Two-site substrate recognition model for the Keap1-Nrf2 system: a hinge and latch mechanism.* Biol Chem, 2006. **387**(10-11): p. 1311-20.

242. McMahon, M., *et al.*, *Dimerization of substrate adaptors can facilitate cullin-mediated ubiquitylation of proteins by a "tethering" mechanism: a two-site interaction model for the Nrf2-Keap1 complex.* J Biol Chem, 2006. **281**(34): p. 24756-68.

243. Baird, L., *et al.*, *Regulatory flexibility in the Nrf2-mediated stress response is conferred by conformational cycling of the Keap1-Nrf2 protein complex.* Proc Natl Acad Sci U S A, 2013. **110**(38): p. 15259-64.

244. Kundu, J.K. and Y.J. Surh, *Inflammation: gearing the journey to cancer.* Mutat Res, 2008. **659**(1-2): p. 15-30.

245. Kensler, T.W., N. Wakabayashi, and S. Biswal, *Cell survival responses to environmental stresses via the Keap1-Nrf2-ARE pathway.* Annu Rev Pharmacol Toxicol, 2007. **47**: p. 89-116.

246. Zhuang, C.L., *et al.*, *Ginsenoside Rb1 improves postoperative fatigue syndrome by reducing skeletal muscle oxidative stress through activation of the PI3K/Akt/Nrf2 pathway in aged rats.* Eur J Pharmacol, 2014. **740**: p. 480-7.

247. Li, L., *et al.*, *Nrf2/ARE pathway activation, HO-1 and NQO1 induction by polychlorinated biphenyl quinone is associated with reactive oxygen species and PI3K/AKT signaling.* Chem Biol Interact, 2014. **209**: p. 56-67.

248. Kang, K.W., *et al.*, *Phosphatidylinositol 3-kinase regulates nuclear translocation of NF-E2-related factor 2 through actin rearrangement in response to oxidative stress.* Mol Pharmacol, 2002. **62**(5): p. 1001-10.

249. Tao, S., *et al.*, *Oncogenic KRAS confers chemoresistance by upregulating NRF2.* Cancer Res, 2014. **74**(24): p. 7430-41.

250. Yamadori, T., *et al.*, *Molecular mechanisms for the regulation of Nrf2-mediated cell proliferation in non-small-cell lung cancers.* Oncogene, 2012. **31**(45): p. 4768-77.

251. DeNicola, G.M., *et al.*, *Oncogene-induced Nrf2 transcription promotes ROS detoxification and tumorigenesis.* Nature, 2011. **475**(7354): p. 106-9.

252. Hybertson, B.M. and B. Gao, *Role of the Nrf2 signaling system in health and disease.* Clin Genet, 2014. **86**(5): p. 447-52.

253. Pergola, P.E., *et al.*, *Bardoxolone methyl and kidney function in CKD with type 2 diabetes.* N Engl J Med, 2011. **365**(4): p. 327-36.

254. de Zeeuw, D., *et al.*, *Bardoxolone methyl in type 2 diabetes and stage 4 chronic kidney disease.* N Engl J Med, 2013. **369**(26): p. 2492-503.

255. Liu, J., *et al.*, *Nrf2 protection against liver injury produced by various hepatotoxicants.* Oxid Med Cell Longev, 2013. **2013**: p. 305861.

256. Ramos-Gomez, M., *et al.*, *Sensitivity to carcinogenesis is increased and chemoprotective efficacy of enzyme inducers is lost in nrf2 transcription factor-deficient mice.* Proc Natl Acad Sci U S A, 2001. **98**(6): p. 3410-5.

257. Iida, K., *et al.*, *Nrf2 is essential for the chemopreventive efficacy of oltipraz against urinary bladder carcinogenesis.* Cancer Res, 2004. **64**(18): p. 6424-31.

258. Xu, C., *et al.*, *Inhibition of 7,12-dimethylbenz(a)anthracene-induced skin tumorigenesis in C57BL/6 mice by sulforaphane is mediated by nuclear factor E2-related factor 2.* Cancer Res, 2006. **66**(16): p. 8293-6.

259. Osburn, W.O., *et al.*, *Increased colonic inflammatory injury and formation of aberrant crypt foci in Nrf2-deficient mice upon dextran sulfate treatment.* Int J Cancer, 2007. **121**(9): p. 1883-91.

260. Khor, T.O., *et al.*, *Nrf2-deficient mice have an increased susceptibility to dextran sulfate sodium-induced colitis.* Cancer Res, 2006. **66**(24): p. 11580-4.

261. Khor, T.O., *et al.*, *Increased susceptibility of Nrf2 knockout mice to colitis-associated colorectal cancer.* Cancer Prev Res (Phila), 2008. **1**(3): p. 187-91.

262. Huang, C.F., *et al.*, *Clinical significance of Keap1 and Nrf2 in oral squamous cell carcinoma.* PLoS One, 2013. **8**(12): p. e83479.

263. Solis, L.M., *et al.*, *Nrf2 and Keap1 abnormalities in non-small cell lung carcinoma and association with clinicopathologic features.* Clin Cancer Res, 2010. **16**(14): p. 3743-53.

264. Shibata, T., *et al.*, *Genetic alteration of Keap1 confers constitutive Nrf2 activation and resistance to chemotherapy in gallbladder cancer.* Gastroenterology, 2008. **135**(4): p. 1358-1368, 1368.e1-4.

265. Konstantinopoulos, P.A., *et al.*, *Keap1 mutations and Nrf2 pathway activation in epithelial ovarian cancer.* Cancer Res, 2011. **71**(15): p. 5081-9.

266. Park, J.Y., Y.W. Kim, and Y.K. Park, *Nrf2 expression is associated with poor outcome in osteosarcoma.* Pathology, 2012. **44**(7): p. 617-21.

267. Hartikainen, J.M., *et al.*, *Genetic polymorphisms and protein expression of NRF2 and Sulfiredoxin predict survival outcomes in breast cancer.* Cancer Res, 2012. **72**(21): p. 5537-46.

268. Hayden, A., *et al.*, *The Nrf2 transcription factor contributes to resistance to cisplatin in bladder cancer.* Urol Oncol, 2014. **32**(6): p. 806-14.

269. Hu, X.F., *et al.*, *Nrf2 overexpression predicts prognosis and 5-FU resistance in gastric cancer.* Asian Pac J Cancer Prev, 2013. **14**(9): p. 5231-5.

270. Soini, Y., *et al.*, *Nuclear Nrf2 expression is related to a poor survival in pancreatic adenocarcinoma.* Pathol Res Pract, 2014. **210**(1): p. 35-9.

271. Ji, L., *et al.*, *Correlation of Nrf2, NQO1, MRP1, cmyc and p53 in colorectal cancer and their relationships to clinicopathologic features and survival.* Int J Clin Exp Pathol, 2014. **7**(3): p. 1124-31.

272. Kang, K.A., *et al.*, *Epigenetic modification of Nrf2 in 5-fluorouracil-resistant colon cancer cells: involvement of TET-dependent DNA demethylation.* Cell Death Dis, 2014. **5**: p. e1183.

273. Akhdar, H., *et al.*, *Involvement of Nrf2 activation in resistance to 5-fluorouracil in human colon cancer HT-29 cells.* Eur J Cancer, 2009. **45**(12): p. 2219-27.

274. Yoo, N.J., *et al.*, *Somatic mutations of the KEAP1 gene in common solid cancers.* Histopathology, 2012. **60**(6): p. 943-52.

275. Kim, Y.R., *et al.*, *Oncogenic NRF2 mutations in squamous cell carcinomas of oesophagus and skin.* J Pathol, 2010. **220**(4): p. 446-51.

276. Hanada, N., *et al.*, *Methylation of the KEAP1 gene promoter region in human colorectal cancer.* BMC Cancer, 2012. **12**: p. 66.

277. Maruichi, T., *et al.*, *Transcriptional regulation of human carboxylesterase 1A1 by nuclear factor-erythroid 2 related factor 2 (Nrf2).* Biochem Pharmacol, 2010. **79**(2): p. 288-95.

278. Walsh, J., *et al.*, *Identification and quantification of the basal and inducible Nrf2-dependent proteomes in mouse liver: biochemical, pharmacological and toxicological implications.* J Proteomics, 2014. **108**: p. 171-87.

279. Kitteringham, N.R., *et al.*, *Proteomic analysis of Nrf2 deficient transgenic mice reveals cellular defence and lipid metabolism as primary Nrf2-dependent pathways in the liver.* J Proteomics, 2010. **73**(8): p. 1612-31.

280. Yueh, M.F. and R.H. Tukey, *Nrf2-Keap1 signaling pathway regulates human UGT1A1 expression in vitro and in transgenic UGT1 mice.* J Biol Chem, 2007. **282**(12): p. 8749-58.

281. Wang, M., *et al.*, *Effects of co-treatment with sulforaphane and autophagy modulators on uridine 5'-diphospho-glucuronosyltransferase 1A isoforms and cytochrome P450 3A4 expression in Caco-2 human colon cancer cells.* Oncol Lett, 2014. **8**(6): p. 2407-2416.

282. Buckley, D.B. and C.D. Klaassen, *Induction of mouse UDP-glucuronosyltransferase mRNA expression in liver and intestine by activators of aryl-hydrocarbon receptor, constitutive androstane receptor, pregnane X receptor, peroxisome proliferator-activated receptor alpha, and nuclear factor erythroid 2-related factor 2.* Drug Metab Dispos, 2009. **37**(4): p. 847-56.

283. Adachi, T., *et al.*, *Nrf2-dependent and -independent induction of ABC transporters ABCC1, ABCC2, and ABCG2 in HepG2 cells under oxidative stress.* J Exp Ther Oncol, 2007. **6**(4): p. 335-48.

284. Balstad, T.R., *et al.*, *Coffee, broccoli and spices are strong inducers of electrophile response element-dependent transcription in vitro and in vivo - studies in electrophile response element transgenic mice.* Mol Nutr Food Res, 2011. **55**(2): p. 185-97.

285. Nair, S., W. Li, and A.N. Kong, *Natural dietary anti-cancer chemopreventive compounds: redox-mediated differential signaling mechanisms in cytoprotection of normal cells versus cytotoxicity in tumor cells.* Acta Pharmacol Sin, 2007. **28**(4): p. 459-72.

286. Wang, Y.Y., *et al.*, *Bardoxolone methyl (CDDO-Me) as a therapeutic agent: an update on its pharmacokinetic and pharmacodynamic properties.* Drug Des Devel Ther, 2014. **8**: p. 2075-88.

287. Honda, T., *et al.*, *Design and synthesis of 2-cyano-3,12-dioxoolean-1,9-dien-28-oic acid, a novel and highly active inhibitor of nitric oxide production in mouse macrophages.* Bioorg Med Chem Lett, 1998. **8**(19): p. 2711-4.

288. Yates, M.S., *et al.*, *Pharmacodynamic characterization of chemopreventive triterpenoids as exceptionally potent inducers of Nrf2-regulated genes.* Mol Cancer Ther, 2007. **6**(1): p. 154-62.

289. Wang, Y.Y., H. Zhe, and R. Zhao, *Preclinical evidences toward the use of triterpenoid CDDO-Me for solid cancer prevention and treatment.* Mol Cancer, 2014. **13**: p. 30.

290. Hong, D.S., *et al.*, *A phase I first-in-human trial of bardoxolone methyl in patients with advanced solid tumors and lymphomas.* Clin Cancer Res, 2012. **18**(12): p. 3396-406.

291. Gao, A.M., *et al.*, *Chrysin enhances sensitivity of BEL-7402/ADM cells to doxorubicin by suppressing PI3K/Akt/Nrf2 and ERK/Nrf2 pathway.* Chem Biol Interact, 2013. **206**(1): p. 100-8.

292. Tang, X., *et al.*, *Luteolin inhibits Nrf2 leading to negative regulation of the Nrf2/ARE pathway and sensitization of human lung carcinoma A549 cells to therapeutic drugs.* Free Radic Biol Med, 2011. **50**(11): p. 1599-609.

293. Liu, J.H., *et al.*, *A new triterpenoid from Brucea javanica.* Arch Pharm Res, 2009. **32**(5): p. 661-6.

294. Ren, D., *et al.*, *Brusatol enhances the efficacy of chemotherapy by inhibiting the Nrf2-mediated defense mechanism.* Proc Natl Acad Sci U S A, 2011. **108**(4): p. 1433-8.

295. Zhao, M., *et al.*, *Seven quassinoids from Fructus Bruceae with cytotoxic effects on pancreatic adenocarcinoma cell lines.* Phytother Res, 2011. **25**(12): p. 1796-800.

296. Sharpless, N.E. and R.A. Depinho, *The mighty mouse: genetically engineered mouse models in cancer drug development.* Nat Rev Drug Discov, 2006. **5**(9): p. 741-54.

297. Roper, J. and K.E. Hung, *Priceless GEMMs: genetically engineered mouse models for colorectal cancer drug development.* Trends Pharmacol Sci, 2012. **33**(8): p. 449-55.

298. Anisimov, V.N., *et al.*, *Long-live euthymic BALB/c-nu mice. II: spontaneous tumors and other pathologies.* Mech Ageing Dev, 2001. **122**(5): p. 477-89.

299. Miyamoto, M. and Y. Tani, *A study on colon cancer-prone rats of WF-Osaka strain.* Med J Osaka Univ, 1989. **38**(1-4): p. 1-12.

300. Miyamoto, M., *et al.*, *Morphology on spontaneous regression of the autochthonous colon carcinoma in WF Osaka rat strain.* Med J Osaka Univ, 1989. **38**(1-4): p. 19-25.

301. Laqueur, G.L., *Carcinogenic effects of cycad meal and cycasin, methylazoxymethanol glycoside, in rate and effects of cycasin in germfree rats.* Fed Proc, 1964. **23**: p. 1386-8.

302. Fiala, E.S., *Investigations into the metabolism and mode of action of the colon carcinogens 1,2-dimethylhydrazine and azoxymethane.* Cancer, 1977. **40**(5 Suppl): p. 2436-45.

303. Yamada, Y., *et al.*, *Frequent beta-catenin gene mutations and accumulations of the protein in the putative preneoplastic lesions lacking macroscopic aberrant crypt foci appearance, in rat colon carcinogenesis.* Cancer Res, 2000. **60**(13): p. 3323-7.

304. Neufert, C., C. Becker, and M.F. Neurath, *An inducible mouse model of colon carcinogenesis for the analysis of sporadic and inflammation-driven tumor progression.* Nat Protoc, 2007. **2**(8): p. 1998-2004.

305. Rosenberg, D.W., C. Giardina, and T. Tanaka, *Mouse models for the study of colon carcinogenesis.* Carcinogenesis, 2009. **30**(2): p. 183-96.

306. Long, M., *et al.*, *Nrf2-dependent suppression of azoxymethane/dextran sulfate sodium-induced colon carcinogenesis by the cinnamon-derived dietary factor cinnamaldehyde.* Cancer Prev Res (Phila), 2015. **8**(5): p. 444-54.

307. Kato, R., *Metabolic activation of mutagenic heterocyclic aromatic amines from protein pyrolysates.* Crit Rev Toxicol, 1986. **16**(4): p. 307-48.

308. Nakagama, H., M. Nakanishi, and M. Ochiai, *Modeling human colon cancer in rodents using a food-borne carcinogen, PhIP.* Cancer Sci, 2005. **96**(10): p. 627-36.

309. Ito, N., *et al.*, *A new colon and mammary carcinogen in cooked food, 2-amino-1-methyl-6-phenylimidazo[4,5-b]pyridine (PhIP).* Carcinogenesis, 1991. **12**(8): p. 1503-6.

310. Canene-Adams, K., *et al.*, *Dietary chemoprevention of PhIP induced carcinogenesis in male Fischer 344 rats with tomato and broccoli.* PLoS One, 2013. **8**(11): p. e79842.

311. Toyota, M., *et al.*, *Genetic alterations in rat colon tumors induced by heterocyclic amines.* Cancer, 1996. **77**(8 Suppl): p. 1593-7.

312. Sugimura, T. and S. Fujimura, *Tumour production in glandular stomach of rat by N-methyl-N'-nitro-N-nitrosoguanidine.* Nature, 1967. **216**(5118): p. 943-4.

313. Narisawa, T., *et al.*, *Carcinoma of the colon and rectum of rats by rectal infusion of N-methyl-N'-nitro-N-nitrosoguanidine.* Gann, 1971. **62**(3): p. 231-4.

314. So, B.T., N.E. Magadia, and E.L. Wynder, *Induction of carcinomas of the colon and rectum in rats by intrarectal instillation of N-methyl-N'-nitro-N-nitrosoguanidine.* J Natl Cancer Inst, 1973. **50**(4): p. 927-32.

315. Nakayama, Y., *et al.*, *Chemopreventive effect of 4-[3,5-Bis(trimethylsilyl) benzamido] benzoic acid (TAC-101) on MNU-induced colon carcinogenesis in a rat model.* Anticancer Res, 2009. **29**(6): p. 2059-65.

316. Perse, M. and A. Cerar, *Morphological and molecular alterations in 1,2 dimethylhydrazine and azoxymethane induced colon carcinogenesis in rats.* J Biomed Biotechnol, 2011. **2011**: p. 473964.

317. Kishimoto, Y., *et al.*, *Effects of cyclooxygenase-2 inhibitor NS-398 on APC and c-myc expression in rat colon carcinogenesis induced by azoxymethane.* J Gastroenterol, 2002. **37**(3): p. 186-93.

318. Tuominen, I., *et al.*, *Diet-induced obesity promotes colon tumor development in azoxymethane-treated mice.* PLoS One, 2013. **8**(4): p. e60939.

319. Kobaek-Larsen, M., *et al.*, *Review of colorectal cancer and its metastases in rodent models: comparative aspects with those in humans.* Comp Med, 2000. **50**(1): p. 16-26.

320. Derry, M.M., *et al.*, *Characterization of azoxymethane-induced colon tumor metastasis to lung in a mouse model relevant to human sporadic colorectal cancer and evaluation of grape seed extract efficacy.* Exp Toxicol Pathol, 2014.

321. Bissahoyo, A., *et al.*, *Azoxymethane is a genetic background-dependent colorectal tumor initiator and promoter in mice: effects of dose, route, and diet.* Toxicol Sci, 2005. **88**(2): p. 340-5.

322. Evans, J.P., *et al.*, *From mice to men: Murine models of colorectal cancer for use in translational research.* Crit Rev Oncol Hematol, 2016. **98**: p. 94-105.

323. Kinzler, K.W., *et al.*, *Identification of a gene located at chromosome 5q21 that is mutated in colorectal cancers.* Science, 1991. **251**(4999): p. 1366-70.

324. Korinek, V., *et al.*, *Constitutive transcriptional activation by a beta-catenin-Tcf complex in APC-/- colon carcinoma.* Science, 1997. **275**(5307): p. 1784-7.

325. Moser, A.R., H.C. Pitot, and W.F. Dove, *A dominant mutation that predisposes to multiple intestinal neoplasia in the mouse.* Science, 1990. **247**(4940): p. 322-4.

326. Fodde, R., *et al.*, *A targeted chain-termination mutation in the mouse Apc gene results in multiple intestinal tumors.* Proc Natl Acad Sci U S A, 1994. **91**(19): p. 8969-73.

327. Oshima, M., *et al.*, *Loss of Apc heterozygosity and abnormal tissue building in nascent intestinal polyps in mice carrying a truncated Apc gene.* Proc Natl Acad Sci U S A, 1995. **92**(10): p. 4482-6.

328. Aoki, K., *et al.*, *Colonic polyposis caused by mTOR-mediated chromosomal instability in Apc+/Delta716 Cdx2+/- compound mutant mice.* Nat Genet, 2003. **35**(4): p. 323-30.

329. Takaku, K., *et al.*, *Intestinal tumorigenesis in compound mutant mice of both Dpc4 (Smad4) and Apc genes.* Cell, 1998. **92**(5): p. 645-56.

330. Batlle, E., *et al.*, *EphB receptor activity suppresses colorectal cancer progression.* Nature, 2005. **435**(7045): p. 1126-30.

331. Dopeso, H., *et al.*, *The receptor tyrosine kinase EPHB4 has tumor suppressor activities in intestinal tumorigenesis.* Cancer Res, 2009. **69**(18): p. 7430-8.

332. Petrova, T.V., *et al.*, *Transcription factor PROX1 induces colon cancer progression by promoting the transition from benign to highly dysplastic phenotype.* Cancer Cell, 2008. **13**(5): p. 407-19.

333. Edelmann, W., *et al.*, *Mutation in the mismatch repair gene Msh6 causes cancer susceptibility.* Cell, 1997. **91**(4): p. 467-77.

334. Edelmann, W., *et al.*, *Tumorigenesis in Mlh1 and Mlh1/Apc1638N mutant mice.* Cancer Res, 1999. **59**(6): p. 1301-7.

335. Edelmann, L. and W. Edelmann, *Loss of DNA mismatch repair function and cancer predisposition in the mouse: animal models for human hereditary nonpolyposis colorectal cancer.* Am J Med Genet C Semin Med Genet, 2004. **129c**(1): p. 91-9.

336. Kuraguchi, M., *et al.*, *The distinct spectra of tumor-associated Apc mutations in mismatch repair-deficient Apc1638N mice define the roles of MSH3 and MSH6 in DNA repair and intestinal tumorigenesis.* Cancer Res, 2001. **61**(21): p. 7934-42.

337. Shibata, H., *et al.*, *Rapid colorectal adenoma formation initiated by conditional targeting of the Apc gene.* Science, 1997. **278**(5335): p. 120-3.

338. Saam, J.R. and J.I. Gordon, *Inducible gene knockouts in the small intestinal and colonic epithelium.* J Biol Chem, 1999. **274**(53): p. 38071-82.

339. Robanus-Maandag, E.C., *et al.*, *A new conditional Apc-mutant mouse model for colorectal cancer.* Carcinogenesis, 2010. **31**(5): p. 946-52.

340. el Marjou, F., *et al.*, *Tissue-specific and inducible Cre-mediated recombination in the gut epithelium.* Genesis, 2004. **39**(3): p. 186-93.

341. Haigis, K.M., *et al.*, *Differential effects of oncogenic K-Ras and N-Ras on proliferation, differentiation and tumor progression in the colon.* Nat Genet, 2008. **40**(5): p. 600-8.

342. Trobridge, P., *et al.*, *TGF-beta receptor inactivation and mutant Kras induce intestinal neoplasms in mice via a beta-catenin-independent pathway.* Gastroenterology, 2009. **136**(5): p. 1680-8.e7.

343. Kucherlapati, M.H., *et al.*, *An Msh2 conditional knockout mouse for studying intestinal cancer and testing anticancer agents.* Gastroenterology, 2010. **138**(3): p. 993-1002.e1.

344. Babaei-Jadidi, R., *et al.*, *FBXW7 influences murine intestinal homeostasis and cancer, targeting Notch, Jun, and DEK for degradation.* J Exp Med, 2011. **208**(2): p. 295-312.

345. Hioki, K., *et al.*, *Suppression of intestinal polyp development by low-fat and high-fiber diet in Apc(delta716) knockout mice.* Carcinogenesis, 1997. **18**(10): p. 1863-5.

346. Taketo, M.M., *Cyclooxygenase-2 inhibitors in tumorigenesis (Part II).* J Natl Cancer Inst, 1998. **90**(21): p. 1609-20.

347. Chulada, P.C., *et al.*, *Genetic disruption of Ptgs-1, as well as Ptgs-2, reduces intestinal tumorigenesis in Min mice.* Cancer Res, 2000. **60**(17): p. 4705-8.

348. Steinbach, G., *et al.*, *The effect of celecoxib, a cyclooxygenase-2 inhibitor, in familial adenomatous polyposis.* N Engl J Med, 2000. **342**(26): p. 1946-52.

349. Dangles-Marie, V., *et al.*, *Establishment of human colon cancer cell lines from fresh tumors versus xenografts: comparison of success rate and cell line features.* Cancer Res, 2007. **67**(1): p. 398-407.

350. Cho, Y.B., *et al.*, *Colorectal cancer patient-derived xenografted tumors maintain characteristic features of the original tumors.* J Surg Res, 2014. **187**(2): p. 502-9.

351. Kruse, J., *et al.*, *Macrophages promote tumour growth and liver metastasis in an orthotopic syngeneic mouse model of colon cancer.* Int J Colorectal Dis, 2013. **28**(10): p. 1337-49.

352. Lechner, M.G., *et al.*, *Immunogenicity of murine solid tumor models as a defining feature of in vivo behavior and response to immunotherapy.* J Immunother, 2013. **36**(9): p. 477-89.

353. Hemmerle, T. and D. Neri, *The antibody-based targeted delivery of interleukin-4 and 12 to the tumor neovasculature eradicates tumors in three mouse models of cancer.* Int J Cancer, 2014. **134**(2): p. 467-77.

354. Nakamura, S., *et al.*, *TGF-beta1 in tumor microenvironments induces immunosuppression in the tumors and sentinel lymph nodes and promotes tumor progression.* J Immunother, 2014. **37**(2): p. 63-72.

355. Sasaki, T., *et al.*, *Serum CD10 is associated with liver metastasis in colorectal cancer.* J Surg Res, 2014.

356. Senger, S., *et al.*, *Darbepoetin-alpha Accelerates Neovascularization and Engraftment of Extrahepatic Colorectal Metastases.* Eur Surg Res, 2014. **53**(1-4): p. 25-36.

357. Badiola, I., *et al.*, *Discoidin domain receptor 2 deficiency predisposes hepatic tissue to colon carcinoma metastasis.* Gut, 2012. **61**(10): p. 1465-72.

358. Robinson, S.M., *et al.*, *The potential contribution of tumour-related factors to the development of FOLFOX-induced sinusoidal obstruction syndrome.* Br J Cancer, 2013. **109**(9): p. 2396-403.

359. de Heer, P., *et al.*, *Celecoxib inhibits growth of tumors in a syngeneic rat liver metastases model for colorectal cancer.* Cancer Chemother Pharmacol, 2008. **62**(5): p. 811-9.

360. Boni, L., *et al.*, *Injection of colorectal cancer cells in mesenteric and antimesenteric sides of the colon results in different patterns of metastatic diffusion: an experimental study in rats.* World J Surg Oncol, 2005. **3**: p. 69.

361. Kyriazis, A.P., *et al.*, *Growth patterns and metastatic behavior of human tumors growing in athymic mice.* Cancer Res, 1978. **38**(10): p. 3186-90.

362. Giavazzi, R., *et al.*, *Metastatic behavior of tumor cells isolated from primary and metastatic human colorectal carcinomas implanted into different sites in nude mice.* Cancer Res, 1986. **46**(4 Pt 2): p. 1928-33.

363. Bresalier, R.S., *et al.*, *An animal model for colon cancer metastasis: establishment and characterization of murine cell lines with enhanced liver-metastasizing ability.* Cancer Res, 1987. **47**(5): p. 1398-406.

364. Goi, T., *et al.*, *The anti-tumor effect is enhanced by simultaneously targeting VEGF and PROK1 in colorectal cancer.* Oncotarget, 2015.

365. Duquet, A., *et al.*, *A novel genome-wide in vivo screen for metastatic suppressors in human colon cancer identifies the positive WNT-TCF pathway modulators TMED3 and SOX12.* EMBO Mol Med, 2014. **6**(7): p. 882-901.

366. Zhou, Y., *et al.*, *Spontaneous genomic alterations in a chimeric model of colorectal cancer enable metastasis and guide effective combinatorial therapy.* PLoS One, 2014. **9**(8): p. e105886.

367. Tseng, W., X. Leong, and E. Engleman, *Orthotopic mouse model of colorectal cancer.* J Vis Exp, 2007(10): p. 484.

368. Seguin, J., *et al.*, *Evaluation of Nonradiative Clinical Imaging Techniques for the Longitudinal Assessment of Tumour Growth in Murine CT26 Colon Carcinoma.* Int J Mol Imaging, 2013. **2013**: p. 983534.

369. Kashtan, H., *et al.*, *Intra-rectal injection of tumour cells: a novel animal model of rectal cancer.* Surg Oncol, 1992. **1**(3): p. 251-6.

370. Donigan, M., *et al.*, *Novel murine model for colon cancer: non-operative trans-anal rectal injection.* J Surg Res, 2009. **154**(2): p. 299-303.

371. Goldrosen, M.H., *Murine colon adenocarcinoma: immunobiology of metastases.* Cancer, 1980. **45**(5 Suppl): p. 1223-8.

372. Flatmark, K., *et al.*, *Twelve colorectal cancer cell lines exhibit highly variable growth and metastatic capacities in an orthotopic model in nude mice.* Eur J Cancer, 2004. **40**(10): p. 1593-8.

373. Cespedes, M.V., *et al.*, *Orthotopic microinjection of human colon cancer cells in nude mice induces tumor foci in all clinically relevant metastatic sites.* Am J Pathol, 2007. **170**(3): p. 1077-85.

374. Donigan, M., *et al.*, *A metastatic colon cancer model using nonoperative transanal rectal injection.* Surg Endosc, 2010. **24**(3): p. 642-7.

375. Tao, L., *et al.*, *Weichang'an and 5-fluorouracil suppresses colorectal cancer in a mouse model.* World J Gastroenterol, 2015. **21**(4): p. 1125-39.

376. Puig, I., *et al.*, *A personalized preclinical model to evaluate the metastatic potential of patient-derived colon cancer initiating cells.* Clin Cancer Res, 2013. **19**(24): p. 6787-801.

377. Zhang, Y., *et al.*, *Development and characterization of a reliable mouse model of colorectal cancer metastasis to the liver.* Clin Exp Metastasis, 2013. **30**(7): p. 903-18.

378. Kemeny, N., *Presurgical chemotherapy in patients being considered for liver resection.* Oncologist, 2007. **12**(7): p. 825-39.

379. Gonzalez, M., *et al.*, *Risk factors for survival after lung metastasectomy in colorectal cancer patients: a systematic review and meta-analysis.* Ann Surg Oncol, 2013. **20**(2): p. 572-9.

380. Szabo, V., *et al.*, *Mechanism of tumour vascularization in experimental lung metastases.* J Pathol, 2015. **235**(3): p. 384-96.

381. Garofalo, A., *et al.*, *Comparative study on the metastatic behavior of human tumors in nude, beige/nude/xid and severe combined immunodeficient mice.* Invasion Metastasis, 1993. **13**(2): p. 82-91.

382. Lafreniere, R. and S.A. Rosenberg, *A novel approach to the generation and identification of experimental hepatic metastases in a murine model.* J Natl Cancer Inst, 1986. **76**(2): p. 309-22.

383. Urosevic, J., *et al.*, *Colon cancer cells colonize the lung from established liver metastases through p38 MAPK signalling and PTHLH.* Nat Cell Biol, 2014. **16**(7): p. 685-94.

384. Chang, Y.J., *et al.*, *Combined therapeutic efficacy of Re-liposomes and sorafenib in an experimental colorectal cancer liver metastasis model by intrasplenic injection of C26-murine colon cancer cells.* Mol Clin Oncol, 2014. **2**(3): p. 380-384.

385. Mook, O.R., *et al.*, *Visualization of early events in tumor formation of eGFP-transfected rat colon cancer cells in liver.* Hepatology, 2003. **38**(2): p. 295-304.

386. Cai, S.R., *et al.*, *A mouse model for developing treatment for secondary liver tumors.* Int J Oncol, 2005. **27**(1): p. 113-20.

387. Thalheimer, A., *et al.*, *Noninvasive visualization of tumor growth in a human colorectal liver metastases xenograft model using bioluminescence in vivo imaging.* J Surg Res, 2013. **185**(1): p. 143-51.

388. Wiegering, A., *et al.*, *The impact of pyrvinium pamoate on colon cancer cell viability.* Int J Colorectal Dis, 2014. **29**(10): p. 1189-98.

389. Seol, H.S., *et al.*, *Development and characterization of a colon PDX model that reproduces drug responsiveness and the mutation profiles of its original tumor.* Cancer Lett, 2014. **345**(1): p. 56-64.

390. de Jong, M., J. Essers, and W.M. van Weerden, *Imaging preclinical tumour models: improving translational power.* Nat Rev Cancer, 2014. **14**(7): p. 481-93.

391. Becker, C., M.C. Fantini, and M.F. Neurath, *High resolution colonoscopy in live mice.* Nat Protoc, 2006. **1**(6): p. 2900-4.

392. Waldner, M.J., *et al.*, *Confocal laser endomicroscopy and narrow-band imaging-aided endoscopy for in vivo imaging of colitis and colon cancer in mice.* Nat Protoc, 2011. **6**(9): p. 1471-81.

393. Foersch, S., *et al.*, *VEGFR2 Signaling Prevents Colorectal Cancer Cell Senescence to Promote Tumorigenesis in Mice with Colitis.* Gastroenterology, 2015.

394. Koba, W., L.A. Jelicks, and E.J. Fine, *MicroPET/SPECT/CT imaging of small animal models of disease.* Am J Pathol, 2013. **182**(2): p. 319-24.

395. Xia, J. and L.V. Wang, *Small-animal whole-body photoacoustic tomography: a review.* IEEE Trans Biomed Eng, 2014. **61**(5): p. 1380-9.

396. Zhou, Y., *et al.*, *Calibration-free in vivo transverse blood flowmetry based on cross correlation of slow time profiles from photoacoustic microscopy.* Opt Lett, 2013. **38**(19): p. 3882-5.

397. Chatni, M.R., *et al.*, *Tumor glucose metabolism imaged in vivo in small animals with whole-body photoacoustic computed tomography.* J Biomed Opt, 2012. **17**(7): p. 076012.

398. Filonov, G.S., *et al.*, *Deep-tissue photoacoustic tomography of a genetically encoded near-infrared fluorescent probe.* Angew Chem Int Ed Engl, 2012. **51**(6): p. 1448-51.

399. Wu, L., *et al.*, *A Green Synthesis of Carbon Nanoparticle from Honey for Real-Time Photoacoustic Imaging.* Nano Res, 2013. **6**(5): p. 312-325.

400. Ritman, E.L., *Current status of developments and applications of micro-CT.* Annu Rev Biomed Eng, 2011. **13**: p. 531-52.

401. Greer, L.F., 3rd and A.A. Szalay, *Imaging of light emission from the expression of luciferases in living cells and organisms: a review.* Luminescence, 2002. **17**(1): p. 43-74.

402. Frangioni, J.V., *In vivo near-infrared fluorescence imaging.* Curr Opin Chem Biol, 2003. **7**(5): p. 626-34.

403. Ballou, B., L.A. Ernst, and A.S. Waggoner, *Fluorescence imaging of tumors in vivo.* Curr Med Chem, 2005. **12**(7): p. 795-805.

404. Ho, C.J., *et al.*, *Multifunctional photosensitizer-based contrast agents for photoacoustic imaging.* Sci Rep, 2014. **4**: p. 5342.

405. Edinger, M., *et al.*, *Advancing animal models of neoplasia through in vivo bioluminescence imaging.* Eur J Cancer, 2002. **38**(16): p. 2128-36.

406. Adams, S.T., Jr. and S.C. Miller, *Beyond D-luciferin: expanding the scope of bioluminescence imaging in vivo.* Curr Opin Chem Biol, 2014. **21**: p. 112-20.

407. Griswold, D.P. and T.H. Corbett, *A colon tumor model for anticancer agent evaluation.* Cancer, 1975. **36**(6 Suppl): p. 2441-4.

408. Cory, A.H., *et al.*, *Use of an aqueous soluble tetrazolium/formazan assay for cell growth assays in culture.* Cancer Commun, 1991. **3**(7): p. 207-12.

409. Smith, P.K., *et al.*, *Measurement of protein using bicinchoninic acid.* Anal Biochem, 1985. **150**(1): p. 76-85.

410. Chen, H.Y., *et al.*, *miR-103/107 promote metastasis of colorectal cancer by targeting the metastasis suppressors DAPK and KLF4.* Cancer Res, 2012. **72**(14): p. 3631-41.

411. van der Geest, L.G., *et al.*, *Nationwide trends in incidence, treatment and survival of colorectal cancer patients with synchronous metastases.* Clin Exp Metastasis, 2015. **32**(5): p. 457-65.

412. Limani, P., *et al.*, *Selective portal vein injection for the design of syngeneic models of liver malignancy.* Am J Physiol Gastrointest Liver Physiol, 2016. **310**(9): p. G682-8.

413. Ducrest, A.-L., *et al.*, *Detection of promoter activity by flow cytometric analysis of GFP reporter expression.* Nucleic Acids Research, 2002. **30**(14): p. e65-e65.

414. Yu, Y.A. and A.A. Szalay, *A Renilla luciferase-Aequorea GFP (ruc-gfp) fusion gene construct permits real-time detection of promoter activation by exogenously administered mifepristone in vivo.* Mol Genet Genomics, 2002. **268**(2): p. 169-78.

415. Yamano, S., J. Dai, and A.M. Moursi, *Comparison of transfection efficiency of nonviral gene transfer reagents.* Mol Biotechnol, 2010. **46**(3): p. 287-300.

416. Yalvac, M.E., *et al.*, *Comparison and optimisation of transfection of human dental follicle cells, a novel source of stem cells, with different chemical methods and electro-poration.* Neurochem Res, 2009. **34**(7): p. 1272-7.

417. Anson, D.S., *The use of retroviral vectors for gene therapy-what are the risks? A review of retroviral pathogenesis and its relevance to retroviral vector-mediated gene delivery.* Genet Vaccines Ther, 2004. **2**(1): p. 9.

418. Vorburger, S.A. and K.K. Hunt, *Adenoviral gene therapy.* Oncologist, 2002. **7**(1): p. 46-59.

419. Jinek, M., *et al.*, *A programmable dual-RNA-guided DNA endonuclease in adaptive bacterial immunity.* Science, 2012. **337**(6096): p. 816-21.

420. Tseng, W., X. Leong, and E. Engleman, *Orthotopic Mouse Model of Colorectal Cancer.* Journal of Visualized Experiments : JoVE, 2007(10): p. 484.

421. Haydon, A., *Adjuvant chemotherapy in colon cancer: what is the evidence?* Intern Med J, 2003. **33**(3): p. 119-24.

422. Sikorski, R. and B. Yao, *Visualizing the landscape of selection biomarkers in current phase III oncology clinical trials.* Sci Transl Med, 2010. **2**(34): p. 34ps27.

423. Kawasaki, Y., *et al.*, *Clinicopathological significance of nuclear factor (erythroid-2)-related factor 2 (Nrf2) expression in gastric cancer.* BMC Cancer, 2015. **15**: p. 5.

424. Liew, P.L., *et al.*, *Prognostic and predictive values of Nrf2, Keap1, p16 and E-cadherin expression in ovarian epithelial carcinoma.* Int J Clin Exp Pathol, 2015. **8**(5): p. 5642-9.

425. Kononen, J., *et al.*, *Tissue microarrays for high-throughput molecular profiling of tumor specimens.* Nat Med, 1998. **4**(7): p. 844-7.

426. Shousha, S., *Oestrogen receptor status of breast carcinoma: Allred/H score conversion table.* Histopathology, 2008. **53**(3): p. 346-7.

427. Franken, N.A., *et al.*, *Clonogenic assay of cells in vitro.* Nat Protoc, 2006. **1**(5): p. 2315-9.

428. Hata, R., *et al.*, *Suppressed rate of carcinogenesis and decreases in tumour volume and lung metastasis in CXCL14/BRAK transgenic mice.* Sci Rep, 2015. **5**: p. 9083.

429. Chou, T.C., *Drug combination studies and their synergy quantification using the Chou-Talalay method.* Cancer Res, 2010. **70**(2): p. 440-6.

430. Motohashi, H. and M. Yamamoto, *Nrf2-Keap1 defines a physiologically important stress response mechanism.* Trends Mol Med, 2004. **10**(11): p. 549-57.

431. Wang, X.J., *et al.*, *Oxaliplatin activates the Keap1/Nrf2 antioxidant system conferring protection against the cytotoxicity of anticancer drugs.* Free Radic Biol Med, 2014. **70**: p. 68-77.

432. Hu, T., *et al.*, *Clinicopathologic significance of CXCR4 and Nrf2 in colorectal cancer.* J Biomed Res, 2013. **27**(4): p. 283-90.

433. Hall, I.H., *et al.*, *Antitumor agents XLVI: In vitro effects of esters of brusatol, bisbrusatol, and related compounds on nucleic acid and protein synthesis of P-388 lymphocytic leukemia cells.* J Pharm Sci, 1982. **71**(3): p. 345-8.

434. Liou, Y.F., *et al.*, *Antitumor agents XLVIII: Structure-activity relationships of quassinoids as in vitro protein synthesis inhibitors of P-388 lymphocytic leukemia tumor cell metabolism.* J Pharm Sci, 1982. **71**(4): p. 430-5.

435. Vartanian, S., *et al.*, *Application of mass spectrometry profiling to establish brusatol as an inhibitor of global protein synthesis.* 2015.

436. Olayanju, A., *et al.*, *Brusatol provokes a rapid and transient inhibition of Nrf2 signaling and sensitizes mammalian cells to chemical toxicity—implications for therapeutic targeting of Nrf2.* Free Radical Biology and Medicine, 2015. **78**: p. 202-212.

437. Huang, R., *et al.*, *ATP-binding cassette transporters modulate both coelenterazine- and D-luciferin-based bioluminescence imaging.* Mol Imaging, 2011. **10**(3): p. 215-26.

438. Willingham, W., Jr., *et al.*, *Mechanism of eukaryotic protein synthesis inhibition by brusatol.* Biochim Biophys Acta, 1981. **654**(2): p. 169-74.

439. Willingham, W., 3rd, *et al.*, *Reversibility of protein synthesis inhibition by quassinoid antineoplastic agents in a rabbit reticulocyte system.* Biochem Pharmacol, 1984. **33**(2): p. 330-3.

440. Liesmann, J., *et al.*, *Phase I study on bruceantin administered on a weekly schedule.* Cancer Treat Rep, 1981. **65**(9-10): p. 883-5.

441. Bedikian, A.Y., *et al.*, *Initial clinical studies with bruceantin.* Cancer Treat Rep, 1979. **63**(11-12): p. 1843-7.

442. Wiseman, C.L., *et al.*, *Phase II trial of bruceantin in metastatic breast carcinoma.* Am J Clin Oncol, 1982. **5**(4): p. 389-91.

443. Arseneau, J.C., *et al.*, *A Phase II study of Bruceantin (NSC-165, 563) in advanced malignant melanoma.* Invest New Drugs, 1983. **1**(3): p. 239-42.

444. Zieske, L.R., *A perspective on the use of iTRAQ reagent technology for protein complex and profiling studies.* J Exp Bot, 2006. **57**(7): p. 1501-8.

445. Bradford, M.M., *A rapid and sensitive method for the quantitation of microgram quantities of protein utilizing the principle of protein-dye binding.* Anal Biochem, 1976. **72**: p. 248-54.

446. Schmittgen, T.D. and K.J. Livak, *Analyzing real-time PCR data by the comparative CT method.* Nat. Protocols, 2008. **3**(6): p. 1101-1108.

447. Subramanian, A., *et al.*, *Gene set enrichment analysis: a knowledge-based approach for interpreting genome-wide expression profiles.* Proc Natl Acad Sci U S A, 2005. **102**(43): p. 15545-50.

448. Chen, P., *et al.*, *Oleanolic acid attenuates obstructive cholestasis in bile duct-ligated mice, possibly via activation of NRF2-MRPs and FXR antagonism.* Eur J Pharmacol, 2015. **765**: p. 131-9.

449. Roberts, M.D., *et al.*, *Western diet-induced hepatic steatosis and alterations in the liver transcriptome in adult Brown-Norway rats.* BMC Gastroenterol, 2015. **15**: p. 151.

450. Ceddia, R.B., *The role of AMP-activated protein kinase in regulating white adipose tissue metabolism.* Mol Cell Endocrinol, 2013. **366**(2): p. 194-203.

451. Kang, K.W., S.J. Lee, and S.G. Kim, *Molecular mechanism of nrf2 activation by oxidative stress.* Antioxid Redox Signal, 2005. **7**(11-12): p. 1664-73.

452. Lin, A.H., *et al.*, *Activation of Nrf2 is required for up-regulation of the pi class of glutathione S-transferase in rat primary hepatocytes with L-methionine starvation.* J Agric Food Chem, 2012. **60**(26): p. 6537-45.

453. Roskoski Jr, R., *ERK1/2 MAP kinases: Structure, function, and regulation.* Pharmacological Research, 2012. **66**(2): p. 105-143.

454. Shen, G., *et al.*, *Regulation of Nrf2 transactivation domain activity. The differential effects of mitogen-activated protein kinase cascades and synergistic stimulatory effect of Raf and CREB-binding protein.* J Biol Chem, 2004. **279**(22): p. 23052-60.

455. Cong, Z.X., *et al.*, *ERK and PI3K signaling cascades induce Nrf2 activation and regulate cell viability partly through Nrf2 in human glioblastoma cells.* Oncol Rep, 2013. **30**(2): p. 715-22.

456. Choi, H.Y., *et al.*, *Oxyresveratrol abrogates oxidative stress by activating ERK-Nrf2 pathway in the liver.* Chem Biol Interact, 2016. **245**: p. 110-21.

457. Bettenworth, D., *et al.*, *Endoscopy-guided orthotopic implantation of colorectal cancer cells results in metastatic colorectal cancer in mice.* Clin Exp Metastasis, 2016. **33**(6): p. 551-62.

458. Ramasawmy, R., *et al.*, *Monitoring the Growth of an Orthotopic Tumour Xenograft Model: Multi-Modal Imaging Assessment with Benchtop MRI (1T), High-Field MRI (9.4T), Ultrasound and Bioluminescence.* PLoS One, 2016. **11**(5): p. e0156162.

459. Lin, P.L., *et al.*, *Cytoplasmic localization of Nrf2 promotes colorectal cancer with more aggressive tumors via upregulation of PSMD4.* Free Radic Biol Med, 2016. **95**: p. 121-32.

460. Zhao, X.Q., *et al.*, *Promoter demethylation of nuclear factor-erythroid 2-related factor 2 gene in drug-resistant colon cancer cells.* Oncol Lett, 2015. **10**(3): p. 1287-1292.

461. Yokoo, Y., *et al.*, *Effects of Nrf2 silencing on oxidative stress-associated intestinal carcinogenesis in mice.* Cancer Med, 2016. **5**(6): p. 1228-38.

462. Ford, J., *et al.*, *Multiple and Co-Nanoprecipitation Studies of Branched Hydrophobic Copolymers and A–B Amphiphilic Block Copolymers, Allowing Rapid Formation of Sterically Stabilized Nanoparticles in Aqueous Media.* Macromolecules, 2015. **48**(6): p. 1883-1893.

463. Mosallaei, N., *et al.*, *Solid lipid nanoparticles containing 7-ethyl-10-hydroxycamptothecin (SN38): Preparation, characterization, in vitro, and in vivo evaluations.* Eur J Pharm Biopharm, 2016. **104**: p. 42-50.

464. Essa, S., *et al.*, *SN-38 active loading in poly(lactic-co-glycolic acid) nanoparticles and assessment of their anticancer properties on COLO-205 human colon adenocarcinoma cells.* J Microencapsul, 2015. **32**(8): p. 784-93.

465. Zhang, Q., *et al.*, *Determination of a potential antitumor quassinoid in rat plasma by UPLC–MS/MS and its application in a pharmacokinetic study.* Journal of Pharmaceutical and Biomedical Analysis, 2016. **124**: p. 143-148.

466. Chio, II, *et al.*, *NRF2 Promotes Tumor Maintenance by Modulating mRNA Translation in Pancreatic Cancer.* Cell, 2016. **166**(4): p. 963-76.

Appendix 1 – comparison of phenotypes in the CT26 parent and CT26lucA6c clonal populations

a)

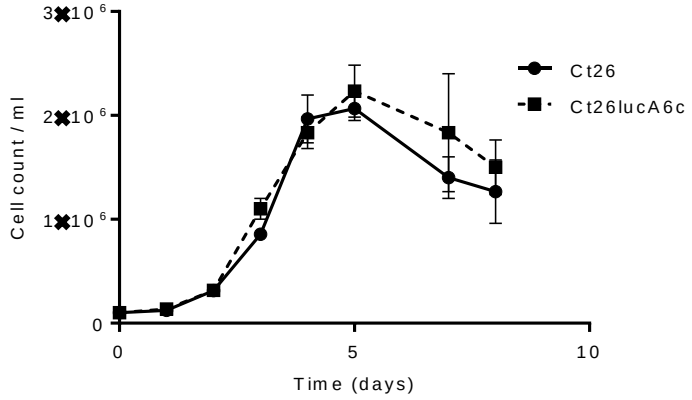

b)

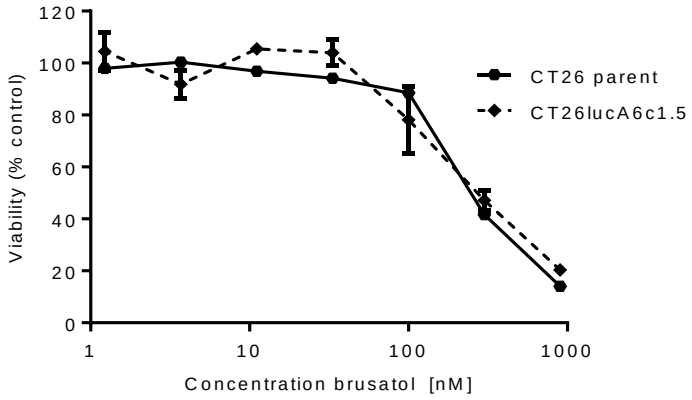

Figure A1 – a) Graph displays the growth rate of the CT26 parent population in comparison to the CT26lucA6c clonal cell line used *in vivo,* assessed by cell counting using the Countess™ automated cell counter. No significant differences were observed. b) Brusatol dose-response curves demonstrated similar IC50 values in the parent and clonal population (CT26 versus CT26lucA6c brusatol IC50 = 266 versus 290, non-significant by sum of squares F-test)

Appendix 2 – lines of best fit and comparison of tumour growth rates between treatment groups in the orthotopic model

a)

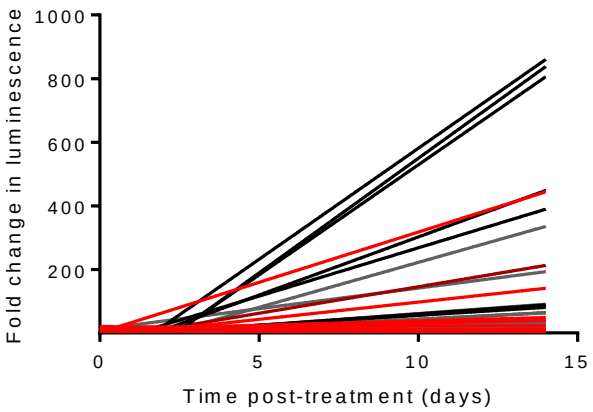

b)

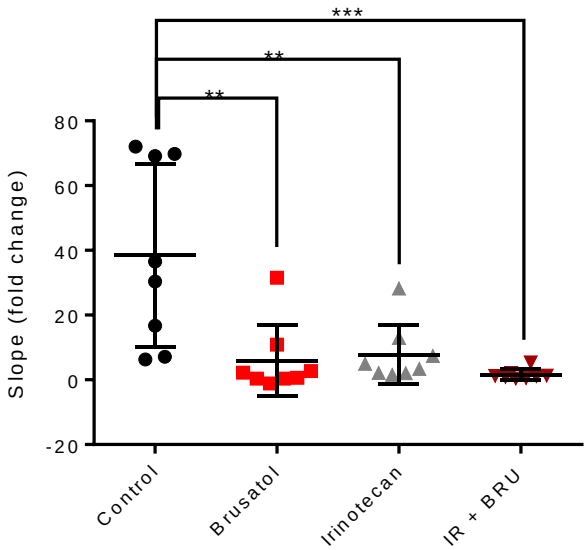

Figure A2 – a) Graph displays the lines of best fit for fold change in luminescence for each individual mouse, with the slope representing tumour growth rate; colours divide mice by treatment group. b) Scatter plots display the slope values for each individual mouse with the mean +/- SD for each treatment group. All treatments inhibited tumour growth significantly (one-way ANOVA). (IR = irinotecan, BRU = brusatol)

Appendix 3 – Supporting Publications, Presentations and Prizes

Accepted Manuscripts

Evans JP, Sutton PA, Winiarski BK, Fenwick SW, Malik HZ, Vimalachandran D, Tweedle EM, Costello E, Palmer DH, Park BK, Kitteringham NR. **From mice to men; murine models of colorectal cancer for use in translational research**. Crit Rev Oncol Hematol. 2016 Feb; 98: 94-105. (PMID: 26558688 DOI: 10.1016/j.critrevonc.2015.10.009)

Sutton PA, Jones RP, Evans JP, Kitteringham N, Goldring C, Palmer DH, Vimalachandran D and Malik HZ. **Predicting response to neoadjuvant treatment for advanced colorectal cancer – a review of relevant mechanisms and potential biomarkers.** Colorect. Cancer. 2015 May; 4(2): 85–95

Manuscripts in Preparation

Jonathan P Evans, Boleslaw K Winiarski, Paul A Sutton, Robert P Jones, Lorenzo Ressel, Carrie A Duckworth, D Mark Pritchard, Zhi-Xiu Lin, Ian M Copple, Elizabeth M Tweedle, Eithne Costello, Christopher E Goldring, B Kevin Park, Daniel H Palmer and Neil R Kitteringham. **The Nrf2 inhibitor brusatol is a potent antitumour agent in an orthotopic mouse model of colorectal cancer.** Submitted to Oncotarget.

Jonathan P Evans, Boleslaw K Winiarski, Paul A Sutton, Robert P Jones, Lorenzo Ressel, Carrie A Duckworth, D Mark Pritchard, Elizabeth M Tweedle, Eithne Costello, Christopher E Goldring, B Kevin Park, Daniel H Palmer and Neil R Kitteringham. **The development of an orthotopic syngeneic metastatic murine model of colorectal cancer for use in translational research.**

Presentations and Published Abstracts

Evans JP, Winiarski, BK, Sutton PA, Jones RP, Rooney PS, Palmer DH and Kitteringham NK. **The Nrf2 inhibitor brusatol is a potent antitumour agent in an orthotopic mouse model of colorectal cancer.**

Oral presentation at West Midlands Surgical Society Nov 2016

Won the runners up prize

Evans JP, Winiarski, BK, Sutton PA, Jones RP, Rooney PS, Palmer DH and Kitteringham NK. **The development of an orthotopic syngeneic murine model of colorectal cancer for use in translational research.** Abstract Colorectal Disease Oct 2016: 18(S2): 1-82 (DOI: 10.1111/codi.13499)

Poster of distinction ACPGBI 2016

Evans JP, Winiarski, BK, Sutton PA, Jones RP, Palmer DH and Kitteringham NK. **Nrf2 inhibition offers a therapeutic strategy in the treatment of colorectal cancer.** Abstract Colorectal Disease Oct 2016: 18(S2): 1-82 (DOI: 10.1111/codi.13499)

Poster ACPGBI 2016

Evans JP, Winiarski, BK, Sutton PA, Jones RP, Palmer DH and Kitteringham NK. **Nanoparticle technology for the direct delivery of SN-38 in the treatment of colorectal cancer.** Abstract Colorectal Disease Oct 2016: 18(S2): 1-82 (DOI: 10.1111/codi.13499)

Poster ACPGBI 2016

Sutton PA, Evans JP, Jones RP, Sahgal O, Malik H, Vimalachandran D, Palmer DH, Goldring C and Kitteringham NK. **Inhibition of NQO1 improves chemosensitivity in an *in vitro* model of colon cancer.** Abstract Colorectal Disease Oct 2016: 18(S2): 1-82 (DOI: 10.1111/codi.13499)

Poster ACPGBI 2016

Evans JP, Winiarski BK, Sutton PA, Rooney PS, Palmer DH and Kitteringham N. **Modulation of the NRF2 pathway alters the responsiveness of colorectal cancer cells to irinotecan.** Abstract Gut June 2015; 64: Suppl 1 A531 (doi:10.1136/gutjnl-2015-309861.1160)

Poster DDF 2015

Evans JP, Al-Khafaji, Sutton PA, Bowden D, Rooney PS, Vimalachandran D and Jenkins JR. β-**Catenin expression in the primary tumour is associated with lymph node status in colorectal cancer.** Abstract Gut 2015; 64: Suppl 1 A530 (doi:10.1136/gutjnl-2015-309861.1158)

Poster DDF 2015

Evans JP, Winiarski BK, Sutton PA, Rooney PS, Palmer DH and Kitteringham N. **Inhibition of NRF2 sensitises colorectal cancer cells to irinotecan cytotoxicity.** Abstract Diseases of the Colon & Rectum May 2015; 58(5):e89-e389 (P1281)

Poster ASCRS 2015

Sutton P, Evans J, Jones R, Malik H, Vimalachandran D, Palmer D, Goldring C and Kitteringham N. **Proteomic analysis to identify biomarkers in the primary tumour that predict response to neoadjuvant chemotherapy in liver metastases.** Abstract The Lancet February 2015; 385: Special Issue S95 (doi: 10.1016/S0140-6736(15)60410-X.)

Poster Academy of Medical Sciences 2015

Sutton P, Evans J, Jones R, Malik H, Vimalachandran D, Palmer D, Goldring C and Kitteringham N. **Nqo1 is a predictive biomarker and therapeutic target in metastatic colorectal cancer.** Gut June 2015; 64: Suppl 1 A345 (doi:10.1136/gutjnl-2015-309861.751)

Poster DDF 2015

Grants

Arising from and for the continuation of work completed during this PhD thesis

Cancer Research UK (2014)	£1786
Cancer Research UK (2015)	£1.5M